A STUDY OF THE CARINA DWARF SPHEROIDAL GALAXY

Philip John Godwin

A Thesis submitted for the degree of

Doctor of Philosophy

Edinburgh University 1986

This Thesis is an account of work carried out at Edinburgh University between October 1981 and May 1986. It consists entirely of my own work except where specifically indicated in the text. Some of the results presented in chapter 5 have been published in the proceedings of IAU Symposium number 113 'Dynamics of Star Clusters' (eds. Goodman J. and Hut P. p.77) and some of the results from the initial reductions of chapter 6 have been published under joint authorship with D. Lynden-Bell and R.D. Cannon (M.N.R.A.S 1983 204, 87P).

Department of Astronomy,
Blackford Hill,
Edinburgh University.

May 1st 1986

Acknowledgements

I should particularly like to thank my supervisors Mary Bruck and Russell Cannon for their help, support and encouragement with this Thesis over the period of my stay in Edinburgh. Special thanks must also go to Harvey MacGillivray for his ever diligent care in providing the best quality COSMOS data available, and to Mike Hawkins, Douglas Heggie, Ram Sagar, Richard Prestage, Donald Lynden-Bell, Steve Heathcote, Paul Hodge, Denis Kelly, Annie Robin, Clinton Blackman, Gerry Gilmore, Neill Reid, John Palmer, Paul Hewett, Steven Beard, Colin Aspin, Serge Demers, Gene Byrd and Nick Kaiser for useful and stimulating discussions.

I also wish to thank all members of the University Astronomy Department, ROE library, photolaboratories, IDPU unit and UKSTU plate library staff for their ever ready willingness to help.

My thanks must also be expressed to Alice Julier and Chris Godfrey for their help and assistance in the preparation of this manuscript.

Finally, I acknowledge the financial assistance of a Science and Engineering Research Council (SERC) studentship.

To my wonderful parents

ABSTRACT

The structure and chemical composition of the Carina dwarf spheroidal galaxy is studied, using COSMOS measures of deep UKST and AAT plates. A (B-V,V) colour magnitude diagram is constructed, and such parameters as this galaxy's heliocentric distance (91 ± 9 kpc), giant branch metallicity parameters ($\Delta V_{1.4} = 3.0\pm0.3$, $S = 5.0\pm1.1$, $(B-V)_{og} = 0.74\pm0.06$) and Mironov Index (0.09 ± 0.03) estimated.

The low luminosity counterpart of the extended giant branch found by Mould et al (1982) in this galaxy has been identified and separated from the first ascent giant stars. This latter branch is shown to be possibly intrinsically broad, implying a mean metallicity [Fe/H] = -1.8 with a possible real spread of about 0.26. Any broadness has been calculated to be far too large to be explained solely in terms of age e.g. by a continuous star formation history since the Carina dwarf was formed. The results are consistent however with e.g. (a) the dwarf spheroidals originating in a much more massive external system (e.g. the Magellanic Clouds) where metal enrichment occurred, and later being tidally 'ripped' out of this system with their presently estimated masses or (b) if the dwarf spheroidals evolved as isolated systems, then in the case of the Carina dwarf, it must have lost more than 70% of its original mass.

Core ($9.7'\pm0.8'$) and tidal ($38'\pm10'$) radii as well as the orientation position angle (72 ± 2^{o}) and mean ellipticity of the Carina dwarf's isopleths (0.31 ± 0.03) have been calculated, the latter result showing that there exists very little variation of the ellipticity of the isopleths with radius. These values, together with this galaxy's mass of $(0.3,6.1,17.5)\times10^{5}$ $M_{\odot}$ (calculated by the Hodge (1971) method of assuming that globular cluster and dwarf spheroidal galaxy luminosity functions are similar) have been used to show that this galaxy is interacting strongly with the Galaxy's gravitational field. It is surmised that this could be one mechanism whereby the Carina dwarf has lost mass (as required by case (b) above), after a number of perigalactic passages.

More evidence, complementing that of Mould and Aaronson (1983), that a substantial fraction of the Carina dwarf's membership is younger than 15 Gyr has been found. This comes from (a) the comparison of its luminosity function to that of M3 over a substantial range of absolute magnitude, (b) the identification of another carbon star in this galaxy and confirmation of the previously suspected six by optical spectra, (c) the lack of variables and (d) isochrone fits over both the giant and main sequence branches taken together (for the first time).

The absolute magnitude of the Carina dwarf is estimated to be $M_V = -9.6$ with a range from -8.8 to -10.8, making it one of the least luminous objects in the Local Group. Its central surface density and brightness are so low ($\rho_0 = (5 \pm 4) \times 10^{-3}$ $M_\odot/pc^3$, $b(B) = 25.3 \pm 1.0$ magnitudes/arcsec^2) that it would be barely detectable on IIIaJ UKST plates at five times the distance of M31.

Spectra of carbon stars, using the RGO spectrograph with the IPCS on the AAT have been used to question whether dwarf spheroidals contain large quantities of non-luminous matter. The major 'evidence' for this latter point comes from velocity dispersion measures using carbon star spectra in some of the other dwarf spheroidals. It is shown here, under the assumption of negligible variability of these stars and using only the internal errors on the carbon stars' velocities, that the velocity dispersion of the Carina dwarf is 10.4 ± 3.0 kms^{-1} implying a large M/L ratio for this galaxy.

The Galactocentric velocity of the Carina dwarf derived using these spectra suggests that instead of being one of the Galaxy's fastest moving satellites as previously thought (Cannon, Niss and Norgaard-Nielsen 1981), it is practically stationary (15 ± 5kms^{-1}), removing some of the previous evidence for a Galactic heavy halo.

TABLE OF CONTENTS

Chapter 1 : INTRODUCTION AND AIMS OF THESIS

1.1 : Introduction

Our Galaxy is located within a small cluster of galaxies usually referred to as the 'Local Group', which in turn is part of a supercluster centered on the famous Virgo cluster of galaxies. Probably the best known members of the Local Group besides our own Galaxy are the Andromeda Nebula (M31), the Triangulum Nebula (M33) and the two Magellanic Clouds, the latter being satellites of our Galaxy (at least in the sense of being affected by the Galaxy's gravitational field) together with the almost spherical halo of dynamically bound globular clusters. It is within this halo, extending out to some 250kpc that the Galaxy's dwarf spheroidal galaxy companions are found, of which the one located in the constellation of Carina is the subject of this thesis. Hereafter, 'dsph' will be used to denote one of our Galaxy's 'dwarf spheroidal' galaxies and 'CDG' will refer to the 'Carina dwarf spheroidal galaxy'.

The name dwarf spheroidal galaxy is usually used to label galaxies of (a) low surface brightness, (b) small intrinsic size and (c) small absolute luminosity. Their masses ($10^5 \leq M/M_\odot \leq 10^7$) and absolute magnitudes ($-15 \leq M_V \leq -7$) derived by Hodge (1971) range from those of massive globular clusters to low mass elliptical galaxies and their Galactocentric distances from about 80 to 220 kpc (Hodge 1971), i.e. they reside in the Galaxy's outer halo. They contain large numbers of red giants, but no very luminous blue stars (Tammann 1980) and very little neutral hydrogen, upper limits being of the order 10^{-3} to 10^{-4} of their total mass (Huchtmeier 1980). The Galaxy's other dwarf spheroidal members, which like the CDG (see plates 1.1a and b) are also thought to be satellites of our own Galaxy (Pagel and Edmunds 1981), are to be found in the constellations of Sculptor, Fornax, Draco, Leo (two dwarfs, usually labelled I and II) and Ursa-Minor.

Plate 1.1a. The Carina dwarf spheroidal galaxy, taken from a UK Schmidt telescope J survey plate (×2). Normal contrast print.

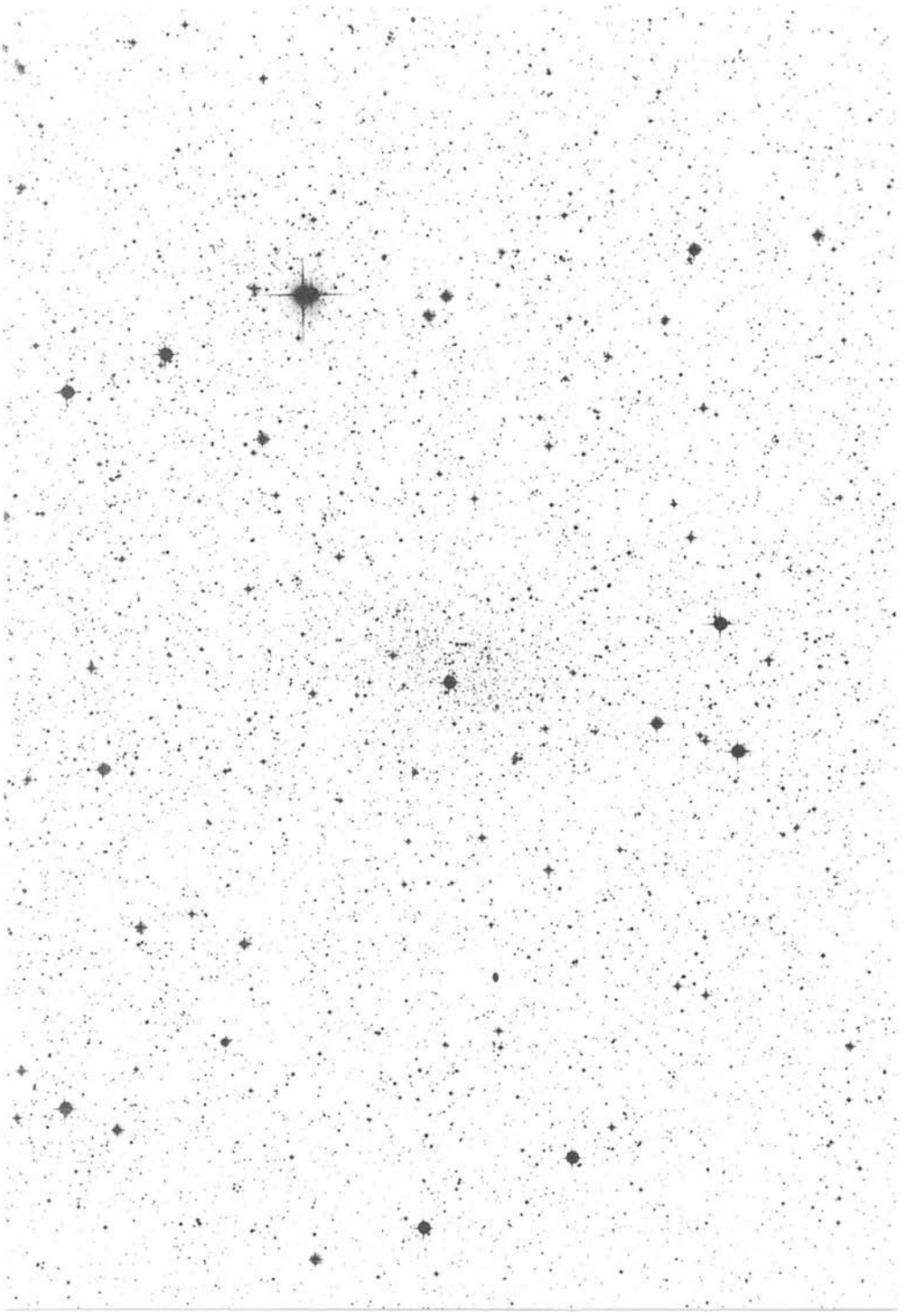

Plate 1.1b. The Carina dwarf spheroidal galaxy, taken from a UK Schmidt telescope J survey plate (×2). High contrast print.

The Local Group also contains a number of dwarf irregular galaxies which contain copious amounts of neutral hydrogen and in many cases HII gas. These galaxies are mainly situated in low density environments whereas the known dwarf spheroidal galaxies tend to favour the neighbourhood of M31 and that of our own Galaxy (van den Bergh 1980). Together they are the most numerous constituents of the Local Group, and it seems likely that they are also the most common type of galaxy in the Universe (van den Bergh 1980). Reaves (1967) concluded that although the dwarf spheroidals are more numerous than the more massive (and rarer) giant ellipticals, their contribution to the total mass in the Universe must be very small. However, spiral and elliptical galaxy rotation curves (e.g. Roberts 1975, Appleton and Davies 1983) and group mass to light ratios of elliptical galaxies show strong evidence for there to be some form of missing mass in the best studied of these galaxies, but it is unclear whether the dwarf spheroidals contain any of this matter. The evidence for any tendency for the dwarf spheroidal galaxies to be found only around larger galaxies is scanty, searches being hampered by their intrinsic faintness and very low surface densities. To emphasize this point, it is noted that the SERC IIIaJ survey of the southern skies has resulted in only one new dsph galaxy member, that in Carina (Cannon, Hawarden and Tritton 1977), to the previously known six, all of which had been found within the last 50 years (Shapley 1938, 1939, Harrington and Wilson 1950, Wilson 1955).

The majority of the dsph galaxies and many of the very distant and therefore tidally undisrupted globular clusters together with the LMC and SMC (the Large and Small Magellanic Clouds respectively), define a plane passing through the Galactic centre and inclined at a large angle to the Galactic plane; the so called 'Magellanic Plane' (Mathewson, Cleary and Murray 1974, Fujimoto and Murai 1984). A long filament of neutral hydrogen, extending from the Magellanic Clouds down to the South Galactic Pole (SGP), together with the Ursa-Minor and Draco dsph galaxies defines another plane, the 'Magellanic Stream', inclined at approximately 35 ^{o} to the former one (Kunkel 1979). Lynden-Bell (1982b) has shown that it is probable that the CDG is also associated with this Stream, and that the Fornax, Sculptor

and Leo systems lie on another great circle as seen from the Galactic centre. All of the Local Group dwarf spheroidals appear at the present time to be interacting to some degree with the Galaxy's gravitational field, and in the case of the Ursa-Minor dsph galaxy, it has been speculated that the tidal force of the Galaxy will permanently disrupt it on its next passage around the Galaxy, by pulling a large fraction of its stellar membership completely away (Hodge and Michie 1969). Lynden-Bell (1982a) found that the elongation of this dwarf galaxy implied that it is being disrupted in the plane defined by the Magellanic Stream, leading to speculations (Lynden-Bell 1976, 1982b, Kunkel 1979) that the dsph galaxies are the evolved tidal debris of a past close encounter, shortly after the formation of the globular cluster halo, between the Magellanic Clouds (treated as a single entity) and the Galaxy.

Evidence for a more recent disruptive event ($<$ 1 Gyr ago), possibly on a successive passage of the Magellanic Clouds around the Galaxy, comes mainly from two observations. The first is that a wing of the SMC is known to be primarily composed of young stars (Westerlund and Glaspey 1971) indicating a recent triggering process, and secondly, there exists very fine structure in the filaments of the Magellanic Stream that could not have survived for more than 10^8 years (Mathewson, Schwartz and Murray 1977). There are problems with this idea though, of the dsph galaxies being the stellar remnants torn from a 'Greater Magellanic Galaxy'. One of these is that there is now thought to be a dominant <u>intermediate</u> age stellar population in the Magellanic Clouds with an age of around 2 to 4 Gyr (Bruck and Hawkins 1983, Hardy and Durand 1984, Hardy et al 1984). Hence if the Magellanic Stream consists of material drawn out of the Clouds, then it should presumably contain stars already in existence. However very few stars (if any) have been found to be associated with the Magellanic Stream (see e.g. Tanaka and Hamajima 1982, Bruck and Hawkins 1983). Another problem is that the radial velocities obtained for the Draco and Ursa-Minor dsph galaxies by Hartwick and Sargent (1978) differ greatly from those of the nearby high velocity clouds of hydrogen, which should also be associated with the Stream, if this picture is correct (Lynden-Bell 1982a). The idea of dual formation of

these systems though, still seems very attractive (see e.g. Gerola, Carnevali and Salpeter 1983), with the Galaxy tidally stripping their gas away and halting any further star formation at the instant of separation from the Magellanic Clouds; this would mean that the age of the last period of star formation in the dsph galaxies would be that at which they were pulled away.

It can be seen that there are still some uncertainties as to whether this was the origin of the dsph galaxies. There are numerous other theories though. Could they be the after effects of core collapse in globular clusters; the remnants of the early fragmentation of isolated primordial gas clouds as Hodge and Michie (1969) have theorised, or have they been simply gravitationally captured by our Galaxy as the Magellanic Clouds appear to have been? Saito (1979), in order to explain why the mass density of these galaxies is so low, proposed that they were born as dense systems, but expanded at a later time due to supernovae driven gas ejection. Van den Bergh (1980), Lin and Faber (1983) and Faber and Lin (1983) have speculated that the dsph galaxies near giant galaxies were originally dwarf irregulars, and were stripped of their gas by the ram pressure of their parent galaxies. This would mean however that the dsph galaxies should be flattened which is not the case. Gerola, Seiden and Schulmann (1980) have postulated in a similar vein that the dsph galaxies and dwarf irregular galaxies interchange identities due to bursts and quiescent periods of stochastic self-propagating star formation.

Is their origin alternatively directly tied to our Galaxy's own evolution, as the Galaxy's system of globular clusters are now generally accepted to be? Radial abundance gradients in the Galaxy's halo, determined by looking at the metallicities of star clusters at different distances from the Galactic centre (see e.g. Freeman and Norris 1981, Harris and Racine 1979, Pilachowski 1984), provides an insight into the possible formation of the dwarf spheroidals and distant clusters out of the Galaxy's proto-gas cloud, but the picture is far from clear. Searle and Zinn (1978) suggested that the evidence for a metallicity gradient outside 10 to 20 kpc from the Galactic

centre is not very strong, and that it is not true that only extremely metal poor clusters are found at the large Galactocentric distances that the dwarf spheroidals are located. Pilachowski (1984) on the other hand finds that the average metallicity of the globular clusters declines slowly with Galactocentric distance, following an exponential law out to at least 100 kpc.

Is the origin and evolution of the dsph galaxies in some way linked to that of the globular clusters? In the past, both these systems have been thought to be similar, not only in age and origin but in structure and chemical composition too. Recent observations have thrown serious doubts on these ideas though, and it is now known that there are major differences between them. The most striking are as follows:

(1) There exists a spread in heavy element abundance within (at least) the best studied of the dsph galaxies (e.g. the Sculptor and Fornax systems), whereas the bulk of the globular clusters are known to be chemically homogeneous (there are exceptions though e.g. ω Cen, Cannon and Stobie 1973). This spread is deduced from the large differences seen in the spectral scans of some of the dwarf spheroidals' constituent red giants, located on opposite sides of their giant branches (Zinn 1978a, Zinn 1981). Possible intrinsically broad giant branches for these galaxies could be further evidence for this spread (Demers, Kunkel and Hardy 1979, Norris and Bessel 1978). If the composition of the planetary nebula in Fornax is indicative of the primordial composition of its progenitor star then the spread in Fornax of [Fe/H] could be as high as 1 (Zinn and Persson 1981). This range in abundance suggests either, or some combination of the following:

(a) More than one episode of star formation in the dsph galaxies, unlike the globular clusters where it is thought that all of the stars formed at one epoch, approximately 15 to 18 Gyr ago (VandenBerg 1983). Mould (1982) has suggested the possibility that the Fornax dsph galaxy's intermediate age population (Aaronson and Mould 1980) could merely be due to the recycling of mass lost by the original

generation of stars; the large mass of Fornax ($\sim 10^7$ $M_\odot$, Hodge 1971) being able to retain the ejected supernova material whilst the globular clusters were not (Zinn and Persson 1981).

(b) There existed large chemical abundance variations in the primordial gas cloud out of which the dsph galaxies may have formed, perhaps induced by the self pollution of an early generation of stars.

(c) Incomplete mixing processes within some of the red giants (see e.g. Kraft 1979, Zinn and Persson 1981).

Simple chemical evolutionary models of elliptical galaxies (e.g. Audouze and Tinsley 1976), taking into account mass loss appear to be consistent with the observations of a chemical abundance range in the dsph galaxies (Zinn 1978a). They predict that Fornax, the most massive of the dsph galaxies, should have retained and converted into stars the largest fraction of its initial mass and hence should have the richest mean metal abundance of these systems, which appears to be the case. It would also mean however from the metallicity spread observed in the Draco dsph galaxy, that this particular galaxy was ~100 times more massive than it appears to be today (Zinn 1978a). However the models do not explain why the majority of Galactic globular clusters have very little if any internal dispersion in [Fe/H], and this could be seen as evidence for a different origin for the two types of systems, perhaps giving weight to the tidal scenario for the dsph galaxies mentioned above (Zinn 1978b).

(2) All dsph galaxies so far searched for variables, contain at least two 'anomalous Cepheids' of which only one has been found in a globular cluster (Zinn and Dahn 1976, in the metal poor globular cluster NGC5466), and no type II Cepheids. At a given luminosity the periods of the anomalous Cepheids are shorter than those of the type II Cepheids by large amounts. Norris and Zinn (1975), and Demarque and Hirshfeld (1975) have shown that the periods, luminosities and evolutionary histories of these variables can be understood if they are factors of two or three times more massive than RR Lyrae

variables. Observations in the Draco dsph galaxy (Zinn and Searle 1976) confirm this large mass difference. They show that the large masses could be the result of either relatively young ages (~1 Gyr) or the coalescence of mass in close binary systems. Renzini, Mengel and Sweigart (1977) assuming the latter case deduced that these variables would not be found in globular clusters due to a binary of the required separation (a lower limit of 0.25 astronomical units) not being able to survive the required 12 Gyr for their production, due to stellar encounters.

The RR Lyrae variables that some of the dsph galaxies contain (van Agt 1973) also appear to be peculiar, since only a few can be classified into either of the two Oosterhoff groups that those found in globular clusters can be (Zinn 1978b). The Oosterhoff groups classify the mean periods of the (ab) RR Lyraes; those in Oosterhoff group I having $<P_{ab}> = 0.55$, and those in group II, $<P_{ab}> = 0.65$. The dsph galaxy (ab) RR Lyrae variables have been found to have values of $<P_{ab}>$ intermediate to these values, the exceptions being these types of star found in the Sculptor and Ursa-Minor dsph galaxies (Cacciari and Renzini 1976, van Agt 1973) which are thought to belong to groups I and II respectively. It is known that the Oosterhoff segregation effect is weakly correlated with metal abundance (Madore 1978); group I clusters (e.g. M3) being more metal rich than group II clusters (e.g. M92), the reason behind this being unknown. In the case of the dsph galaxies, the broad giant branches and hence the dispersion in metallicity that this presumably reflects, could be an explanation for the intermediate value of this period.

(3) In common with the outer halo globular clusters, the majority of the dsph galaxies have predominantly red horizontal branches despite their generally large metal deficiencies. The exception to this is the Ursa-Minor dsph galaxy (Schommer, Olszewski and Kunkel 1978, Olszewski and Aaronson 1985) which has been found to have a blue horizontal branch. Hence they do not follow the conventional relation between horizontal branch type and metal abundance that the vast majority of globular clusters do (NGC7006 being one exception, McClure and Hesser 1981), and are consequently said to suffer from

the 'second parameter anomaly'. In globular cluster colour magnitude diagrams, the giant branch can be described very well in terms of one parameter namely [Fe/H]. What causes the type of observed horizontal branch (blue, intermediate or red) however is much more difficult to ascertain since e.g. there is known to be a large range in type for globular clusters having the same metallicity. This is not surprising, since horizontal branch morphology is known to be sensitive to a number of parameters e.g. age, He and Z_{CNO} abundance, and any process causing mass loss on the first ascent of the giant branch (Rood 1973, Rood and Seitzer 1981).

In order to examine what the second parameter could be for the dsph galaxies, it is obviously desirable to know something about their origin. The Galaxy collapse model of Eggen, Lynden-Bell and Sandage (1962) established a relation between the shape of a star's orbit in the Galaxy and its stellar chemical abundance. This was interpreted as evidence that the stars with the highest velocities formed in a relatively short interval of time forming the Galactic spheroid, whilst the gas clouds which became the Galaxy collapsed later, with considerable energy dissipation and angular momentum redistribution to form the flattened and rotating Galactic disk. If this is to be believed then the spread in Galactic globular cluster ages should be small and so the search for a second parameter in these systems has usually concentrated on the Z_{CNO} and/or the He abundance. Recent re-calculations of model stellar atmospheres and new opacity determinations have led to the construction of reliable theoretical constant age loci (isochrones), that confirm that the globular clusters have ages in the range 15 to 18 Gyr (VandenBerg 1983), reinforcing the idea that these clusters were born (almost) simultaneously during the collapse of the protogalactic gas cloud. In the case of the dsph galaxies however, an age spread now seems to be the most likely candidate for this second parameter (Kraft 1979, Freeman and Norris 1981), and this fits in well with the results of Searle and Zinn (1978), who showed that clusters with unusually blue horizontal branches for their metal abundances are on average more tightly bound than those with red ones, and postulated that both type of system are found in the outer halo due simply to orbital mixing.

They found this idea to be consistent with the hypothesis that the loosely bound clusters of the outer halo have a broader range in age than the more tightly bound clusters, and formed from protogalactic fragments after the central regions of the Galaxy had collapsed. Rood and Seitzer (1981) though, still think that Z_{CNO} is a plausible candidate too for this parameter in dsph galaxies.

(4) At least one carbon and/or CH star has now been positively identified in each of the seven known dsph galaxies (Westerlund 1979, Aaronson and Mould 1980, Cannon, Niss and Norgaard-Nielson 1981, Aaronson, Liebert and Stocke 1982, Aaronson, Olszewski and Hodge 1983, Azzopardi, Lequeux and Westerlund 1985). They are bolometrically the most luminous stars in all of these galaxies (apart from the Ursa-Minor dsph galaxy), the redder and brighter ones being found in those galaxies having relatively greater luminosities and metallicities (Aaronson and Mould 1985). Carbon stars are however very rare in globular clusters and so the environment of the dsph galaxies seems to be favourable for their formation although theories of the origin of these stars are still very uncertain. This suggests that outer halo carbon stars could be escapees from dsph galaxies, or might be situated in this type of galaxy with too small a central density to be easily detected as such. Van den Bergh and Lafontaine (1984) showed that this second possibility cannot be true in the case of one particular halo carbon star, unless the assumed dsph galaxy had a very low absolute magnitude ($M_V > -5.7$).

Carbon stars are also much commoner in old open clusters than in globular clusters, so it would appear that these stars belong to the old population I class rather than to the (metal-poor) population II class. Hence their presence in the dsph galaxies indicates at least a small percentage of a younger (1 to 10 Gyr) intermediate age population of stars (Mould and Aaronson 1980), instead of simply the old population II component that was previously thought to be their only constituent. If this is so, and these galaxies contain old as well as intermediate age stars, then this naturally poses further questions about their origin e.g. do the dsph galaxies contain missing mass in order that the chemically enriched material was not

lost and could then be recycled for further star formation episodes after an initial burst, or did star formation suddenly cease after the dsph galaxies were torn away from a more massive parent galaxy?

(5) At least one of the dsph galaxies (Fornax) contains six globular clusters (Hodge 1971). It has been shown (Zinn and Persson 1981) that the metallicity range and ages of these globular clusters are comparable to those of the oldest ones in the Magellanic Clouds.

(6) Their much larger spatial dimensions and their comparable number of stars to globular clusters (of the order 10^6 to 10^7), result in the dsph galaxies having very small stellar densities in their central cores (typically $\sim 10^{-3}$ $M_\odot/pc^3$), making their relaxation times ($\sim 10^{11}$ to 10^{13} years) longer than the probable age of the Universe.

It would seem then that the two types of system not only evolved but originated in certain markedly differing ways. The mounting new CCD colour-magnitude diagram data for dsph galaxies (e.g. Mould and Aaronson 1983 for the CDG, Da Costa 1984 for Sculptor, Stetson et al 1985 for Draco, and Olszewski and Aaronson 1985 for Ursa-Minor) seems to confirm this, by showing that some of these galaxies contain a proportion of stars which are substantially younger than previously thought and also resemble the more luminous early type galaxies than the globular clusters. Evidence for the latter point comes from the work of Aaronson and Mould (1985) who showed that there is a well defined (abundance,M_V) relation amongst the known dsph galaxies which when extended, joins smoothly onto the same relation for the less luminous elliptical galaxies implying that the two types of galaxy are in fact very similar. Two pieces of evidence for the former point come from

(a) the presence of extended giant branches in at least five of the dsph galaxies. This is thought to be an indicator that an intermediate age population is present (Mould and Aaronson 1980), since it means that there are more massive stars present in the galaxy, better able to survive the mass loss mechanisms (Renzini

1981) that are thought to take place during evolution on the giant branch. Recent work by Aaronson and Mould (1985) using an age calibration dependent upon the extent of the asymptotic giant branches in the dsph galaxies (Mould and Aaronson 1980) found that star formation in Fornax could have occured of the order of 2 Gyr ago, and in the Carina, Sculptor and Leo systems ~10 Gyr ago. By this method Da Costa and Mould (in preparation) and Olszewski and Aaronson (1985) deduce that there has not been significant star formation in Draco or Ursa-Minor (respectively) over a period less than the age of M92 ago (~15 Gyr). Aaronson and Mould (1985) also find that the intermediate age population ranges from 5% of the Sculptor system to 25% in Fornax and in the case of Carina, the majority. Hodge (1983) however, has questioned this method of age calibration by comparing these age estimates with those derived from main sequence turn off predictions in Magellanic Cloud clusters.

(b) The main sequence turn off points for the CDG and Sculptor dwarf found by Mould and Aaronson (1983) and Da Costa (1984) respectively have been found to be more luminous than those of the globular clusters. If their identifications are correct, then this is prima facie evidence for a younger population of stars (compared to those found in globular clusters) in these two dsph galaxies. Although quantitatively, the absolute ages of the dsph galaxies may not be able to be pinned down with much accuracy, it is clear that the current theory of main sequence turn off luminosities, extended giant branches and carbon stars, gives strong support to the claim that there does exist a spread of age in at least some of these galaxies.

1.2 : Specific aims and outline of Thesis

It can be seen from the above resume why the study of dsph galaxies is of such considerable astrophysical interest, not only providing possible clues to our own Galaxy's evolution, but also as objects in their own right. They are close enough, in fact closer than any other type of galaxy apart from the Magellanic Clouds, that their structure can be examined in great detail as well as their individual stars, making their study a very important part of present

day Astronomy. Although modern CCD techniques have enabled data to be obtained at very faint levels (that is, down to the main sequence turn off and beyond in some of the dwarf spheroidals), it is clear that there is still room for large (relatively bright) stellar sample studies to be done, enabling the chemical and structural morphology of these galaxies to be examined in more detail, and to see how the derived results accord with current theories concerning their origin and evolution.

The data used in chapters 2,3,4 and 5 of this thesis come from photographic plate measurements obtained from the COSMOS automatic plate measuring machine at the Royal Observatory Edinburgh (ROE). One of the main aims here is to see if reliable photometric and number count data from these measures can be obtained for objects such as the dwarf spheroidals where e.g. the crowding of stellar images or sky background variations could very easily render the data unworkable. Previous colour magnitude diagrams of the CDG have been made by Cannon et al (1986) using PDS photographic data, and by Mould and Aaronson (1983) using CCD techniques over a very small area. This latter study deals with the Carina dwarf's main sequence component, whereas this thesis, using a larger and hence more statistically significant sample of stars than either of the two previous works, considers the red giant and horizontal branch populations. Optical spectra of carbon stars presented in chapter 6 come from an observing run at the Anglo-Australian Telescope (AAT) during January 1983.

Some of the astrophysical questions that will be attempted with this data are e.g. what is the Carina dwarf's metallicity ? Is there a spread of metallicity, and if so how can this be interpreted? Can an estimate of its luminosity and mass be made? What do its constituent stars and luminosity function infer about its age? How do the adopted isochrones for determining its age depend upon the choice of input parameters? Do the carbon stars found in the dsph galaxies have an intrinsic variability, or can their parent galaxy's true velocity dispersion be calculated using their observed radial velocities? Very little to date is known about these problems and hence work is badly needed in these areas if e.g. constraints are to

be obtained on the formation environments and the subsequent evolution of these galaxies.

Answers relating to the structural nature of the dsph galaxies should also enable an examination of the way in which the CDG (in particular) is interacting with the Galaxy's gravitational field. The mass of the dsph galaxies as well as that of our own Galaxy is a critical factor in this argument, but by using the radial velocities of stars within the dwarf spheroidals, as well as the heliocentric velocities of these galaxies, it is hoped to address the important question of whether there is any evidence for non-luminous matter in the CDG and if so what the dynamical effect could be. The main conclusions of each chapter are brought together in chapter 7.

2.1 : Introduction

The material used for the derivation of a colour magnitude diagram for the CDG consisted of six AAT plates, three taken in the photographic B band and the rest in V over two observing runs during 1977. The two plates taken with the doublet corrector were of good quality whilst the remainder taken with the triplet corrector were somewhat poorer (see table 2.1). The COSMOS automatic plate measuring machine specification has been extensively reviewed by numerous authors (see e.g. Stobie 1982) and so this will not be discussed here. However a brief outline of the way data is processed by COSMOS relevant to the projects undertaken in the following chapters is given, and the techniques used to derive a colour magnitude diagram from the resulting measures of these AAT plates is also presented.

At the beginning of this project it was unclear as to whether the thresholding technique used by COSMOS to estimate the brightness of a stellar image would be suitable for use on the available AAT plates of the CDG due to possible crowding, sky background or field effect problems. A number of other standard magnitude estimator algorithms available on the STARLINK VAX network were used to investigate this.

2.2 : A brief description of the COSMOS machine

The COSMOS machine is a high speed microdensitometer. Its main purpose is to convert the information contained on a photographic plate into digitised form which can be readily accessed for astronomical analysis. The procedure for measurement can be summarised as follows. The photographic plate is mounted into a sturdy holder and scanned by light from a microspot cathode ray tube (CRT) focussed onto the plate emulsion. The transmitted light is recorded by a photomultiplier and is compared with the light recorded by a second photomultiplier looking directly at the CRT face. These

TABLE 2.1

AAT PLATE MATERIAL

Name	Exposure	Corrector	∿seeing	Date	Emulsion/filter
B1386	40 mins	Doublet	2"	17-18.4.77	IIaO GG385
B1510	20 mins	Triplet	2"+	08-09.9.77	IIaO GG385
B1530	40 mins	Triplet	2"+	10-11.9.77	IIaO GG385
V1387	35 mins	Doublet	2"	17-18.4.77	IIaD GG495
V1511	25 mins	Triplet	2"+	08-09.9.77	IIaD GG495
V1529	40 mins	Triplet	2"+	10-11.9.77	IIaD GG495

two readings are then used to eliminate variations in sensitivity across the face of the CRT and the normalised output is converted to a transmission value by means of an analogue/digital convertor. These transmission values, which range from 0 to 255 inclusive, can then be converted to relative intensity values using the step wedge or spot calibration markings on the plate.

In 'mapping mode' (MM) operation, COSMOS simply retains these transmission values for every pixel. In 'threshold mode' (TM) the machine determines a smoothed local sky background (see section 2.3) and applies a threshold at a fixed percentage level in intensity space above the background. It then only accepts those pixels with intensity values above this level for output or further analysis. The 'image analysis mode' (IAM) software is applied to these data, determining which pixels are connected together to form a coherent image, and also calculating for this image such parameters (that are relevant here) as its area in square pixels, integrated magnitude, x and y intensity weighted centroid coordinate, intensity weighted orientation and the size of its semi-major/minor axes.

For work involving photographic photometry, the following points have to be given serious consideration before any reliable results can be obtained;

(a) The density to intensity calibration. The choice of pixel size to be used can be crutial if there exists large scale density variations over the size chosen, or if saturation effects are present. The two doublet plates had relative intensity to density conversion step wedges taken with an experimental spot calibrator. This meant that the value of γ (i.e. the 'contrast' of the emulsion - see section 2.3) had to be estimated from the type of emulsion (Malin, private communication) since the values in the Anglo-Australian Observatory (AAO) provided tables were not known with very great certainty.

(b) The accuracy and reliability of the magnitude calibration, taking into account any colour effects that may arise from the standard star photoelectric magnitudes not being in exactly the same pass-band as

the photographic material. The colours of the standard stars have to cover the range over which results are required (i.e. in this case for the CDG, the horizontal branch to the high luminosity tip of the giant branch). It is also important that the standards to be used are spatially distributed as much as possible over the area of the photographic plate that is to be used. This helps to reduce the effect of any position and/or colour dependent magnitude residuals in the derived calibrated magnitudes. These residuals can arise from e.g. emulsion variations, image profile variations due to the telescope corrector that is being used or even atmospheric effects at the time of observation.

(c) It is necessary that at least three plates of reasonable quality are available in each colour so that a 'reliable' mean calibrated magnitude can be derived for each stellar image.

(d) Sky background determination and subtraction or division from the data.

These points are discussed further below.

2.3 : Sky background determination and threshold level

After COSMOS has mapped a plate in 'mapping mode' i.e. for every increment in the scan a value of the transmission T has been recorded, calibration of these values to intensity is performed. This transformation is done by adopting a Baker density formulation which can be defined by

$$\log_{10} (I) = \gamma \log_{10} (\omega - 1) + C \quad \text{where} \qquad (2.1)$$

$$\omega = \frac{T_c - T_b}{T - T_b} \qquad (2.2)$$

In these formulae, I is the required pixel intensity, T_c is the transmission value recorded for chemical fog, T_b is the transmission recorded when no incident light is recorded by the detector, and γ measures the 'contrast' of the emulsion. The additive constant C is chosen such that a change in transmission from 255 to 254 units corresponds to a change in intensity of one unit.

The sky background level is determined by dividing each scan up every lane (which is 128 pixels wide) into blocks of 128x128 pixels, and for each of these a (T value,frequency) histogram is calculated with data drawn from every second pixel in the x and y directions. The median points of these histograms are chosen as the sky background values per block and assigned to each image falling within this region. Hence a discrete set of values are determined which for a strongly varying background caused by e.g. the stellar density in the centre of a star cluster, may not be good enough to enable a reliable thresholded magnitude to be obtained.

A preliminary set of COSMOS thresholded data measures was generated from one doublet and one triplet V plate of the CDG, to investigate the relative success of this standard (1 dimensional) sky background determination in coping with the vignetting (which is a more serious problem on the doublet plate) and the actual presence of the dsph galaxy. Figure 2.1a shows that apart from the central regions, the calculated sky background varies by as much as 0.025 magnitudes over the sampling size of one block, and by about 1.2 magnitudes from the centre to the edge of the measured region. To see whether a better determination of the sky background could be done, a 2 dimensional filter technique developed by MacGillivray (private communication) was tried. Each 22x22 pixel area had its mean intensity value calculated. These measurements over the whole of the plate were then compressed into a 512x512 array and a median filter

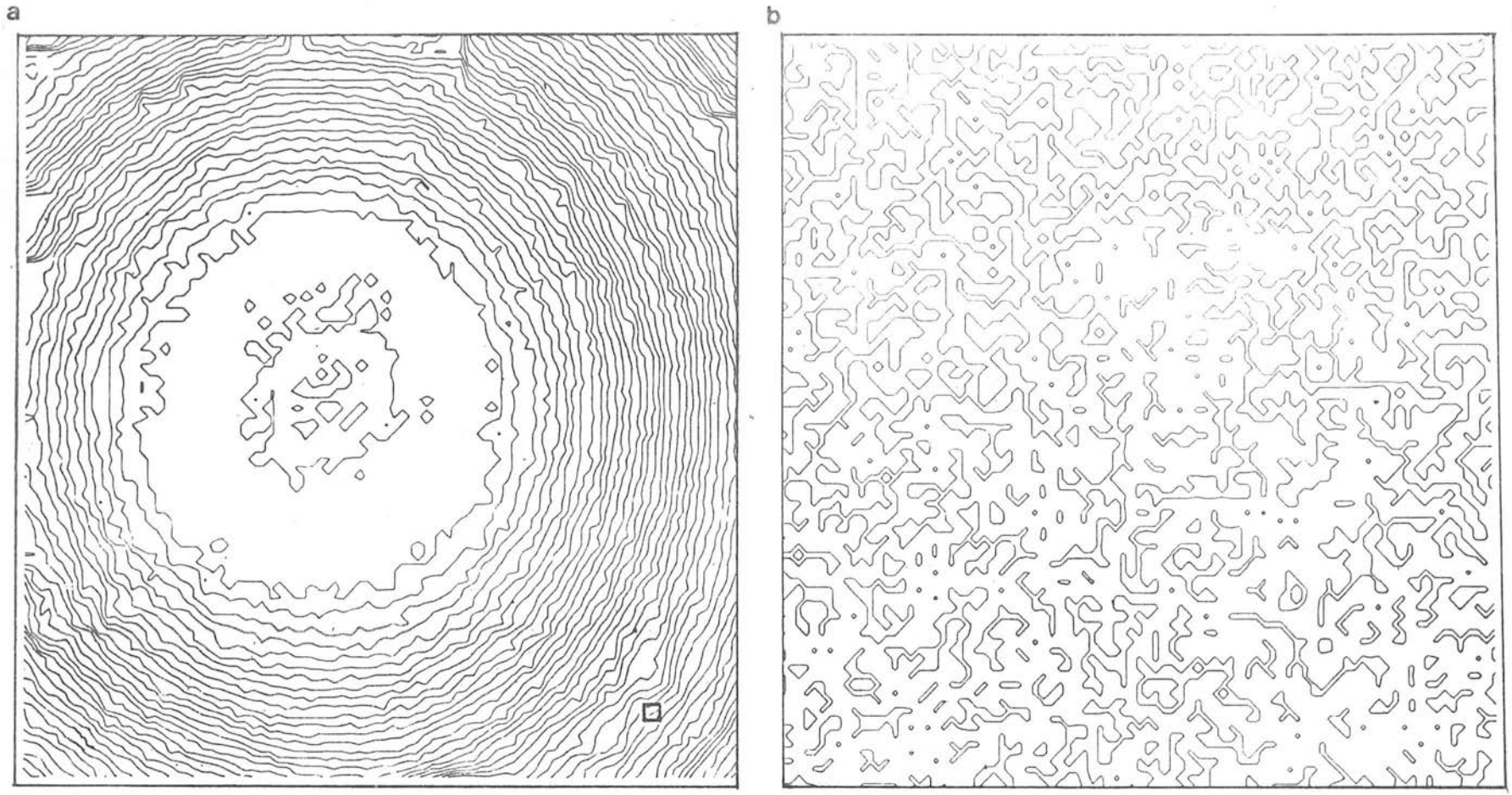

Figure 2.1a,b. (a) Sky background values for doublet plate (B1386) contoured in $\log_{10}$ (I) (interval = 0.01). The approximate block size is shown in the bottom right hand corner. (b) Same plot as in (a) except flat - fielded sky background values.

passed through the array elements to eliminate any sharp features and stars. The resulting 2-D 'bullseye' intensity profile was then divided out of the data. Figure 2.2 shows a slice across this profile (smooth line) compared with a slice across the original data (line with superimposed stars). The 'bump' in the middle is due to the presence of the dsph galaxy contributing to the sky background. The effect of this operation is shown in the new sky background plot of figure 2.1b, which implies a sky background magnitude shift across the whole of the measured region of about 0.03 magnitudes. The obvious success of this latter technique gave confidence in using the 2-D method for the two doublet plates, but it was found that the 1-D filtering was quite adequate for the triplet plates.

All of the six AAT plates used here were then mapped by COSMOS and thresholded at 10% above the local sky background level in intensity space. This level was chosen as being a good compromise between (a) enabling faint images to be detected down to the horizontal branch with a relatively high signal to noise (S/N) ratio (low threshold) thus enabling reliable calibration at these faint levels and (b) reducing the effects of crowding and hence making the blending of images less severe (high threshold). Once the thresholding base has been determined, all photometric parameters are then measured relative to this. To obtain the correct thresholded magnitude, the COSMOS σ_I output parameter for each image (divided by 100) namely

$$\sigma_I = -2.5\log_{10}\left[\sum_i (I_i - I_{sky})\right] \qquad (2.3)$$

(where the sum is performed over all pixels of the image), must be divided by the calculated sky background intensity. If this is done for the sky intensity per square arcsecond, then the resulting magnitude (σ_{CG}) gives a measure of the thresholded magnitude above sky i.e.

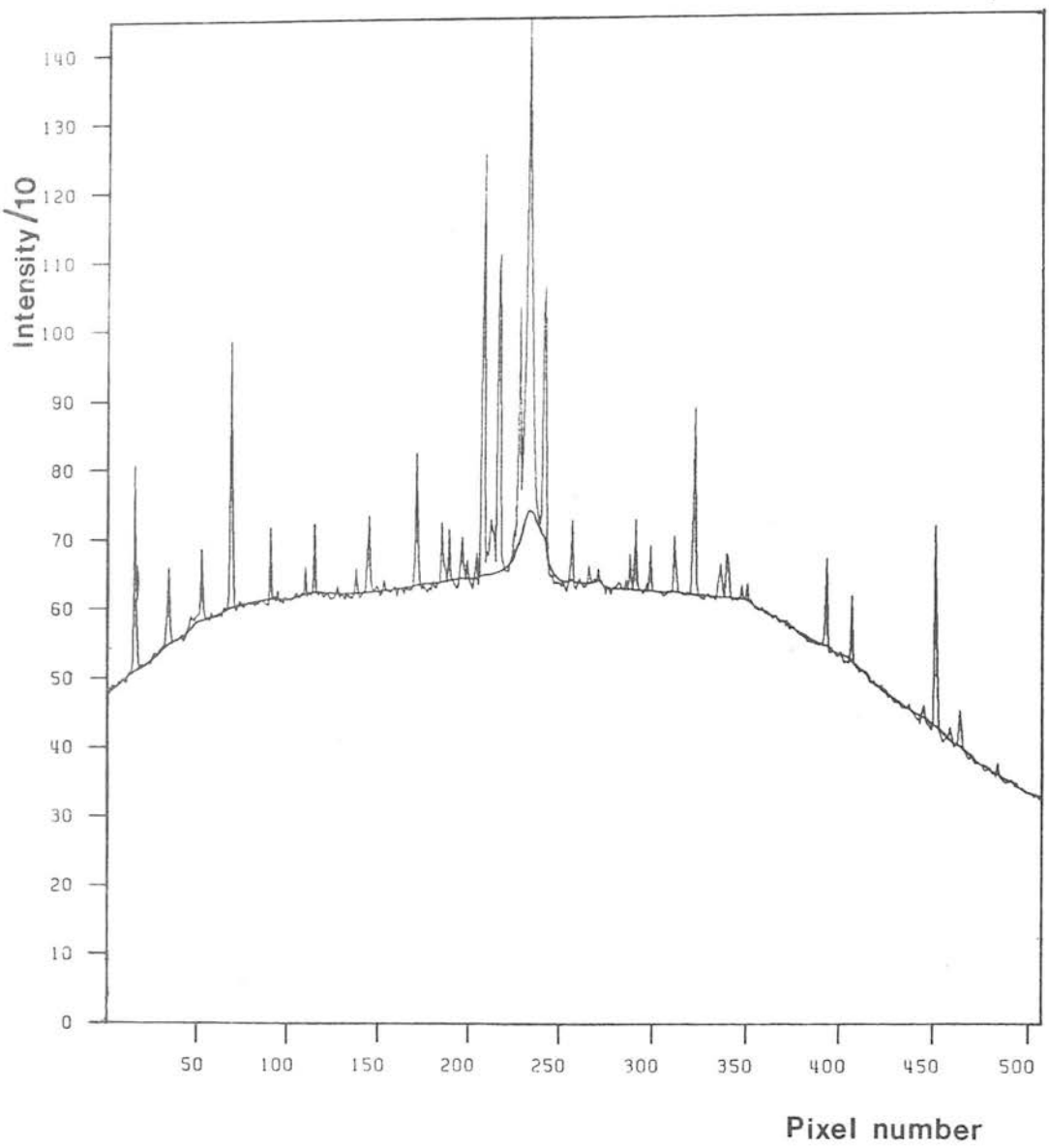

Figure 2.2. Slice taken across the doublet 'bullseye' profile. The effect of the flat-fielding represented by the smooth line can be seen to have eliminated all of the unwanted sharp features (i.e. the images) in the unflatfielded data (jagged line).

$$\sigma_{CG} = \sigma_I + 2.5\log_{10}\left(\frac{I_{sky}}{\beta}\right) \qquad (2.4)$$

where

$$\beta = (\epsilon\Omega)^2.10^{-6} \qquad (2.5)$$

ϵ is the pixel size used in microns and Ω is the plate scale in arcsec/mm. Since the two doublet measures were flat fielded there was no need to correct them for sky. For additive sky background variations due to e.g. chemical fog variations, low surface brightness nebulosity, division by local sky background is not the correct procedure to use. However since the COSMOS threshold level is set as a percentage above sky and will be incorrectly set when additive corrections are present, COSMOS cannot take these latter effects into account anyway, and so it must be assumed that they are negligible.

2.4 : AAT distortions

The spatial distortions introduced by using the doublet and triplet correctors are by no means negligible (Argue and Sullivan 1980) in so far that a simple linear translation, rotation and stretch method for the purpose of pairing the plates could not be used until these effects had been taken out of the data. The fact that the plates were not centred on exactly the same absolute point on the sky also contributed to this pairing problem, since the distortions are radial from the centre of the plate. They are also non-linear in the sense of turning a rectangular image into a pincushion shape (see figures 2.3a and b). Hence they can be considered as an increasing function of plate scale (i.e. fewer arcsec/mm) at larger distances from the centre of the plate.

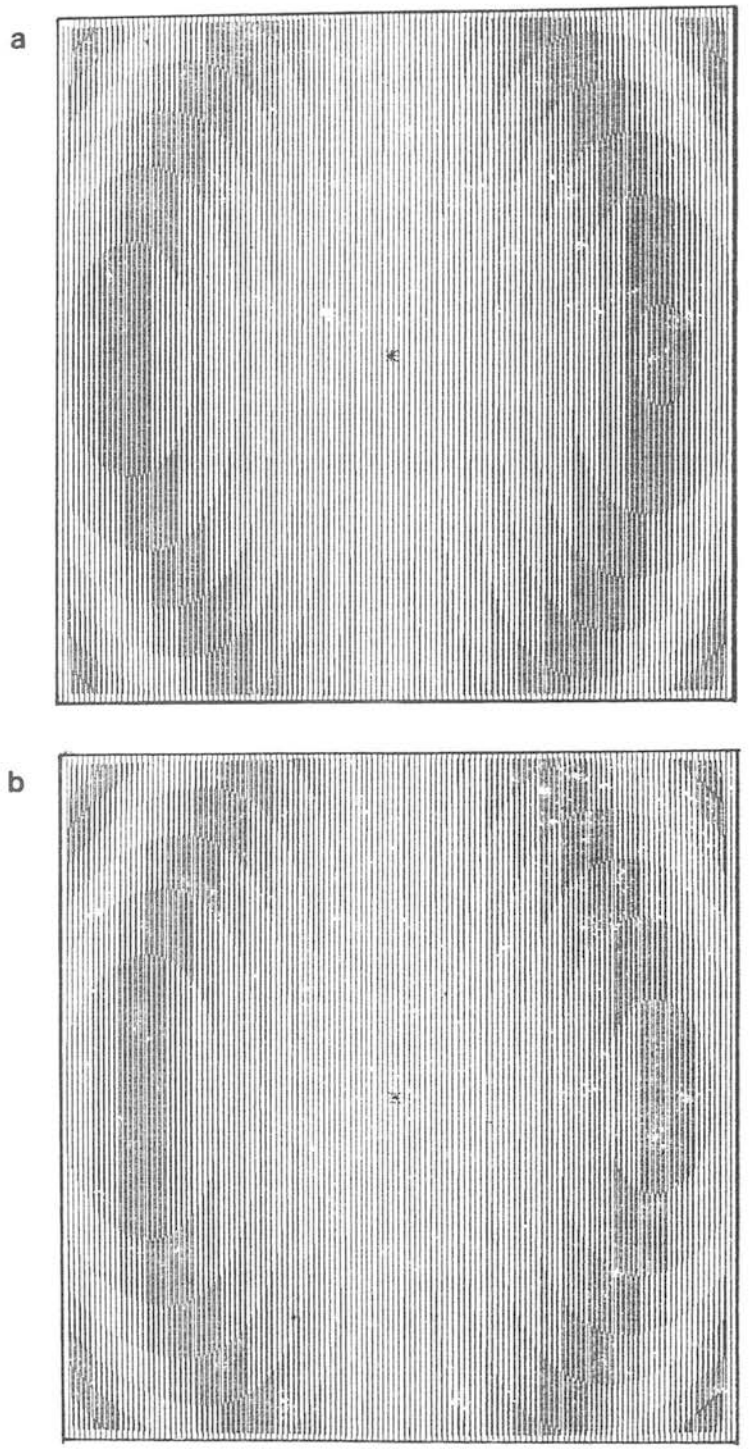

Figure 2.3a,b.Effect of (a) the doublet and (b) the triplet corrector distortions (shown as curved lines) on 128 vertical linear columns.

If (X,Y) is the coordinate of a star measured from the centre of the plate in units of one focal length, then table 2.2 gives the transformation required to eliminate these distortion effects where ϕ is the distortion coefficient found experimentally to be 147.069 for the doublet and 178.585 for the triplet corrector (Tritton, private communication). (ξ,η) are the undistorted coordinates. The left hand side expression for P is the usual one for pincushion distortion and that for Q on the right hand side is its approximate inverse, derived by using the first iteration in the Newton-Raphson method.

The COSMOS data as it stood could not be paired because of these effects and so a number of programs were written to take these distortions, as well as the difference in plate scales (16.24"/mm for the doublet and 15.3"/mm for the triplet plates) into account. The method finally adopted as most satisfactory was as follows:

(a) From each COSMOS IAM dataset, corresponding to each separate plate, the intensity weighted (x,y) coordinate of each image was transformed to coordinates having the centre of the plate (XC,YC) as origin. The zero point of the COSMOS coordinate system is not necessarily set to be the exact corner of the plate it is measuring. This means that in order to get the precise coordinates of the centre of the plate (where the distortions originate), the offset $(\Delta x,\Delta y)$ between the two coordinate systems had to be found. This was done by using a PACKMAN X-Y measuring machine, which measures the relative positions of a set of objects on a plate to a typical accuracy of 15μm in the following way. Ten unsaturated stars were separately centred (manually) in the PACKMAN view finder and the PACKMAN coordinates reset to the COSMOS coordinates of that particular star. The machine was then driven to the corner of the plate situated nearest to the COSMOS zero point and its coordinate noted. An average value of $(\Delta x,\Delta y)$ for a particular plate was found by averaging the values derived for the ten stars, with typically $1 \leq (\Delta x,\Delta y)/\text{mm} \leq 5$ (see table 2.3).

(b) These coordinates were then divided by the appropriate plate scale to generate 'focal length' coordinates and the formulae on the

TABLE 2.2

AAT DISTORTION TRANSFORMATIONS

$\xi, \eta \rightarrow X, Y$			$X, Y \rightarrow \xi, \eta$		
Define R^2	=	$\xi^2 + \eta^2$	R^2	=	$X^2 + Y^2$
Define P	=	$1 + \phi R^2$	Q	=	$\frac{(1 + 2\phi R^2)}{(1 + 3\phi R^2)}$
Then X	=	ξP	ξ	=	XQ
Y	=	ηP	η	=	YQ

TABLE 2.3

OFFSET OF COSMOS COORDINATE ORIGIN
FROM CORNER OF AAT PLATE IN MM

Name	Δx	Δy
B1386	2.79	3.14
B1510	3.78	4.18
B1530	4.05	3.43
V1387	3.33	3.33
V1511	3.16	2.84
V1529	2.10	2.53

right hand side of table 2.2 applied to take the distortions out. The plate scale differences were also taken out at this stage, with a choice of the data being put onto the doublet or triplet scale. Finally the coordinates were transformed back to those with the original corner of the plate (i.e. the one mentioned above in (a)) as origin.

(c) The (x,y) intensity weighted coordinates of the COSMOS images were then sorted into ascending x values and the data records rebinned into lanes of the original width and the resulting disc file spooled to tape. This sorting operation has to be performed since the procedure in (b) turns the previously linear lanes into 'curved' ones and hence the images of one of these latter lanes are members of at least one (and in fact as it turns out up to three at the edge of the AAT plate) new linear lanes (see figures 2.3a and b). Eliminating the distortions in the software of the pairing programs would have involved a lot more work than the method above.

Being in the standard COSMOS format, IAM data analysis software could then be used on the final (undistorted coordinate) data. Two of these programs worth mentioning at this point since they are used later in this thesis, are called 'IGJOB', which plots COSMOS images in the form of ellipses over a specified area using the unweighted semi-major/minor axes, orientation and (x,y) coordinate values, and 'DOTPLOT' which simply plots a dot for each image at the coordinate of its centre.

Once this distortion software had been applied to the six COSMOS measures, the data was in a form acceptable for input into the pairing programs.

2.5 : Pairing of plates

The pairing programs used here were modified versions of those written at the ROE by Hawkins (private communication). Two 'master' plates were chosen, one in B (B1386) and the other in V (V1387). These were the best plates, this being decided upon primarily by

their 'seeing' quality. For each master plate, all distances between each of the 40 brightest stars were calculated and compared with the corresponding distances on the plate it was to be paired with (the 'slave' plate). Since the areas on the sky of all of the plates were practically identical, this procedure worked well enough to work out an initial rough transformation (translation, rotation and stretch) using a least squares method. The whole procedure was then repeated using this transformation with the 250 to 300 brightest stars to obtain a better one. Images with a deviation from the mean transformation greater than 3σ were rejected, leaving typically 25 to 30 stars with a combined RMS of 16 microns. These final transformation parameters were obtained for all of the required combinations of plates.

Next, for each master image COSMOS recorded, a small area on the slave plate with which it was to be paired (typically a 150 μ^2 box centred on the transformed coordinates), was searched for images. Through a lengthy procedure of calculating the distances between the transformed position and each image in this box, the closest image appearing on the slave was paired with the corresponding master image. When all plates of one colour were paired successfully, the best plate of the two masters was chosen as a 'master-master' and the pairing procedure repeated to correlate the data in the two colour bands. A few points are mentioned here concerning the completeness of the sample of stars left after pairing thresholded COSMOS data (for further discussion see sub-section 3.3.1)

(a) although the plates were all thresholded at the same level, this does not mean that all the blended images in the data set from one plate will be blended in the other sets, simply because the sky background bases and seeing conditions will in general be different for each plate. Hence a 'limit of ellipticity' parameter (LIME) was inserted into the pairing programs. The quotient of the ellipticity of the master image and the slave image it was paired with was calculated and the maximum value of this and its reciprocal found. If this exceeded a certain value, then the master image was rendered unpaired. From visual comparisons of IGJOB ellipse plots of the

images COSMOS had detected with the corresponding photographic plate, a value of 2 for this parameter was found and consequently applied in all of the pairing procedures.

(b) Images with small areas ($\leq$20 pixels) were automatically rejected from the paired data by applying an areacut criterion (see section 3.3.1). In fact most of these images were found to have been rejected by the ellipticity requirement in (a).

(c) COSMOS will create spurious images from the 'outer haloes' of bright stars which will be eliminated from the data to some extent after the pairing has been performed. This however has the effect of leaving the area with an apparent net deficit of stars.

2.6 : Magnitude calibration of plates

The sequence used for the magnitude calibration of the photographic plates came from four sources;

(a) a photoelectric sequence from Cannon et al (1986)

(b) an electronographic sequence obtained by Hawkins (see Cannon et al 1986) using the 8cm McMullan electronographic camera on the Danish 1.5m reflector at La Silla.

(c) another electronographic sequence from the same material as that used in (b) was obtained, consisting of 14 stars centred on the region covered by the stars in (a) above. This was done to increase the reliability of the faint magnitude calibration (see section 2.7 for the reduction technique used).

(d) a CCD sequence taken from Mould and Aaronson (1983), enabling the calibration to go at least as faint as V = 21 magnitudes.

All the sequence stars were identified manually on IGJOB plots and their intensity weighted (x,y) coordinates stored in a disc file. The σ_{CG} and photoelectric magnitude of these stars were then written to

disc by matching up the (x,y) coordinates in this file with the images in the paired file. A 'best order' polynomial fit routine available on the ROE GEC 4090 computer was then applied to a linear plot of this data. This routine enabled polynomial fits of orders 1 to 9 to be successively applied to the data and the coefficients of the polynomial returning the smallest RMS over the whole of the photoelectric magnitude range output. The fit could then be examined by plotting it on a graphics display unit.

A typical calibration curve (in this case for AAT plate B1386) is shown in figure 2.4. Typically the order of fit used was 4th, higher order fits being returned by the fitting package when it was obvious that a sequence star had been misidentified or had been contaminated by other images (i.e. it had been blended). When these stars were rejected, smaller order fits resulted. The σ_{CG} of each of the faintest standards on each plate were noted and no calibration performed beyond them. The coefficients of the derived fits were then applied to the uncalibrated magnitudes of each image in the paired data (see table 2.4 for the RMS values for the fits).

2.7 : Electronographic calibration

Nine B and nine V long and short exposure electronographs (see table 2.5) were measured using the Royal Greenwich Observatory (RGO) PDS microdensitometer employing gaussian profile fitting routines specifically designed for electronographic work (Penny 1976).

2.7.1 : Method of measurement

An area approximately a quarter the size of a full electronograph (a single electronograph covers an area of about 25 arcmin^2) was chosen to be measured. A finding list, written to paper tape, and consisting of 963 COSMOS intensity weighted and AAT distortion corrected (x,y) coordinates for these objects was made from the COSMOS measure of AAT plate B1386. For each electronograph a transformation from COSMOS to PDS coordinates was calculated and a cathode correction map stored on the disc of the PDP 11 computer

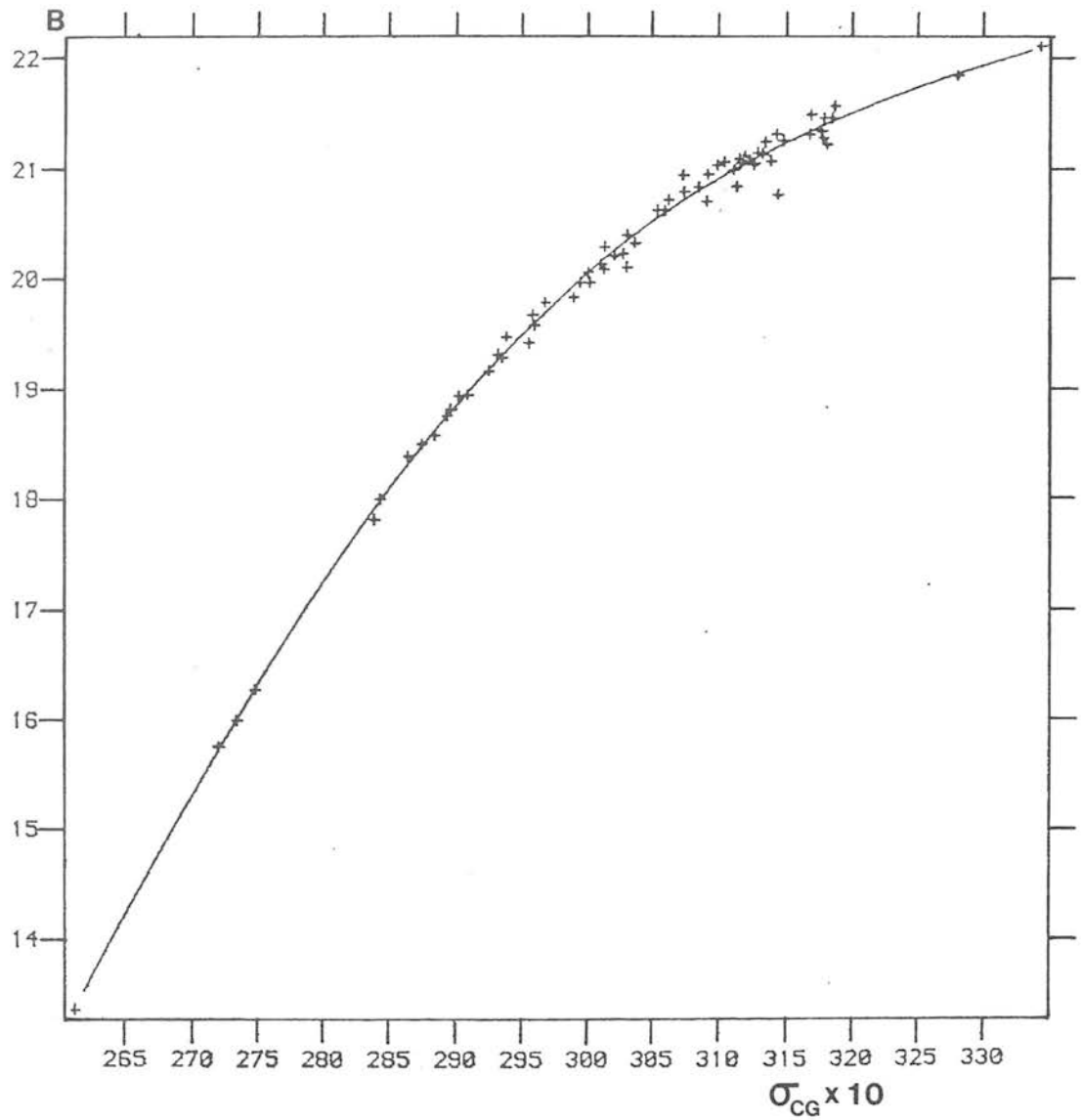

Figure 2.4. Calibration curve for AAT plate B1386. Thresholded COSMOS magnitude above sky (σ_{CG}) plotted against photoelectric B magnitude (B).

TABLE 2.4

ORDER AND RMS VALUES OF THE CALIBRATION CURVE POLYNOMIAL FIT DOWN TO B∿22, V∿21.3

	Plate identification					
	B1386	B1510	B1530	V1387	V1511	V1529
ORDER	4	4	4	4	4	4
RMS (mag)	0.17	0.15	0.10	0.10	0.08	0.13

TABLE 2.5

ELECTRONOGRAPHIC MATERIAL

Name	Colour	Exposure	Date	Emulsion/Filter	Zero point shift*
25.8.15	B	10 mins	22.11.79	L4/PL726	
25.8.16	V	10 mins	22.11.79	"	
25.8.17	B	3 mins	22.11.79	"	
25.8.18	V	3 mins	22.11.79	"	
25.3.1	B	15 mins	17.11.79	"	
25.3.2	V	15 mins	17.11.79	"	
25.2.4	B	75 mins	15.11.79	"	0.15
25.2.5	V	73 mins	15.11.79	"	-0.83
25.4.9	B	60 mins	18.11.79	"	-0.14
25.5.8	V	60 mins	18.11.79	"	-1.01
25.5.9	V	45 mins	19.11.79	G5/PG276	-0.14†
27.10.16	V	60 mins	29.10.81	G5/PL850	-1.46
27.10.17	B	60 mins	29.10.81	"	3.73†
28.1.8	B	60 mins	7.12.82	L4/PL865	-0.79
28.1.9	V	60 mins	7.12.82	"	-1.53
28.1.10	B	60 mins	7.12.82	"	-0.81
28.2.6	V	60 mins	8.12.82	"	-1.57
28.2.7	B	60 mins	8.12.82	"	-0.68

† Electronographs not used in reduction.

* This value has to be applied to the electronographic magnitudes to obtain the photoelectric magnitudes.

(which controls the PDS). This map was then subtracted from the data to correct for any inhomogeneities on the electronographic camera cathode detector surface. A 30x30 pixel raster was then performed on each object and the readings fitted by an iterative least squares procedure to a 2-dimensional gaussian profile of the form

$$D(x,y) = A \exp\left[-\left(\frac{x-x_o}{x^*}\right)^2\right] \exp\left[-\left(\frac{y-y_o}{y^*}\right)^2\right] + B \qquad (2.6)$$

where $D(x,y)$ was the density measured at the position (x,y), x^* and y^* were the X and Y gaussian radii of the profile, (x_o,y_o) was the profile's centroid coordinate, and A and B constants. Initial guesses for x^* and y^* (typically 3 to 5μ) were obtained by averaging the values obtained from three unsaturated images. These radii as well as the pixel size chosen (10 to 15μ here) were found to depend to a large extent upon the seeing conditions prevailing at the time of the electronographic observations.

By successive iterations, A,B,x_o,y_o,x^*,y^* were adjusted so that the sum of the squares of the residuals between the profile and the actual readings was made a minimum. The relative intensities of two images could then be found by comparing these profiles. The intensities were expressed in terms of the volume under the profile namely

$$V = \pi A x^* y^* \qquad (2.7)$$

where A was the height of the profile. This method effectively weights each pixel reading by its expected value so that a change in density near the centre of the image will result in a larger change in the fitted height than the base level, whilst the same change near the edge of the raster will produce the opposite effect. A small correction was applied for the aperture size (chosen to be 1/6 of the seeing disc) and for the slight non-linearity of the emulsion.

Typically these amounted to approximately 0.03 magnitudes for a bright ($<$ 16th magnitude) star. A listing of the (x_o, y_o) coordinate, height, fitted X and Y gaussian radii of the profile, cathode correction used and number of iterations taken to achieve the fit was then generated for each star in the area used.

2.7.2 : Calibration

The calibration technique used for these electronographic measures and the accuracy attainable has been described by Hawkins (1979, 1981). For each colour, a 3, 10 and 15 minute exposure was measured only for the purpose of tying down the bright end calibration of the long exposure measures. Three plots were then made:

(a) PDS 3 minute vs. PDS 10 minute exposure magnitudes

(b) PDS 3 minute exposure magnitudes vs. photoelectric magnitudes

(c) PDS 10 minute exposure magnitudes vs. photoelectric magnitudes

(a) and (b) were used to calculate the zero point of the 10 minute exposure measures, and this together with (c) was then used to get an error estimate on this measurement (typically better than $\pm$ 0.01). A similar procedure was used to get the zero point of the 15 minute exposure measures, this being the one used to calibrate the long exposure (45 to 60 minute) measurements. This was done by plotting the PDS magnitudes of 20 to 30 unsaturated stars with good gaussian fits (number of iterations $\leq$ 10) on both the 15 minute and long exposure electronographs against each other, and the zero point for the long exposure measure was worked out from this relation together with the 15 minute zero point value.

In the short exposure absolute calibration, the photoelectric standards in Cannon et al (1986) were used when at all possible i.e. when a good fit had been achieved and when the standard was not saturated (central height of the fitted profile $\leq$ 1000 units). Only

two of Hawkins' electronographic sequence (H15 and H18) for the fainter end of the 15 minute exposure were used. The zero point corrections used for the long exposure electronographs are listed in table 2.5. To get some idea of the error associated with the calibrated electronographic magnitudes derived above, these latter values were plotted against the original photoelectric magnitude for all of the available standards. One measure in each of B and V was found to be highly discrepant in the sense of deviating significantly from a 45^{o} slope. These were eliminated from the subsequent analysis (see figures 2.5a and b, and also table 2.5).

2.7.3 : Selection of electronographic standards

The criteria used for the inclusion of a mean electronographic (V,B) measure (derived from the remaining films) in the calibration sequence was that;

(i) The image had to be unsaturated on all of the electronographs to be used.

(ii) The derived magnitude (over all of the five electronographs used in each colour) had to have a RMS deviation better than 0.05.

(iii) The image had to have fitted X and Y gaussian radii comparable to the other stellar images on the electronograph, so that the galaxy contamination would be kept to a minimum in the sample. Of these stars, only five coincided with the stars from source (b) (see introduction to section 2.6), the comparision of three of these measures being shown in table 2.6. There was an unacceptable discrepancy between the H17 measures in both B and V, and the measure of F1 in V. H17 was later found to be misidentified in Cannon et al (1986), and so was rejected from the sample. F1 is possibly a variable (Cannon et al 1986) and so obviously cannot be used as a standard. The sequence stars used in the calibration of the AAT plates are identified in plates 2.1a and b, and their magnitudes in table 2.7.

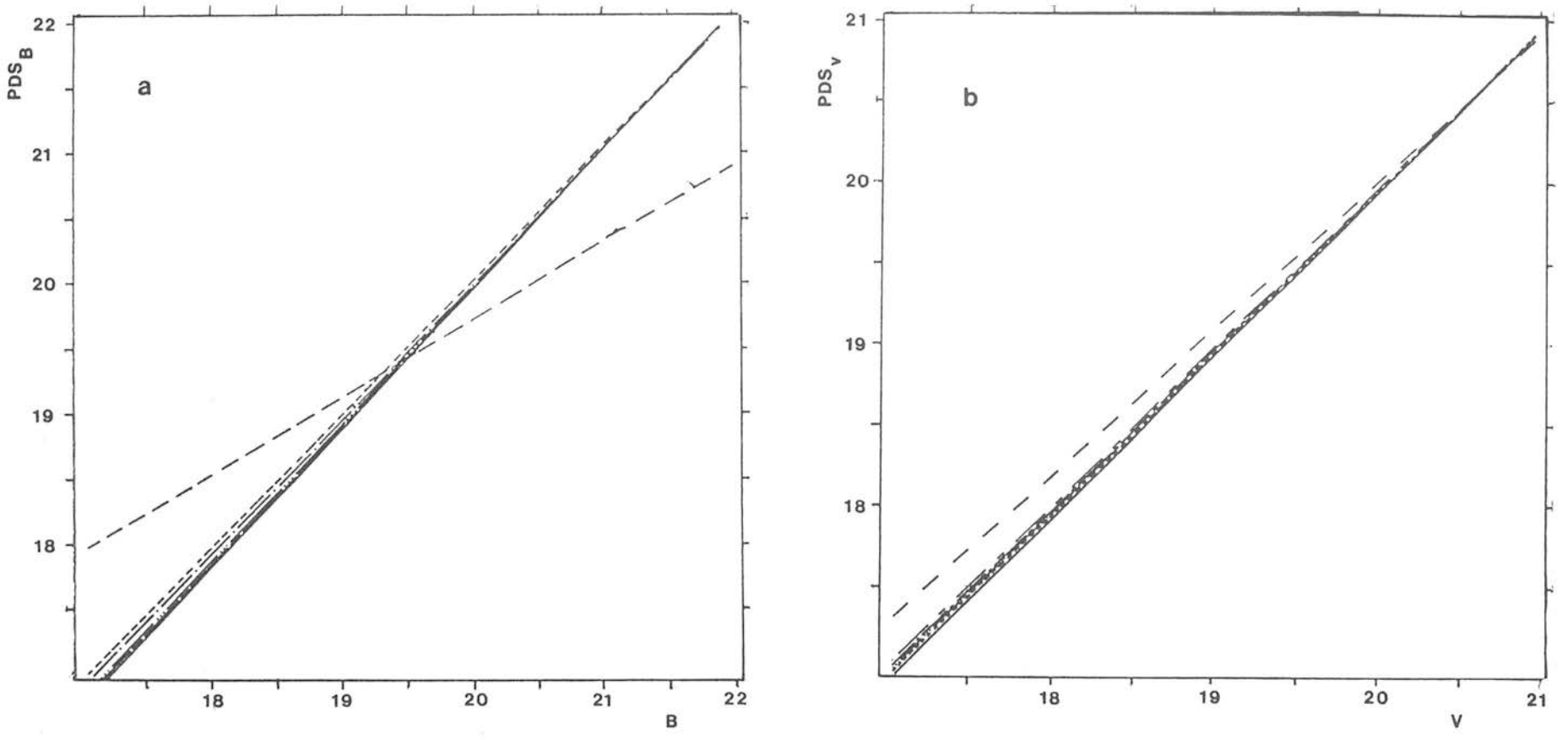

Figure 2.5a,b. The mean line fit to the calibrated electronographic magnitude for each standard star plotted against its photoelectric magnitude for each of the (a) B and (b) V long exposure electronographs. The two dashed (- - - -) lines represent the measures that were rejected from the sample.

TABLE 2.6

MAGNITUDES OF STARS COMMON TO SAMPLES
(b) and (c) (see text)

Cannon et al (1986) identification	PDS identification	V	B	(B-V)
H9		18.88	20.22	1.34
	92	18.86	20.22	1.36
H21		19.63	20.21	0.58
	114	19.54	20.28	0.74
H19		20.06	21.48	1.42
	167	19.99	21.56	1.57

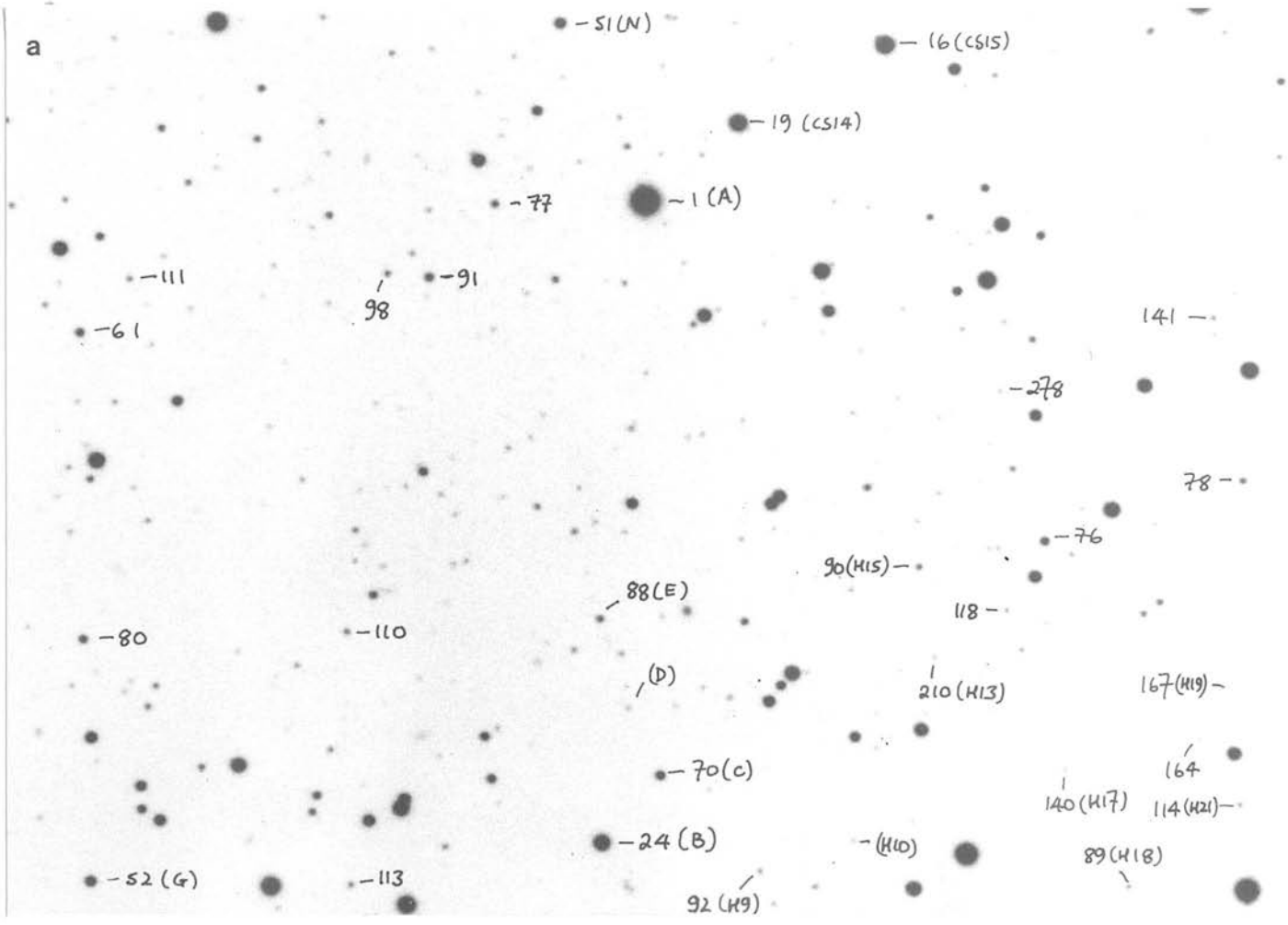

Plates 2.1a,b. Identification photograph for sequence stars used in the calibration. (a) Cannon et al (1986) sequence plus stars from sequence (c) - see section 2.6. (b) Mould and Aaronson (1983) sequence, (see Appendix A for relation of plates 2.1a and b to the central regions of the Carina dwarf).

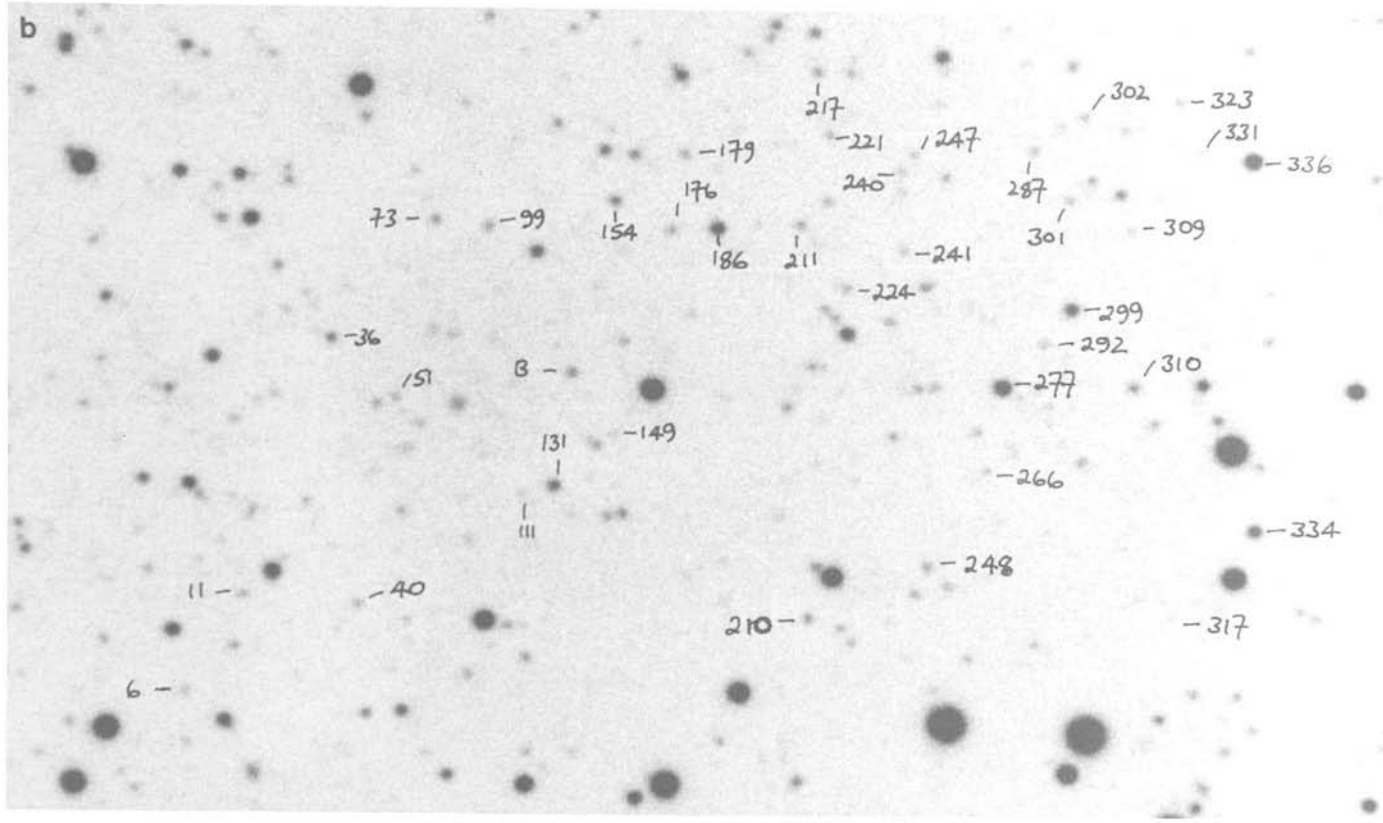

Plate 2.1b (cont.)

TABLE 2.7

STARS USED FOR MAGNITUDE CALIBRATION OF COSMOS MEASURES

Identification						V	B
(a)	(b)	(c)	(d)	(e)	(f)		
1	A	100	1	1		12.28	13.37
2	B	350	20	2		15.64	16.28
70	C	299	72	3		17.92	18.57
	D	298	316	4		20.01	21.24
88	E	295	106	5		18.74	19.67
52	G	371	58	8		17.35	17.82
51	N	22	56	9		17.27	18.00
19	CS14	32	17	10		15.21	16.00
16	CS15	41	13	11		15.08	15.76
92	H9	345	151	101		18.86	20.22
	H10	340	297	102		20.72	21.05
210	H13	317	262	103		20.30	21.04
90	H15	223	130	104		18.66	19.83
140	H17	321	276	105		19.40	20.84
89	H18	335	156	106		18.87	20.10
167	H19	326	369	107		19.99	21.56
114	H21	329	126	108		19.54	20.28
111			117	202		19.11	20.05
61			74	203		17.81	18.81
98			132	205		19.03	19.96
91			79	206		18.59	18.93
77			116	208		18.26	19.42
141			142	212		19.35	20.20
278			304	214		20.42	21.09
78			108	215		18.62	19.58
118			240	217		19.32	20.70
76			84	219		18.15	18.75
80			86	224		18.26	18.94
110			138	225		19.09	19.96
113			158	226		19.08	20.08
164			249	228		19.91	20.99

TABLE 2.7

(cont.)

Identification						V	B
(a)	(b)	(c)	(d)	(e)	(f)		
			125	301	6	20.55	21.34
			108	302	11	20.29	21.07
			69	305	40	20.48	21.06
			126	312	51	20.38	21.28
			41	313	36	19.18	20.12
			51	316	73	19.89	20.71
			30	320	131	18.36	19.78
			130	321	111	21.67	21.89
			157	322	149	20.89	21.83
			24	325	186	18.32	19.16
			71	326	176	20.27	21.03
			49	327	154	19.38	20.31
			93	328	179	20.41	21.11
			55	331	99	20.24	20.94
			57	332	210	19.80	20.62
			68	336	248	20.25	20.95
			119	337	266	20.53	21.31
			187	338	317	20.62	22.10
			29	340	334	18.29	19.31
			13	342	336	17.53	18.38
			132	343	331	20.79	21.93
			103	344	323	20.46	21.31
			44	346	310	19.52	20.39
			114	348	309	20.69	21.22
			99	349	301	20.49	21.13
			118	350	241	21.46	21.45
			23	351	299	18.53	19.28
			109	352	292	20.58	21.25
			12	353	277	17.70	18.49
			117	356	302	20.34	20.76
			98	359	287	20.54	21.14
			53	363	217	19.93	20.79

TABLE 2.7

(cont.)

Identification						V	B
(a)	(b)	(c)	(d)	(e)	(f)		
			121	364	247	20.71	21.45
			87	366	221	20.42	21.09
			111	367	240	21.21	21.48
			65	370	211	20.14	20.83
			73	371	224	20.41	21.05
			60	373	B	19.72	20.62

(a) PDS numbers

(b,c) Cannon et al (1986) numbers

(d) COSMOS numbers

(e) Thesis numbers

(f) Mould and Aaronson (1983) numbers

2.8 : Algorithms for magnitude determination

In this section the relative success of different procedures in calculating the magnitudes of the stars for which photoelectric and electronographic magnitudes were known is examined. COSMOS MM data of AAT plate B1386 (unflatfielded) was used as the raw data, centred on the photoelectric and electronographic region mentioned above. Standard STARLINK FORTRAN algorithms were used as magnitude estimators.

The astrometric (x,y) coordinates of each of the images used was determined by setting a cursor over each image contained in the MM data (displayed on an ARGS TV monitor) in turn. The marginal X and Y distributions for this central area and the image closest to the centre of the fitting area was located and a rectangular sub-area in which the image was located defined. The X and Y positions of the centre of this image were then determined by iteratively fitting gaussians to the X and Y marginal profiles within this sub-area.

(a) : GAUFIT ($^{\sigma}$GT)

The GAUFIT algorithm assumes that in the absence of saturation effects, all stars on a particular photographic plate regardless of magnitude can be represented by the gaussian density profile

$$d(r^2;\ D_o,s,B) = B + D_o \exp\left(\frac{-r^2}{2s^2}\right) \qquad (2.8)$$

where d(r) represents the model image profile on a hypothetical saturationless plate, s its one sigma width, r the radial distance from the image centre, B the background density and D_o the central density. It is further assumed that saturation effects act like a transformation from this model to an observed density profile of the form

$$D(r) = D(d(r)) = (d^{-q} + D_s^{-q})^{-\frac{1}{q}} \qquad (2.9)$$

(Stetson 1979a). This form has no direct physical meaning, but can be thought of as merely providing a numerically convenient form for computation; D_s is the saturation density and q is the saturation exponent, determining the shape of the profile as the image saturates. These last two parameters should be constant for a given plate and were calculated by applying equation 2.9 to three saturated images until a fit (with a low enough number of iterations) was achieved. For the data here, mean values of q = 10 and D_s = 1500 were taken. A magnitude index

$$\mu = k - 2.5\log_{10}(D_o s^2) \qquad (2.10)$$

could then be defined where k is an arbitary constant.

(b) : GAUMAG (σ_{GG})

This routine takes a small area around each star and fits a 2-D gaussian function (with background) to estimate its magnitude.

(c) : APERASP (σ_{AP})

Each image to be used from the test frame was displayed on the ARGS TV monitor and a circular cursor used (size chosen to be 50 pixels in this case, where one pixel = $16\mu^2$), to define the area containing the stellar image and a nearby region of sky. The summed intensities within these areas were then subtracted and a magnitude index calculated, normalised to the local sky background intensity.

(d) : STARFIT/MAG (STARPOW, σ_{SW})

The advantage of this procedure over the others is that it takes into account the ellipticity of an image due to e.g. trailing effects on the plate. Marginal profiles of each star image were formed in four directions inclined at 45^{o} intervals and a gaussian profile fitted to each to derive a mean centre and gaussian width, together with the axis ratio and inclination. The pixels surrounding the centre of each star were then binned into isophotal elliptical annuli (with the parameters defined above) and an average value found for each bin. A gaussian profile was then fitted to these mean values and the derived values normalised to those of the central value. These were then combined with the same data from all of the other stars to be used, giving an average radial profile with the image ellipticity removed. Finally,

$$D = A \exp\left[-\frac{1}{2}\left(\frac{R}{\sigma^*}\right)^{\gamma^*}\right] \qquad (2.11)$$

was fitted to this data, where A was the central amplitude of the star, giving the radial profile parameter γ^* and a final re-estimate of the seeing disk size σ^*. Each image was then fitted with the surface represented by equation 2.11 with a constant added to fit the sky background.

2.8.1 : Results

A linear least squares fit was applied to each of the magnitude data sets generated by the routines (a) to (d) above, and the RMS and gradient of the fits calculated. These are tabulated in table 2.8, and the fits are plotted in figures 2.6 a,b,c,d,e and f. The actual magnitudes calculated are shown in table 2.9. As would be expected, the gaussian fitting routines give the best linear relations although it is surprising how poorly the aperture photometer routine has fared; this could however have something to do with the sharply

TABLE 2.8

THE RMS AND GRADIENT OF A LINEAR LEAST SQUARES FIT BETWEEN THE CALCULATED LABELLED ROUTINE MAGNITUDE AND THE CORRESPONDING PHOTOELECTRIC/ELECTRONOGRAPHIC MAGNITUDE

Magnitude	Gradient and associated error	RMS (real magnitude)
σ_{GT}	1.05 ± 0.02	0.06
σ_{GG}	1.06 ± 0.02	0.07
σ_{SW}	1.01 ± 0.06	0.21
σ_{AL}	-3.94 ± 0.25	0.21
σ_{CG} + CONST	1.04 ± 0.03	0.10
σ_{AP}	-1.17 ± 0.05	0.13

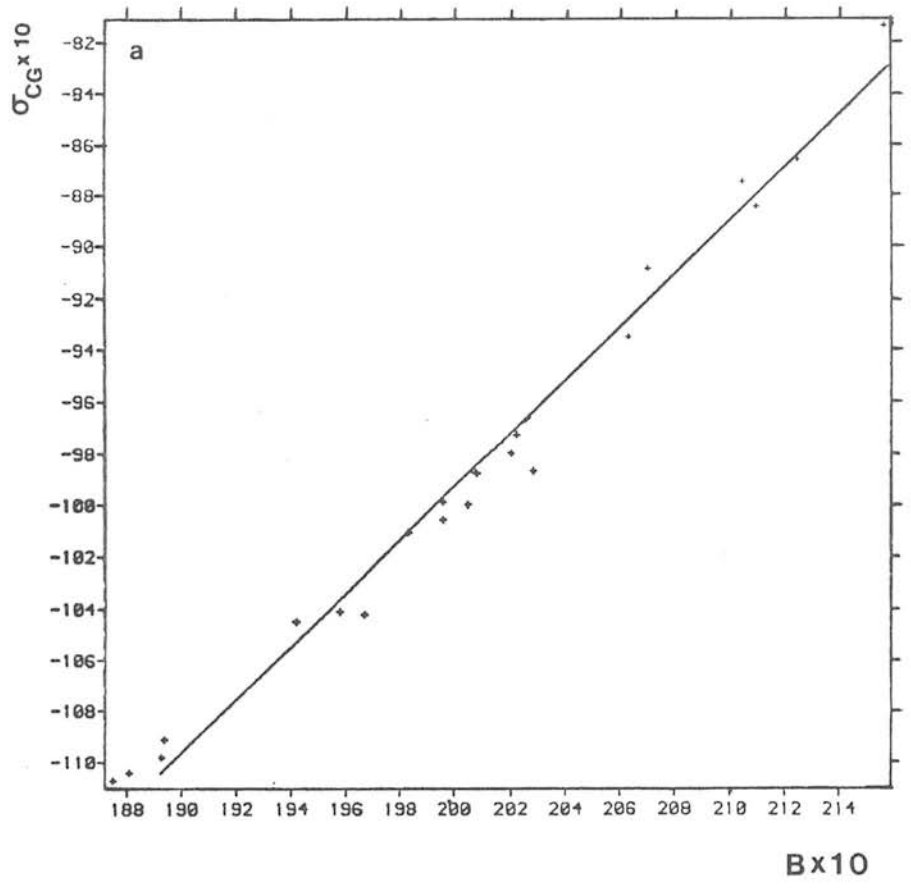

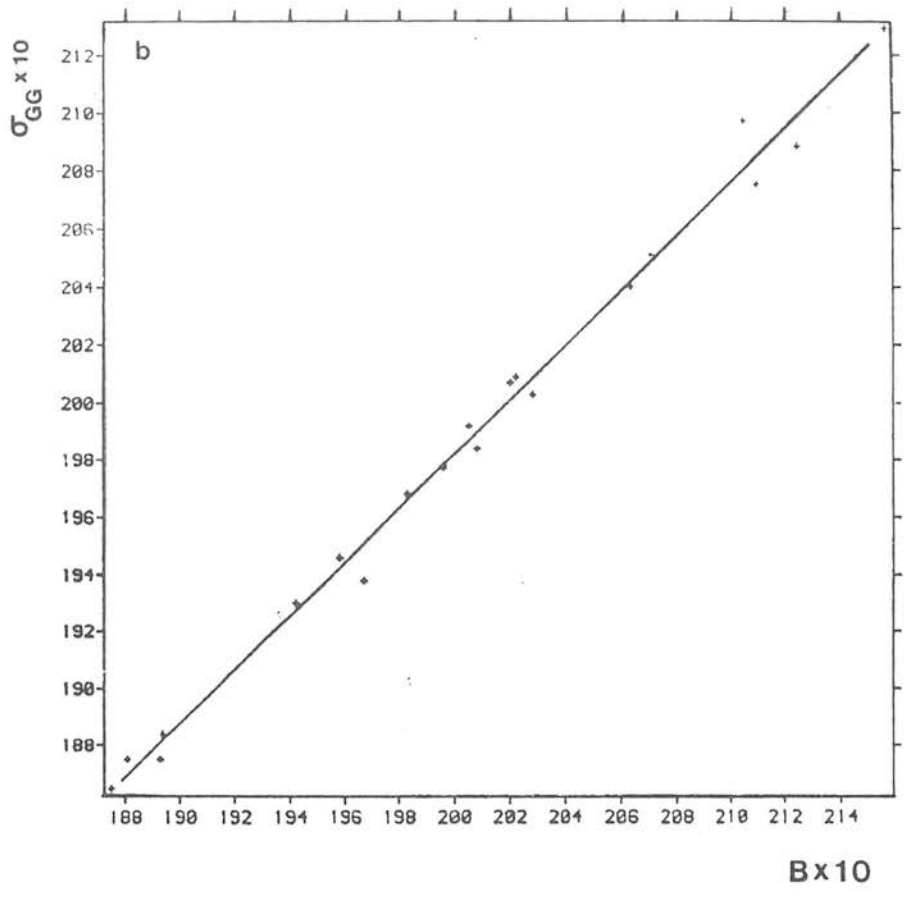

Figure 2.6a,b,c,d,e,f. Magnitude determinations using different algorithms plotted against assumed correct magnitude for each image. (a) σ_{CG}, (b) GAUMAG, (c) σ_{AL}, (d) STARPOW, (e) GAUFIT, (f) APERASP.

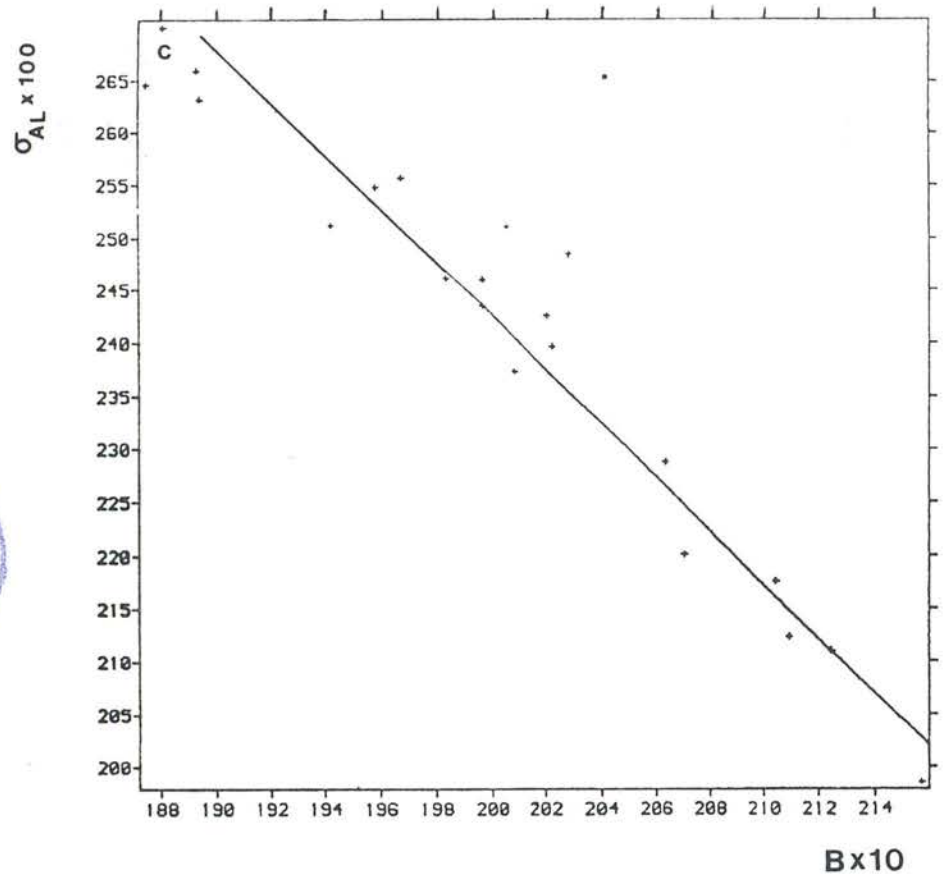

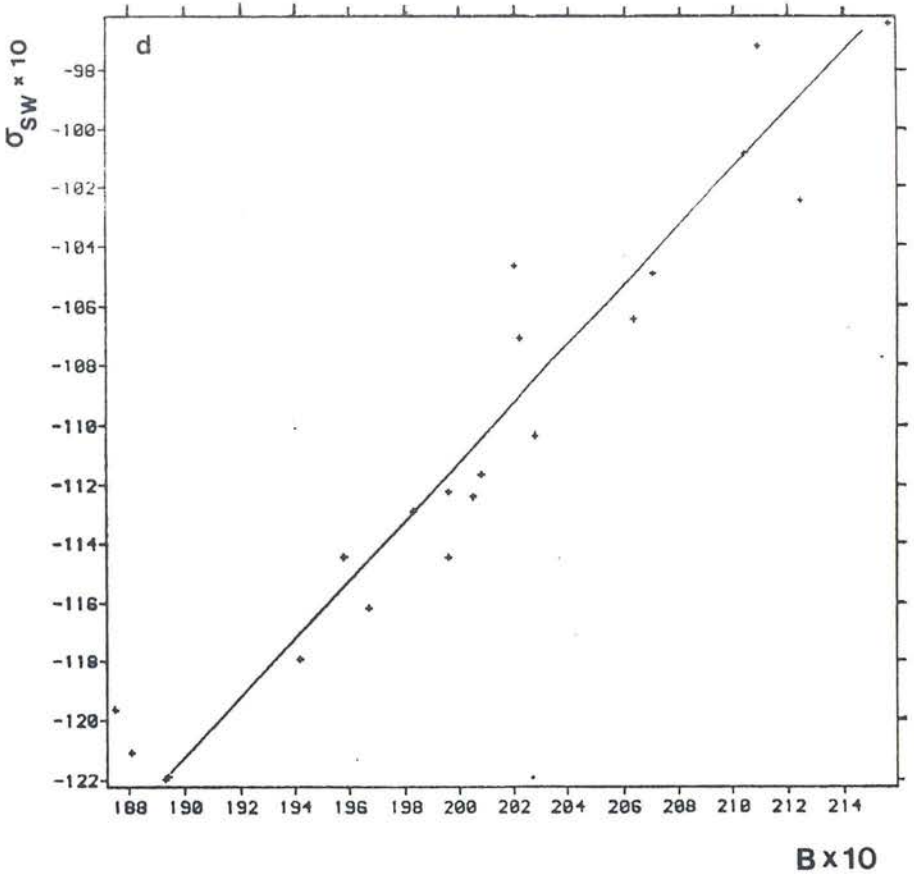

Figure 2.6 (cont.)

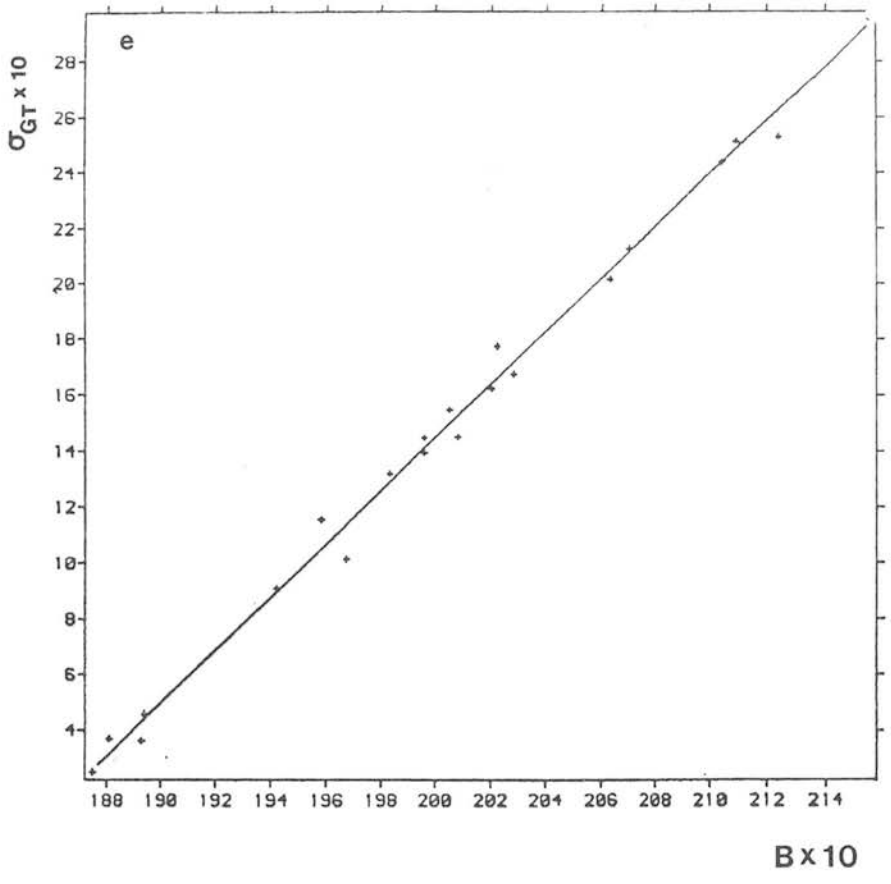

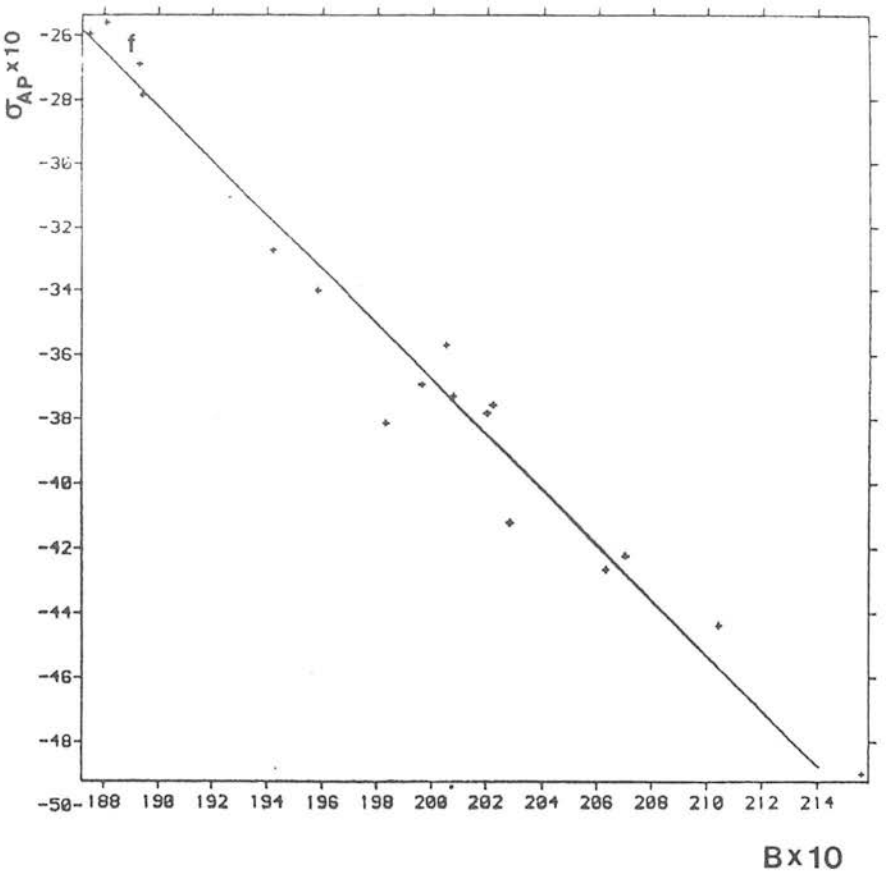

Figure 2.6 (cont.)

TABLE 2.9

MAGNITUDES OF STANDARDS DERIVED

BY DIFFERENT METHODS

Identification*			B	σ_{GF}	σ_{GG}	σ_{SW}	σ_{AA}†	σ_{CG}+CONST	σ_{AP}
(b)	(e)	(a)							
D	4		21.24	2.526	20.88	-10.250	129	- 866	-3.351
E	5	88	19.67	1.014	19.38	-11.615	360	-1042	-3.351
H9	101	92	20.22	1.771	20.09	-10.710	249	- 973	-3.756
H13	103	210	21.04	2.437	20.97	-10.087	150	- 875	-4.437
H15	104	90	19.83	1.318	19.68	-11.290	289	-1011	-3.812
H19	107	167	21.56	2.948	21.29	- 9.643	97	- 814	-4.900
H21	108	114	20.28	1.672	20.03	-11.036	305	- 987	-4.120
	202	111	20.05	1.545	19.92	-11.240	324	-1000	-3.570
	203	61	18.81	0.372	18.75	-12.106	501	-1104	-2.561
	205	98	19.96	1.393	19.77	-11.446	288	-1006	-3.691
	206	91	18.93	0.366	18.75	-12.195	456	-1098	-2.689
	208	77	19.42	0.910	19.30	-11.792	325	-1045	-3.272
	212	141	20.20	1.621	20.07	-10.469	266	- 980	-3.780
	214	278	21.09	2.510	20.75	- 9.722	133	- 885	-5.586
	215	78	19.58	1.154	19.46	-11.445	353	-1041	-3.400
	217	118	20.70	2.125	20.51	-10.494	159	- 909	-4.222
	219	76	18.75	0.254	18.65	-11.963	442	-1107	-2.596
	224	80	18.94	0.459	18.84	-12.185	428	-1091	-2.785
	225	110	19.96	1.446	19.78	-11.223	272	- 999	-3.692
	226	113	20.08	1.449	19.84	-11.165	236	- 988	-3.728

* identification labels as in Table 2.7.

† $\sigma_{AL} = \log_{10}(\sigma_{AA})$.

sloping sky background due to the presence of the dsph galaxy (the raw MM data was unflatfielded). The IAM area in the form $\sigma_{AL} = \log_{10}$ (area of image) has in the past been used as a magnitude estimator (e.g. see Bruck and Hawkins 1983), but it can clearly be seen that the σ_{CG} parameter is the best COSMOS magnitude parameter to use. The systematic dimming of the IAM magnitudes found for the faint stars is caused by the fraction of the light emitted below the intensity threshold becoming an increasingly important fraction of the total light from the star. Hence in the calibration procedure adopted for this parameter, a polynomial fit is applied only over the magnitude range that the standards cover.

2.9 : Field effects

The calibration sequence used, only covers two small areas of the region it is wished to perform photometry over. Hence care must be exercised in extrapolating any calculated magnitude calibration from these areas to larger areas of the plate. A number of FORTRAN programs were written to see to what degree field effects were present in the data, and the following plots were made

(a) In order to look at magnitude shifts, each plate measure of (x,y) coordinates was binned into 5x6 boxes ($\sim 3cm^2$ each on a plate - see figures 2.7 a,b,c,d,e and f) and for each bin a mean magnitude residual value was assigned namely

$$MR = \sqrt{\frac{\left|\sum_{box} (m_{ji} - \mu_{ji})\right|}{N_{box}}} \qquad (2.12)$$

where

$$\mu_{ji} = \frac{\sum_{k=1}^{3} m_{jk}}{3} \qquad (2.13)$$

j refers to either the B or the V magnitude, i is the label for a

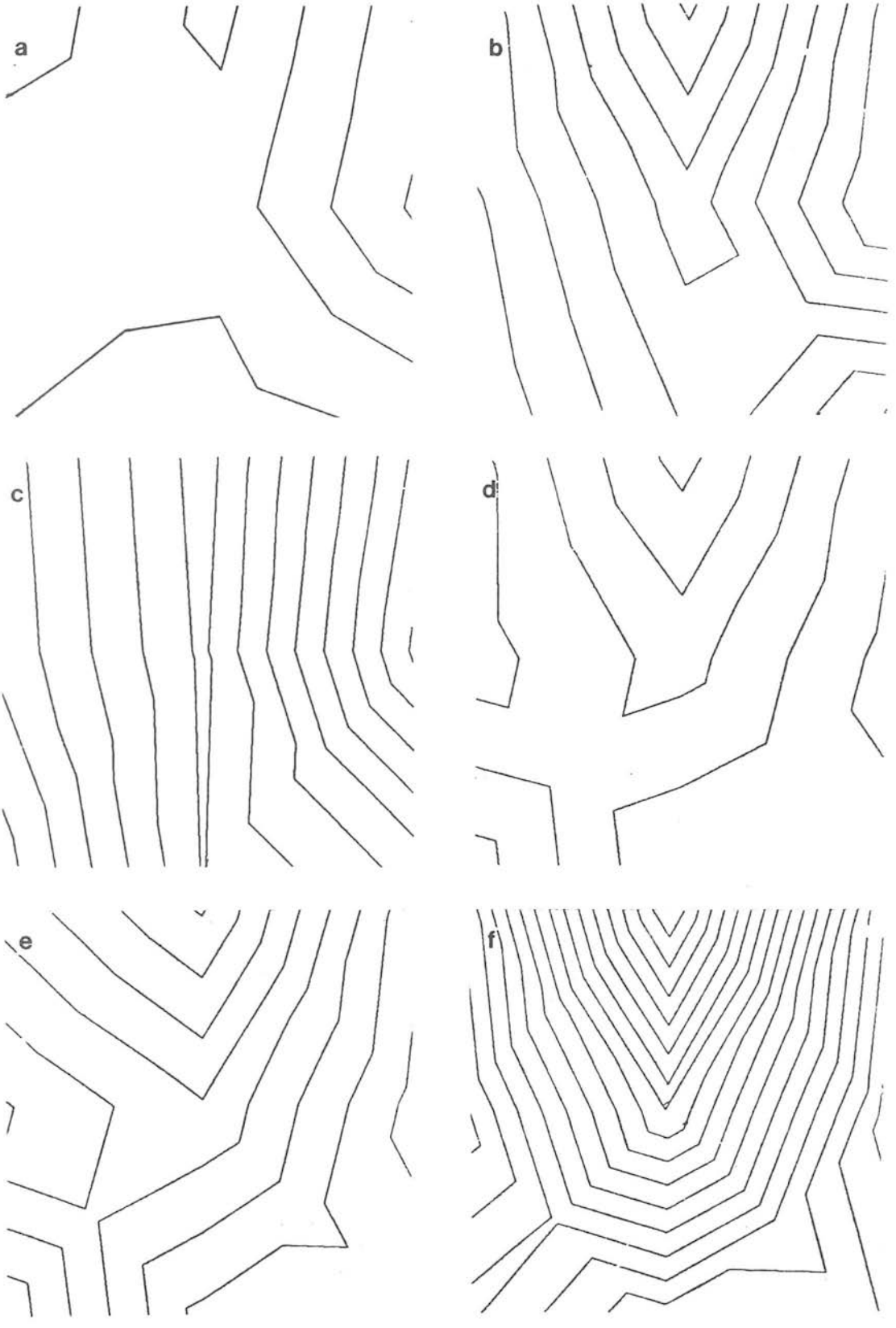

Figure 2.7. Field effects across the whole of each AAT plate (~1 square degree). Each contour corresponds to a change in the MR value of 0.03 magnitudes (a) V1387, (b) B1511, (c) V1529, (d) B1386, (e) B1510 and (f) B1530. (Only the central 0.16 degree^2 area was used in subsequent work).

particular plate of one colour, and so μ_{ji} is the mean magnitude of the image over the three plates of one colour. m_{jk} is the magnitude of the image under consideration and N_{box} is the number of images in the box. The MR values were then contoured. If it is assumed that μ_{ji} is the correct magnitude for the image, then MR should be zero for each box provided only random errors are present i.e. all the errors from the COSMOS and standard magnitude derivations in this case cancel out. From figure 2.7 however, it can be seen that these values are not zero nor constant over the plate.

(b) For each plate and each box, the MR of equation 2.12 was calculated per magnitude bin and histogrammed against that magnitude (see figure 2.8). There is no systematic shift of this MR with magnitude at the bright end although it can be clearly seen from this figure that this is not the case below $B \sim 21$.

(c) For each plate and each image in every box μ_{ji} was plotted against $\Delta = \mu_{ji} - m_{ji}$ (see figure 2.9). Again in the central regions the scatter is random about $\Delta = 0$ for $B \leq 21$ when the uncertainty in the calibration makes the value of Δ increasingly large.

(d) For the importance of colour effects, for each image in every box and plate, $\mu_{Bi} - \mu_{Vi}$ was plotted against $(\mu_{Bi} - \mu_{Vi}) - (m_{B1} - m_{V1})$ where these last two values refer to the magnitudes derived from the B1386 and V1387 measures respectively i.e. it is assumed that these plates give the correct colour. As in (b) and (c) no systematic effects over the calibration colour range (see below and figure 2.11) in the inner regions were found (see figure 2.10).

(e) IGJOB plots were also made to check that there were no systematic shifts of image density across a plate (apart from that towards the centre of the CDG !).

The number-colour diagram for all of the standards used is plotted in figure 2.11 and shows that good calibration should be able to be done at least over the range $0.2 \leq (B-V) \leq 1.4$. Each of the plots considered in this section gives confidence in extrapolating

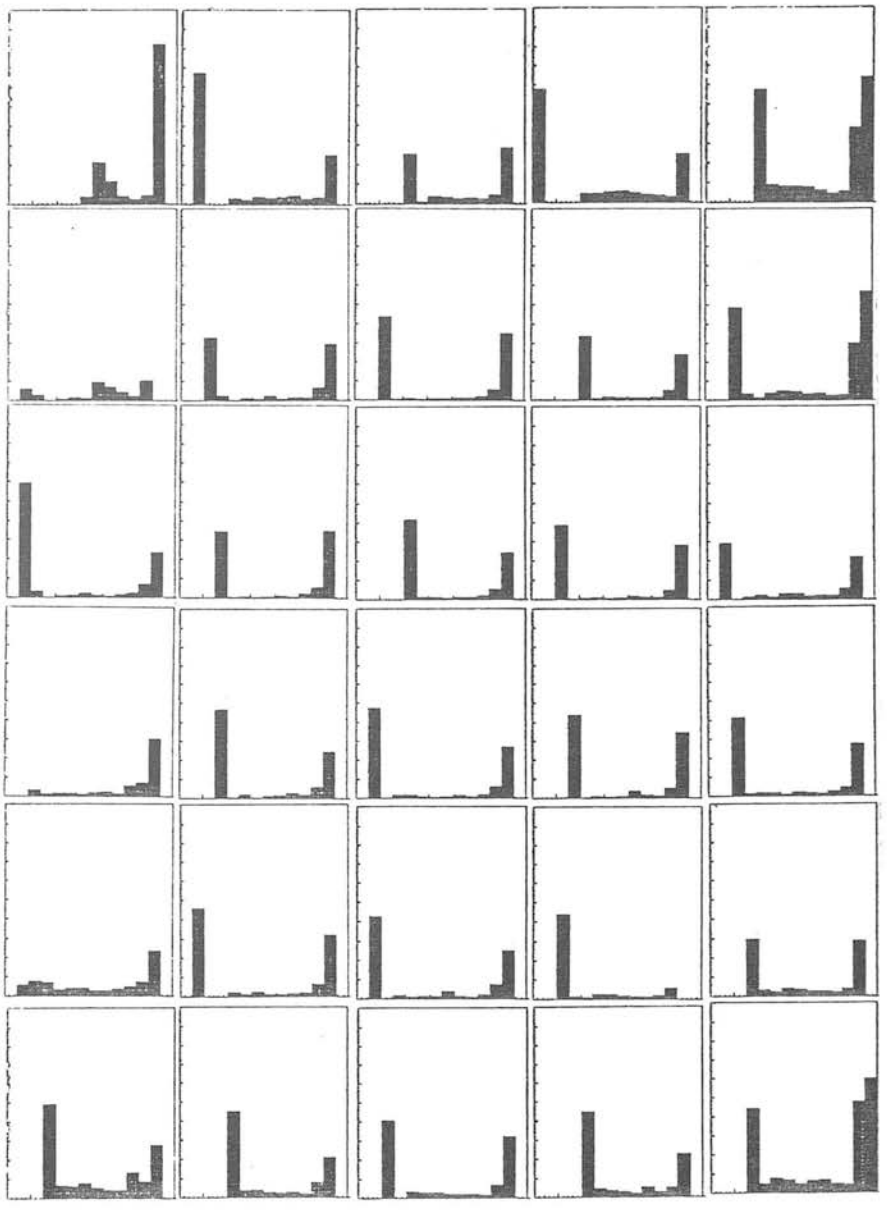

Figure 2.8. MR value per magnitude bin plotted against that magnitude (plate B1386 shown). In each small plot, x axis: start at 10th magnitude, large tick interval is 2 magnitudes. y axis: start at 0 MR, large tick interval is 0.5 magnitudes.

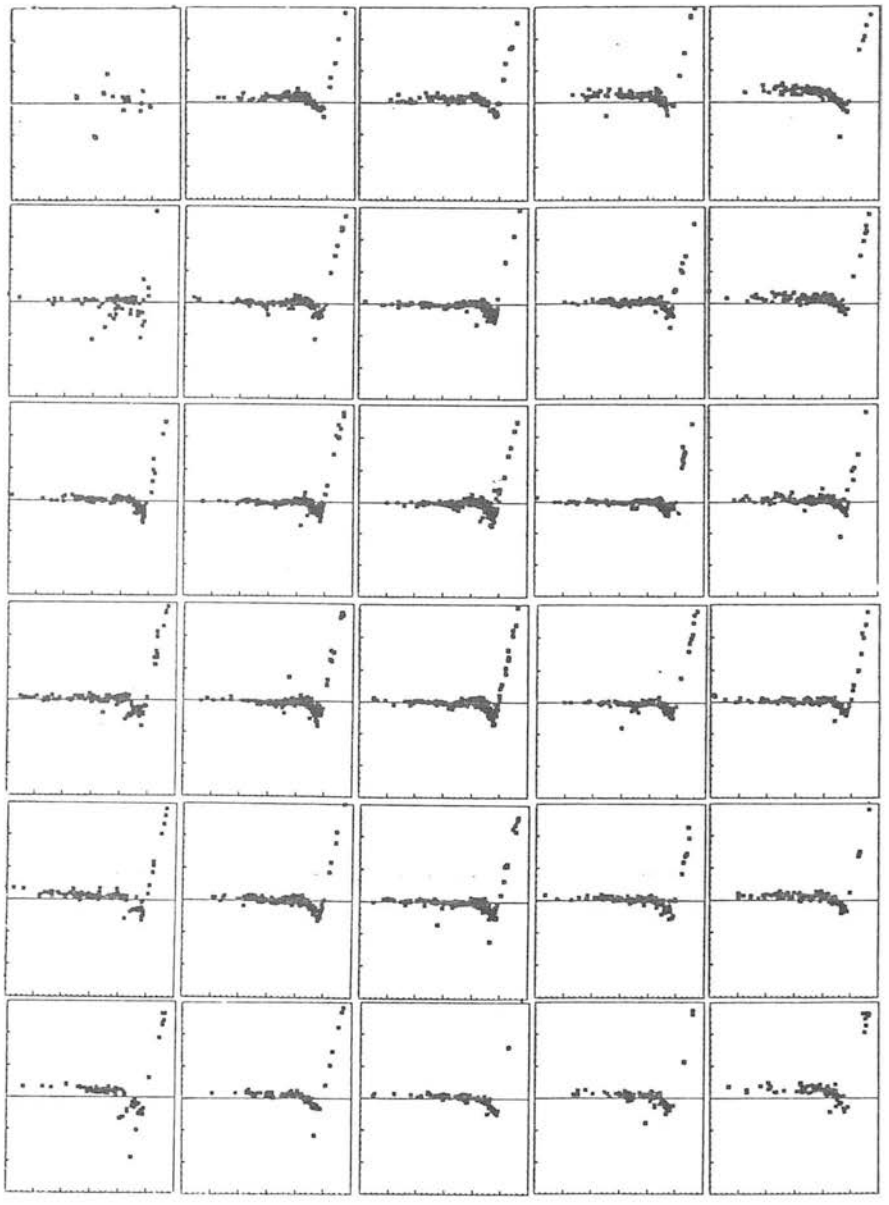

Figure 2.9. Residual ($\Delta = \mu_{ji} - m_{ji}$) versus mean magnitude (μ_{ji}) for each image in each bin. For each small plot, x axis: start at 12th magnitude, large tick interval is 2 magnitudes. y axis: horizontal line represents zero residual, large tick interval is 0.1 magnitudes. Measurements are from plate B1386.

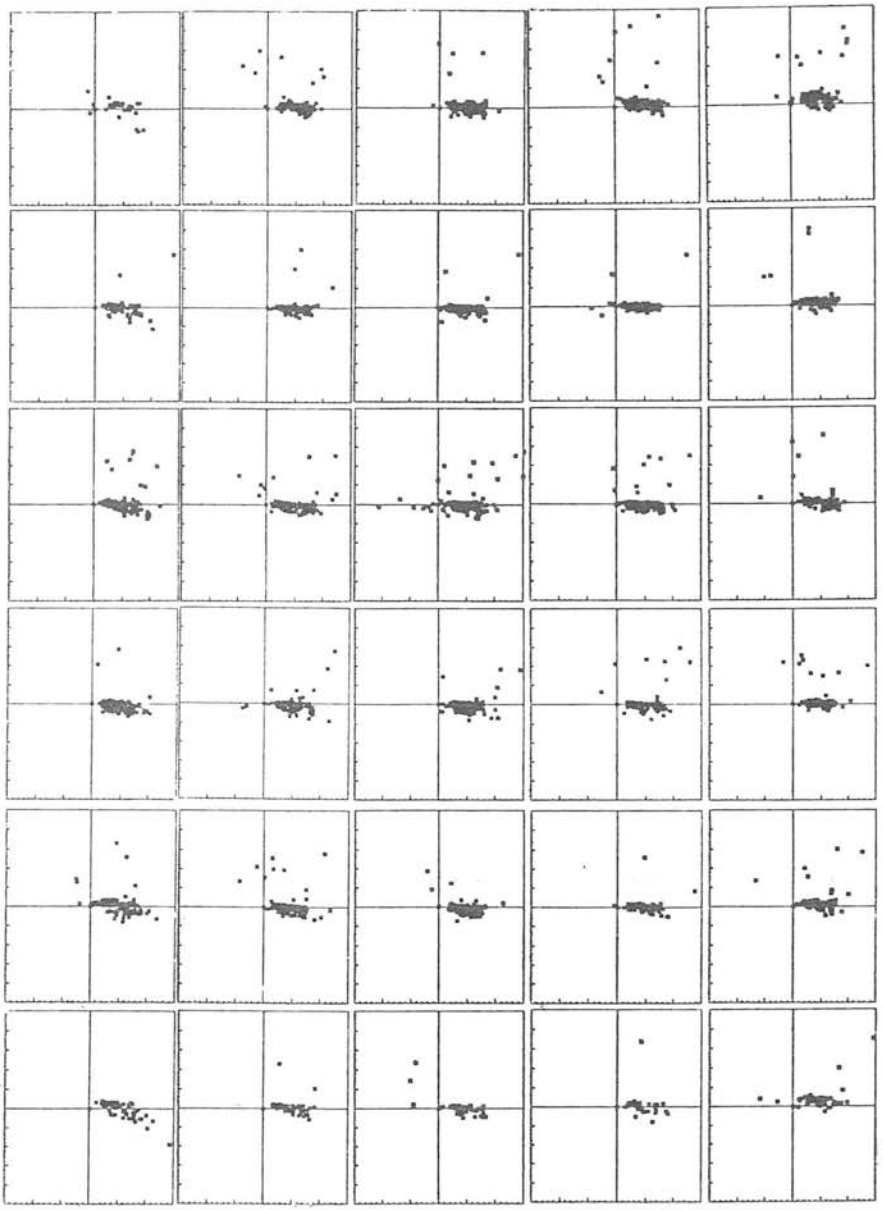

Figure 2.10. Mean colour derived from the six plates (x axis) as a function of the difference between this and the colour derived from the two master plates (y axis). Intersection of central vertical and horizontal lines in each small plot represents the origin (0,0). In each small plot, x axis: large tick interval is equal to B - V=1, y axis: large tick interval is 0.1 magnitudes.

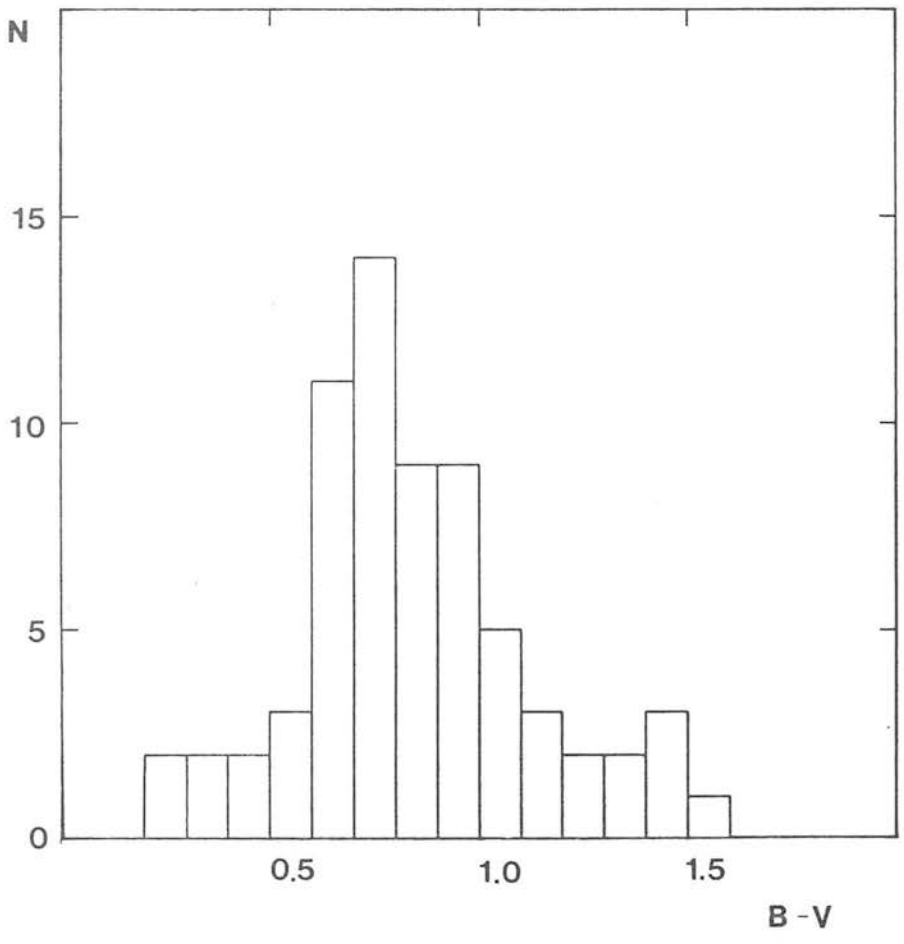

Figure 2.11. Number - colour relation for magnitude standard stars.

the area over which photometry can be performed to a central area of the CDG which was chosen to be $\sim$10x8 cm^2 on the AAT plate, corresponding to about 0.16 $degrees^2$ (see appendix A for finder photograph).

2.10 : Calibration results

Figures 2.12a and b show the standard deviation of the magnitude of each image (calculated over three plates) as a function of its mean magnitude for all of the B and V plates respectively (the data has been binned into one magnitude bins). Figure 2.12c is the same plot for the colour of each image with a (B-V) = 0.1 magnitude bin size. This data gives a measure of the internal errors of the COSMOS data to be $\sim$0.08 or better for both σ(B) (down to B 21.2) and σ(V) (down to V$\sim$20.5) and to be $\sim$0.10 for σ(B-V) (if $0.5 \leq B-V \leq 1.5$).

An estimate of the random external error on the derived magnitudes can be determined by plotting the residuals (calibrated magnitude minus standard photoelectric magnitude) against the photoelectric magnitude of the standard as done in figure 2.13 (it will be assumed in what follows that there are no systematic errors in the photoelectric magnitudes). From this figure down to V$\sim$20.5 and B$\sim$21.2, σ(V)$\sim$0.08, σ(B)$\sim$0.08 and hence σ(B-V)$\sim$0.11 i.e. practically the same as the internal error down to the same magnitude limits adopted, and hence the effect of the random external error on the magnitudes can be taken to be negligible to these limits (if these latter calculated values were significantly different from the internal errors calculated above then the random external error would be important, but it is not). A finder chart and listing of V, B and relative (x,y) coordinates of the stars used is shown in appendix A, and the derived CDG COSMOS giant branch colour magnitude diagram down to V = 21, is shown in figure 3.1a.

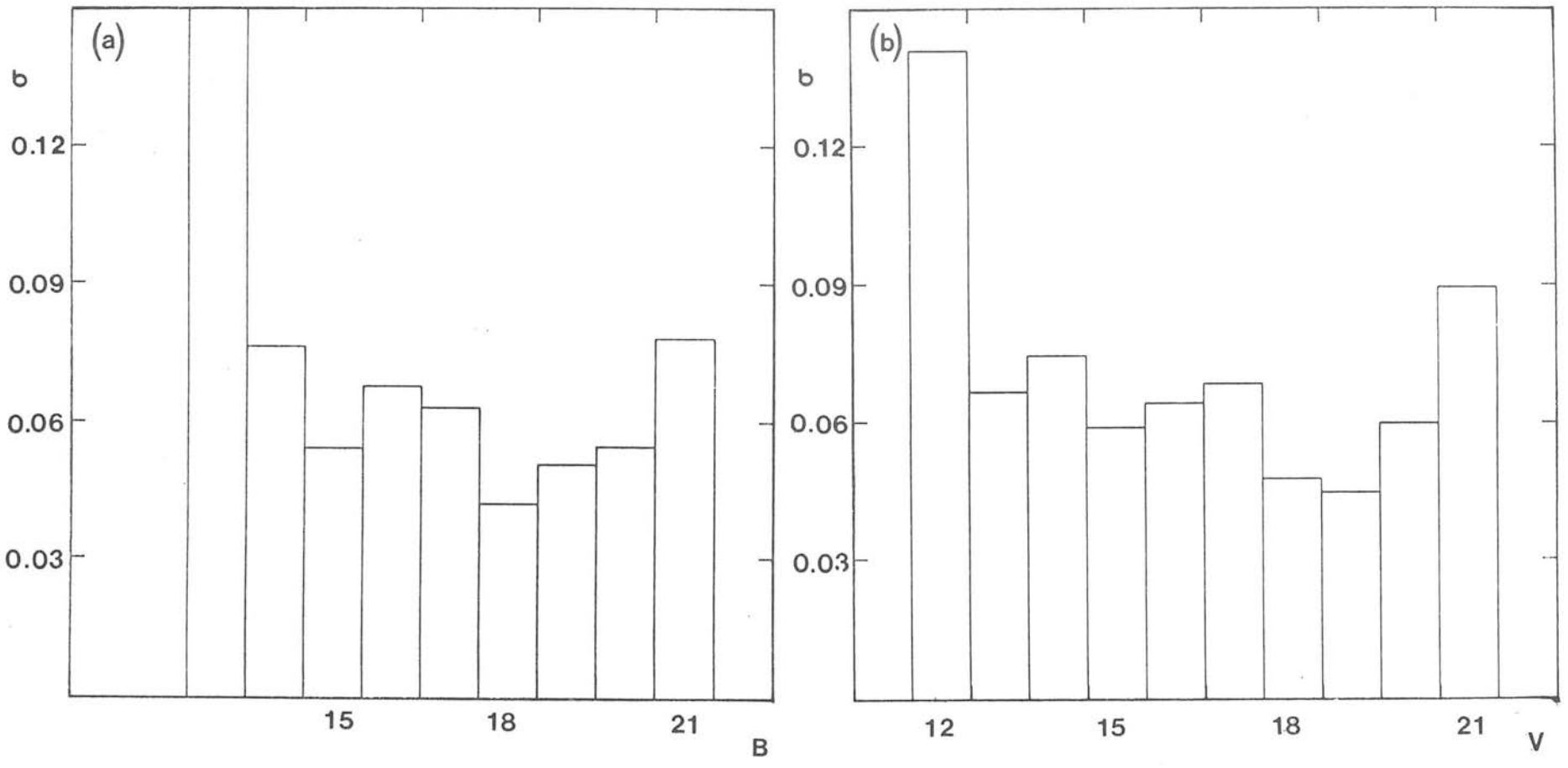

Figure 2.12a,b. The standard deviation of the magnitude of each image (calculated over three plates) as a function of its mean magnitude for all of the (a) B and (b) V photographic plates respectively (the data has been binned into one magnitude bins).

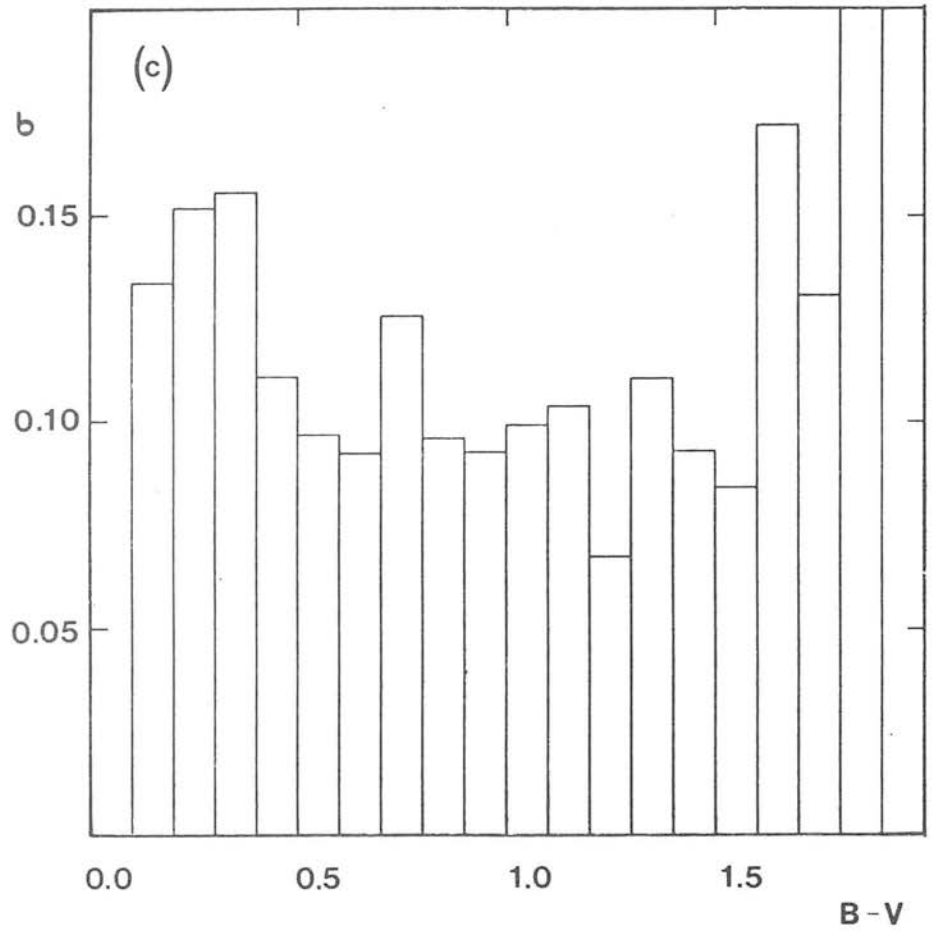

Figure 2.12c. Same plot as for figures 2.12a and b except it has been done for the colour of each image, with a (B-V)=0.1 magnitude bin size.

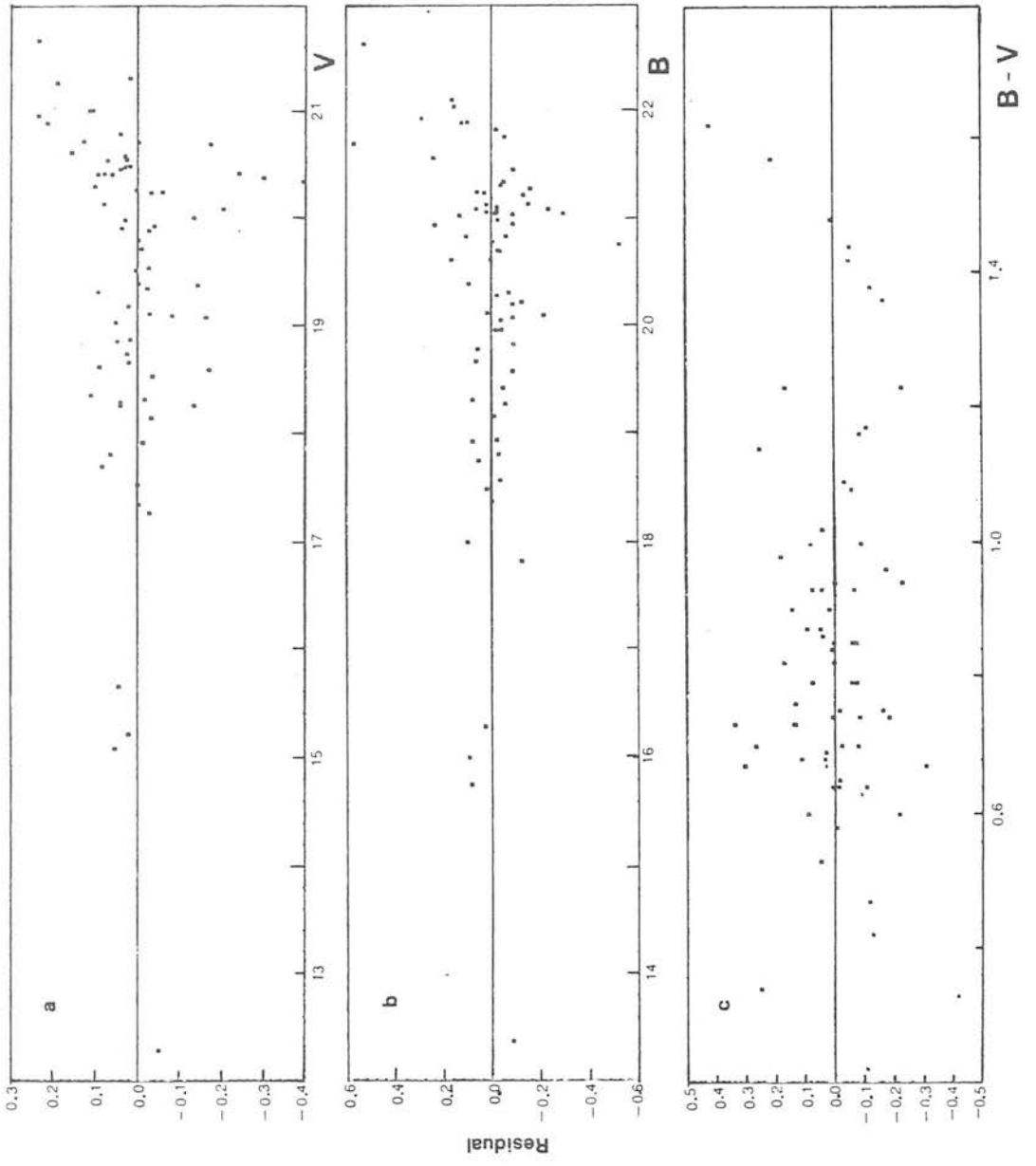

Figure 2.13a,b,c. Standard star magnitude residuals in (a) V, (b) B and (c) B-V.

2.11 : SUMMARY AND CONCLUSIONS

COSMOS has been found to be fully capable of providing accurate magnitudes over a large (spatial) region of the CDG. The problem of AAT distortions in the data have been eliminated, and the COSMOS data duly paired. Electronographic measurements and the CCD data of Mould and Aaronson (1983) have allowed an extension of the Cannon et al (1986) sequence to fainter magnitudes, thus tying down the faint end calibration to about $B \sim 21$. An area over which field effects are not too serious and over which COSMOS has an internal accuracy better than 0.08 magnitudes down to the horizontal branch level $\sim$ 20.5 (see chapter 3) in V has been used to derive a colour magnitude diagram. This diagram will be discussed in an astrophysical context in the next chapter.

Chapter 3 THE COLOUR MAGNITUDE DIAGRAM

3.1 : Introduction

The interpretation of any stellar system's colour magnitude diagram morphology requires an understanding of stellar evolutionary processes and their consequences. A brief outline is given here of present stellar evolutionary ideas in relation to their effects in this diagram, and results derived from the CDG colour magnitude diagram derived in chapter 2 and presented in figure 3.1a are discussed in the light of them.

3.2 : Stellar evolution and the Hertzsprung-Russell diagram

Theoretical calculations of stellar evolutionary processes in clusters involve predictions in the $(\log(T_{eff}),\log(L/L_{\odot}))$ plane, which will be referred to here as the Hertzsprung-Russell (HR) diagram. T_{eff} is the effective temperature of the stellar atmosphere, and $L/L_{\odot}$ is the star's luminosity expressed as a ratio to that of the Sun's. The effective temperature of a star is defined in terms of its luminosity as

$$L = 4\pi R^2 \sigma T_{eff}^4 \qquad (3.1)$$

where R is the radius of the star and σ is the Stefan-Boltzmann constant. To convert this to the observational (B-V,V) parameters, transformations from luminosity to apparent magnitude (m) and from T_{eff} to colour (B-V) have to be used. The first of these incorporates the idea of a bolometric magnitude i.e. the magnitude that would be measured with an ideal bolometer absorbing radiation from a star at all wavelengths with perfect efficiency. A bolometric correction (B.C.) calculated by numerical integration under the energy distribution curves of stars with similar spectral types to those being investigated can then be applied to convert this into the

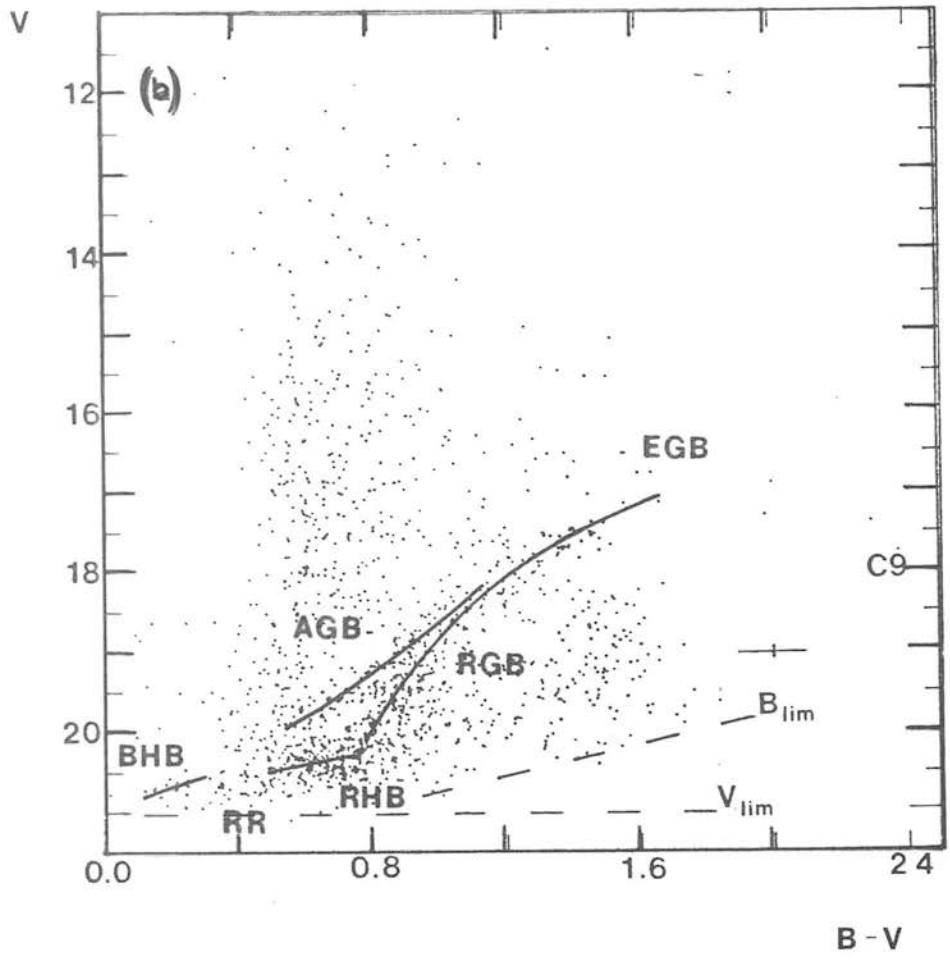

Figure 3.1a,b. (a) The colour magnitude diagram of the Carina dwarf galaxy, derived from COSMOS data (no correction for reddening applied). C9 indicates the position of the new carbon star found in this galaxy, and a typical 1 σ internal error on an individual star magnitude is also marked. B_{lim} and V_{lim} indicate the magnitude limits adopted to construct this diagram. (b) The main morphological features of the colour magnitude diagram in (a) (positions drawn in by hand). Notation used: Blue horizontal branch (BHB), red horizontal branch (RHB), asymptotic giant branch (AGB), red giant branch (RGB), RR Lyrae gap (RR) and extended giant branch (EGB).

absolute magnitude of the pass-band required (M_V in this case) i.e.

$$\log_{10}\left(\frac{L}{L\odot}\right) = 0.4\left[M_{bol}(\odot) - M_{bol}(*)\right] \qquad (3.2)$$

$$M_{bol} = M_V + B.C. \qquad (3.3)$$

where $M_{bol}(\odot)$ and $M_{bol}(*)$ denote the bolometric magnitude of the Sun and observed star respectively. If the apparent distance modulus $|m-M|_V$ of the cluster is known, then this can be used to transform the absolute magnitudes into the required apparent magnitudes.

The T_{eff} to colour transformation is done by interpolation between values of $(B-V)_o$ (o denoting intrinsic values) and $\log(T_{eff})$ for stars of all spectral classes with these parameters well defined from observations. The reddening correction to the cluster is then applied, namely

$$E(B-V) = (B-V) - (B-V)_o \qquad (3.4)$$

and the required observational (B-V) value can then be calculated for each value of T_{eff}.

For the vast majority of stars neglecting for example close binary system components, stars with peculiar rotations (where there exists a latitude dependence of energy flux) etc., stellar evolution is thought to be primarily a function of the mass of the star (M), its age (t) and the original chemical composition of the material it formed from. It is usually assumed that this chemical composition can be spectroscopically determined from the surface layers of luminous highly evolved stars. Star cluster colour magnitude diagrams in

particular are extremely valuable tools for examining new theories in stellar evolution since unlike stars in the solar neighbourhood, the cluster members are all assumed to be at the same distance, have the same age, initial chemical composition and reddening. Hence star clusters provide 'snapshots' of the evolution of stars of different masses. In particular the colour magnitude diagrams of globular clusters provide a complete picture of the evolution of old, metal poor solar mass stars, most of the stars with masses higher than this value having long since evolved and died. Dsph galaxy colour magnitude diagrams have been found to be very similar in shape to those of globular clusters and hence these galaxies are thought to be highly evolved systems too.

3.2.1 : Approach to the main sequence

Stars are assumed to form initially from local enhancements in the interstellar medium, which condense into contracting atomic hydrogen (HI) gas clouds and later fragment into smaller molecular clouds. Gravity dominates the internal pressure of the gas if the density of the cloud is smaller than the critical 'Jeans' density. Any material with higher density is unstable and will disintegrate into smaller (stable) pieces. This collapse is resisted by e.g. magnetic forces, internal turbulence, or if the cloud is rotating, centrifugal forces.

Once the material has fragmented into protostars initially having very large radii and low temperatures (10 to 20K), they evolve into fully convective stars. Hayashi (1961) found that for a star of a given mass and chemical composition, at each luminosity there exists a theoretical maximum radius, and hence a minimum value of T_{eff} at which the star becomes fully convective. The locus of this curve in the HR diagram is almost vertical and is referred to as the 'Hayashi limit'. As gravitational collapse continues, the luminosity of the star increases since the radiative processes are quite efficient at disposing of the energy. Even material at the centre is still transparent to radiation since the density is relatively low. However the core soon becomes dense due to the continued action of

the gravitational forces and hence more and more opaque leading to a gradual rise of temperature in this region. Eventually the dissociation of molecular to atomic hydrogen occurs at a temperature of about 2000K, and the thermal pressure rises to a level that can stop this collapse. However the dissociation provides an energy sink for the newly released energy leading to another free fall collapse of the core, raising the temperature to a level where ionisation of the hydrogen can start. A state of hydrostatic equilibrium between the gravitational and thermal pressures now prevails, the core being gradually heated and becoming more opaque; theoretical models predict that at this stage the star's luminosity falls with a corresponding increase in T_{eff}.

3.2.2 : The main sequence

The locus of points in the HR diagram where the thermo-nuclear conversion of hydrogen into helium first starts is defined as the zero age main sequence (ZAMS). This is well defined theoretically (e.g. VandenBerg and Bridges 1984 for the metallicities associated with open clusters), although different studies (e.g. Mengel et al 1979) have revealed that systematic differences do begin to appear for low mass stars. Stars of different masses encounter this sequence at different luminosities and temperatures in the sense that the higher the mass, the larger the values of the luminosity and temperature.

In the stellar systems considered here, the concern is with low mass stars where the principal energy source is the proton-proton (p-p) cycle which is much less sensitive to variations in temperature than the energy source of the higher mass stars, namely the CN cycle. Both create He nuclei; the p-p cycle fusing four H nuclei together, whilst the CN cycle uses C, N and O to do the same conversion. Energy rates that are very temperature sensitive lead to the development of convective cores (because temperature sensitive sources tend to be centrally concentrated) which in turn leads to large radiative temperature gradients. In order to reduce these gradients, the core becomes convective. Reaction rates for the p-p chain are far less

sensitive to temperature and radiative transport is therefore possible for reasonable temperature gradients.

Stars in which the p-p chain dominates are usually referred to as being on the lower main sequence. Typically their central temperatures are below 20 million K and their masses less than $2M_{\odot}$. When these stars encounter the main sequence, most develop radiative cores, which are surrounded by convective envelopes extending to the base of the photosphere. The depth of this convective envelope is determined by the mass of the star; the envelope extends deeper into a star the less massive it is.

3.2.3 : The red giant phase

The lifetime of a star on the main sequence is determined by the length that its ZAMS luminosity can be maintained by the hydrogen to helium thermonuclear reactions. When the central hydrogen has been exhausted, the star is temporarily out of fuel and must contract. This is the point where stars turn off the main sequence and marks the onset of their red giant evolution. This contraction leads to a release of gravitational energy, and eventually a region in a shell outside the exhausted core becomes hot enough for H shell burning. During this phase, the star moves nearly horizontally in the HR diagram (i.e. at nearly constant luminosity) towards cooler temperatures. The core of a low mass star becomes isothermal when nuclear burning ceases there and the shell burning gradually adds more mass to it. This leads to it contracting and a slight rise in the temperature, which leads to the surface layers being driven outwards. Eventually, the envelope becomes convectively unstable and the star moves up the red giant branch to even cooler temperatures and higher luminosities.

The strength of the convection in evolutionary models is usually handled by the parameter α, which equals the ratio of the mixing length ℓ (i.e. the distance over which a typical convective eddy moves) to the pressure scale height H_p. For $\alpha = 0$, convection does not contribute to the energy flux, and radiative energy transport

dominates; as α gets larger, the structure of the region tends to adiabatic equilibrium. Changes in the value of α can produce large differences in the computed radius of a star and hence the temperature, and so theoretical interpretations have to be gauged against the numerical choice of this parameter. α has little effect on the luminosity of a star though, and hence on its rate of evolution, but there is a problem as to whether it remains constant with varying evolutionary phase and/or chemical composition; this is not known (see section 4.2.1). The possibility of convective overshooting of the material from the helium burning core into the hydrogen burning shell has been examined in open clusters by Maeder (1975, 1976). He found that most of the effects of overshoot had a decreasing importance with decreasing stellar mass (if the mixing length ratio does not change with stellar mass).

The red giant phase ends when the central core temperature becomes so large ($\sim$ 80 million K) as to ignite the triple alpha process, converting the helium to carbon in the core. For stars below a certain mass, electron degeneracy provides a significant and growing contribution to the core pressure before this happens, so that when helium burning begins, it does so explosively since the degenerate electrons conduct very efficiently. This is the 'helium flash'. For higher mass stars this is a much more gradual process (critical mass is $\sim 2.3 M_{\odot}$). This release of energy, raises the temperature of the gas, but since it is degenerate, the pressure does not rise significantly. The increased temperature of the core leads to further energy release and a thermal runaway develops. Eventually, the large amount of energy released lifts the electron degeneracy, allowing the gas pressure to increase with increasing temperature, and hence the core expands and cools.

3.2.4 : The horizontal branch

The star now has a helium burning core with a hydrogen burning shell, and is positioned on the zero age horizontal branch (ZAHB). From theoretical models, the mass of stars on the ZAHB is found to be somewhat smaller than those on the red giant branch, and the smaller

widths of the observed horizontal branches to those calculated from theory implies that some process inducing mass loss has occured (Renzini 1981). Castellani and Tornambe (1981) found that the total amount of mass lost during the first ascent giant branch phase of Population II red giants is proportional to the metallicity content in the sense of being more when the metallicity is higher.

The position of a star on the ZAHB is a function of its total mass, CNO and helium abundance. The luminosity of a star on this branch is primarily dependent upon the mass of the central He core at the helium flash, and its effective temperature upon the mass of the hydrogen rich envelope, which in turn is dependent upon the amount of mass loss. The larger the He core the more luminous the star; the larger the envelope the redder the star. For all other parameters fixed, the smaller the value of Z, the bluer is the colour of the star on the horizontal branch. Iben (1968) found that the number ratio of first ascent giant branch stars above the horizontal branch luminosity to horizontal branch stars is primarily a function of the original He abundance since by increasing the He abundance, the horizontal branch luminosity increases which in turn decreases the portion of the first giant branch that is being looked at (the 'R method' of Demarque, Sweigart and Gross 1972). This provides a valuable method for predicting this parameter which is very difficult to determine observationally.

3.2.5 : Advanced stages of evolution

Evolving stars build up nuclear ash of increasing atomic weight in their cores, in an analogous manner to the H shell burning phase, as they ascend up the asymptotic giant branch. Dynamical instabilities such as relaxation oscillations (see e.g. Iben 1974), and also more mass loss from the outer envelope occur (Fusi-Pecci and Renzini 1979). This leaves the core exposed (for low mass stars) with the envelope being blown off, and forming a planetary nebula. The core evolves very quickly, rapidly losing its luminosity and ending its life as a very dense white dwarf. Verification from observations of the theoretical prediction of a well populated low luminosity

white dwarf population in e.g. globular clusters awaits confirmation however.

3.3 : The Carina dwarf galaxy's colour magnitude diagram features

The CDG has a very low galactic latitude and so a certain amount of Galactic extinction and reddening can be expected. Cannon et al (1986), using the HI column density in the direction of Carina determined by Heiles and Cleary (1979) together with the relation between HI and E(B-V) of Burstein and Heiles (1978) derived a reddening E(B-V) = 0.045. Mould and Aaronson (1983) using the reddening maps of Burstein and Heiles (1983) found a value of 0.025 $\pm$ 0.01. This value (which is surprisingly small considering the low galactic latitude of the CDG) will be the one adopted here. A composite colour magnitude diagram derived from the COSMOS data is shown in figure 3.1a (no correction for reddening made).

The colour magnitude diagrams of the other dsph galaxies can be easily compared with that of the CDG by plotting them as they would appear at the same distance as this galaxy, with the differences in reddenning taken into account. This can be done using the following formulae

$$V_{ca} = V_{ga} + (|m-M|^{*}_{v,ca} - |m-M|^{*}_{v,ga}) \qquad (3.5)$$

$$(B-V)_{ca} = (B-V)_{ga} + [E(B-V)_{ca} - E(B-V)_{ga}] \qquad (3.6)$$

where ga denotes the comparison galaxy values, ca those for the CDG and the * denotes that the apparent distance moduli are to be used, together with the data in table 3.1. The resulting colour magnitude diagrams are shown in figure 3.2. The data for the (composite) CDG colour magnitude diagram brighter than V = 21 comes from the COSMOS

TABLE 3.1

LOCAL GROUP DWARF SPHEROIDAL GALAXY AND GLOBULAR CLUSTER DATA

Name	E(B-V)	$\|m-M\|_V^\dagger$	Mironov Index	$(B-V)_{og}$ (calibrated equations 3.14	$\Delta V_{1.4}$ metallicity and 3.15	S from brackets)	[Fe/H] (spectroscopic)
Leo I	0.02[6]	21.7 ± 0.6[7]					
Leo II	0.02[6]	21.7 ± 0.6[7]					
Fornax	0.00[5]	21.30 ± 0.5[7]					
Ursa-Minor	0.06 ± 0.03[3]	19.2[3]	0.7[9]				
Carina	0.025 ± 0.01[11]	19.8 ± 0.2[14]	0.09 ± 0.03[14]	0.74 ± 0.06[14] (-1.82±0.26)	3.0 ± 0.3[14] (-1.86±0.23)	5.0 ± 1.1[14]	
Draco	0.03 ± 0.01[2]	19.4[2]	0.07[12]				
Sculptor	0.02[1]	19.47 ± 0.1[1]	0.09[13]				
47 Tuc	0.04[10]	13.46[4]	0.07[4]	0.88 ± 0.07[4] (-1.22±0.30)	2.08[4] (-1.0)	3.4[4]	-0.48 ± 0.04[4]
M3	0.01[10]	15.00[4]	0.56[4]	0.77 ± 0.04[4] (-1.69±0.17)	2.67[4] (-1.55)	4.9[4]	-1.48 ± 0.09[4]
M92	0.01[10]	14.50[4]	0.83[4]	0.69 ± 0.02[4] (-2.03±0.09)	2.96[4] (-1.82)	6.5 ± 0.3[15]	-2.1 ± 0.1[4]

TABLE 3.1 (cont'd)

[1] Kunkel and Demers (1977)

[2] Stetson (1979c)

[3] Schommer, Olszewski and Kunkel (1978)

[4] Madore (1978)

[5] Demers, Kunkel and Hardy (1979)

[6] Demers and Harris (1983)

[7] Hodge (1971)

[8] Canterna and Schommer (1978b)

[9] Derived from colour magnitude diagram in [3].

[10] VandenBerg (1983)

[11] Mould and Aaronson (1983)

[12] Derived from colour magnitude diagram in Stetson (1979b)

[13] Derived from colour magnitude diagram in Kunkel and Demers (1977)

[14] This Thesis

[15] Sandage (1970)

(Note: † denotes true distance modulus)

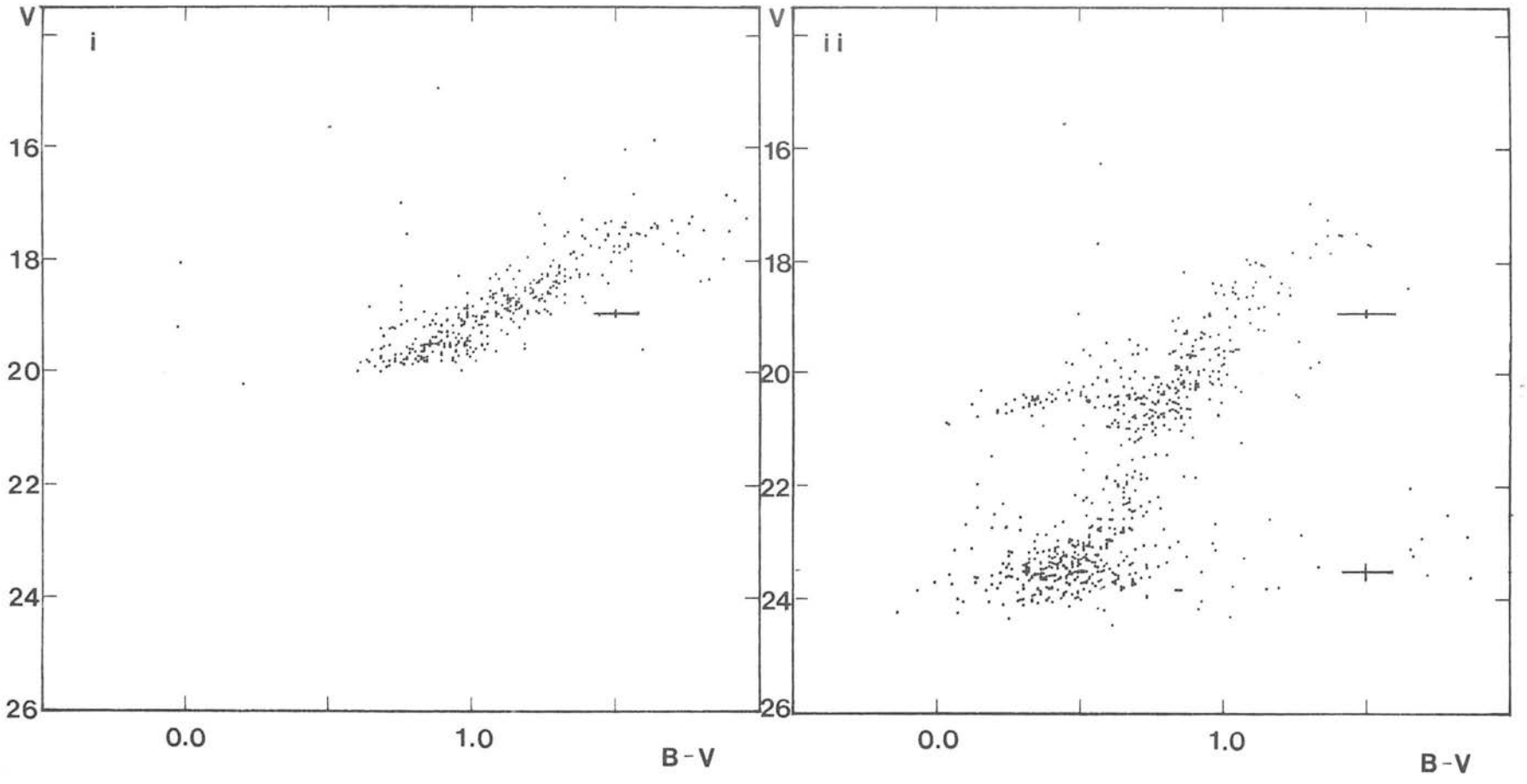

Figure 3.2. The unreddened colour magnitude diagrams of (i) Leo II, (ii) Sculptor, (iii) Carina, (iv) Draco. (i), (ii) and (iv) are drawn as they would appear at the distance of the Carina dwarf. All data brighter than V~ 21 magnitude are derived from photographic plates. The sub-giant and main sequence data below V ~ 21 is used in (iii) from Mould and Aaronson (1983), in (ii) from Da Costa (1984) and in (iv) from Stetson et al. (1985). The 1σ internal error on an individual star measure is shown.

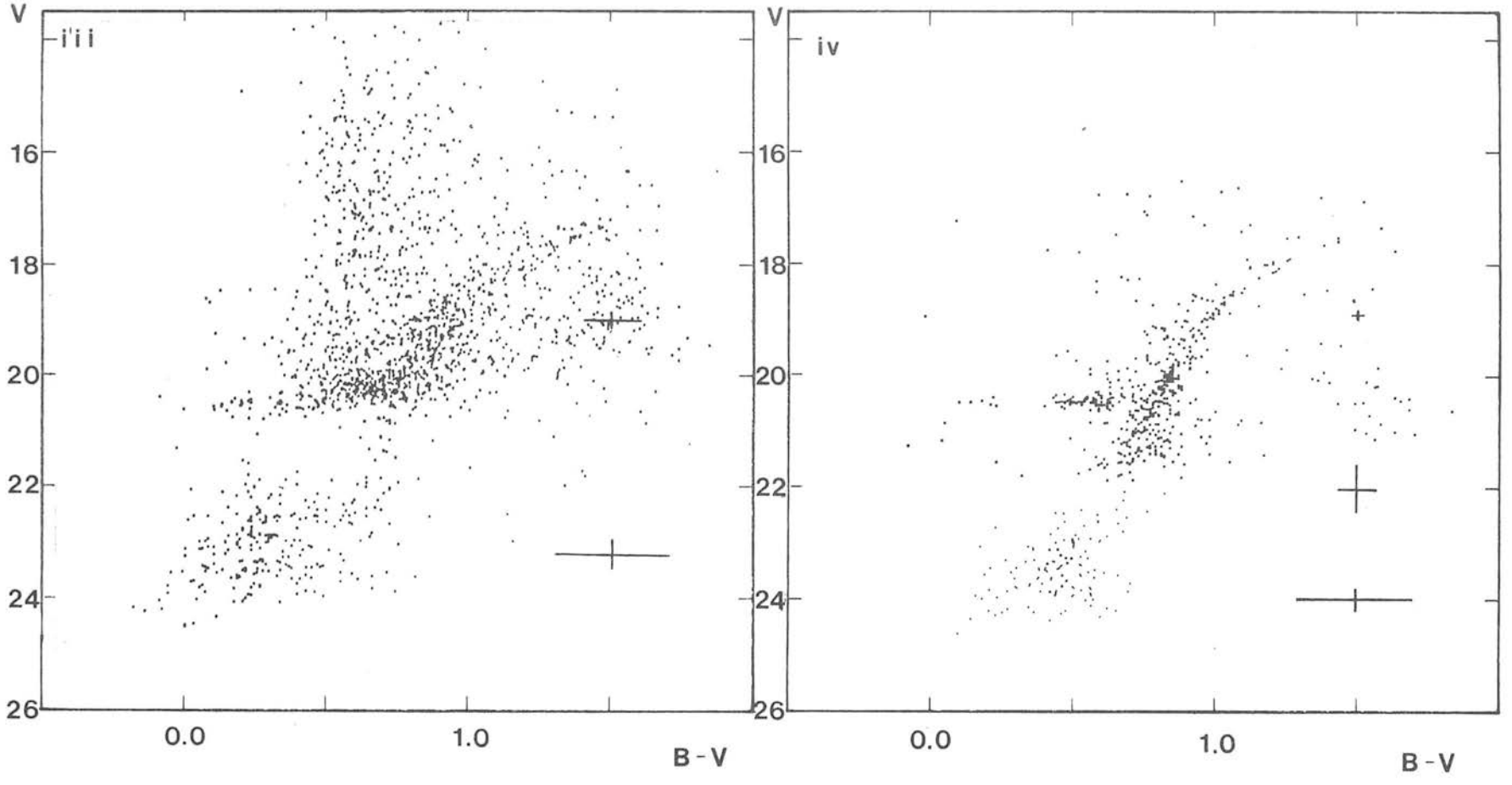

Figure 3.2 (contd.)

data presented in chapter 2 and that fainter than this limit from the CCD work of Mould and Aaronson (1983). In the case of the (composite) Sculptor colour magnitude diagram, all data brighter than 21 in V comes from Kunkel and Demers (1977) and that fainter from Da Costa (1984) and for the (composite) Draco colour magnitude diagram, all data brighter than 21 in V comes from Stetson (1979b) and that fainter from Stetson et al (1985). It can be clearly seen that the giant branches of the Sculptor, Draco and Carina dwarf galaxies are quite similar in slope (see sub-section 3.3.3) with the Leo II giant branch being somewhat shallower. Also, the former dwarf galaxies' horizontal branches are all predominantly red, the Leo II observations not going faint enough to reach this level.

3.3.1 : Contamination and completeness of the COSMOS sample

At this stage it is well to say something about the completeness of the sample of stars selected for the COSMOS colour magnitude diagram. The paired COSMOS data used in figure 3.1a covers an area centred on the CDG of approximately 0.16 degrees^2 and consists of 1471 stars each of which

(i) was paired across all six plates (both V and B), in order that a reliable mean magnitude in each colour could be obtained.

(ii) was not rejected via tha LIME parameter criterion (see section 2.5) i.e. images were rejected from the sample if they were blended on one or more of the plates.

(iii) had an ellipticity (ELLIM) $\leq$ e, where e is to be determined (see below). This was inserted to reject images blended over <u>all</u> plates and also some of the background galaxy contamination (ELLIM = 1 represents a circle). An estimate of this contamination can be made by assuming that the average value of $(B-V)_o$ for galaxies (in general) is about 0.70 (e.g. see Allen 1955); then a limiting magnitude of V = 20.50 $\pm$ 0.20 (which is approximately equal to the limit that is to be taken later) corresponds to a B magnitude limit of about 21.20 $\pm$ 0.20. If the absorption in V is given by

$$A_V = R.E(B-V) \text{ , where } R = 3.1 \qquad (3.7)$$

then using equation 3.4, the absorption in B is given by

$$A_B = \frac{(1+R)A_V}{R} \qquad (3.8)$$

Hence a B magnitude of 21.20 $\pm$ 0.20 at the Galactic latitude of the CDG corresponds to a B magnitude at the SGP of approximately 21.10 $\pm$ 0.20. The galaxy counts of MacGillivray (private communication, see e.g. Shanks et al 1984) indicate that the background galaxy contribution to the number counts down to this limit in the J band (which corresponds approximately to the B band) equals $10^{(3.02\pm0.02)}$/degree^2 where the error in the fit of the counts of MacGillivray has been taken to be negligible in comparison with the error on the limiting magnitude estimate (0.2 magnitudes). Hence over the area considered here of 0.16 degrees^2, this contamination is 167 $\pm$ 8 galaxies which is about 9% of the total sample of images (1774) (see table 3.2).

(iv) had a standard deviation better than 3σ in B, V and colour, where the standard deviation is measured over the three plates of each colour and σ is taken from the data used to plot figure 2.12.

A comparison of the images detectable by eye with those picked up in the raw COSMOS data (before the criteria (i) to (iv) above had been applied) from the V1387 measure in an 'uncrowded' and 'crowded' (i.e. away/towards the centre of the CDG respectively) region of the plate containing a large selection of both faint and unsaturated bright images, made it evident that there was a vast quantity of (small pixel area) spurious images in the COSMOS data amounting to anything up to 50% of the sample with no optical counterparts on the plate. These can be due to a number of causes, the main ones being

TABLE 3.2

PAIRING STATISTICS OF THE IMAGES USED
FOR THE COLOUR MAGNITUDE DIAGRAM

Number of images in region = 3552 (no ACUT applied)
Number of images in region = 1774 (ACUT = 20)

Paired images

Operation	no. of images	Operation	no. of images remaining
ELLIM > 1.2		ELLIM $\leq$ 1.2	
ACUT = 20		ACUT = 20	
MAGLIM > 19.75	115 (p_1)	MAGLIM = 20.50	1507 (p_3)
MAGLIM $\leq$ 19.75	40 (p_2)	3σ rejection	1471 (p_4)

Unpaired images

Operation	no. of images	Operation	no. of images
ELLIM > 1.2		ELLIM $\leq$ 1.2	
ACUT = 20		ACUT = 20	
MAGLIM > 19.75	34 (u_1)	MAGLIM = 20.50	60 (u_3)
MAGLIM $\leq$ 19.75	18 (u_2)		

the effect of very faint stars with such low S/N ratios that no reliable photometry can be performed on them, and also variations in the emulsion. They can be eliminated by inserting either a magnitude or pixel area cut and also by pairing the plates. Examination of the COSMOS data of plate V1387 showed that all images with area less than (at least) 20 pixels (ACUT) were not actually visible on the plate. This areacut was subsequently used.

A series (corresponding to various values of ELLIM) of two separate plots were then made of all the images in the object area. Sample (a) consisted of those images with area greater than 20 pixels, ellipticity less than ELLIM and with a magnitude brighter than V = 20.50 (the approximate horizontal branch level - see section 3.3.2). Sample (b) contained all images with area greater than 20 pixels and ellipticity greater than ELLIM. The images of both these plots were examined on a photographic print of plate V1387 magnified six times, in order to see at what value of ELLIM only blended images (as well as single galaxies) were contained in sample (b). A value of e = 1.2 (see criterion (iii) above) was found for ELLIM, which is presumably a function of the seeing conditions when the plate was taken, and also trailing effects. The images in sample (a) were examined by eye on the same prints, and only three galaxies were positively identified; it must be stressed here though that it became increasingly difficult to decide whether an image was a star or galaxy fainter than about V~20 magnitudes. However for the purposes here, this sample was defined as being all stellar images and sample (b) the blended images (star-star, star-galaxy, galaxy-galaxy, multiple blends etc.).

Can an estimate of the degree of blending be made? Consider the following. It was assumed that all images on the plate down to a specified magnitude level (in this case V~20.50) had been picked up by COSMOS as such on the V1387 measure. That is, the number of stars not detected due to for example variations in the sky-background around bright stars was negligible (a few such images were indeed found). It was further assumed that a blended image from sample (b) consisted of two objects, let them have magnitudes m_1 and m_2, and to

a first approximation COSMOS converts this blend into an image of magnitude

$$M = -2.5\log_{10} (10^{-0.4m_1} + 10^{-0.4m_2}) \qquad (3.9)$$

In particular, if we let $m_1 = m_2 = 20.50$, then $M = 19.75$. Hence if a blended image has a magnitude fainter than 19.75, then one component must be fainter than 20.50 and so this image in the following blending analysis is counted only once. If M is brighter than 19.75, then we do not know anything about the assumed two components since one could be very bright and the other fainter than 20.50, or both could be brighter than 20.50. These images are counted twice in the analysis.

The statistics of the pairing are shown in table 3.2. For a (very) rough guide as to the number of images lost due to the pairing and blending effects down to a magnitude of V 20.50, the assumptions in the previous paragraph and the further assumption that the galaxy contamination (N_g) is contained in the blended image sample with ACUT = 20 and ELLIM>1.2 was made. Hence the total number of stellar images down to a magnitude of V = 20.50 equals

$$N_{tot} = (p_1 + 2p_2 - N_g + p_3) + (u_1 + 2u_2 + u_3) \qquad (3.10)$$

and hence the percentage of stellar images lost (and rejected) equals

$$P_{lost} = \frac{(N_{tot} - p_4).100}{N_{tot}} \% \qquad (3.11)$$

(see table 3.2 for notation). This came out to be approximately (12 $\pm$ 3)% of the defined stellar sample. It is interesting to note that Shanks et al (1984) give the total number of galaxies down to V = 19.75 as 82$\pm$4, and from table 3.2, there are $p_2 + u_2 = 58\pm8$

elliptical images brighter than V = 19.75. Hence it would seem that statistically (i.e. within the 3σ limits), the blended images are accounted for by galaxies to this magnitude limit (and so crowding is not too serious a problem down to this magnitude limit). Fainter than V = 19.75, but brighter than V = 20.5, this leaves $p_1 + u_1$ blended images = 149 ± 12 and the number of galaxies from Shanks et al (1984) in this interval is 85 ± 9, hence the number of stars in blends can be estimated to be 64 ± 15. Adding the 60 (u_3) stars unpaired gives 124 ± 17 lost implying a % loss of (10 ± 3)% i.e. within the (12 ± 3)% loss calculated earlier in this sub-section.

The composition of the Galactic field contamination can be examined by using one of the many Galaxy models available at the present time, predicting the colour magnitude distribution of Galactic stars in a particular region of sky. Such a model has been developed by Robin and Creze (1984), and their predicted Galactic field colour magnitude diagram over a region of 0.25 degrees^2 in the direction of the CDG is shown in figure 3.3 (Robin, private communication). From this model, the prominent clump appearing at V~19 and (B-V)~1.5 in the colour magnitude diagram of the CDG (see figure 3.1a) can be interpreted as disk and intermediate age population II main sequence stars.

Since the AAT measures used to derive the colour magnitude diagram here only covered a central area of the CDG, this model will be used to calculate the effect of (a) image losses on magnitude limit adopted and (b) the background count. In order to do this, the colour magnitude diagram of the CDG has to be subtracted from the COSMOS data leaving only the Galactic contamination. By comparing the COSMOS colour magnitude diagram of the CDG with that of e.g. the Sculptor and Draco dsph galaxies (see figures 3.2(ii) and (iv) respectively) and with those of globular clusters having well defined colour magnitude diagrams (e.g. M3 and M92, Sandage 1970), approximate limits can be drawn on figure 3.4a separating the bulk of the Galactic contamination from the CDG stars. These limits were estimated to be

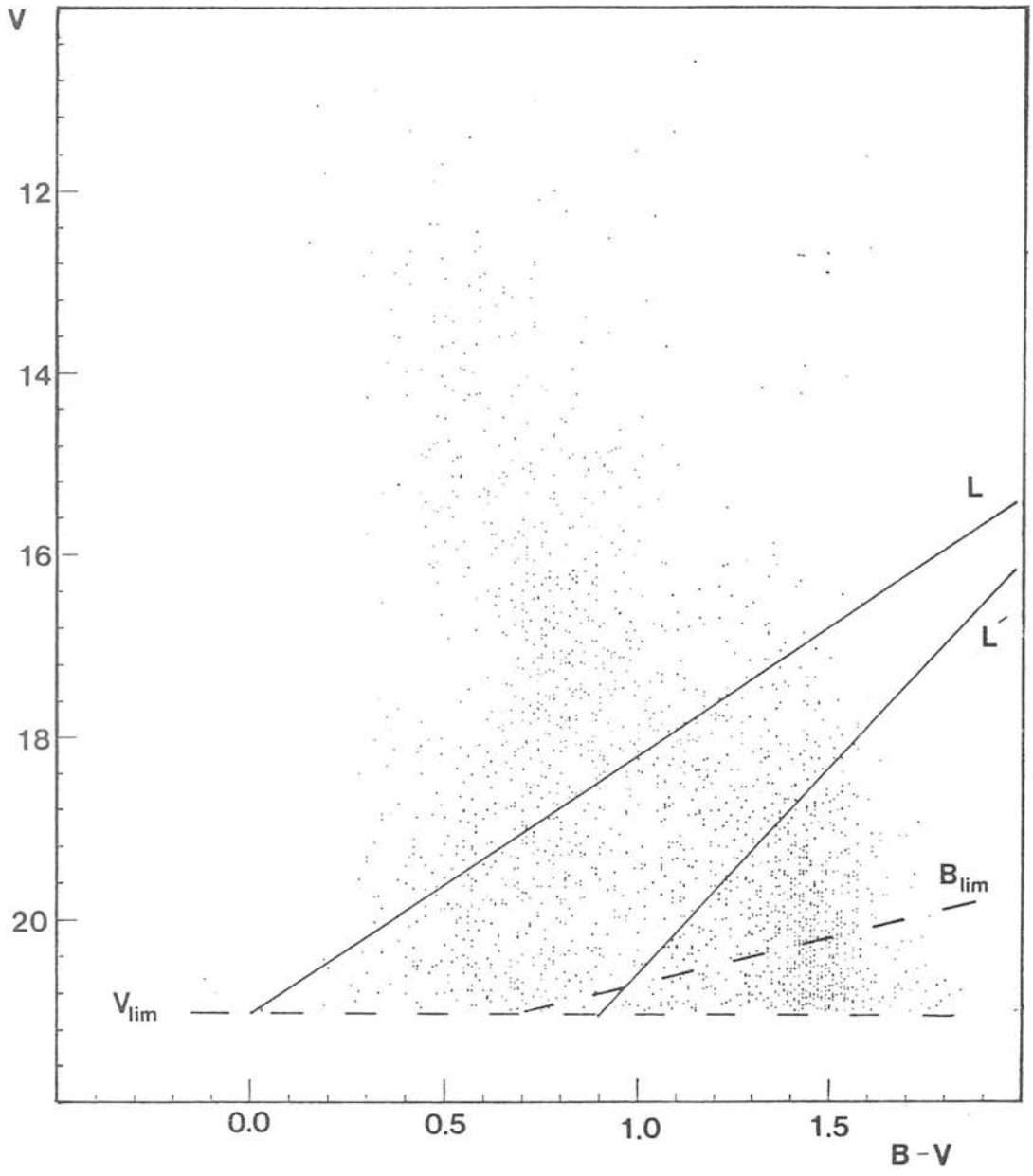

Figure 3.3. The predicted (reddened) colour magnitude diagram of the Galactic field star contamination in the direction of the Carina dwarf galaxy for an area of 0.25 degrees^2 (Robin, private communication). The solid lines (L and L') represent the selection limits for the Carina dwarf data (see text), and V_{lim} and B_{lim} the V and B magnitude limits (respectively), used to determine incompleteness and background corrections.

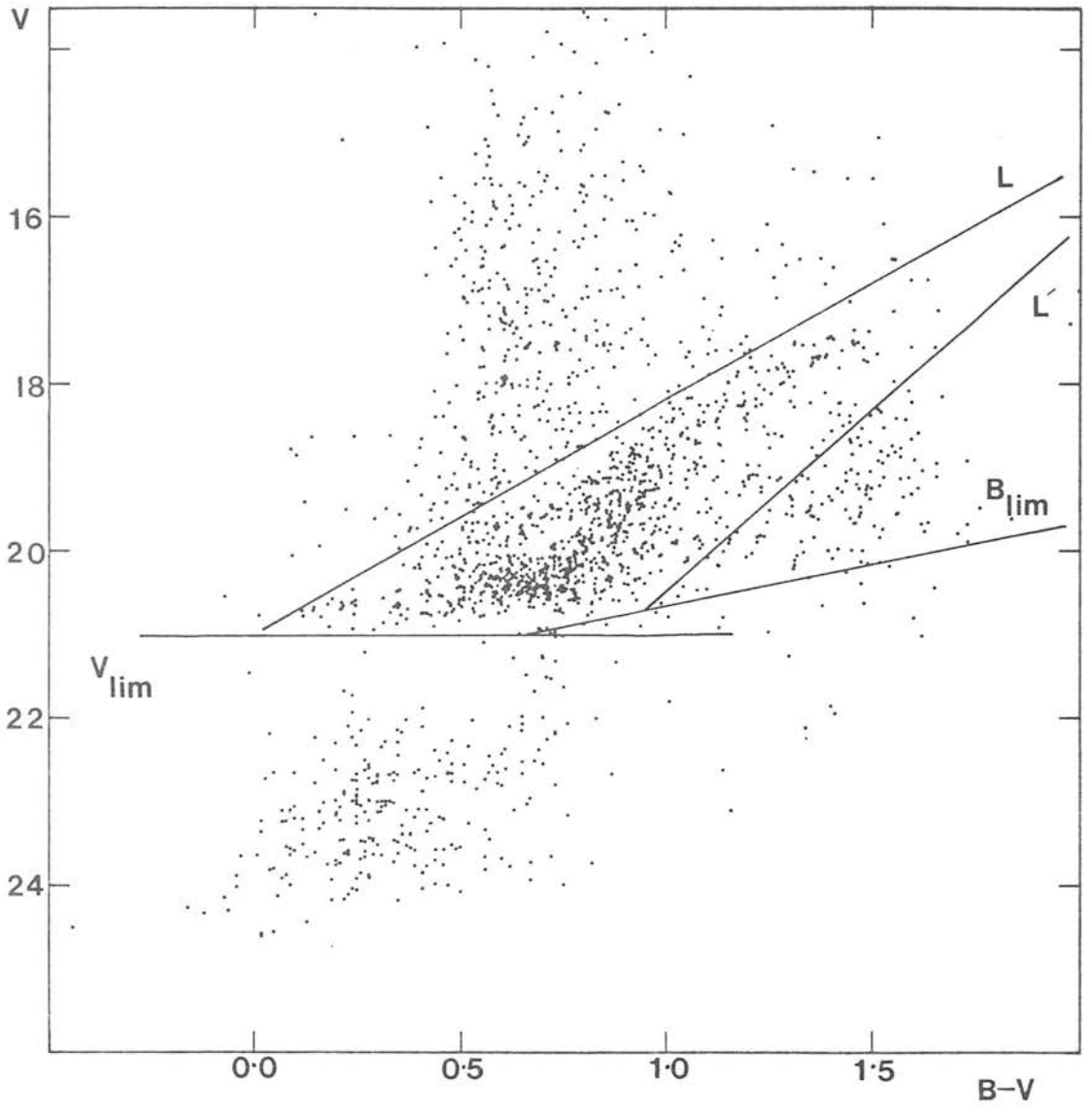

Figure 3.4 a. The selection limits (L and L') used to determine membership of the Carina dwarf (see equation 3.12, and figure 3.3).

$$-2.8(B-V) + 21.00 \leq V \leq -4.3(B-V) + 24.80 \qquad (3.12)$$

Table 3.3 shows the number of foreground COSMOS images (classified as stellar from table 3.2) as a function of magnitude together with the Robin counts corrected for the difference in areas of the two regions. It is clear from this data that the loss of images from the COSMOS sample due to blending only begins to occur at a serious level fainter than V~19.5 magnitudes confirming the conclusion drawn above from analysis of the COSMOS data.

3.3.2 : The horizontal branch and distance determination

If it is assumed that the derived colour magnitude diagram for the CDG covers the regime of all the horizontal branch stars of this system, then from (e.g.) figure 3.1a, this dwarf spheroidal's horizontal branch can be seen to be predominantly red. This is in agreement with the work of Cannon et al (1986) and Mould and Aaronson (1983). From figure 3.1a, the red horizontal branch can be estimated to lie approximately between the limits $0.5 \leq (B-V) \leq 0.8$ and a small blue horizontal branch population with $0.1 \leq (B-V) \leq 0.3$ can also be identified, where the Galactic field contribution has been estimated from figure 3.3. Hence it would seem that the Ursa-Minor dsph galaxy (Schommer, Olszewski and Cudworth 1981) remains the only known dsph galaxy to have a substantially blue (as compared to its red) horizontal branch although the available Fornax (Demers, Kunkel and Hardy 1979, Cannon, Hawkins and Sagar 1985) and Leo I/II (Demers and Harris (1983), Hodge private communication) observations do not go faint enough in order that a reliable magnitude level for the horizontal branch can be identified in these systems. However, the magnitude of the observed horizontal branch in the CDG being close to the magnitude limit applied to the COSMOS data does not rule out altogether the possibility of a more populous blue horizontal branch in this galaxy.

A number of colour magnitude diagram morphological parameters

TABLE 3.3

FOREGROUND STELLAR CONTAMINATION OUTSIDE THE SELECTION LIMITS L AND L' AND BRIGHTER THAN V_{lim} AND B_{lim} (SEE FIGURES 3.3 AND 3.4a) FOR THE CARINA DWARF GALAXY

m_V (apparent)	COSMOS COUNTS	ROBIN COUNTS†
15 - 16	63 ± 8	59 ± 6
16 - 17	99 ± 10	96 ± 8
17 - 18	99 ± 10	108 ± 8
18 - 19	106 ± 10	106 ± 8
19 - 19.5	68 ± 8	56 ± 6
19.5 - 19.75	26 ± 5	46 ± 5
19.75 - 20	20 ± 4	45 ± 5
20 - 21	22 ± 4	72 ± 7

†scaled for difference in area between COSMOS counts (0.16 degrees^2) and Robin counts (0.25 degrees^2).

can now be estimated for the CDG. The Mironov Index for a globular cluster is defined as B/(B+R), where B and R are the number of blue and red horizontal branch stars respectively, and measures the 'redness' or 'blueness' of the horizontal branch. For the CDG COSMOS data here, a number of assumptions have to made before an estimate of this quantity can be calculated. These are

(a) the incompleteness corrected COSMOS counts at the magnitude level of the horizontal branch can be calculated by scaling the raw COSMOS counts by the ratio of the number of foreground stars taken from the Robin and Creze (1984) model to those actually counted by COSMOS at this magnitude level (taken as $20 \leq V \leq 21$) (see table 3.3).

(b) the background count needed to be subtracted from both the B and R COSMOS counts can again be calculated from the Robin and Creze (1984) model by comparing the number of stars at the horizontal branch level within the selection limits of figures 3.3 and 3.4a.

(c) defining the B count to be all those stars within the limits $0.1 \leq (B-V) \leq 0.3$, $20 \leq V \leq 21$, and the R count as those between $0.5 \leq (B-V) \leq 0.8$, $20 \leq V \leq 21$.

(d) all of the stars comprising the intrinsic blue and red horizontal branches of the CDG fall above the limiting magnitude of the colour magnitude diagram in figure 3.1a. This might not be true since these particular branches in globular cluster colour magnitude diagrams appear at the position of the (absolute) magnitude limit adopted here.

After correcting for incompleteness and background counts and assuming (a) to (d) to hold, a Mironov Index of 0.09 ± 0.03 was obtained. From the data in table 3.1, this makes the 'redness' of the Carina dwarf's horizontal branch comparable with that of the Sculptor and Draco dsph galaxies in contrast to the higher Mironov indices of 0.83 and 0.56 (Madore 1978) for M92 (a strongly blue horizontal branch cluster) and M3 (with both a blue and red horizontal branch) respectively.

From (e.g) figures 3.1a and b, it is clear that there is some uncertainty in defining the error on the magnitude level of the RR Lyrae gap. The internal error on the V magnitude of each star at the RR Lyrae gap end of each of the red and blue horizontal branches is ~0.08 (see figure 2.12), but the error on the mean position of the red and blue horizontal ridge lines will be very much better than this assuming a negligible intrinsic width. Using this fact, it is clear that the error on the magnitude level of the RR Lyrae gap is going to be dominated by the visual estimate error i.e. the limits between which this gap can be estimated to lie by eye, and from figure 3.1a this horizontal branch level can be estimated to be V_{HB} = 20.5±0.2. Adopting an absolute magnitude for an RR Lyrae star to be M_V = 0.6 (see e.g. Madore 1978), then this gives a true distance modulus $|m-M|_V^{\dagger}$ = 19.8±0.2 (the absorption in V is given by equation 3.7). Hence using the equation

$$|m-M|_V^{\dagger} = 5\log_{10}d - 5 \text{ , where d is in pc} \qquad (3.13)$$

the distance to the CDG can then be calculated to be 91kpc with an estimated error of about 9kpc. One of the uncertainties in this calculation is the value used for the luminosity of an RR Lyrae star. Clube and Dawe (1980) found that for a particular metal poor RR Lyrae star that M_V = 1.0 instead of the generally adopted value of 0.6 used above, and there is now evidence to suggest that the luminosity of the horizontal branch level depends upon cluster metallicity (see e.g. Sandage 1982). However, an absolute magnitude of M_V = 0.6 for an RR Lyrae as is generally adopted for the other dsph galaxies and globular clusters will be used in the work here, as will the distance (and error) to the CDG derived using this value.

3.3.3 : The asymptotic, first and sub-giant branches

The CDG giant branch is steep, and extends out to at least (B-V)~1.5, with very red objects in the colour magnitude diagram of

figure 3.1a with (B-V)~2 being possible carbon star members (see section 3.3.5). The classification of globular cluster giant branches is usually defined in terms of three parameters namely $(B-V)_{og}$, $\Delta V_{1.4}$ and S. $(B-V)_{og}$ is the unreddened colour of the intersection of the giant and horizontal branches (Sandage and Smith 1966). Field star contamination makes this difficult to determine with any high accuracy. By comparison with the shapes of the colour magnitude diagrams of globular clusters, the CDG presumably has a sub-giant branch extending fainter than the horizontal branch level, from the red end of the horizontal branch. From the ridge line diagram of figure 3.4b (see sub-section 3.3.4 for the definition and estimated errors on the ridge line), this latter point can be estimated to be probably no redder than (B-V) = 0.82 and no bluer than 0.70, and so a value for $(B-V)_{og}$ = 0.74±0.06 (i.e. unreddened) will be taken.

Using the apparent magnitude in sub-section 3.3.2 for the horizontal branch, $\Delta V_{1.4}$ (Sandage and Wallerstein 1960) which measures the height of the giant branch above the horizontal branch at $(B-V)_o$ = 1.4, equals 3.0 ± an estimated error of 0.25 where the value of V at $(B-V)_o$ = 1.4 on the giant branch is taken to be 17.50 ± 0.15 (see figures 3.4b and c and explanation of ridge line errors in sub-section 3.3.4). S (Hartwick 1968) is another metallicity parameter and is equal to the slope of the line joining the intersection of the horizontal and sub-giant branches to a point on the giant branch 2.5 magnitudes above the horizontal branch. A similar analysis to that used for deriving $\Delta V_{1.4}$ and $(B-V)_{og}$ gave S = Tan β = 5.0 (see figure 3.4c) with an estimated error of 1.1, comparable to the value for M3.

Zinn and West (1985) have calibrated $\Delta V_{1.4}$ and $(B-V)_{og}$ with [Fe/H], and their results show that

$$[Fe/H] = -0.924\Delta V_{1.4} + 0.913 \qquad (3.14)$$

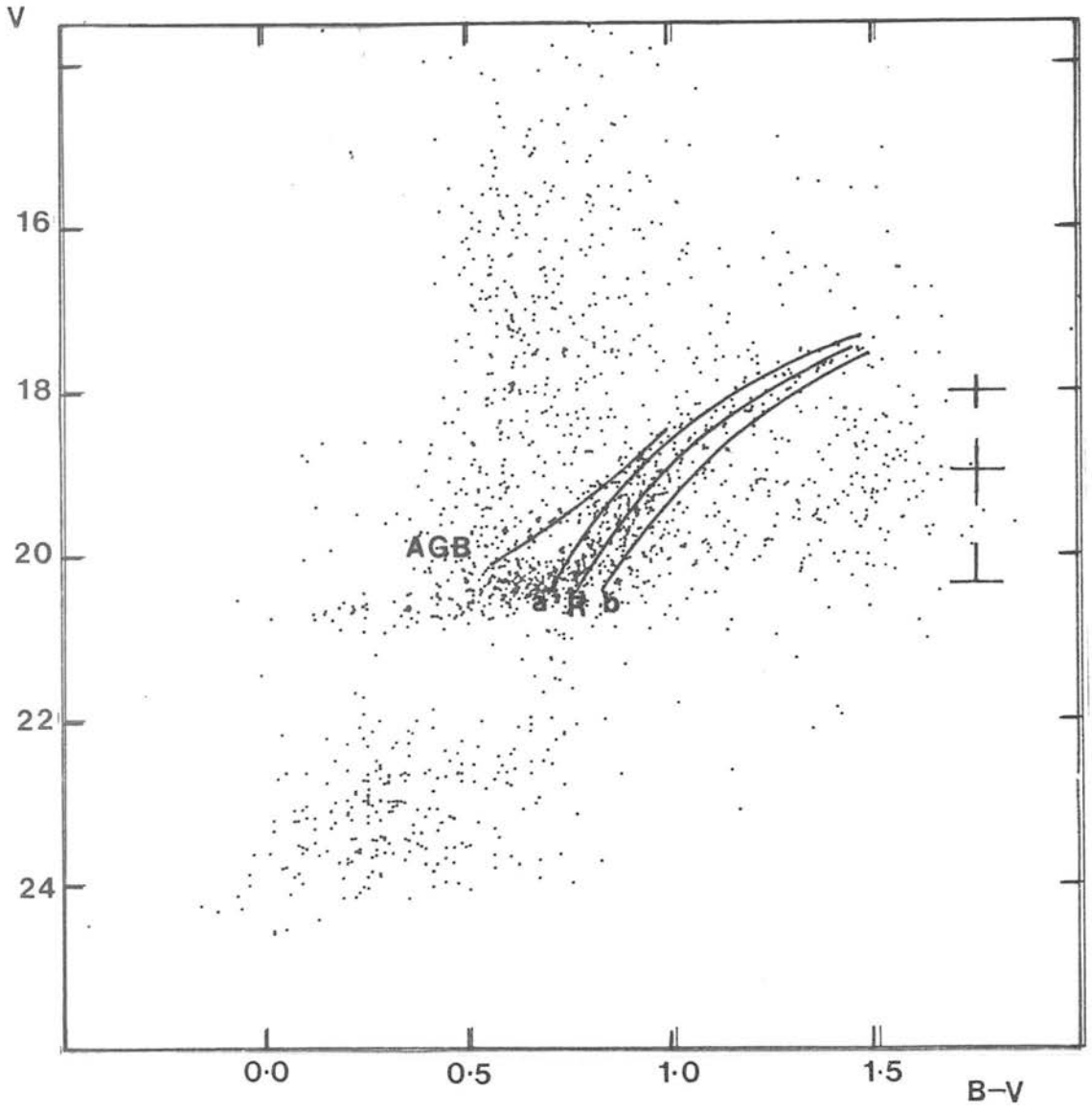

Figure 3.4b. The adopted ridge line (R) for the Carina dwarf's red giant stars assumed to lie between the lines (a) and (b), drawn on this galaxy's colour magnitude diagram (not corrected for reddening). Compensation has been made for the asymptotic giant branch lying at a slightly higher luminosity than that of the red giant branch. The position of the low luminosity asymptotic giant branch predicted by Lee (1976) for globular clusters with the same metallicity as that of the Carina dwarf (found in section 3.3.3) is also marked as AGB. The errors shown are those estimated for defining the position of R.

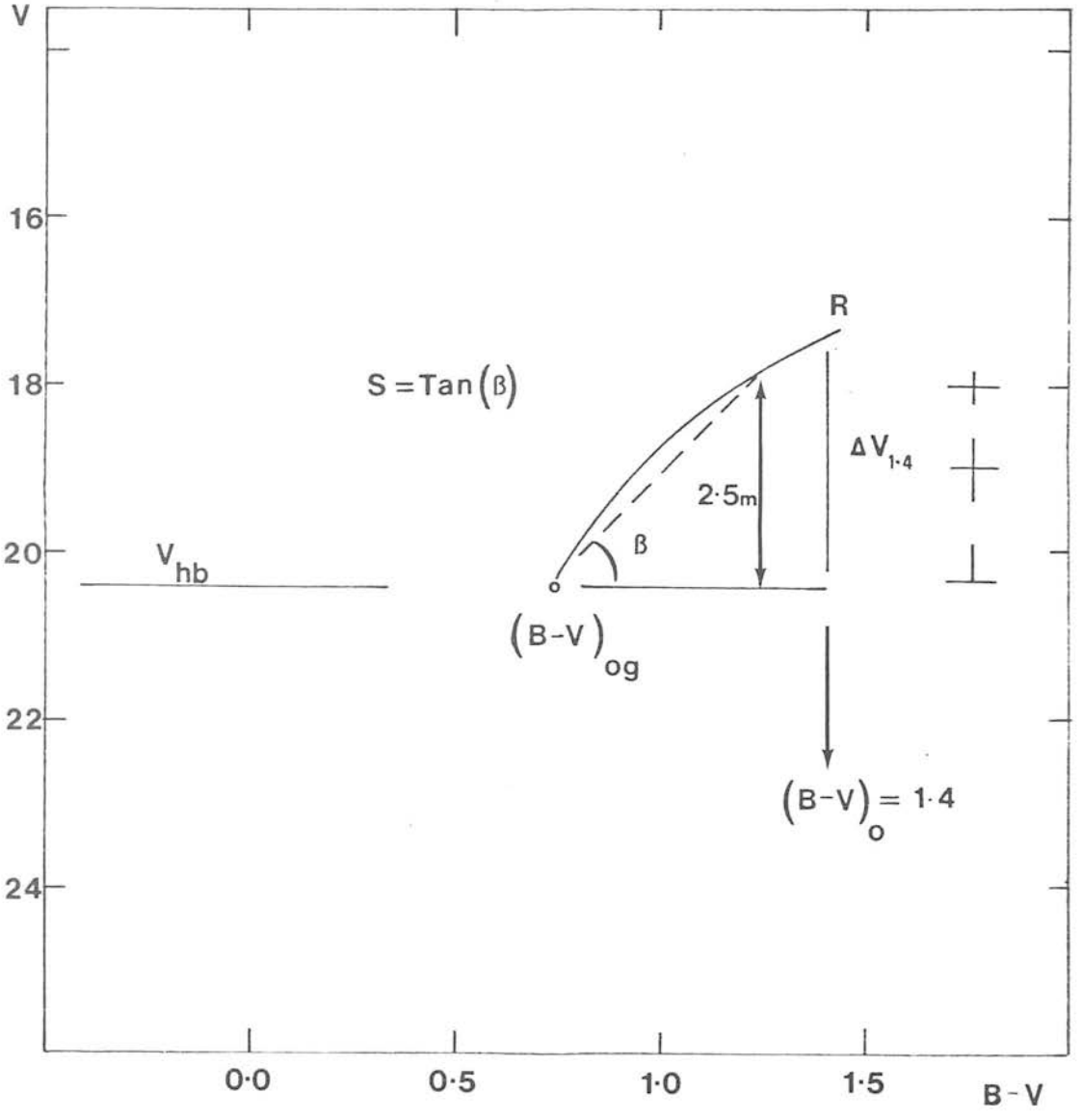

Figure 3.4c. The giant branch parameters of the Carina dwarf marked on the unreddened red giant ridge line (R) defined in figure 3.4b.

$$[Fe/H] = -5.00 + 4.3(B-V)_{og} \qquad (3.15)$$

Hence with the values derived here for the CDG, equation 3.14 yields [Fe/H] = -1.86 $\pm$ 0.23 and equation 3.15, -1.82 $\pm$ 0.26. However, these calibrations which are usually used to derive the metallicites of globular clusters, have to be treated with caution when applying them to any other systems since in particular for the dsph galaxies, an abundance spread appears to be present. Also, all of the calibrations have their drawbacks. For example $(B-V)_{og}$ has been shown to be fairly insensitive to [Fe/H] when [Fe/H] $\leq$ -2.0, and S, the only reddening independent parameter of the three, has been shown to lose sensitivity for [Fe/H] $\sim$ -1.4 (Kraft 1979). Table 3.1 lists the metallicity obtained from equations 3.14 and 3.15 for the two parameters discussed above for three globular clusters, against their spectroscopic metallicity. From this data (especially that of M3 and M92) it can be seen that both $(B-V)_{og}$ and $\Delta V_{1.4}$ seem reasonable measures to infer a system's metallicity from, for a spectroscopic metallicity between -1.5 and -2.1.

It is concluded that these giant branch morphological parameters indicate that the CDG has a low metallicity, probably somewhere in the range of [Fe/H] = -1.6 to -2.0. This result fits in well with the corresponding values of the metallicity for the other dsph galaxies except (possibly) Fornax (see table 5.4). This latter galaxy was thought at one time to be quite metal rich with [Fe/H]$\sim$-0.5 (Demers, Kunkel and Hardy 1979), a deduction made from looking at the shallowness of the observable high luminosity end of its giant branch (see figure 3.7). However, from the work of Aaronson and Mould (1985), Cannon, Hawkins and Sagar (1985) and Buonanno et al (1984a), it is clear that its metal abundance is less than this, although it is still thought to be one of the most metal rich dsph galaxies with [Fe/H]$\sim$-1.7 (Aaronson and Mould 1985). Spectroscopic evidence (from e.g. Zinn 1978a, 1981, Stetson 1980) also indicates that the heavy metal abundance of the dsph galaxies is low (see table 5.4).

Another way to infer information about the metallicity of the CDG is to compare the slope of its giant branch with the giant branch mean ridge lines of globular clusters with a known range of metallicity e.g. M92 (Sandage 1970), M3 (Sandage 1970) and 47Tuc (Cannon 1974). These are plotted in figure 3.5, with the data having been corrected for the different reddenings and distances to these clusters. It is well known that these three clusters form a sequence in metallicity from metal poor (M92) through intermediate metallicity (M3) to metal rich (47Tuc). This is reflected in the slope of their respective giant branches immediately above their horizontal branches, being steep for M92, shallow for 47Tuc and intermediate for M3 (see figure 3.5). The vertical positional error in this figure for the ridge line of the globular clusters is dominated by the uncertainty in the distance modulus of the clusters, which is typically 0.3 magnitudes. The globular cluster colour magnitude diagrams being much tighter sequences that that for the CDG and the large number of stars that make them up, contributes to making the error in the colour of their ridge lines very small (typically better than 0.05 in B-V - see Sandage 1970 and Cannon 1974).

The position and slope of the giant branch of the CDG suggest that its mean metallicity lies somewhere between that of M92 ([Fe/H] = -2.1 ± 0.1) and that of M3 ([Fe/H] = -1.48 ± 0.09), these latter two metallicity values being taken from Madore (1978). Hence, from this method the mean metallicity of the CDG must be around -1.8 ± 0.3. This compares favourably with the metallicity value found from the colour magnitude morphological parameters above, and so this value will now be adopted. The Mironov index which is a horizontal branch index, is not used as a metallicity indicator. Its anomalous nature is discussed below (see subsection 3.3.7).

3.3.4 : The metallicity dispersion

The giant branch in the colour magnitude diagram for the Sculptor dsph galaxy has been found to have an intrinsic width over and above the calculated photometric errors (Kunkel and Demers 1977, Norris and Bessell 1978, Smith and Dopita 1983), and although it has

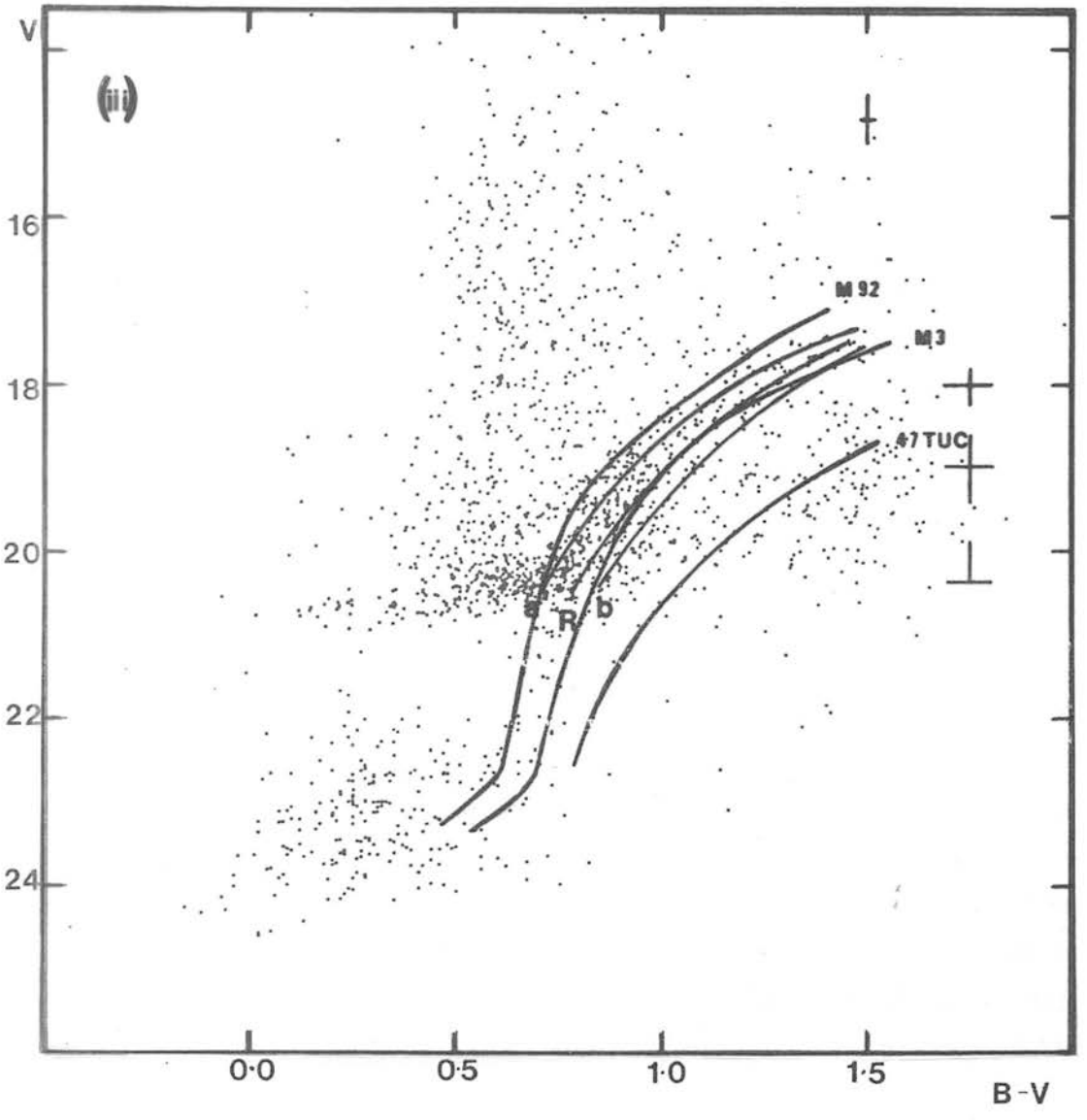

Figure 3.5. Giant branch ridge lines of M92, M3 and 47Tuc (see (i)) indicating possible bounds for the metallicity of the Carina dwarf. The error in the defined ridge line for the Carina dwarf data (see (ii)) as marked is that of figure 3.4b. In addition, there is an error of ±0.2 magnitudes in the distance modulus to this galaxy (i.e. a shift in the vertical direction of ±0.2). A typical error for the globular cluster ridge lines is also shown,with the distance modulus error incorporated into it.

been unclear in the past whether this was the case for the Draco dwarf (see Stetson 1979b), recent evidence suggests that this phenomenon occurs in all of the dsph Galaxies (see e.g. Carney 1984). It is thought that this primarily arises due to a metallicity dispersion within these galaxies, and although this is very rare in globular clusters, there are notable exceptions e.g. ω Cen (Cannon and Stobie 1973) and possibly M22 (Norris and Freeman 1983).

The CDG colour magnitude data derived earlier can be used to see if such a dispersion is present in this galaxy. Before doing this, it is necessary to see if an asymptotic giant branch is present, so that its contamination of the first ascent giant branch can be properly accounted for. The (B-V,V) colour magnitude diagram data for the CDG were binned in bins of width 0.1 and 0.5 in colour and V magnitude respectively, and histogram plots made of the stellar number density as a function of colour (see figure 3.6). This figure together with figure 3.1a suggest that there is a population of stars lying at a slightly higher luminosity than the horizontal, and first ascent giant branches, inclined at $\sim 45^{o}$ in the latter figure. This is possibly the low luminosity end of the extended asymptotic giant branch found by Mould et al (1982). A theoretical estimate of the expected separation of the asymptotic and first ascent giant branches is not easy, being a function of many factors such as the mass of the stellar envelope, chemical composition, mixing and mass loss (Buonanno, Corsi and Fusi-Pecci 1981), but an empirical guide can be deduced from the work of Lee (1976) who from his study of six Galactic globular clusters, was able to classify their asymptotic branches using the $(B-V)_{og}$ and $\Delta V_{1.4}$ parameters. The position of his predicted (mean) asymptotic giant branch, using the metallicity parameters derived here for the CDG is plotted on figure 3.4b, and seems to suggest that the stars making up this relatively low luminosity asymptotic branch population are present in the CDG. This identification would not be new in dsph galaxies e.g. Sculptor (Norris and Bessel 1978), Ursa-Minor (Schommer, Olzewski and Cudworth 1981), LeoII (Demers and Harris 1983) and Draco (Stetson 1979b) all appear to have them too, but it is unclear in all of these latter cases whether it is in fact a broad giant branch that is causing the

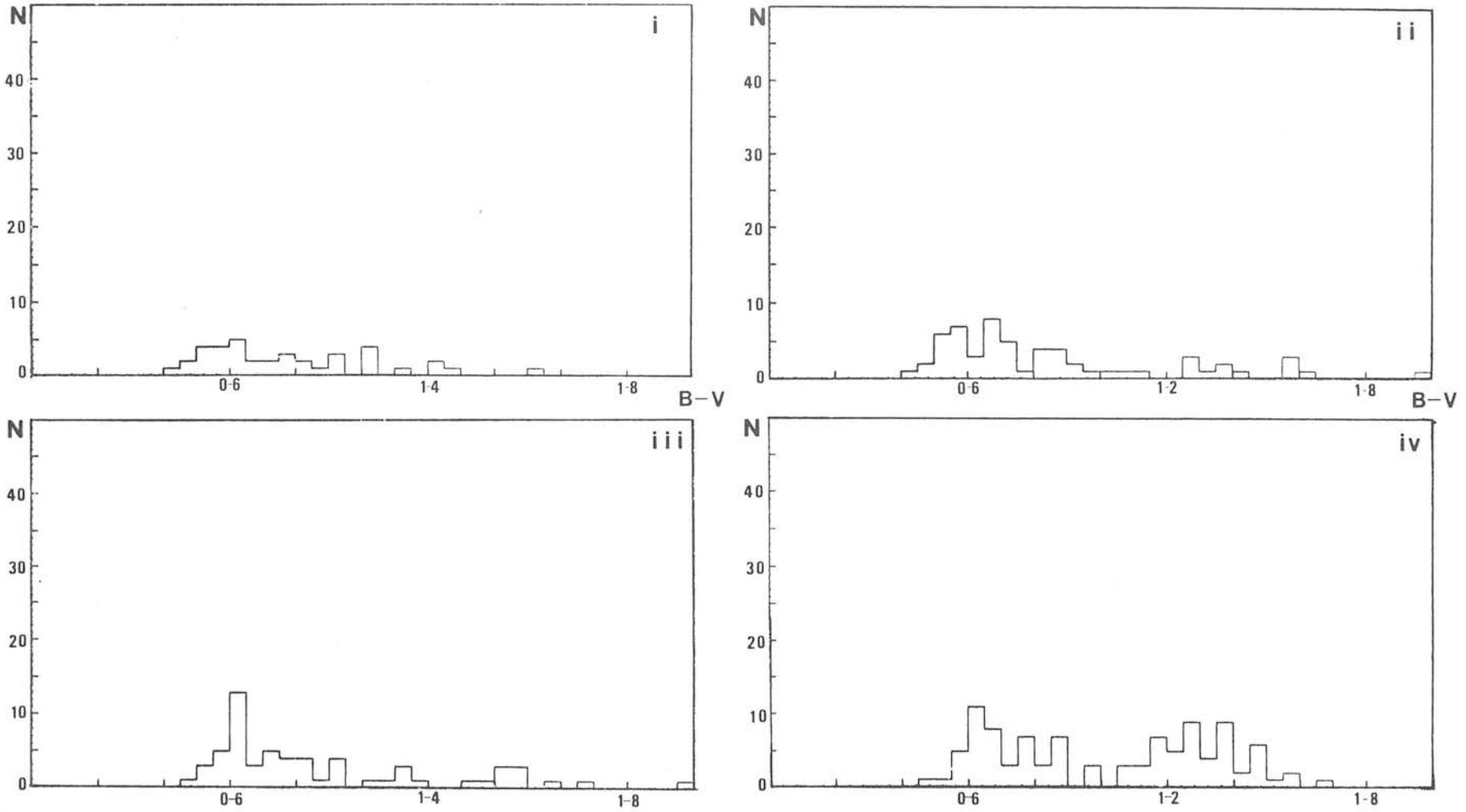

Figure 3.6. Colour-number density plots of the Carina dwarf spheroidal galaxy. (i) 16.00<V<16.50, (ii) 16.50<V<17.00, (iii) 17.00<V<17.50, (iv) 17.50<V<18.00, (v) 18.00<V<18.50, (vi) 18.50<V<19.00, (vii) 19.00<V<19.50 (viii) 19.50<V<20.00, (ix) 20.00<V<20.50, (x) 20.50<V<21.00

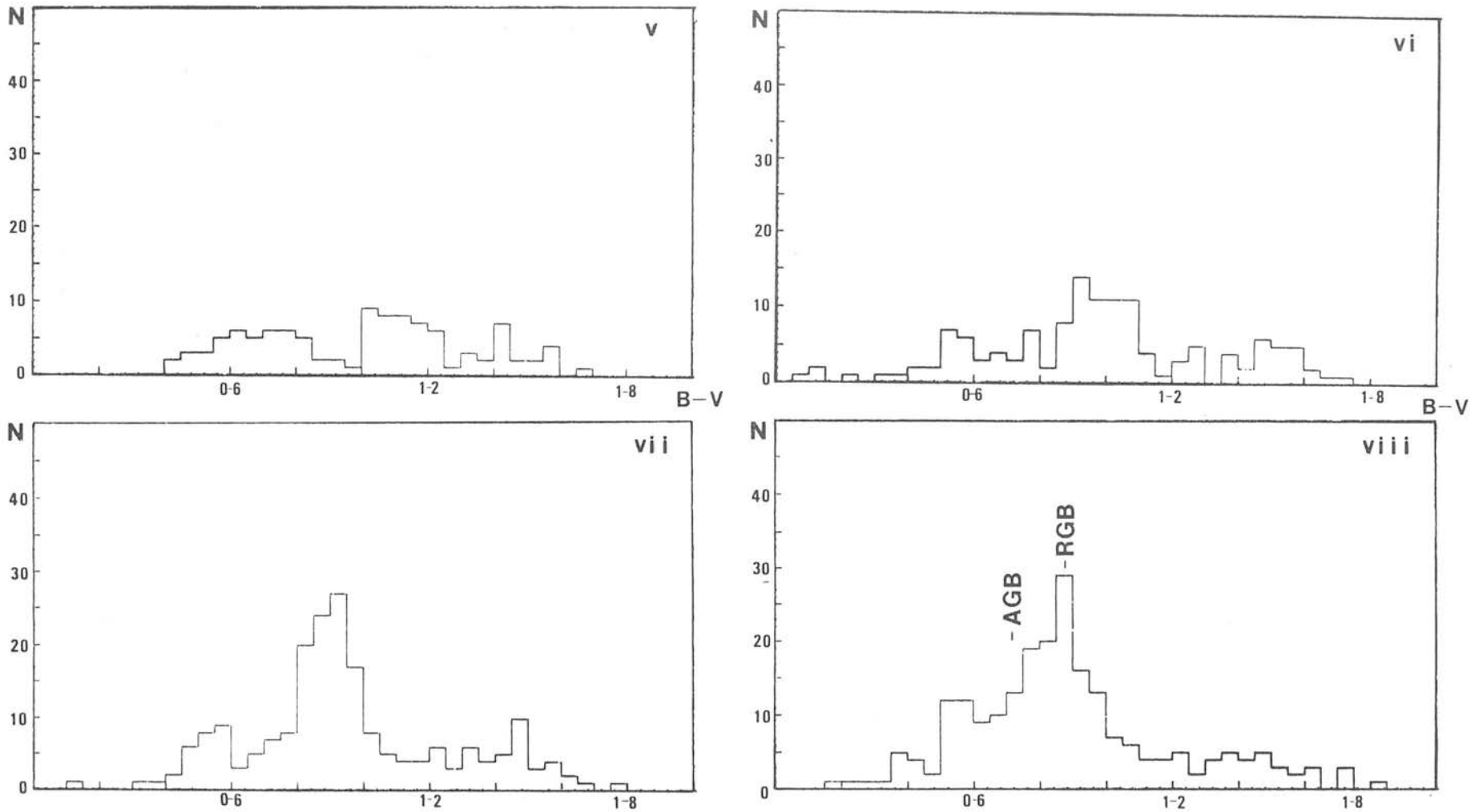

Figure 3.6 (cont.) AGB: Asymptotic giant branch, RGB: Red giant branch.

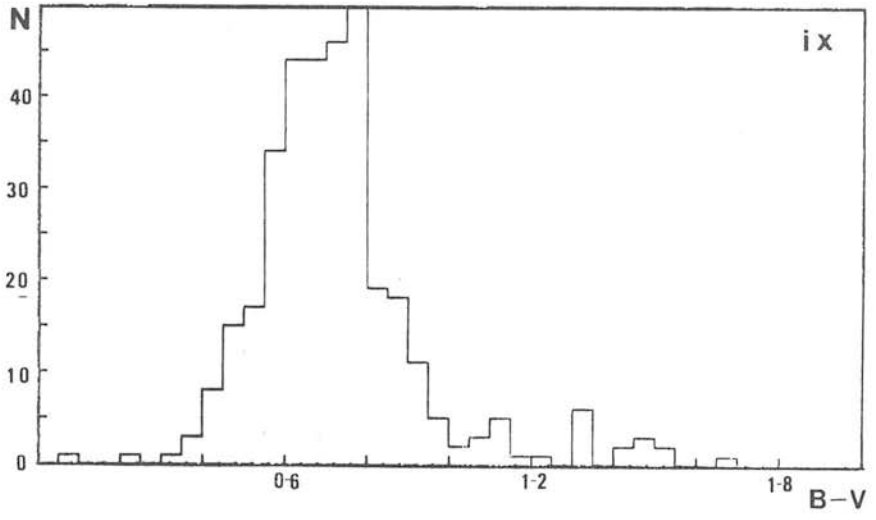

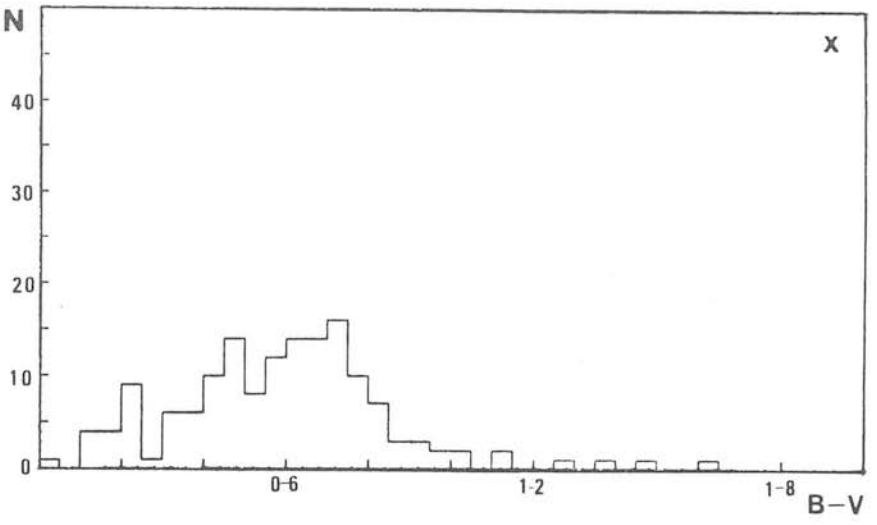

Figure 3.6 (cont.)

confusion.

Assuming that an asymptotic giant branch does exist in the CDG, a simple calculation can be done to derive a value for the possible spread in metallicity present (see e.g. Sandage and Katem 1982). If the number count data redward of the peak indicated in figure 3.6 (viii) as 'RGB' is taken to be first ascent giant stars, and this distribution is assumed to be the same as that of the giants on the blueward side, then fitting a gaussian function to this data by allowing the σ and the mean of this distribution function to be free fitting parameters (see e.g. the routine NONLIN, Bevington 1969), a value of the observed dispersion $\sigma_{obs} = 0.11$ was obtained. If the intrinsic width of the giant branch is given by

$$\sigma^2_{GB} = \sigma^2_{obs} - \sigma^2_{B-V} \qquad (3.16)$$

(see e.g. Buonanno et al 1984b), where σ_{GB} is the intrinsic σ of the giant branch width then using σ_{B-V} at the colour of the first ascent giant branch peak (see figure 3.6 (viii)) to be 0.09 (internal error, from figure 2.12), $\sigma_{GB} = 0.06$. This implies that there exists an intrinsic width of the giant branch, but it must be stressed that since σ_{GB} is of the same order as that of the internal error in the colour (σ_{B-V}), the conclusion from this data that there exists a metallicity spread in the CDG can only be tentative. A quantative estimate for such a spread (if real) can be deduced from e.g. equation 3.15. Taking the mean value of $(B-V)_{og}$ to be 0.74 (as found earlier) and σ_{GB} found above to be comparable with the value of σ_{GB} at the V magnitude of $(B-V)_{og}$ (the large population of red horizontal branch stars makes σ_{GB} difficult to find here), then this implies a real spread of about 0.26 in metallicity. This spread agrees well with the globular cluster ridge line comparisons made earlier, where a mean metallicity of -1.80 was found with an error of 0.3 which can probably be taken as as an upper bound to any metallicity dispersion present.

The ridge lines for the CDG and the other dsph galaxies can be easily constructed from the published colour magnitude diagrams (or taken from the literature in the case of the Draco dsph galaxy colour magnitude diagram of Stetson 1979b), and plotted as they would appear at the distance and direction of the CDG by using equations 3.5 and 3.6. If it is assumed that the giant branch of the CDG lies between the limits (a) and (b) shown in figure 3.4b, where compensation for the asymptotic giant branch found in this sub-section has been made, then the ridge line can be taken to be their mean. The error can then be defined by the limits (a) and (b) (the mean ridge line determined by this method for the red giant branch is confirmed by comparing these values with the red giant branch ridge lines obtained from figure 3.6). These are plotted in figures 3.7a and b. The vertical error shown in these figures is an estimate composed of that in the distance modulus and in the bounds of the visual estimate of the ridge lines (cf limits (a) and (b) above for the CDG). The error in the colour shown is an estimate of that of the visual estimate of the ridge line locus. Both errors are quite large and so it is difficult to deduce anything conclusive from these figures, but it seems reasonable to suppose that the Draco, Sculptor and Carina dwarf galaxies all have similar giant branch slopes, implying that they have comparable metallicities. Fornax, as previously stated appears to have a shallow giant branch (relative to those of the other dwarf galaxies shown), usually indicative of a metal rich system, and neither it nor (possibly) the Leo I's giant branch seem to correspond to any of the well known Galactic globular cluster giant branches. It could well be that in these two cases it is only the tip of an extended giant branch that is being seen, as found in some of the other dsph galaxies and also the Magellanic Cloud globulars (N.B. the ridge line in figure 3.7a for Leo I has been derived from only a preliminary colour magnitude diagram, Hodge private communication).

3.3.5 : Carbon stars

Images that COSMOS had detected with a $(B-V) > 1.8$, V brighter than 20th magnitude, and positioned towards the centre of the CDG were examined visually on the best AAT plate. Artificially large red

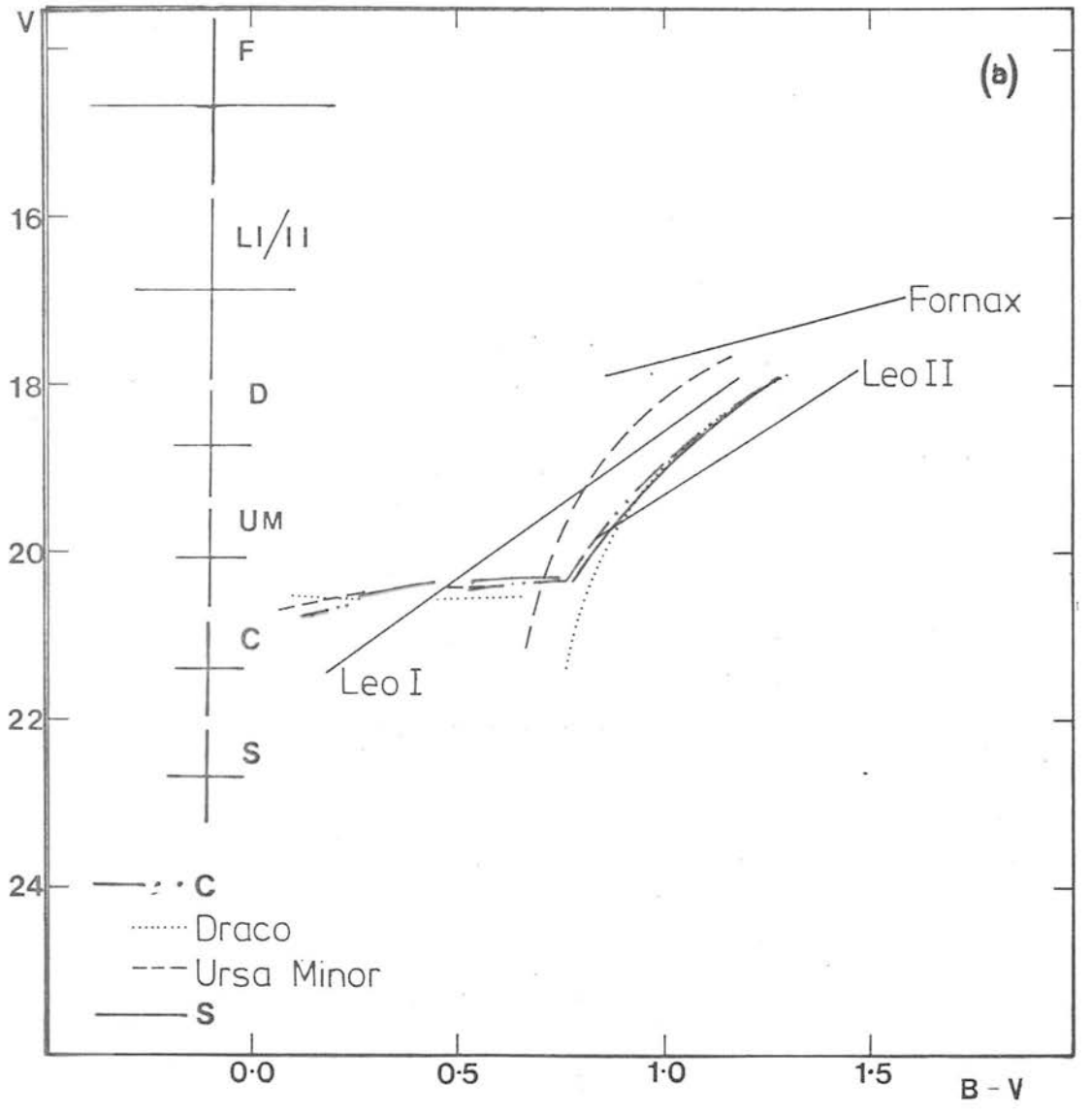

Figure 3.7a,b. The ridge lines of the dwarf spheroidals with estimated average errors (deduced from the literature - see text for references) including that due to the distance modulus error. C=Carina, S=Sculptor, F=Fornax, LI/II=Leo I and Leo II, D=Draco, UM=Ursa-Minor.

colours for the images could be present in the data if there was one or more incorrect measure(s) of the magnitude (especially since the data consists of only three plates in each colour). This was found to be the case in some of the selected images due to them appearing in the vignetted or step-wedge regions of one of the plates causing a false value of the sky background to be calculated and hence an incorrect magnitude determination for the star. When all these images had been eliminated from the sample, 21 remained, and these were examined on a direct IIIaJ and a prism plate of the CDG (plate numbers J8382 and YR7607P respectively).

The vast majority of these stars (as expected) were indeed objects with their flux concentrated towards the red end of their spectrum. In addition to picking up four of the known carbon stars though (C1, C2, C4, C5 in Mould et al 1982), an extra candidate emerged which had the characteristics of these former carbon stars (see plate 3.1, figure 3.1a and table 3.4). For this star (now labelled C9), the apparent V and B magnitudes were 17.75 $\pm$ 0.16 and 20.12 $\pm$ 0.24 respectively, giving an apparent colour of (B-V) = 2.37 $\pm$ 0.29 (see figure 3.1a for its position in the COSMOS colour magnitude diagram for the CDG); however due to the colour of the star being so red, from figure 2.11 it can be seen that the calibration is not well defined. A comparison of the magnitudes of C1 and C6 obtained by Mould et al (1982) is shown in table 3.5, where as they state, their magnitudes too could be in error by as much as 0.1 magnitudes for the same reason.

A recent grism survey of the central regions of the CDG by Azzopardi, Lequeux and Westerlund (1985) confirms the nature of the carbon star candidate found here.

3.3.6 : Variable stars

Searches for variable stars are important since in particular for the RR Lyrae variety, they can provide valuable information on the distance, and indications of the age of the stellar systems in which they are located. Finder charts of the 36 objects rejected from

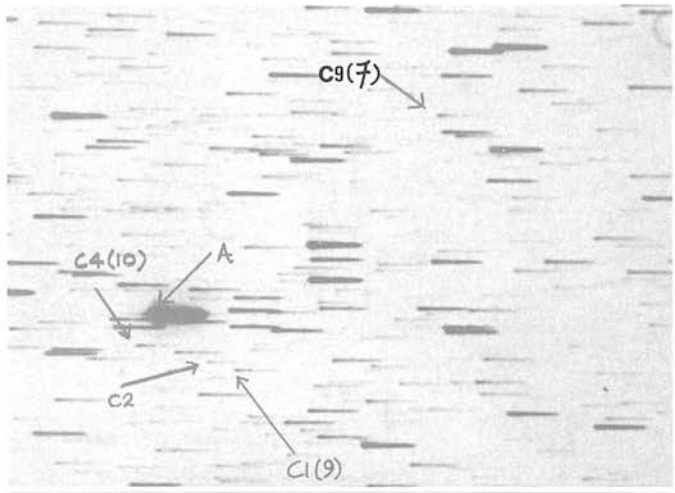

Plate 3.1. Carbon stars in the Carina dwarf galaxy taken from UKST prism plate YR7607P. C1, C2, C4 are three of the carbon stars found by Mould et al (1982), C9(7) is the one identified in this thesis. Numbers in brackets refer to the identifications in table 3.4. Star 'A' is SAO 234657.

TABLE 3.4

MAGNITUDES (X100) OF CARBON STAR CANDIDATES IN THE CARINA DWARF SPHEROIDAL GALAXY

Plate identification

Id	X*	Y	B1386	B1510	B1530	V1387	V1511	V1529	NOTES
1	73	49	1823	2187	2168	1764	1787	1785	1
2	73	55	1948	1966	1973	1750	1760	1768	1
3	72	193	1615	1630	2108	1570	1566	1674	2
4	74	201	1615	1637	2139	1574	1577	1654	2
5	77	214	1597	1634	2145	1560	1573	1610	2
6	101	139	2025	2005	2167	1868	1884	1885	2
7	116	148	2039	1993	2005	1794	1765	1766	C9
8	121	100	2114	2189	2131	1957	1968	1958	2
9	131	127	1890	1884	1890	1701	1685	1679	C1
10	139	129	1983	1974	1942	1736	1741	1734	C4
11	151	141	1901	1940	1936	1724	1735	1725	C6
12	161	57	2106	2178	2131	1951	1958	1949	2
13	166	198	2000	2022	2008	1830	1821	1821	2
14	173	52	2117	2119	2163	1984	1719	2002	1
15	173	214	2068	2194	2082	1925	1923	1924	1
16	175	59	2132	2146	2165	1967	1972	1963	2
17	176	86	2128	2189	2152	1967	1972	1955	2
18	179	78	1948	1951	1968	1760	1758	1771	1
19	178	195	2017	2008	1989	1810	1823	1812	1
20	204	121	2100	2125	2096	1935	1931	1898	1
21	207	218	1933	2176	1946	1811	1810	1829	1

*See Appendix A for finder photograph.

Notes: 1 = Red object but no carbon bands visible

2 = Object not visible on prism plate or overlapped

TABLE 3.5

APPARENT VISUAL MAGNITUDE COMPARISONS
OF KNOWN CARBON STARS

Name	COSMOS Calibrated magnitudes			Mould et al (1982)	
	B	V	B-V	V	B-V
C1	18.88 ± 0.03	16.88 ± 0.11	2.0 ± 0.11	16.92	1.91
C4	19.66 ± 0.22	17.37 ± 0.04	2.29 ± 0.22		
C6	19.26 ± 0.21	17.28 ± 0.06	1.98 ± 0.22	17.39	1.94

the sample of stars by criterion (iv) in sub-section 3.3.1 were made and the corresponding objects examined on the plate material. This was done to see if these objects could be identified as variables, but all were found to be either saturated images, or had pixel areas very close to the corresponding magnitude limit used, making it very difficult to decide whether they were in fact exhibiting real variability. This null result is consistent with the study of Cannon et al (1986) who also found no variables.

3.3.7 : Discussion

The steep giant branch together with the low Mironov index (i.e. red horizontal branch) means that the CDG suffers from the 'second parameter' anomaly. This means that it does not obey the relationship found amongst the vast majority of the Galactic globular clusters between metal abundance and horizontal branch type namely that red horizontal branch clusters are metal rich and blue ones are metal poor (cf 47Tuc data from table 3.1). This is predicted if the clusters have the same ages, helium abundances and C, N and O to Fe ratios but different Fe to H values (the so called 'first parameter'). Stellar evolution calculations have shown that variations in any of the former quantities whilst holding the [Fe/H] ratio fixed can produce the observed range of horizontal branch types among clusters of similar metallicity (Rood 1973, Rood and Seitzer 1981), suggesting that one of these former quantities is the required second parameter needed to explain the colour magnitude diagrams of the dsph galaxies. However, current data on these galaxies is not good enough to conclusively solve the problem, and its solution will have to wait until more accurate and reliable faint photometry down to and below the main sequence turn off point can be made available (to obtain ages to within at most a few Gyr), together with detailed spectroscopic information of their giant branch stars. Faint photometry in Leo I (Olszewski, Suntzeff and Hodge 1985, in preparation) should be published soon and its analysis go some way to resolving this problem, but much more data on all of the dsph galaxies is required.

A red horizontal branch is found in the globular cluster NGC7006 (Sandage and Wildey 1967), which is known from photometry of individual stars to be extremely metal deficient (Canterna and Schommer 1978a). A blue horizontal branch is found in NGC288, which is known to have a fairly high metal content (Cannon 1974, Godwin and Sagar 1986 in preparation). Hence whilst a red horizontal branch may indicate a metal enrichment (as compared to say the majority of halo clusters), it is certainly not a sufficient condition. Rood (1973) and Renzini (1981) showed that even quite small changes in the essentially arbitary mass loss parameter for stars on the first giant branch evolving towards the horizontal branch could lead to great variations in the latter's structure. Rood and Seitzer (1981) showed that minor variations in any of several parameters especially at the low metallicities of the dsph galaxies (e.g. $Z \sim 0.001$ to 0.0001) could also suffice to do the same trick. If the evolutionary model of Hartwick (1976) is to be believed, where the metal poor globular clusters formed first with the metal rich ones forming later after the proto-Galaxy gas cloud collapse time of 150 million years (Eggen, Lynden-Bell and Sandage 1962) then Rood (1973) calculated that this short time scale would produce negligible effect on horizontal branch morphology, a time scale of at least 1 Gyr being required. Hence it would seem on the face of it that age cannot be the second parameter needed to explain the anomalous globular cluster colour magnitude diagrams in this picture of the latter's formation. However, age could still be the second parameter in the case of the outer halo red horizontal branch clusters and dsph galaxies, since it is reasonable to expect that either tidal forces (creating the necessary conditions for the formation of tidal shocks) or the passage of a globular cluster/dwarf spheroidal through the Galactic disk could lead to an environment ready for star formation. This is given added weight by the observational evidence of Da Costa (1984) and Mould and Aaronson (1983) which suggests that star formation did not occur at one particular epoch in these systems but over a number of generations (for Sculptor and Carina respectively).

To examine this further, figure 3.8 shows the metallicity gradient in the Galaxy, using globular cluster data taken from Zinn

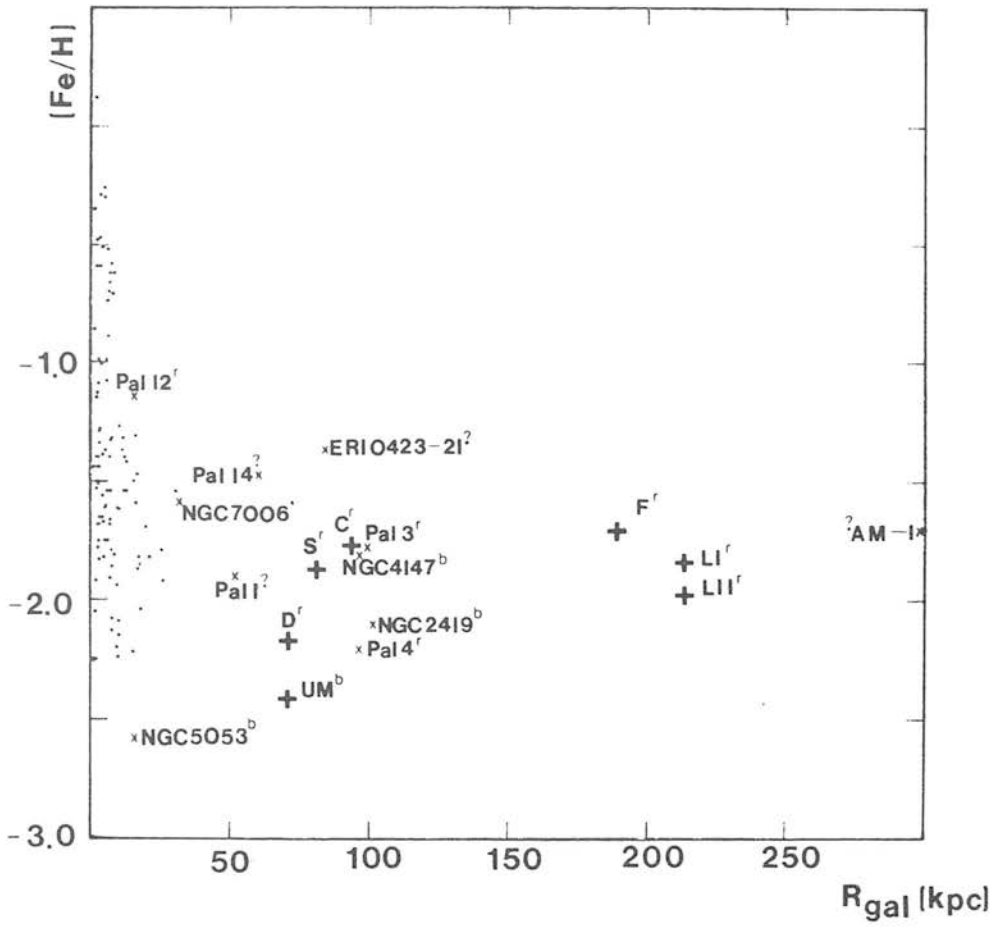

Figure 3.8. The metallicity gradient in the Galaxy (for errors on the mean metallicities and the distances to the dwarf spheroidals, see table 5.4). Error on globular cluster mean metallicities are typically better than 0.1 (Zinn and West 1984), and the error on their distances better than 10 kpc (Madore 1978). The key to the symbols is as follows:

^{r} denotes red horizontal branch type
$_{b}$ denotes blue horizontal branch type
$^{?}$ denotes unknown horizontal branch type
+ denotes dwarf spheroidal galaxy
and . denotes Galactic globular clusters

and West (1984) and the mean metallicities of the dsph galaxies from table 5.4 . Also plotted is the type of horizontal branch present in the system (for the outer halo clusters) including that of the CDG. As can be seen, if all the clusters plotted are directly related to the early evolution of our Galaxy, then a theory for their origin has to explain e.g. (a) the mixture of blue and red horizontal branch objects in the inner and outer halo, and (b) the apparent flattening of the metallicity gradient at 10 to 20 kpc (but see Pilachowski 1984). Searle and Zinn (1978) explained this by suggesting that during the very early stages of the Galaxy's formation, the metal abundance of the central regions grew rapidly, out of which the metal rich clusters formed quickly. The clusters in the outer regions then formed over a prolonged period out of the much more slowly free falling uncontaminated material giving rise to the observed spectrum of horizontal branch types. Orbital mixing could then populate the outer halo with both red and blue horizontal branch type systems. This contradicts the Eggen, Lynden-Bell and Sandage (1962) picture, but a prolonged formation time to account for these differences has also been put forward by Yoshii and Saio (1979) who claim that a slow contraction of the Galaxy on a time scale $\sim$3 Gyr can give rise to all of the kinematical properties of old Galactic stars if the primordial gas had random motions.

Alternatively, the fact that amongst the outer halo clusters both red (e.g. NGC7006, Pal 4, 12, 13) and blue horizontal branches are found, could be suggesting something completely different e.g. that the globular clusters and the dsph galaxies originated in different environments. The tidal origin (Lynden-Bell 1976, Kunkel 1979), in which the dwarf spheroidals (and perhaps the 'anomalous' globular clusters too) were tidally pulled from a 'Greater Magellanic Cloud', the precursor of the presently observed LMC and SMC is particularly appealing since these systems have been found to be non-randomly distributed in the sky, being aligned in one of two Magellanic Planes (see section 1.1). This in relation to the gravitational influence that the Galaxy must now be exerting on the dsph galaxies is discussed further in chapter 5.

3.4 : SUMMARY AND CONCLUSIONS

The results of this chapter show that the CDG is similar to the majority of the other dsph galaxies (apart from possibly Ursa-Minor) in the sense of : (a) suffering from the second parameter anomaly (b) having a predominantly red horizontal branch, (c) an (extended) asymptotic giant branch, (d) a steep giant branch and hence presumably a relatively low metallicity as compared to the Galactic globular clusters and (e) the hint of an intrinsically broad first ascent giant branch which indicates a possible spread in metal abundance. This latter feature deserves further comment as it could provide possible clues to the origin and subsequent evolution of these galaxies. Five possible explanations (not necessarily mutually exclusive) are that any broadness is

(a) caused solely by the presence of an asymptotic giant branch. Although this is unclear from the previous work on other dsph galaxies, it does appear from the data here that this is not the case for the CDG. This is because the low luminosity counterpart of the extended giant branch has been identified in this galaxy by essentially comparing its position in the colour magnitude diagram with that predicted by Lee (1976) from globular clusters of similar metallicity, and separating it out from the population of first ascent giant stars. The broadness is still apparent when compared with the tight giant branches of the chemically homogeneous globular clusters which are known to have very little metallicity dispersion from spectroscopy of their giant stars.

(b) due to the metallicity spread resulting from e.g. the galaxy forming out of an inhomogeneous proto-galactic gas cloud. Globular cluster ridge line comparisons and the value of the dispersion in the colour of the first ascent giant branch, over the magnitude range slightly brighter than that of the intersection of this branch with the red horizontal branch have been used to give an estimate of the mean metallicity of the CDG to be [Fe/H] = -1.8 ± 0.3 with a possible spread ~ 0.26. Chemical variations within the dsph galaxies have been found in e.g. Draco (Zinn 1978a), Ursa-Minor (Zinn 1981) and

Fornax (Zinn and Persson 1981). In the case of the Sculptor dsph galaxy, [Fe/H] and/or [Ca/H] variations have been identified (Norris and Bessell 1978) and it is thought to contain cyanogen enhanced giants (Smith and Dopita 1983). In Ursa-Minor, oxygen rich first ascent giant branch stars have been found, unlike any in the other dsph galaxies, which may account for the anomalous blue horizontal branch found in this galaxy (Aaronson and Mould 1985), but this is uncertain.

(c) a result of the mixing of nuclearly processed material into the envelope of a stellar member during evolution, or due to some sort of binary accretion process. If this is to be believed though, it is unclear why this should happen in dwarf spheroidals and not in the vast majority of the globulars, unless perhaps their origins were significantly different.

(d) due to an age spread, caused by multiple or continuous star formation periods. This could also lead to a metallicity dispersion being present. The possibility of the broadness of the giant branch being caused solely by an age spread is examined in the next chapter.

(e) related to another scenario for their origin. It could be that the large masses of the dsph galaxies (Hodge 1971), unlike the globular clusters, were capable of retaining their nuclearly procesed material of highly evolved stars for further star formation periods. The Draco dsph galaxy with a mass that is thought to be similar (see table 5.4 and chapter 5) to that of the CDG, has been found to have practically the same spread in [Fe/H] (Zinn 1978a) as tentatively suggested here for the CDG, and gives some encouragement to this idea.

Only two globular clusters are known to have a significant metallicity dispersion, viz. M22 (Norris and Freeman 1983) and ω Cen (Cannon and Stobie 1973). The latter cluster also appears to have a broad giant branch, and is also the most luminous (M_V = -10.4, Webbink 1985), and hence is presumably the most massive globular cluster. Using a globular cluster M/L ratio of 1.7 (see e.g.

Illingworth 1975), and a value of $M_V(\theta) = 4.71$ (Allen 1955), an approximate mass of $2 \times 10^6 M_\theta$ is obtained for this cluster, which is intermediate to the masses obtained by Hodge (1971) for the Leo II and Sculptor dsph galaxies (see table 5.4). Hence the idea of the more massive systems having larger ranges in metallicity and the capability for further periods of star formation than the less massive ones simply because of their larger velocity of escape, might go some way towards explaining the broad giant branches in the dsph galaxies. There is some doubt now (see chapter 5) as to whether the Hodge (1971) masses of the dsph galaxies are reliable, being based on an assumption that the luminosity functions of these galaxies and the globular clusters are similar in shape. This is explored further in the following chapters.

Another similarity between the dsph galaxies and the globular cluster ω Cen is that both contain carbon stars (Azzopardi, Lequeux and Westerlund 1985) which are generally associated with a young to intermediate age population. This type of star identified in the CDG here (see also chapter 6), together with the lack of variable stars and the extended asymptotic giant branch in the CDG, all seem to be consistent with the idea that a large proportion of the Carina dwarf's population is significantly younger than that of the globular clusters (~15Gyr). This is in accord with the main sequence turn-off age for the CDG found by Mould and Aaronson (1983) to be 7 ± 2 Gyr. This is also discussed further in the next chapter in relation to the Carina dwarf's luminosity function, and the fitting of isochrones to its giant branch.

4.1 : Introduction

In this chapter, the Ciardullo and Demarque (1977a, hereafter CD) isochrones are fitted to the (V,B-V) values of the COSMOS CDG giant branch stars. Mould and Aaronson used their CCD main sequence data to infer from the main sequence portion of these isochrones a turn off point yielding an age of 7 ± 2 Gyr. There are uncertainties in the way that these latter isochrones have been fitted though e.g. (a) it is unknown whether there is a blue straggler population in the CDG which would tend to make the turn off point apparently more luminous than it actually is and hence the galaxy would be older than 7 ± 2 Gyr, and (b) the CD isochrones have all been calculated for a convective mixing length parameter $\alpha = 1.0$ which from the work of VandenBerg (1983) seems to be an underestimate. He finds $1.5 \leq \alpha \leq 1.7$ a more appropriate value for globular cluster main sequence fitting. The effect of this parameter on giant branch morphology is also examined here, using the mean metallicity value for the CDG found in chapter 3.

Luminosity functions are important since they are determined by exactly the same parameters that affect the morphology of the colour magnitude diagram discussed in chapter 3. Such a function is presented here for the CDG, based on COSMOS counts, reaching down to a luminosity slightly greater than the horizontal branch. This, together with that derived for the main sequence by Mould and Aaronson (1983), is compared to the observational luminosity function of the globular cluster M3 (Sandage 1957). The practical problems of obtaining reliable star counts, such as those due to crowding, foreground stars/background galaxy and incompleteness are also discussed.

4.2 : Isochrone modelling

Isochrone fitting to the observational data depends essentially upon six parameters associated with the object concerned. These are

(a) the reddening in the direction of the cluster
(b) its apparent distance modulus
(c) its age
(d) its metallicity
(e) the helium abundance Y adopted, and
(f) the value chosen for the parameter α

To convert the CD isochrones to those with a different α, the following corrections can be applied to their tabulated values of T_{eff} and log(g) (where g is the surface gravity of the star) with $\alpha = 1$

$$\delta(\log_{10}(T_{eff})) = \beta^{*}.[0.021\log_{10}\left(\frac{L}{L\odot}\right) + 0.143]\log_{10}\alpha \qquad (4.1)$$

$$\delta(\log_{10}(g)) = 4.0\delta(\log_{10}(T_{eff})) \qquad (4.2)$$

where β^{*} = 1 for the giant branch and 0.2 for the main sequence (Ciardullo and Demarque 1979). The change in luminosity due to a change in α is minimal (Sweigart 1978) and hence the correction represented by equation 4.2 will not be used here. Although $\log(T_{eff})$ is approximately proportional to $\log(\alpha)$ on the giant branch, it certainly is not on the main sequence, a point which can be seen quite clearly from the evolutionary tracks of Sweigart and Gross (1978). The CD isochrones will be used here to fit the COSMOS CDG giant branch data, employing equation 4.1 to give isochrones with differing values of α.

Formal statistical fitting procedures of isochrones to observational data are surprisingly few. Flannery and Johnson (1982) used a χ^2 statistic to measure the goodness of fit of a colour magnitude diagram to the CD main sequence and sub-giant branch isochrones. Janes (1981) used a (M_V,B-V) classification of the colour magnitude diagram ridge line by comparing the theoretical predictions at M_V = 0 through to 6 for $(B-V)_o$ with observations. It is important to stress however, that the best fitting isochrone is obtained from the visual inspection of the whole of the available colour magnitude diagram features, not separate portions, which is why the composite colour magnitude diagram of the CDG has been constructed here to do this fitting to (see e.g. figure 3.2).

There are a number of useful points that can be derived by simply comparing theoretically constructed isochrones which can be borne in mind when fitting them to the data (see figure 4.1). For example the blueward shift of the red giant branch as Y or α increases and an opposite shift as age or Z increases. Figure 4.1 also shows just how important the choice of mixing length parameter α is in affecting the position of the giant branch. For the CDG, the mean value of Z will be used, as found in chapter 3 , and Y will be taken to be 0.2 (VandenBerg 1983). This latter parameter is a big uncertainty in all evolutionary predictions since it cannot be measured directly; it is not observable in the relatively cool unevolved main sequence stars nor in the red giants. Hence the main parameter allowed to vary in the fitting procedure below is the age, and on the giant branch α.

Transformations from the theoretical to observational planes can be achieved by using a grid of model stellar atmospheres, with bolometric corrections and colours computed for low metallicities and the known reddening corrections. The VandenBerg (1983) main sequence isochrones (shown in figure 4.1) are given in a form ready for direct comparison with observations, and so no such transformations were required for this data. However a transformation was needed for the conversion of the CD isochrones. All the data in (V,B-V) space from the theoretically defined (T_{eff},M_{bol}) CD isochrones were calculated

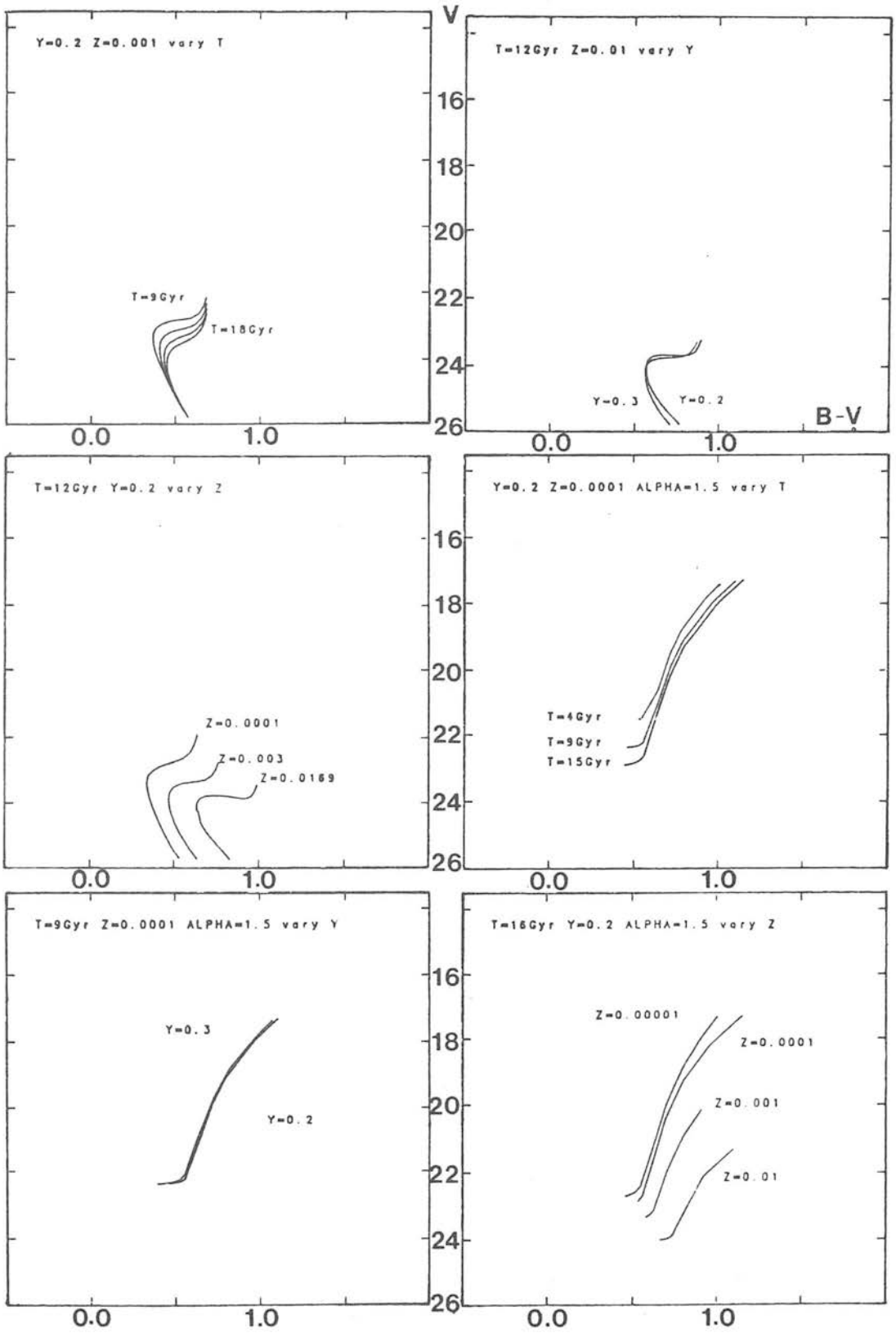

Figure 4.1. Theoretically defined main sequence and giant branch isochrones from VandenBerg (1983) and Ciardullo and Demarque (1977a) respectively. These plots are on the same relative scale as figure 3.1a, and are adjusted for the reddening and distance to the Carina dwarf galaxy.

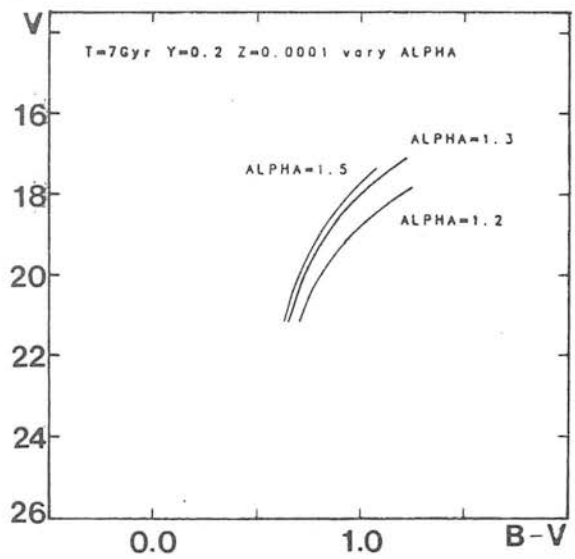

Figure 4.1 (cont.)

by fitting polynomial functions to the (T_{eff},B-V) and (T_{eff},B.C.) data for [Fe/H] = -2.0 taken from Bell and Gustaffson (1978), and the resulting transformations were applied to the isochrones. The polynomial fitting package mentioned in chapter 2 allowing fits of up to order 9 was used and the one giving the smallest RMS deviation was employed. For the $\log(T_{eff})$ to (B-V) transformation, a fifth order polynomial was used and a third order one for the $\log(T_{eff})$ to bolometric correction transformation. The method of fitting the isochrones to the colour magnitude data was then as follows:

(a) fix the helium abundance at Y = 0.2

(b) fix the age via the main sequence turn off point

(c) Use the mean metallicity found in chapter 3 and a suitable value of α to fit the giant branch, trying at the same time to get the slopes of the sub-giant branches correctly aligned.

A graphics package available on the STARLINK VAX 11/780 (Aspin, private communication) then allowed direct overplotting of the isochrones onto the relevant colour magnitude diagram displayed on an ARGS TV display unit.

4.2.1 : Carina and Sculptor dwarf isochrone fits

Consider first the fit of the main sequence Carina dwarf stars to the CD isochrones for α= 1.0 as done by Mould and Aaronson (1983) in order to pin down the Carina dwarf's age. The CD main sequence isochrones for Y = 0.2, Z = 0.0003 (interpolated value from CD isochrone tables), α = 1.0 and T = 7 and 9 Gyr are shown in figure 4.2a. VandenBerg (1983) found that for main sequence stars in globular clusters a more appropriate value for α was 1.5, but as mentioned earlier, a shift in this parameter has negligible effect on the luminosity of the main sequence turn off point, and from the VandenBerg (1983) and Ciardullo and Demarque (1979) isochrones it can be calculated that the biggest shift in the colour due to α varying from 1.0 to 1.5 at this metallicity and age would be $\sim$0.03 magnitudes

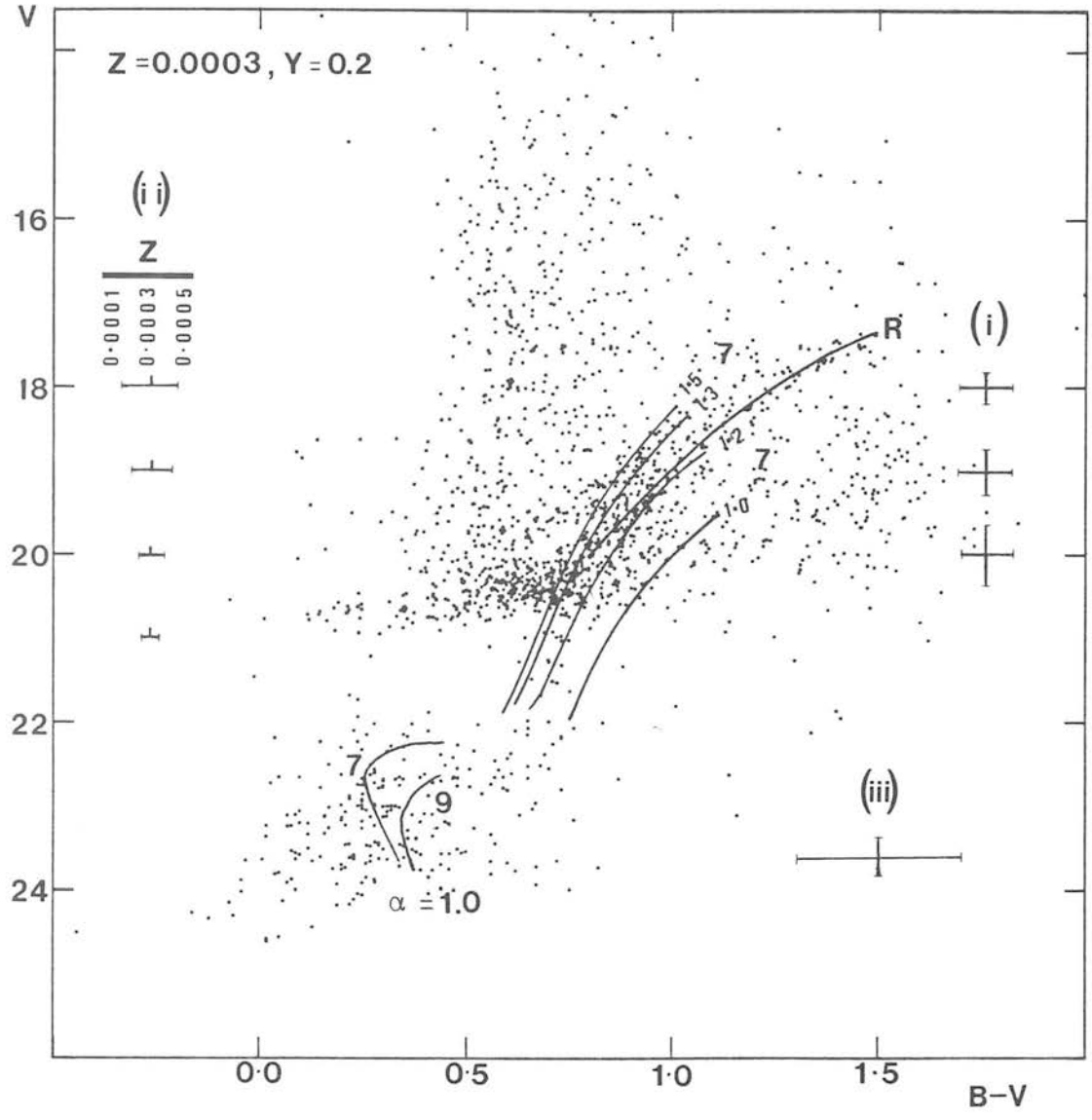

Figure 4.2a. Isochrone fits to the Carina dwarf galaxy giant branch COSMOS, and main sequence Aaronson and Mould (1983) data. R denotes ridge line for the red giant branch found in chapter 3. CD giant branch isochrones shown for α=1.5, 1.3, 1.2 and 1.0, T=7 Gyr, z = 0.0003 and Y = 0.2. CD main sequence isochrones shown for T = 7 and 9 Gyr with α=1.0, z=0.0003 and Y=0.2. Error bars (i) show estimated error on ridge line R definition. Error bars (ii) show the range allowed in the mean metallicity of the Carina dwarf ($0.0001 \leq z \leq 0.0005$), and error bars (iii) the internal 1σ error on each individual star magnitude in the Mould and Aaronson (1983) main sequence data.

to the blue. Hence if the clump of stars in their data at $V \sim 23$ magnitude is interpreted as the real main sequence (i.e. neglecting any contamination from the possible presence of blue stragglers), then their age estimate of 7 ± 2 Gyr seems quite reasonable (and in any case is a good lower limit to the age of the CDG). Adopting this value, consider now the fit of the CD isochrones to the COSMOS giant branch data. Figure 4.2a shows the 7Gyr isochrones for various values of α and Z = 0.0003, Y = 0.2. The left hand error bars (ii) are those on the isochrones due to the error on the mean metallicity found in chapter 3 ([Fe/H] = -1.8 ± 0.3). Using a solar metallicity of 0.0169 (see e.g. VandenBerg 1983) then by definition of Z

$$\log_{10} Z_{obj} = [Fe/H]_{obj} - 1.772 \qquad (4.3)$$

Hence the range for the mean value of [Fe/H] above implies a range of 0.0002 either side of 0.0003 in the value of Z for the CDG. The error bars on the right hand side (i) are due to the error in the definition of the ridge line R of the red giant branch. These error bars effectively rule out a value of $\alpha = 1.0$ on the CDG giant branch, even for the metal rich end of the range (0.0005), a value of $\alpha = 1.25\pm0.1$ seeming more likely.

However, what happens if the Mould and Aaronson (1983) age estimate is incorrect and e.g. there does exist a blue straggler population in the CDG which makes the main sequence turn off point indeterminate. The age in this case has to be older than 7Gyr and figure 4.2b shows the fit of a 12 and 15 Gyr isochrone to the CDG data for Y = 0.2, Z = 0.0003 and $\alpha = 1.5$. The ridge line in this case can barely fit the 12 and 15 Gyr isochrones to within the errors even if a metallicity of Z = 0.0005 is taken (cf especially the high luminosity end of R). If α is taken to be smaller than 1.5, a fit can be achieved but in both these cases the slope of the theoretical giant branches are not as similar in the previous case to that of R. This result is also found to be true for Sculptor. Da Costa (1984) has fitted the CD main sequence and sub-giant branch isochrones,

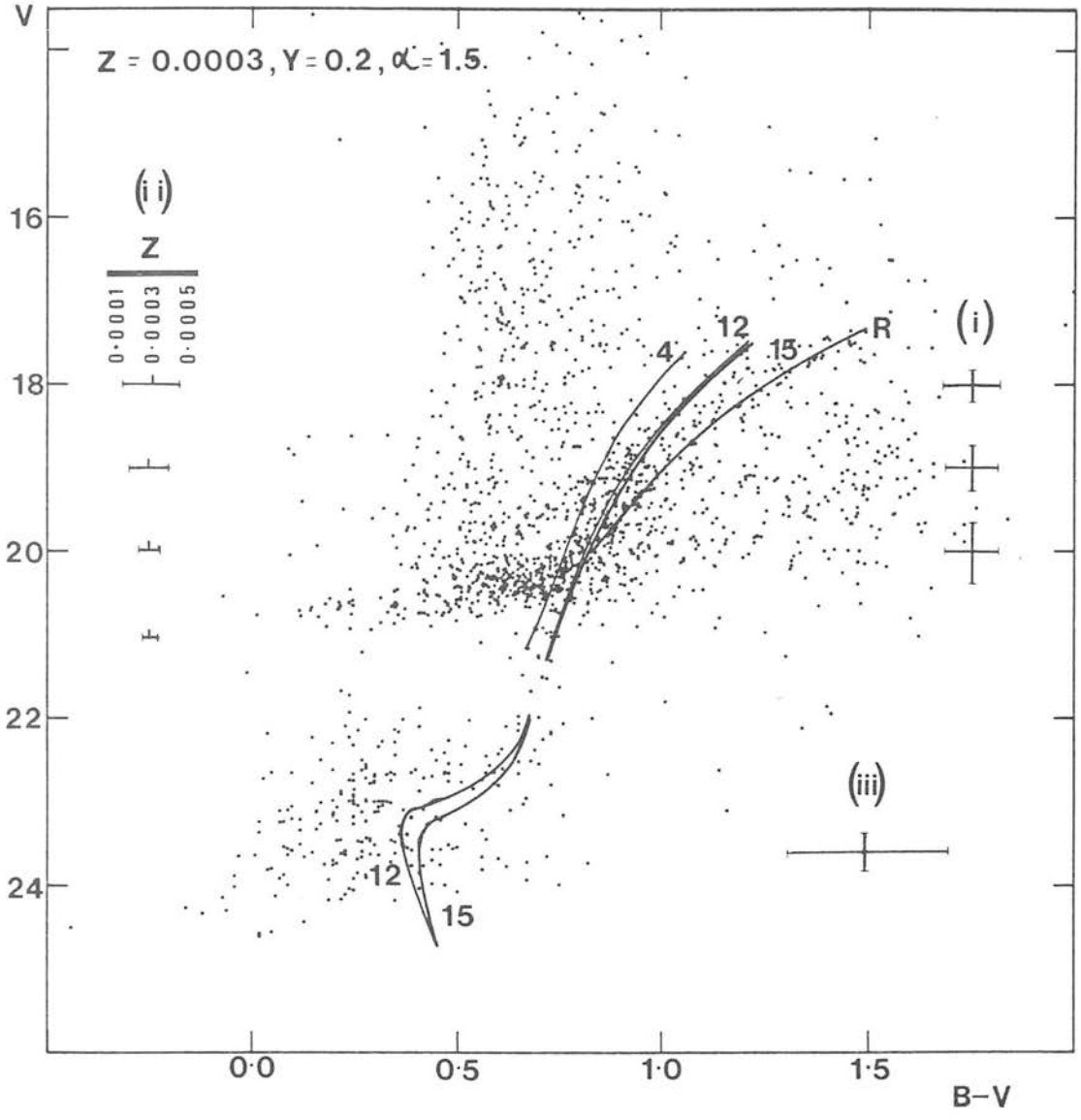

Figure 4.2b. Isochrone fits to the Carina dwarf galaxy giant branch COSMOS, and main sequence Aaronson and Mould (1983) data. R denotes ridge line for the red giant branch found in chapter 3. CD giant branch isochrones shown for T=4, 12, 15 Gyr, z=0.0003, Y=0.2 and α=1.5. VandenBerg (1983) main sequence isochrones shown for T=7 and 9 Gyr with z=0.0003, Y=0.2 and α=1.5. Error bars as in figure 4.2a.

shifted to a value of α = 1.5, to his CCD data for the Sculptor dwarf. Spectroscopy in this galaxy seems to indicate that $-1.5 \geq [Fe/H] \geq -2.2$ (Norris and Bessell 1978) i.e. using equation 4.3, $0.0005 \geq Z \geq 0.0001$, which puts constraints on the metallicity Z of the isochrones to try for the fitting.

Figure 4.3 shows the composite colour magnitude diagram of the Sculptor dsph galaxy, and also the new VandenBerg (1983) main sequence isochrones and the CD giant branch isochrones for the labelled different values of the age and α respectively. The red giant branch ridge line R' was found in an analogous way to that of the Carina dwarf's R red giant branch ridge line, but using the data of Kunkel and Demers (1977). Da Costa (1984) found an age of 13 ± 2 Gyr for the Sculptor dwarf from the luminosity of its main sequence turn off point (see figure 4.3), and like the CDG data, the whole of the giant branch (especially the slope of this latter branch's high luminosity tip) when the errors on the observational data are considered (see figure 4.3) fits best when a value of α is chosen $<$ about 1.35 and $>$ 1.0. This again is somewhat lower than that derived empirically by VandenBerg (1983) for the main sequence stars of 15 Galactic globular clusters, but with the constraints (a) to (c) in section 4.2, this seems the only way to achieve reasonable fits to the data of these galaxies.

4.2.2 : Discussion

There are a number of problems associated with fitting isochrones to the CDG and Sculptor observational data. Perhaps the most important of these with this data is that of the possible presence of a blue straggler population (more noticible in the CDG data - cf. figures 4.2 and 4.3) at a luminosity slightly above that of the main sequence. This makes the age determination of the CDG uncertain. These stars are thought to be hydrogen burning stars anything up to twice as massive as the current turn off point stars (Cannon 1968), and a number of explanations for their existence have been made e.g. that they have their origin in binary mass transfer or are simply stars that for some reason have been born late (Wheeler

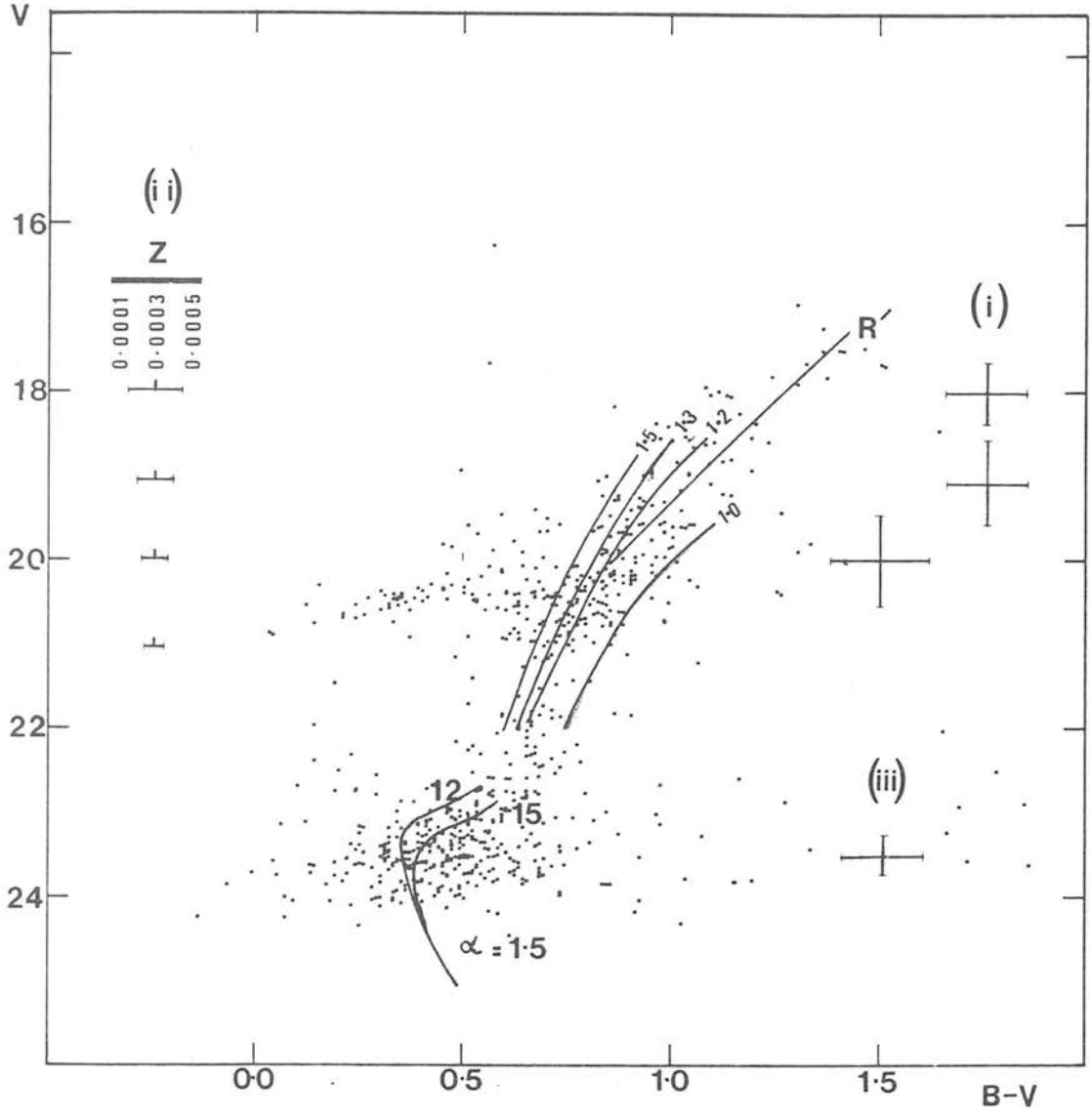

Figure 4.3. Isochrone fits to the Sculptor dwarf galaxy (composite) colour magnitude diagram data. R' denotes ridge line for the Sculptor dwarf's red giant branch. CD giant branch isochrones shown for Y=0.2, T=12 Gyr, z=0.0003, α = 1.0, 1.2, 1.3, 1.5. VandenBerg (1983) main sequence isochrones shown for T=12 and 15 Gyr with Y = 0.2, z = 0.0003, α=1. 5. Error bars (as in figure 4.2a) for (i) the ridge line R', (ii) the metallicity variation $0.0001 \leq z \leq 0.0005$ and (iii) the internal 1σ error on each individual star magnitude in the Da Costa (1984) main sequence Sculptor dwarf data.

1979). It could well be though that the not very well defined turn off points in the dsph galaxies' colour magnitude diagrams might be due to some other phenomenon such as multiple star formation episodes as discussed in chapter 3. Another problem is that the CD isochrones do not take into account mass-loss on the giant branch, and equation 4.1 is at best only an approximation for the whole of the giant branch. However, this may not be a serious problem at the low metallicities involved here (see e.g. Castellani and Tornambe 1981).

The discrepancy in α on the giant branch to that generally adopted on the main sequence for the observational data if real is interesting since it implies a change in a star's atmospheric structure as it evolves. Here, a value of α certainly < 1.5 and probably somewhere between 1.35 and 1.0 seems to fit the giant branch best; most of the previous work suggesting that α be taken to be 1.5 or slightly greater has come from main sequence studies e.g. VandenBerg (1983), VandenBerg and Bridges (1984). Could therefore this be (very) tentative evidence to suggest that this parameter can change with different evolutionary phases? There is no particular reason to suppose that it remains constant throughout a star's evolution and in fact Simoda and Iben (1970) suggested that α may well vary for stars with different surface temperatures, but they also found that similar effects were caused by changes in the opacity determination. Armandroff and Demarque (1984) tried to explain the gaps seen on the sub-giant branches of several globular clusters in terms of variations in α, but without success, and Deupree (1979) seriously questioned the 'crude' nature of the α formalism in handling the convection theory. Hence it could well be that it is the method itself that is too simplistic.

Earlier in sub-section 3.3.4 an estimate of the metallicity dispersion required to explain the width of the giant branch was made. Could a large age difference also explain this? From figure 4.2b, the difference between the T = 4 and 15 Gyr theoretical isochrones (Z = 0.0003, Y = 0.2, α = 1.5) in (B-V) measured at the same luminosity level as σ_{GB} in sub-section 3.3.4 is approximately 0.05 magnitudes. If this difference is considered to be a 4σ spread,

then a galaxy with a continuous star formation history over a period of 11 Gyr starting at the time of formation of the globular clusters should have this fact reflected in its giant branch having an intrinsic width $\sim$ 0.01 magnitudes in (B-V) (neglecting any metallicity dispersion that may or may not result). This is too small an effect to disentangle from the effect of a metallicity dispersion (changing α to a smaller value has little effect on this result) i.e. an age spread of 11 Gyr alone cannot account for the intrinsic width of the Carina dwarf's giant branch found earlier.

4.3 : The luminosity function of the Carina dwarf

To determine a luminosity function for the CDG in the case of the present data involves two difficulties: the loss of images at the faint end of the photometric range, and the contamination by foreground stars and background galaxies. These questions of completeness and contamination were discussed in some detail in sub-section 3.3.1 where it was shown that galaxy images are effectively removed through the reduction procedures and also that loss of images becomes significant only at magnitudes V $\sim$ 19.5 (table 3.3).

The efficiency of rejection of the blended image and galaxy component from the initial sample of images used by simply inserting an ellipticity cut, can be seen by plotting the magnitude against the logarithm of the pixel area of each image (see figures 4.4a and b). The blended image/galaxy component of the sample can be seen to lie in the region of images with a higher area for their magnitudes relative to stellar images. In the sample of images taken here as 'stellar' (see sub-section 3.3.1) for the luminosity function derivation, the approximate contamination by this component is 2%. This was calculated by assuming that the stellar sequence is symmetrical about a mean locus and manually drawing a star-blended image/galaxy separation line (see figure 4.4b). This contamination value can then be evaluated by calculating the ratio of the number of images above this line to those below it. This result confirms that of chapter 3, that the ellipticity cut ELLIM used for the COSMOS data

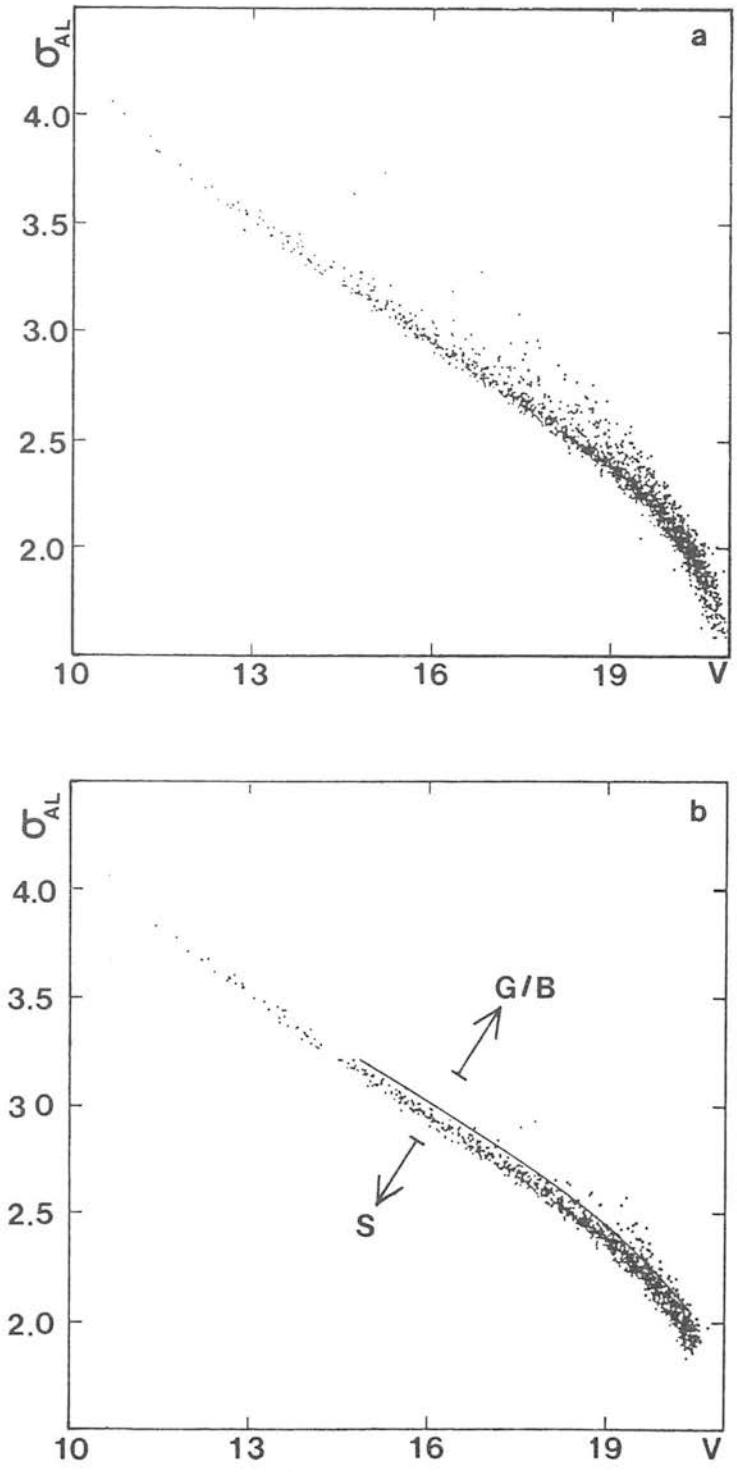

Figure 4.4.a,b. Star-galaxy separation plots for (a) all images in selected region, (b) images classified as 'stellar' (see sub-section 3.3.1). The solid curve in (b) represents the manually drawn star-galaxy separation line with those objects in the direction of 'S' from this line being defined as stellar images, and those in the direction G/B being defined as background galaxy and blended objects.

has eliminated most of the background galaxy contamination from the 'stellar sample' defined in that chapter.

As described in chapter 3, the Galactic star count model of Robin and Creze (1984) was used both to calculate the correction for image losses among the faint stars and also to provide the foreground Galactic star correction. The stars of the CDG falling in the giant and horizontal branch regions of the colour magnitude diagram between the limits shown in figure 3.4a, satisfying the inequalities 3.12, were binned differentially in absolute magnitude bins of size 0.2 magnitudes (columns 1 and 2 of table 4.1). Star counts in the same magnitude bins and within the same limits on Robin and Creze's colour magnitude diagram of Galactic stars (figure 3.3) gave foreground counts. In the case of the faintest bins, where the present counts suffer image losses, a comparison of the purely Galactic counts outwith the set limits in the CDG and Galactic colour magnitude diagrams gives the fraction of images lost in each bin in the CDG field. The counts within the set limits were scaled up to allow for the lost images before subtraction of the foreground counts. The correction virtually doubles the observed counts in the faintest two bins, with correspondingly large uncertainties in the final numbers. The last column of table 4.1 gives fully corrected star counts in the CDG for the giant and horizontal branches.

4.3.1 : Comparison of the Carina dwarf and M3 luminosity functions

The results of chapter 3 indicate that M3, at least as far as the slope of its giant branch (and hence metallicity) is concerned would be a good globular cluster with which to compare the luminosity function of the CDG. The usual procedure of comparing globular cluster luminosity functions is to normalise the two data sets at the horizontal branch level, but as discussed above and in the previous chapter, the CDG is now thought to contain a population of stars much younger than those found in globular clusters, and since the horizontal branch numbers are strongly dependent upon age, this would not be a sensible way to proceed for the comparison being done here. The way adopted here to normalise the CDG and M3 data sets therefore

TABLE 4.1

THE LUMINOSITY FUNCTION OF THE CARINA DWARF GALAXY

	WITHIN SELECTION LIMITS[1]		FOREGROUND COUNT[2]		
M_V	$\Delta N \pm \sqrt{N}$ (COSMOS counts)	ROBIN AND CREZE (1984) counts[3]	COSMOS data	ROBIN AND CREZE (1984) counts[3]	COSMOS count[4]
-3.0	0	0			0
-2.8	2 ± 1	0			2 ± 1
-2.6	3 ± 2	1 ± 1			2 ± 2
-2.4	14 ± 4	2 ± 1			12 ± 4
-2.0	17 ± 4	5 ± 2			12 ± 4
-1.8	12 ± 3	7 ± 2			5 ± 4
-1.6	16 ± 4	11 ± 2			5 ± 4
-1.4	19 ± 4	13 ± 3			6 ± 5
-1.2	24 ± 5	16 ± 3			8 ± 6
-1.0	27 ± 5	19 ± 4			8 ± 6
-0.8	39 ± 6	16 ± 3			23 ± 7
-0.6	45 ± 7	23 ± 4			22 ± 8
-0.4	52 ± 7	19 ± 4			33 ± 8
-0.2	65 ± 8	19 ± 4			46 ± 9
+0.0	66 ± 8	23 ± 4	19 ± 4	29 ± 4	78 ± 29
+0.2	65 ± 8	17 ± 3	23 ± 5	25 ± 4	53 ± 21
+0.4	109 ± 10	19 ± 4	15 ± 4	28 ± 4	185 ± 65
+0.6	132 ± 11	16 ± 3	17 ± 4	39 ± 5	286 ± 84

TABLE 4.1 (contd.)

[1]Count taken within the selection limits L and L' of figures 3.3 (Robin and Creze 1984) and 3.4a (COSMOS).

[2]Count taken outside the selection limits L and L' of figures 3.3 (Robin and Creze 1984) and 3.4a (COSMOS).

[3]Scaled to same area as COSMOS counts.

[4]The final Carina dwarf giant branch luminosity function, corrected for incompleteness and foreground count.

is to assume that the shape of the ZAMS luminosity function of both these systems are the same. This means that the Mould and Aaronson (1983) counts will have to be used since the COSMOS counts do not reach as faint as the main sequence. Further, since the main sequence turn-off for M3 occurs at around $M_V = +3.9 \pm 0.1$ (see VandenBerg 1983) and the Mould and Aaronson (1983) counts only go as faint as $M_V = +4.1$, then the normalisation will be done at the faint end. Figure 4.5a shows the main sequence counts of Sandage (1957) for M3 shifted in logN space by -1.01 to coincide with the Mould and Aaronson (1983) main sequence counts (plotted on figure 4.5b), which had already been corrected for incompleteness). It is seen that the shape of the two luminosity functions in figure 4.5 have the same overall trend. This normalises the Mould and Aaronson (1983) data with that of M3. What is now required is the normalisation of the Mould and Aaronson (1983) data with the COSMOS giant branch data so that the latter data can be normalised to that of M3.

The area of sky covered by Mould and Aaronson's investigation is smaller by a factor of 35 than in the present work. However, the latter very extended field has a considerably lower overall star density than that of Mould and Aaronson's which is close to the centre of the CDG. To allow for the difference in star density between the two fields the results of chapter 5 are anticipated, where the profile of the CDG, in the form of relative star numbers per unit area as a function of radial distance from the centre of the CDG, is fitted to a theoretical model (figure 5.5) in which radial distance is in units of the core radius of 9.7'. It is assumed that the luminosity function of the CDG is the same throughout; therefore the magnitude limit of the stars used to establish the profile is not of interest at the present juncture. Mould and Aaronson's field is at a distance of 1.33' from the centre of the CDG where from figure 5.5 the star density is 0.97 of the central density. The average density from the same model over the area covered by the present anaysis is 0.31 of the central density. To normalise Mould and Aaronson's counts to the present ones requires multiplication by a factor $35 \times 0.31/0.97$ or a shift of 1.05 (± 0.08) in logN space, the uncertainty allowing for the errors attached to the profile fitting discussed in chapter

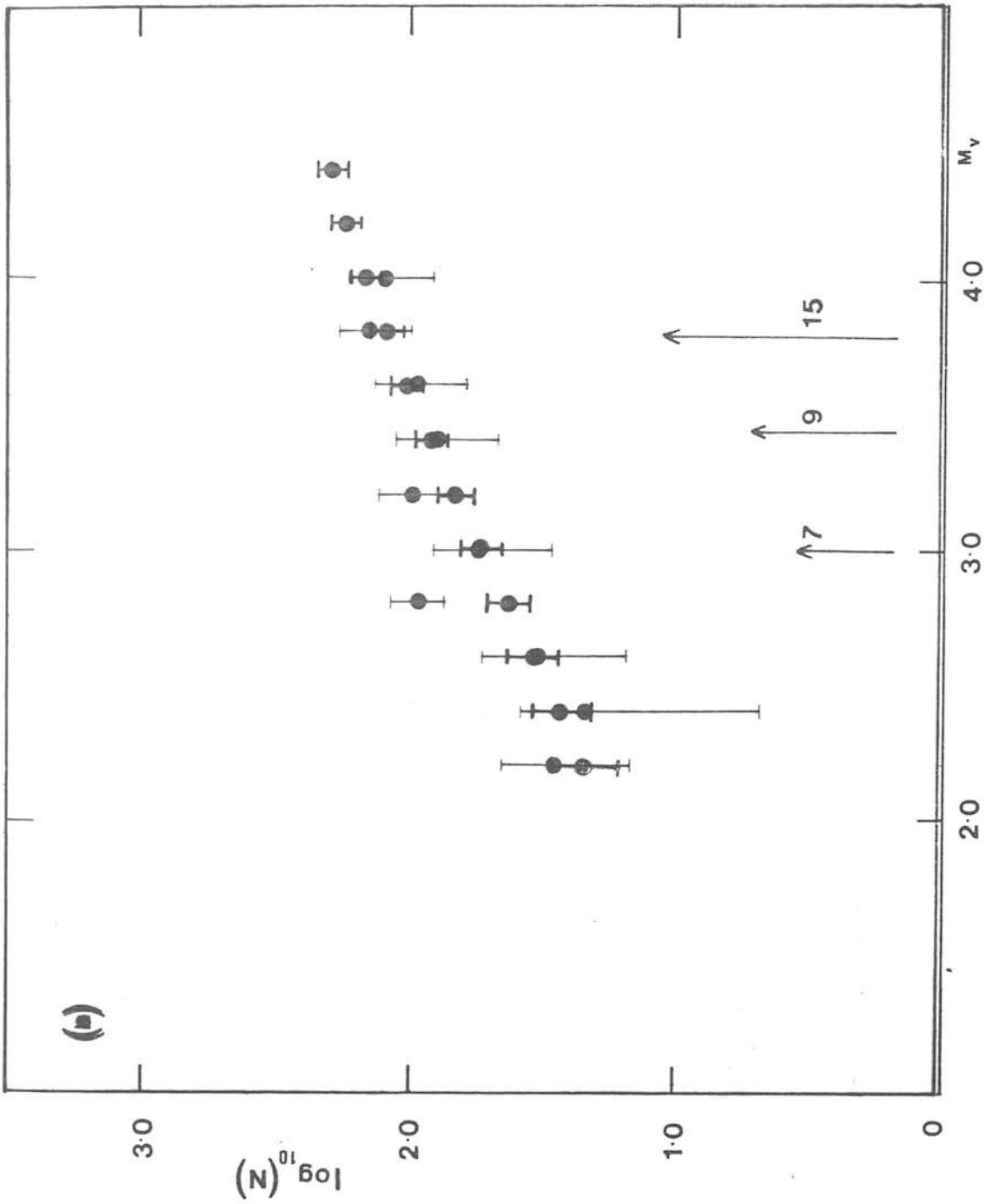

Figure 4.5a,b. (a) The main sequence luminosity function of M3 from Sandage (1957) shifted in log N to normalise the data with that of Mould and Aaronson (1983) shown in figure 4.5b. The 7, 9 and 15 Gyr turn off luminosities (Vanden Berg 1983) are indicated.

Hence to obtain the M3 and CDG giant counts on the same scale, the M3 counts have to be shifted by 0.04 (i.e. 1.05-1.01) in logN. This is shown in figure 4.6a and b. However there are uncertainties in the fitting of a and b in figure 4.6. The first is the vertical fitting uncertainty in logN of a to b in figure 4.5 estimated to be 0.15. Another consideration is the effect of the uncertainties in the distance moduli of the CDG ($\pm$0.2 magnitudes) and M3 ($\pm$0.1 magnitudes) which can be estimated over the main part of the giant branch to be about $\pm$0.1 in logN. Hence the total uncertainty is the logN shift for the giant branch amounts to about 0.33.

To within the errors it can be seen that the giant branches are similar apart from the very bright end of the luminosity function (approximately $-2.8 \leq M_V \leq -2.4$) and the counts around an absolute magnitude $M_V \sim +2.8$. The former point can be interpreted as due to the presence of more massive stars in the CDG as compared to their counterparts in M92 being able to attain higher luminosities on the asymptotic giant branch before exhausting their hydrogen envelopes. The presence of the 'resulting' extended giant branches in a stellar system has been interpreted by Mould and Aaronson (1980) as indicating the existence of an intermediate age population. This is also the domain where the more luminous carbon stars, rarely found in globular clusters, but common in the intermediate age clusters, reside. The latter point can be attributed to the effect of the main sequence stars in the CDG data appearing at a more luminous point than those in M3 i.e. the relative age of the CDG is younger than that of M3.

4.4 : SUMMARY AND CONCLUSIONS

The major evidence to date for the CDG to contain an intermediate age population (apart from that discussed in chapter 3) has rested upon

(a) the relatively bright luminosity of its main sequence turn off

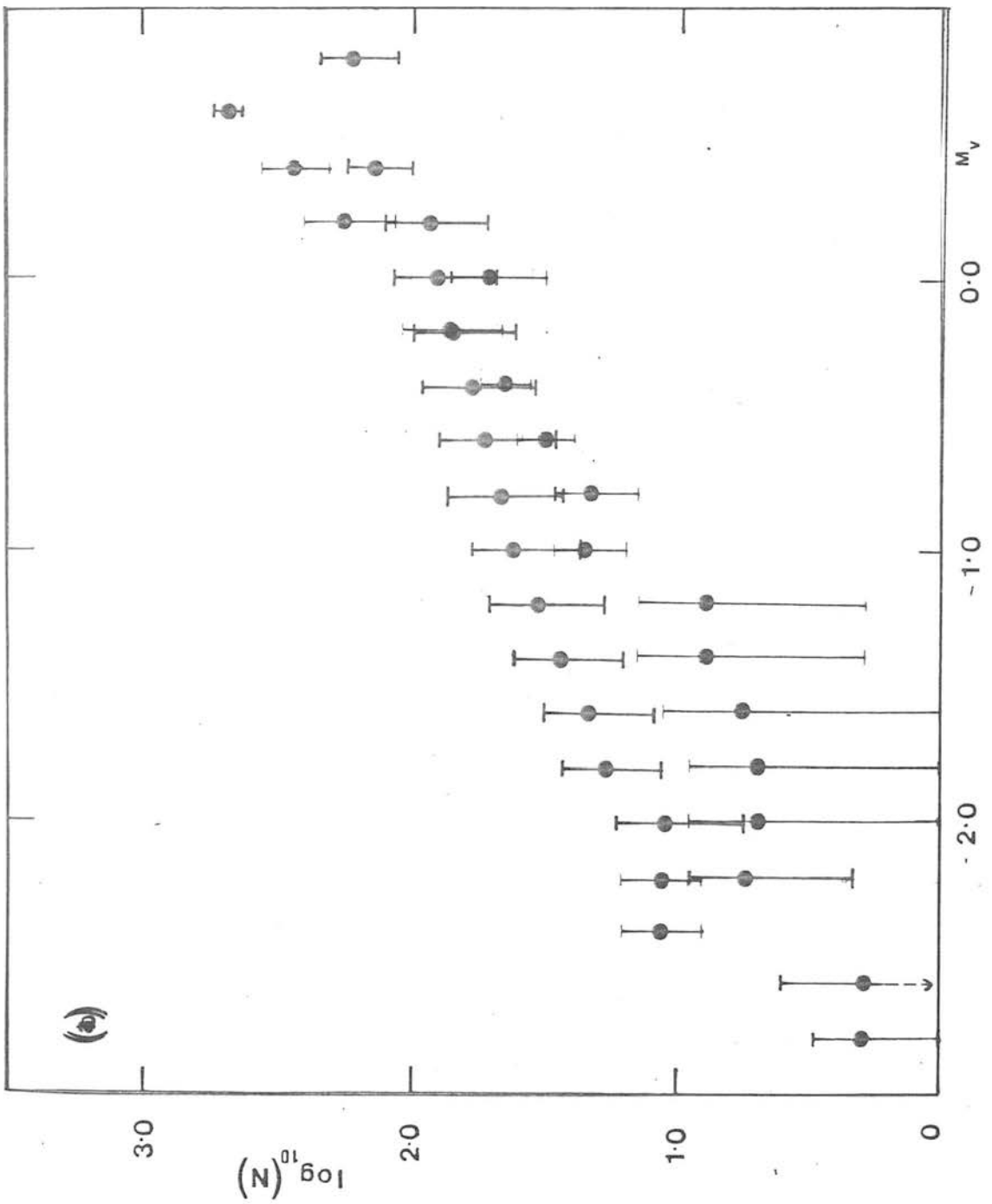

Figure 4.6a,b. (a) The giant branch luminosity function of M3 from Sandage (1957) shifted in log N to normalise the data with the COSMOS giant branch data of the Carina dwarf shown in figure 4.6b. Error in shift estimated to be about 0.33 in log N.

point derived by Mould and Aaronson (1983) as compared to Galactic globular clusters. If this identification is real, then the bulk of the stars in the CDG have an age of around 7±2 Gyr (Mould and Aaronson 1983) deduced by fitting the CD isochrones or as done here, those of VandenBerg (1983). However, it could be that there is a blue straggler population present, giving the appearance of a more luminous and hence younger turn off point and therefore the CDG could be older than this. Da Costa (1984) has also postulated that these stars are present in the Sculptor dwarf spheroidal.

(b) the comparison by Mould and Aaronson (1983) of their main sequence luminosity function with the theoretical luminosity functions of Ciardullo and Demarque (1977b and c). They found the main sequence luminosity function consistent with a 7Gyr population of stars.

The comparison of the COSMOS CDG giant branch luminosity function and the main sequence luminosity function of Mould and Aaronson (1983) covering a substantial range in absolute magnitude and hence evolutionary phases, to that of M3, provides further evidence, complementing that of chapter 3 and Mould and Aaronson (1983) that this galaxy contains a proportion of stars that must be younger than those stars found in the vast majority of globular clusters. This is in agreement with the currently held viewpoint that most if not all of the dsph galaxies contain a population of intermediate age stars, implying that some recent star formation has taken place in these systems. Whether the CDG contains completely younger stars is difficult to assertain though, and clearly one requirement in determining this is a consistent set of theoretical isochrones (and luminosity functions) covering all of the stellar evolutionary phases. Another necessity is that more comparisons (as has been done here) of the observational colour magnitude diagrams covering more than one evolutionary stage (e.g. horizontal/giant branches and main sequence) with theoretical isochrones are done, rather than trying to fit parts of this diagram in isolation (e.g. just the main sequence as done in VandenBerg 1983).

This is the first time that a comparison has been made of a dsph galaxy and globular cluster luminosity function over a large range in absolute magnitude (covering the main sequence and horizontal/giant branch stages of evolution). It shows that the luminosity function of the CDG and M3 are quite dissimilar at the high luminosity tip of the giant branch as well as the main sequence turn off regions. This is considered further in the next chapter where in particular, the mass of the CDG determined by the method of Hodge (1971) (which assumes the luminosity functions of globular clusters and dsph galaxies are the same) is compared with that derived from velocity dispersion measures.

5.1 : Introduction

Core (r_c) and tidal (r_t) radii estimates for the CDG are determined by fitting dynamical models to stellar number count radial profiles derived using COSMOS data, and these values are compared with those of the other six known Local Group dsph galaxies. A mass and luminosity are also derived for the CDG, and their implication on its mass to light ratio (M/L) discussed. The relative importance of the internal attractive and Galactic disruptive gravitational forces acting on this galaxy is also considered.

This is the first time in which automatic analysis techniques have been applied to a dsph galaxy member of our own Galaxy to derive number count data. Counts have in the past for these systems been done simply by eye, a method which is prone to many problems e.g.

(a) The determination of the limiting magnitude of the counts.

(b) The scaling up of counts from a small sample field to obtain the total number of stars in a galaxy.

(c) Usually this method only utilises one photographic plate i.e. no colour information about the objects are considered in the counts (in particular see Demers, Beland and Kunkel - hereafter DBK - for the CDG from 1B CTIO prime focus 4-metre plate), nor the effect of any Galactic field contamination. This is particularly important in dsph galaxy number count analysis where the contrast between the dsph galaxy edge and background is so small. Here however, the stars used for the radial profile, come from a selection procedure dependent upon an image's position in the colour magnitude diagram, and an automatic ellipse fitting routine has been developed to fit the resulting stellar isopleths, doing away with the old method of fitting them by hand.

The major problems using COSMOS in this work at the present time are

(i) the effects of sky background variations (caused by the actual presence of the dsph galaxy) on the derived magnitudes and

(ii) blending effects.

COSMOS crowding software (to be introduced in 1986/7) should resolve most of the problems encountered in (ii) and the increased frequency of the sky background sampling that will be incorporated into the new software at the same time should improve (i). Accurate globular cluster number counts present COSMOS with even greater difficulties, primarily due to the very large stellar densities encountered in their cores, anything up to 1000 times that of the dwarf spheroidals (see e.g. for NGC288 Godwin and Sagar 1986, in preparation). Hence with the present capabilities of the COSMOS machine, the dsph galaxies seem to be a good target for dynamical analysis using automatic measuring machine thresholding techniques.

5.2 : Crowding effects

Six good quality UK Schmidt Telescope (UKST) plates (five IIIaJ (blue) and one IIIaF (red) emulsion), were mapped by COSMOS and then thresholded at 10% above the local sky background level in intensity space (see table 5.1 for plate details). The advantage of using UKST as opposed to AAT plates for the CDG counts is that the larger area that they cover allows a sky background count to be determined (the CDG covers practically all of a prime focus AAT plate ($\sim$1 degree^2)). However, the smaller plate scale (that is more arcsec/mm) makes the blending problem somewhat more severe at the same magnitude for the UKST plates.

The same percentage cut was used here as for the AAT plates (the UKST J counts will be limited by how deep the OR magnitudes go). The effect of the loss of images due to blending will have to be assumed not to vary significantly with radial distance away from the centre

TABLE 5.1

UKST PLATE MATERIAL

Plate	Centre (RA, dec)	Date	Emulsion	Exposure	Grade
J8382	06 45.0 -51 00	83-02-06	IIIaJ GG395	60mins	a
J8295	06 45.0 -51 00	82-12-11	IIIaJ GG395	60mins	aI
J8915	06 45.0 -51 30	83-11-13	IIIaJ GG395	60mins	bI
J8965	06 45.0 -51 30	83-12-27	IIIaJ GG395	60mins	bI
J8381	06 40.0 -50 55	83-02-01	IIIaJ GG395	60mins	a
OR8996	06 45.0 -51 30	84-01-24	IIIaF OG590	60mins	a

of the CDG, i.e. the shape of the radial profile is unaltered, only the actual value of the number counts. This latter approximation should be reasonable for the dsph galaxies since the stellar densities are so low, but would be of no use in the dense cores of globular clusters. The loss of stellar images due to a combination of the photometry and blending of images effects can be carried out in a similar fashion to that used in sub-section 3.3.1, and from this analysis, the counts down to the limiting (transformed) V magnitude $\sim$ 20.5 are too low by about (21$\pm$4)%.

5.3 : Preparation and reduction of the data

The six UKST plates were paired and calibrated, using exactly the same method as that used for the AAT plates in chapter 2, enabling reliable J magnitudes to be determined. The B and V magnitudes of the standards were converted to J and OR magnitudes using the colour equations

$$J = B - 0.3(B-V) \qquad (5.1)$$

$$OR = R = V - 0.565(B-V) \qquad (5.2)$$

(Blair and Gilmore 1982) and a (J-R,R) colour magnitude diagram constructed (see figure 5.1). Here with the additional colour provided by the OR plate, as with the luminosity function derivation, the giant and horizontal branch stars could be selected out of this paired dataset by choosing only those stars within the (colour, magnitude) limits used in chapters 3 and 4 (cf. equation 3.12), thus eliminating some of the Galactic field star/background galaxy contamination. Using equations 5.1 and 5.2,

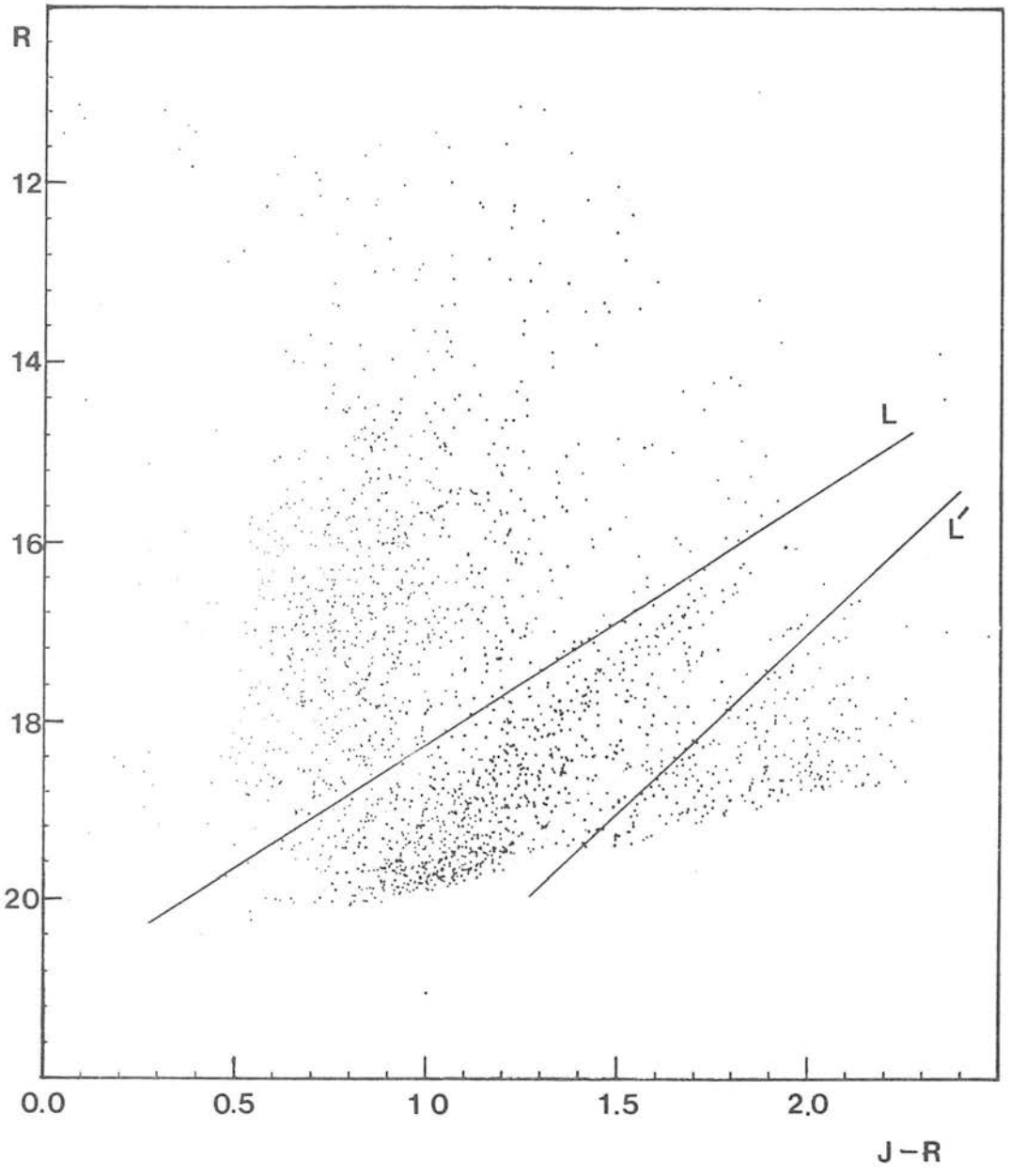

Figure 5.1. A (J-R,R) colour magnitude diagram for the Carina dwarf, indicating the region used for selection of stars (the transformed L and L' selection limits from figures 3.3 and 3.4a).

$$V = R + 0.447(J-R) \qquad (5.3)$$

$$J-R = 1.265(B-V) \qquad (5.4)$$

hence the (V,B-V) luminosity function transformed selection limits become

$$-2.66(J-R) + 21.00 \leq R \leq -3.85(J-R) + 24.80 \qquad (5.5)$$

(see figure 5.1). Being at such a low Galactic latitude, and also since the CDG covers a reasonably large area on the sky (approximately 1 degree^2), very little is known about the patchiness of the Galactic field star spatial distribution, and so this type of selection procedure is very desirable in any future studies.

The (x,y) coordinates of each image in the paired data were binned into bins of size 2 arcmin^2, and the resulting (x,y) array of number density values contoured. Figure 5.2 shows a DOTPLOT of images detected by COSMOS over an area of the master J plate (J8382) and a photographic print of the same area. The bright star SAO 234657 situated towards the centre of the CDG can be seen to have diffraction spikes (aligned N-S, E-W). These are manifested in the data as enhancements in the local pixel intensity values and consequently the applied threshold converts them into spurious images. These are eliminated by pairing the plates to be used, but this does have the effect of leaving the area with a net deficit of stars (see e.g. figure 5.3). A contaminated region of 4x4 bins was 'drilled' out of the data centred on this star. For this reason, and from the fact that the isopleths were too ill defined in this raw

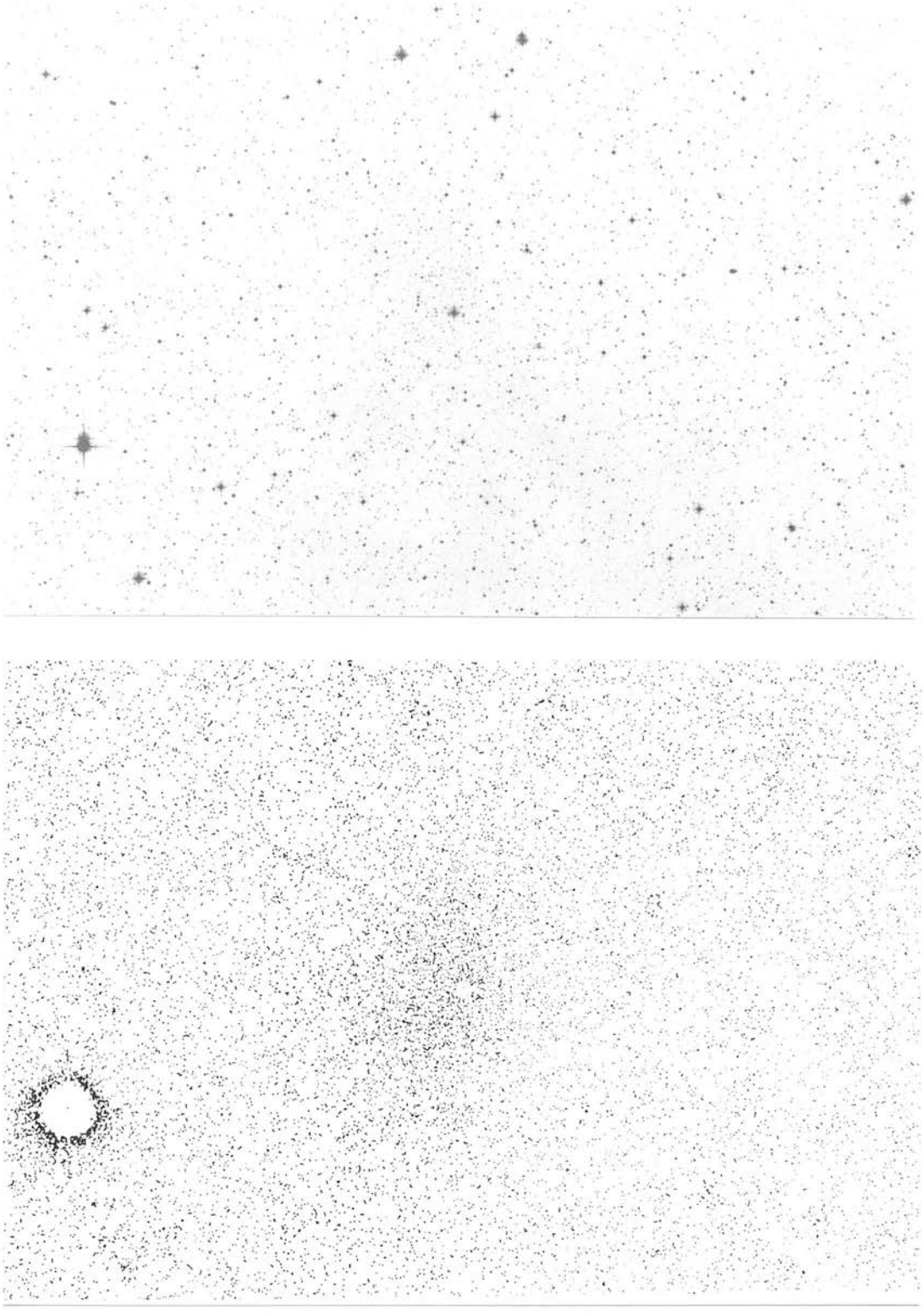

Figure 5.2. A print of the Carina dwarf from UKST plate J8382 and a corresponding DOTPLOT of images detected by COSMOS.

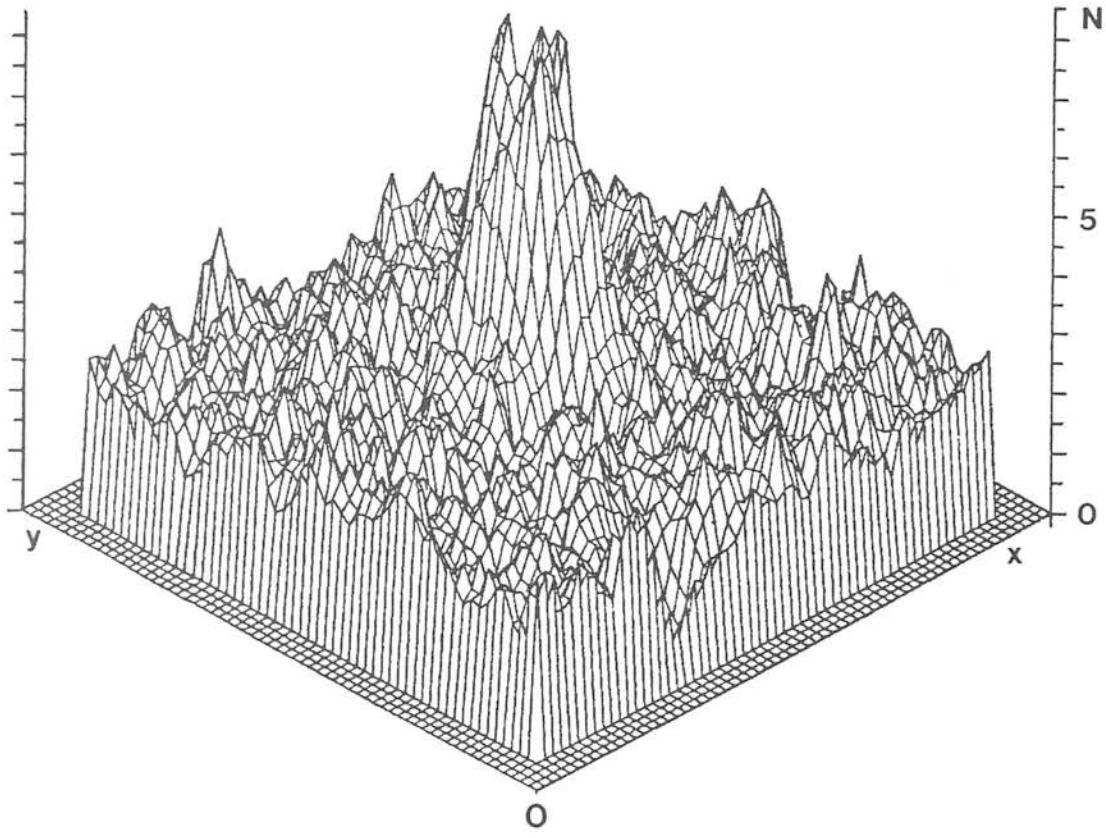

Figure 5.3. A three-dimensional plot of the (x,y) number count array values (3x3 smooth) for the Carina dwarf (2 arcmin^2 bins used). The central deficit of stars is due to the effect of the bright star SAO 234657.

data for the ellipse fitting routine described below to fit their constituent (x,y) coordinates, the binned data was smoothed. Two filters were tested for this purpose; a 'soft' 3x3 and a 'hard' 5x5 filter (Jones et al 1967, see table 5.2), the success of each on the raw number count array data being shown in figures 5.4 a,b and c. It was decided to use the 3x3 filter on the COSMOS measures since this allowed the counts to get further into the dsph galaxy core before being contaminated by the 'hole' left by the drilling out of the bright central star. This filter takes each bin in turn and replaces its value by a weighted mean using the values of the bin it is centred on together with those of the surrounding eight bins. Hence an area 6 bin widths square centred on the bright star were excluded from the data.

Once each bin had a newly assigned number count, marginal x and y profiles were plotted and the centre of the CDG (x_c,y_c) defined as the coordinate of the bin with the maximum count. The (x,y) positions of the bins with a specified count starting at a value slightly higher than that of the background (defined below) were then fitted, after transforming them to polar coordinates (r,θ) with origin at (x_c,y_c) to the generalised functional form of an ellipse namely

$$r^2 = \frac{\alpha^2\beta^2}{\alpha^2\sin^2(\theta+\psi) + \beta^2\cos^2(\theta+\psi)} \qquad (5.6)$$

with the orientation and semi-major/minor axes left as the free fitting parameters (ψ, α β respectively). A non linear least squares procedure was used for this fitting (the routine NONLIN, Bevington 1969).

From the UKST material, very little can be deduced with great certainty about the structure of the central regions of the CDG because of the bright central star. However the AAT material with its larger plate scale can be used for this purpose. Exactly the same procedure of selection for the AAT B and V plates were used as for the UKST J and OR plates, the colour and magnitude limits for the

TABLE 5.2

FILTERS USED FOR SMOOTHING

(a) 3x3 filter ('soft')

1/16	1/8	1/16
1/8	1/4	1/8
1/16	1/8	1/16

(b) 5x5 filter ('hard')

1/256	1/64	3/128	1/64	1/256
1/64	1/16	3/32	1/16	1/64
3/128	3/32	9/64	3/32	3/128
1/64	1/16	3/32	1/16	1/64
1/256	1/64	3/128	1/64	1/256

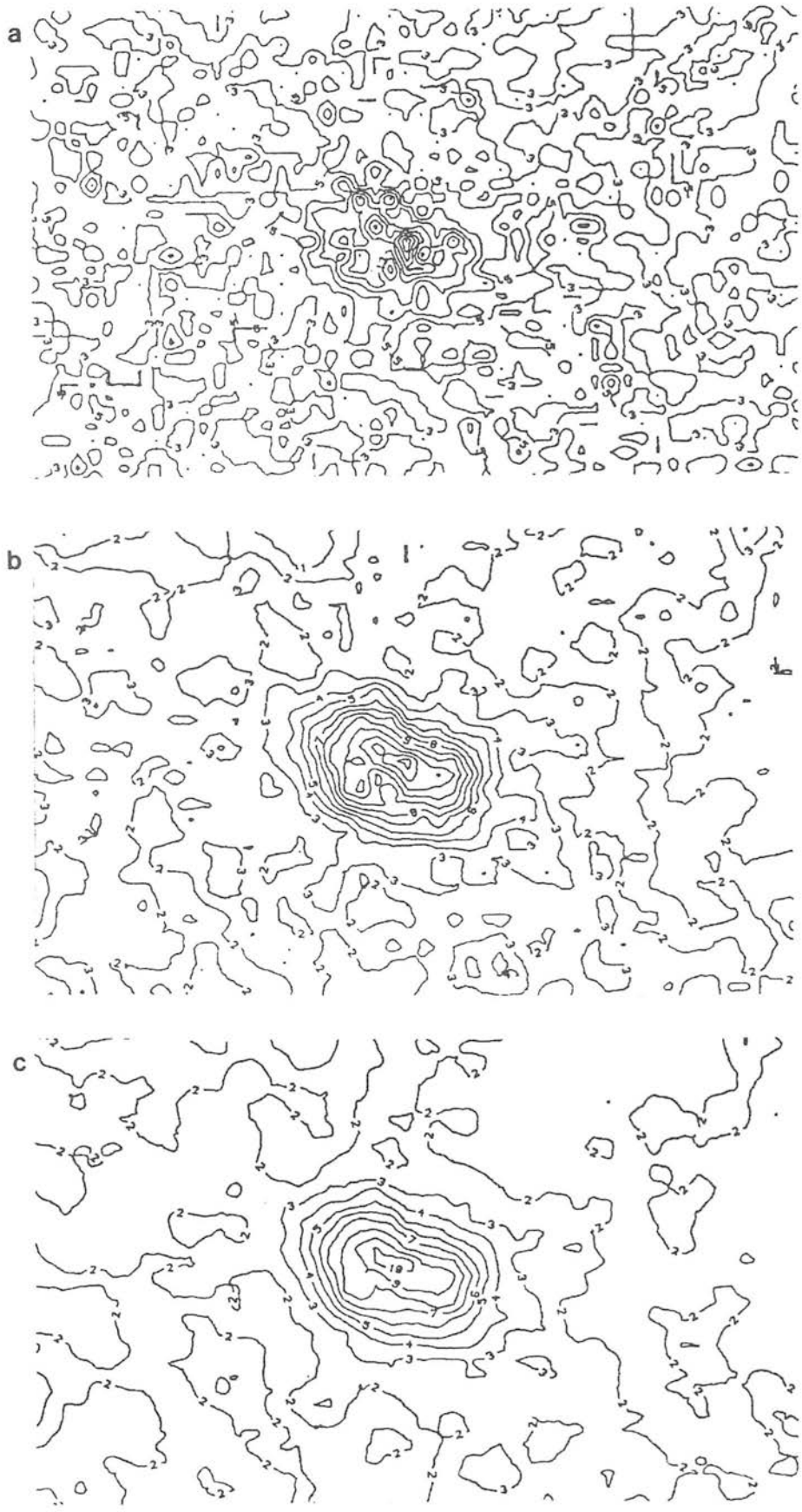

Figure 5.4a,b,c. 2-dimensional plots of the number count array values. Contours are labelled by counts per 2 arcmin^2. Plot (a) is the raw data, (b) after a 3x3 smooth, (c) after a 5x5 smooth.

giant and horizontal branches being exactly the same as those used in chapters 3 and 4. No significant (systematic or otherwise) variation with ellipticity with radius was found in these inner regions using this material, making it comparable to the Fornax dsph galaxy (Hodge and Smith 1974). This latter result for Fornax was taken by Hodge and Smith (1974) to indicate that the central members of the system had no rotation component. Any twisting of the isopleths as found for isophotes in some other elliptical galaxies (King 1978) could indicate that these objects are in fact triaxial ellipsoids (Bertola 1980), but for the CDG data here, any conclusions about its central structure are probably very strongly influenced by the effect in the data of the bright foreground star mentioned earlier.

Using the UKST plates a mean ellipticity (e^*) of 0.31 $\pm$ 0.03 and an orientation position angle of 72 $\pm$ 2^o was found from all of the fitted ellipses. The small spread in the value of this latter parameter implies that this system can be reasonably well represented in 2 dimensions by concentric ellipses of the calculated orientation and ellipticity. The original data were rebinned into ellipses with these parameters and a radial profile with $R = \sqrt{(r_a . r_b)}$ generated, where r_a and r_b are the semi-major and semi-minor axes of each fitted ellipse respectively. The bright central star mentioned earlier (SAO 234657), meant that the radial profile from r = 0 to r = 6' could not be obtained from the UKST plates. The background count was found by finding the value at which the counts summed over these elliptical bins levelled out (0.27 stars/arcmin^2) and this was subtracted from the original counts.

5.4 : The King isotropic velocity spatial density distribution

Previous work on the radial profiles of the dsph galaxies suggest that they do not follow the usual $r^{0.25}$ law of de Vaucouleurs (1958) for isolated elliptical galaxies. This has been interpreted by King (1962) as due to the effect of tidal forces. King (1962) found that most globular clusters had a radial profile that could be fitted by the purely empirical relation

$$f = k\left[\frac{1}{\left[1+\left(\frac{r}{r_c}\right)^2\right]^{\frac{1}{2}}} - \frac{1}{\left[1+\left(\frac{r_t}{r_c}\right)^2\right]^{\frac{1}{2}}}\right]^2 \qquad (5.7)$$

where f is the surface number density of stars, r_t the tidal radius, r_c the core radius and k a scaling factor. In a later paper, King (1966) derived the form of the radial profile of a cluster of stars from theoretical considerations by examining the equation that describes the dynamics of a stellar system in the most general way i.e. the Boltzmann equation

$$\frac{\partial f}{\partial t} + \sum_{k=1}^{6} \dot{x}_k \frac{\partial f}{\partial x_k} = \left(\frac{\partial f}{\partial t}\right)_{enc} \qquad (5.8)$$

f is the phase density defined such that $dN = f(x_1,\ldots,x_6,t)dx_1\ldots dx_6$ is the number of stars at the instant of time t in the volume $dV = dx_1dx_2dx_3$ situated at the point (x_1,x_2,x_3) and having velocities within the differential increments $(x_4,x_4 + dx_4)$, $(x_5,x_5 + dx_5)$, $(x_6,x_6 + dx_6)$. $(^{df}/_{dt})_{enc}$ is the term that takes into account perturbations in the velocity distribution due to stellar encounters, and the left hand side terms are those relating to orbital mixing i.e. the movements of the stars under the smoothed out gravitational potential of the entire system.

The distribution function for a stellar system can be described by a solution of the Boltzmann equation simultaneously solved with Poisson's equation. It is often possible however to assume that stellar encounters have acted for long enough to drive the distribution towards a Maxwellian form. A steady-state solution of the Fokker-Planck equation can be used to derive the velocity dependent part of the distribution function, which then resembles a Maxwellian distribution with modifications near the escape velocity. King (1965,1966) found that such a solution of the Fokker-Planck equation was very nearly a gaussian function minus a constant, and using Jean's Theorem, the phase density at all points in the cluster could be represented by

$$f(r,v) = Ae^{-2j^2(V-V_o)} \left[e^{-j^2v^2} - e^{-j^2v_e^2} \right] \qquad (5.9)$$

where V is the general potential, V_o the potential at the centre of the system, v_e the escape velocity at any point in the cluster (a function of V at that point) and j is the modulus of precision of the velocity distribution. Defining the dimensionless model potential to be

$$W = -2j^2V \quad \text{and} \quad \eta = j^2v^2 \qquad (5.10)$$

from the definition of the phase density, the volume density at any point is

$$\rho = \int_o^{v_e} f(r,v).4\pi v^2 dv = \frac{4}{3}A\pi j^{-3} e^{(W-W_o)} \int_o^W e^{-\eta}\, \eta^{3/2}\, d\eta \qquad (5.11)$$

and Poisson's equation becomes

$$\frac{d^2W}{dR^2} + \frac{2}{R}\frac{dW}{dR} = -9\,\frac{\rho}{\rho_o} \qquad (5.12)$$

where $R = r/r_c$ and ρ_o is the value of the central density. King (1966) found that the parameter r_c was very similar to and hence could be taken to be the core radius of the empirical models if $|\nabla^2 W|_o$ was taken equal to -9.

To solve these equations, a value for the central potential is chosen (W_o) and the density calculated for all values of W in the range $0 < W < W_o$ using equation 5.11. These values are then used to solve equation 5.12 and the density as a function of R results. After

projection of this volume density into a surface density (σ) on the sky using the formula

$$\sigma(R) = 2 \int_{R}^{\infty} \frac{\rho(z) z dz}{(z^2 - R^2)^{\frac{1}{2}}} \qquad (5.13)$$

the predicted run of density with radius for the cluster is found. Using the STARLINK VAX 11/780 at the ROE these models could be generated and compared to the observed radial profile of the CDG obtained in the previous section.

Figure 5.5 shows the observed profile of the CDG and examples of the theoretical King(1966) profiles. It is seen that all the data used lies between the curves $\log_{10}c$ = 0.5 to 0.75, where $c = (r_c/r_t)$. The theoretical models (plotted in $(\log_{10}(f/f_o), \log_{10}(r/r_c))$ parameter space) had to be shifted by an amount $\Delta \log r$ to fit the observational data for the CDG (plotted in $(\log_{10}f, \log_{10}r)$ parameter space) in the sense that $\Delta \log r = \log_{10}r - \log_{10}(r/r_c)$ = 0.99 (+0.03,-0.04) which implies that r_c lies in the range 8.9' to 10.5' say 9.7'$\pm$0.8'. Beyond this core radius, where the tidal effects are strongest, the data lies between the curves $\log_{10}c$ = 0.5 to 0.66. This together with the value of r_c found earlier implies that r_t lies between 28' and 48' say 38'$\pm$10'. These values compare with r_c = 10.7' and r_t = 33' found by DBK (they quote no error), but as stated previously, his results are prone to the problems (a) to (c) mentioned in section 5.1. The ordinate shift ($\Delta \log f$) in the theoretical profiles (in the sense $\log_{10}f - \log_{10}(f/f_o)$) = 0.65 (+0.05,-0.06) yielding a central density f_o lying in the range 3.89 to 5.01 stars/arcmin^2 with a mean of 4.47.

For low values of W_o (<7), King found that these curves agreed well with the empirical ones (represented by equation 5.7) ; this method does have some theoretical basis though whereas the function of equation 5.7 is merely an empirical relation that conveniently mimics the observations. It is assumed however in the theoretical models that the velocity distribution of the 'field' stars involved

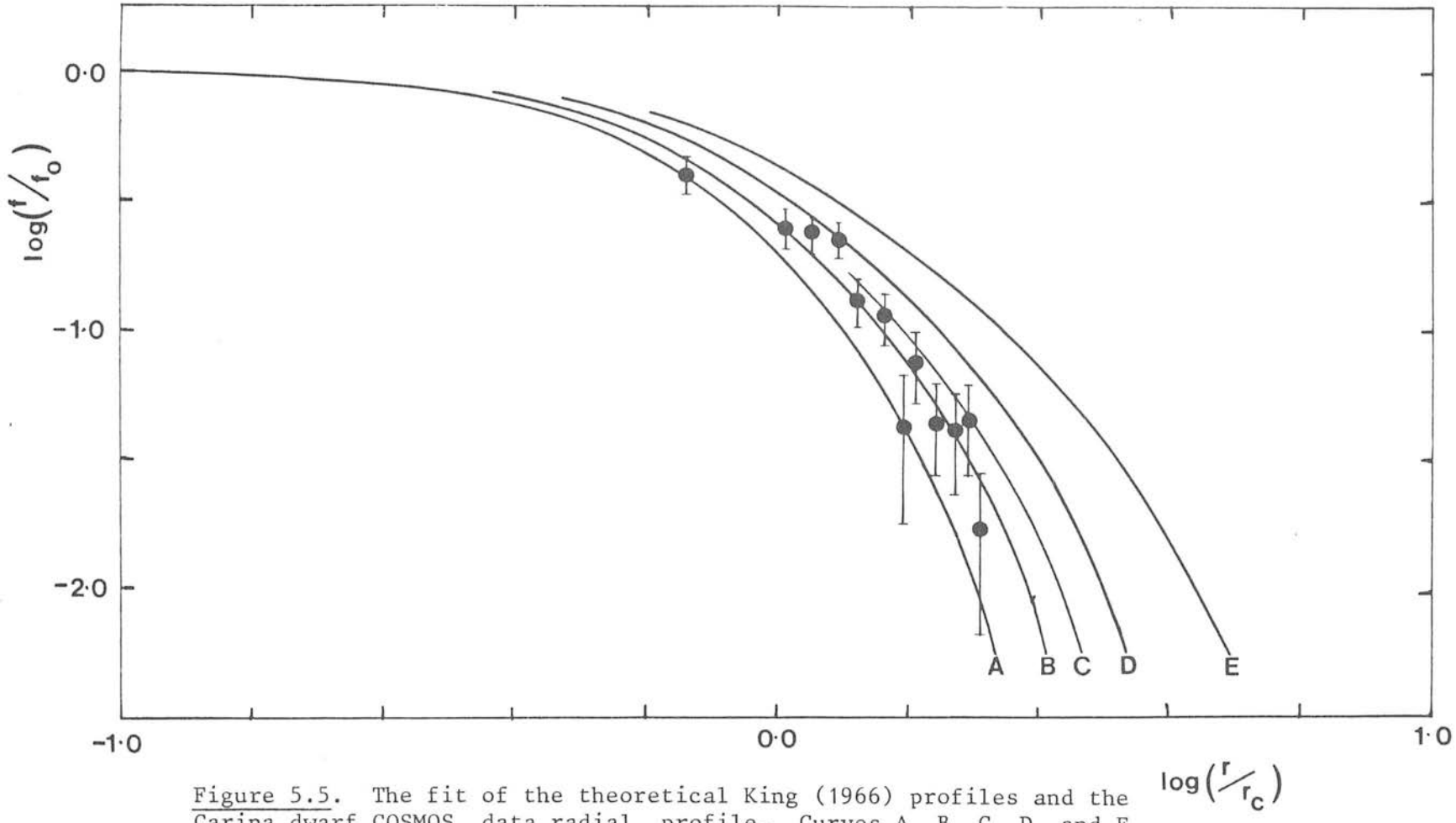

Figure 5.5. The fit of the theoretical King (1966) profiles and the Carina dwarf COSMOS data radial profile. Curves A, B, C, D and E represent a choice of logc=0.5, 0.6, 0.66, 0.75 and 1.0 respectively.

in the stellar encounters is isotropic and gaussian and also the effect of a mass spectrum is not considered. Hence, with these considerations it is somewhat surprising that such a simple model should be able to fit the data so well. The introduction of anisotropy into the models by Hodge and Michie (1969) was found to have the effect of pulling the outer parts of the density distribution down and so in fitting to an observed cluster profile, part of the outer dropoff is provided by the anisotropy, with the tidal part of the dropoff being less severe. They found a small degree of anisotropy in the six dsph galaxies they studied, indicating as well as this more rapid fall off of density (as compared to isotropic models), more elongated orbits with increasing distance from their centres.

5.5 : Luminosity and mass derivation

In the following section, a mass and luminosity for the CDG is estimated by assuming that its luminosity function is similar to that of M3 (see chapter 4). This method has been used by Hodge (1971) to estimate the masses of the other dsph galaxies, and essentially uses the red giant stars as 'tracers' of the main sequence population.

The total number of stars in a stellar system out to a radius r from its centre can be found by integrating equation 5.7 with respect to $2\pi r.dr$, which yields

$$n(x) = \pi r_c^2 \, k \left[\ln(1+x) - \frac{4[(1+x)^{\frac{1}{2}}-1]}{(1+x_t)^{\frac{1}{2}}} + \frac{x}{(1+x_t)} \right] \qquad (5.14)$$

where

$$x = \left(\frac{r}{r_c}\right)^2 \quad \text{and} \quad x_t = \left(\frac{r_t}{r_c}\right)^2 \qquad (5.15)$$

Using equations 5.7 and 5.14, $n(x_t)$, the total number of stars in the

whole system can be expressed solely as a function of c, f_o and r_c. Using the values for these parameters found earlier, the total number of stars down to the faintest V magnitude of the COSMOS sample used (V = 20.5, unreddened i.e. M_V = +0.6±0.2, where the error is that due to the uncertainty in the distance modulus of the CDG found earlier) in the CDG can be calculated to be 2300 with an estimated error of 1000, where the error takes into account the errors in the fitting parameters, and an incompleteness correction has also been applied to the number count data.

The Sandage (1957) counts are assumed to contain all of M3's red giant population out to a radius of 8' from the centre of the cluster, and so putting r = 8' and using values of r_t = 39' and r_c =0.5' from Madore (1978), equation (5.14) can be used to determine k, a parameter related to the central density (see equation 5.7), for any magnitude limit adopted. As done for the CDG counts above, $n(x_t)$ for M3 can then be found. To M_V = +0.6, the number is calculated to be 1240±40.

5.5.1 Luminosity

The method used by Hodge (1971) to determine the luminosity of the dwarf galaxies is essentially that of assuming

$$\frac{N_C^{TOT}}{N_{M3}^{TOT}} = \frac{N_C}{N_{M3}} = \frac{L_C}{L_{M3}} \qquad (5.16)$$

where N_C and N_{M3} are the total number of stars (in this case) in the CDG and M3 respectively down to a particular magnitude, N_C^{TOT}, and N_{M3}^{TOT} are the respective total number of stars in each system and L_C and L_{M3} are their respective total luminosities. Taking M_V(M3) = -8.91±0.25 (Madore 1978, Webbink 1985), $M_V(\odot)$ = +4.71 (see e.g. Allen 1955), then using the values found for N_C and N_{M3} above, M_V(Carina) = -9.58±0.54. This error though does not take into account the uncertainty in the distance modulus error of the CDG (±0.2 magnitudes) e.g. if the distance modulus of the CDG is 20.0 instead

of 19.8 used in the calculations above, then the limiting magnitude that should be used for the M3 counts should be $M_v = +0.4$. Similarly, if the distance modulus is 19.6 for the CDG, then the limiting magnitude of the M3 counts should be $M_v = +0.8$. From the counts of Sandage (1957) the increase in $\log_{10}N$ if counts are extended to 0.2 magnitudes fainter can be estimated (including $\sqrt{N}$ errors) to be 0.09, which means a correction of 0.23 towards a fainter magnitude for M_v(Carina). Similarly, if there are fewer counts in M3 due to the limiting magnitude being chosen as $M_v = +0.4$, the estimated correction in $\log_{10}N$ is 0.26 and a correction of 0.65 towards a brighter magnitude for M_v(Carina). Hence, the absolute magnitude of the CDG can be estimated to be $M_v = -9.6$ with a range from about -8.8 to -10.8. These values imply that the CDG is one of the least luminous objects in the Local Group.

5.5.2 : Central surface density and surface brightness

The spatial density of stars at a particular radius can be found by projecting the 2D counts into a volume count. When this is done for the areal density f in equation 5.7, the result at r = 0 is

$$\rho_o = \frac{k}{\pi r_c} (\cos^{-1} z - z\sqrt{1-z^2}) \qquad (5.17)$$

where $$z = \sqrt{\frac{1}{1+x_t}} \qquad (5.18)$$

(King 1962). The mass density in $M_\odot/pc^3$ can then be evaluated by initially expressing ρ_o as a function of N_c^{TOT}, r_c and c using equation 5.14 with $r = r_t$, and the assumption that

$$\frac{N_c^{TOT}}{N_{M3}^{TOT}} = \frac{N_c}{N_{M3}} = \frac{M_c}{M_{M3}} \qquad (5.19)$$

where M_c and M_{M3} are the respective masses of the CDG and M3 (i.e. this equation implies that the average mass of a star in M3 is equal to that of one in the CDG). Hence taking the dynamical mass of M3 to be $(3.30\pm0.15)\times10^5 M_\odot$ (Da Costa and Freeman 1978),

$$\rho_o = 0.005 \pm 0.004\ M_\odot/pc^3 \qquad (5.20)$$

making the Carina dwarf's central density comparable to that of e.g. the Draco dwarf's (0.0035 - see table 5.4). This indicates just how low the stellar densities are in the dsph galaxies and hence why stellar encounters can be neglected in their dynamical modelling (this compares with ~1 to $\sim10^5 M_\odot/pc^3$ in globular clusters).

Can an estimate of the surface brightness of the CDG be made ? From equation 5.16 it is being assumed that the average luminosity of one CDG and M3 star is equal, hence the central luminosity L' of the CDG can be estimated to be the total central density (in stars/arcmin^2) multiplied by L_{M3}/N_{M3}^{TOT}. Hence using equation (5.14) and the left hand side of equation (5.16) to eliminate N_c^{TOT}, $L' = (0.93\pm0.84)L_\odot/arcsec^2$, which implies a surface brightness of 24.6 ± 1.0 magnitudes/arcsec^2 in V. Using a mean value of (B-V) = 0.7 for a dwarf spheroidal (see e.g. van den Bergh 1972), this corresponds to a B magnitude of 25.3 ± 1.0 magnitudes/arcsec^2 This result gives an indication why this dsph galaxy was not discovered until the SERC survey was undertaken since if it is assumed that the night sky brightness in B is 22.4 magnitudes/arcsec^2, then the calculated mean surface brightness corresponds to $\sim7\%$ of this level.

The detectable minimum size for a faint object is a function of the surface brightness limit i.e. larger objects can be seen a lot better than smaller ones (Cannon 1984). Van den Bergh (1972) found three dwarf spheroidal companions of M31 by a simple visual examination of his photographic material, selecting out faint 'smudges' with low central concentrations of light. A simple order of

magnitude calculation can be made to see at what distance the CDG could be detected on UKST IIIaJ plates if it is assumed that the detection limit for stellar one arcsecond images is around J = 22.4 magnitudes for this emulsion. The observed S/N value for a single star can be expressed as

$$\frac{S}{N} = \frac{N_s}{(N_s+N_b)^{\frac{1}{2}}} \qquad (5.21)$$

where N_s and N_b are the number of photons received from the star and from a corresponding area of background respectively. When $N_b >> N_s$ as is the case here (since we are close to the plate limit), this reduces to $S/N \sim N_s/(N_b{}^{0.5})$. What we require is the maximum distance that (say) the core radius of the CDG could be detected given that this galaxy's surface brightness is 25.3 ± 1.0 magnitudes/arcsec^2 in B. The mean value corresponds to 2.9 magnitudes fainter than the plate limit of 22.4 magnitudes/arcsec^2 (i.e. a factor ~ 14 in luminosity) and so equation 5.21 implies that the galaxy must cover an area of $\sim 10^{2.3}$ arcsec^2 to be detectable. Hence, taking the distance to the CDG as 91kpc (see sub-section 3.3.2), the Carina dwarf's core radius will subtend an angle of 14" (i.e. taking $\sqrt{10^{2.3}}$ arcseconds) (say) at a distance $\sim$3700kpc, which would make it detectable on UKST IIIaJ emulsion at just over five times the distance of M31 ($\sim$700kpc).

5.5.3 Velocity dispersion, mass and the M/L ratio

A star cluster mass can be obtained in a number of ways. Two of these considered in this sub-section are (a) by star counts and (b) by the velocity dispersion present by using some kind of dynamical modelling. Consider first case (a). If the dynamical mass of M3 (which is a more reliable mass to take than that obtained from an observed luminosity function e.g. that of Sandage 1957, since it does not require an unknown extrapolation for the faint stars) is taken to be $(3.3 \pm 0.15)\times10^5 M_\odot$ (Da Costa and Freeman 1976), then using the right hand side of equation 5.19, an estimate for the mass of the CDG can be calculated to be $(6.11\pm2.68)\times10^5 M_\odot$. However, when the error on

the distance modulus ($\pm$0.2 magnitudes) of the CDG is taken into account as described in sub-section 5.5.1, errors of $+8.67\times10^{5}M_{\odot}$ and $-3.10\times10^{5}M_{\odot}$ have to be added, hence

$$\frac{M_{c}^{H}}{M_{\odot}} = 6.1^{+11.4}_{-5.8} \times 10^{5} \qquad (5.22)$$

where the superscript H denotes that the mass has been determined by the Hodge (1971) method. Nothing can be said about the M/L ratio for the CDG from these calculations as it is implicitly being assumed that it is the same as that of M3 (cf equations 5.16 and 5.19).

Case (b) consists of calculating the mass of the CDG using this galaxy's velocity dispersion. This should give a more reliable mass determination than method (a) being based on realistic dynamical models rather than on assumptions about the compatability of dsph galaxy and globular cluster luminosity functions. The results of chapter 6 indicate that the velocity dispersion of the CDG can be taken to be $10.4\pm3.0 kms^{-1}$, and (e.g. Peterson and King 1975, Illingworth 1976) this is related to the mass of the parent galaxy (or stellar system) in solar units by the formula

$$\frac{M}{M\odot} = \alpha r_{c} \mu \langle v_{r}^{2} \rangle_{o} \qquad (5.23)$$

where μ is the dimensionless mass parameter of the theoretical King (1966) model used, α a constant chosen equal to 167 so that the core radius can be used in parsecs and $\langle v_{r}^{2} \rangle_{o}^{0.5}$ is the central velocity dispersion in kms^{-1}. Using the range for the concentration parameter c found in section 5.4, μ can be estimated to lie between 2.7 and 6.4 with a mean of 4.6 (see King 1966). Hence, from the value of r_{c} found in the same section and the distance modulus derived in chapter 3 for the CDG

$$\frac{M_c^V}{M_\odot} = 22^{+35}_{-18} \times 10^6 \qquad (5.24)$$

(the superscript V denotes that the mass has been determined from a velocity dispersion measure).

The implications of this larger mass is that the M/L ratio of the CDG can be estimated to lie in the range from 7 to 105 with a mean $\sim$ 40 which implies that there could be a substantial quantity of mass in this galaxy in the form of low or non-luminous matter. This result is examined further in chapter 6, where the reliability of the velocity dispersion used here is discussed. The main parameters derived in this section are tabulated in table 5.3.

5.5.4 Discussion

Are high M/L ratios common in the other dsph galaxies? Faber and Lin (1983), using tidal interaction arguments (with large uncertainties though) concluded that a difference in M/L ratio between the dsph galaxies and the globular clusters of one order of magnitude could be possible e.g. M/L $\sim$ 10 to 20 say. Aaronson (1983) using a similar argument found a M/L ratio $\sim$ 29 for the Draco dsph galaxy (compare with mean value found above for CDG). Aaronson and Cook (1983) also found a large velocity dispersion from their carbon star spectra and concluded that a large amount of dark matter must be present. Although velocity dispersion measures of carbon stars in the dsph galaxies have provided most of the 'evidence' for these galaxies to contain dark matter, the technique for obtaining radial velocities from these stars is still fraught with uncertainties (e.g. are these stars variable? - see chapter 6). However Aaronson and Olszewski (1985) obtain the radial velocity of the Draco and Ursa-Minor dsph galaxies from carbon star and giant star spectra and still obtain high M/L ratios of 37 $\pm$ 11 and 104 $\pm$ 40 respectively. Hence the evidence for the existence of dark matter in the dsph galaxies seems to be accumulating steadily.

How does this tie in with present ideas on the dsph galaxy's

TABLE 5.3

DERIVED PARAMETERS FOR THE CARINA DWARF GALAXY

r_c	=	9.7' ± 0.8'
$\log_{10} c$	=	0.5 to 0.75
r_t	=	38' ± 10'
*f_o	=	4.47 stars/arcmin² (range from 3.89 to 5.01)
*$n(x_t)$	=	2300 ± 1000 stars
M_V	=	-9.6 (range from -8.8 to -10.8)
ρ_o	=	0.005 ± 0.004 $M_\odot/pc^3$
+b(V)	=	24.6 ± 1.0 mag/arcsec²
+b(B)	=	25.3 ± 1.0 mag/arcsec²
M_V^H	=	6.1 ± 10^5 $M_\odot$ (range from 0.3 to 17.5 x 10^5 $M_\odot$)
M_V	=	22 x 10^6 $M_\odot$ (range from 4 to 57 x 10^6 $M_\odot$)
M_V/L	=	40 (range from 7 to 105) (M/L for M3 = 1.12)

* down to M_V = +0.6 ± 0.2

\+ surface brightness

origin and evolution discussed in chapter 1? Lin and Faber (1983) argue for their origin through the ram stripping of dwarf irregulars which already appear to contain non-luminous matter (Tinsley 1981). The older stars in these systems are smoothly distributed (see e.g. Hodge 1977, 1978), although the overall appearance of these galaxies seems somewhat clumpy, this latter feature being due to the (blue) regions of star formation. If gas could somehow be removed, then Lin and Faber (1983) speculated that this population would fade away leaving behind the old population 'dwarf spheroidal'. They calculated that a dwarf irregular with an initial $M/L_V = 6$ after stripping would yield a final 'dwarf spheroidal' with $M/L_V = 28$ (cf with a $M/L \sim 29$ for Draco found by Aaronson 1983 and the mean value ~ 40 for the CDG found here).

Do the higher masses (relative to those of Hodge 1971) that the dsph galaxies must have if the carbon star velocity dispersion measures reflect that of their parent galaxy, indicate anything about the metal enrichment in these systems to explain their apparent metallicity spread ? The mean metallicities of each of the dsph galaxies are plotted against their Hodge (1971) masses in figure 5.6a together with the values of ($M_c{}^H$,[Fe/H]) for the CDG found earlier in this thesis. No errors are quoted by Hodge (1971) on his masses except to say that they could be in error by large amounts. The mean metallicities come from Aaronson and Mould (1985). There appears to be a hint from this diagram of a mass metallicity relation, even if the Hodge (1971) masses are taken to be order of magnitude estimates only. This could be taken to imply that if the dsph galaxies evolved as isolated systems, the more massive galaxies were able to retain the ejected gas from their evolutionary advanced stars, as predicted in the mass-loss models of Larson (1974), and hence be able to have prolonged star formation periods. Could this be evidence to suppose that the dsph galaxies were <u>once</u> more massive than the Hodge (1971) method predicts (see e.g. Searle and Zinn 1978)? The current (rough) velocity of escape from the CDG can be calculated from the formula

$$v_e = \sqrt{\frac{2GM_c}{r_c}} \qquad (5.25)$$

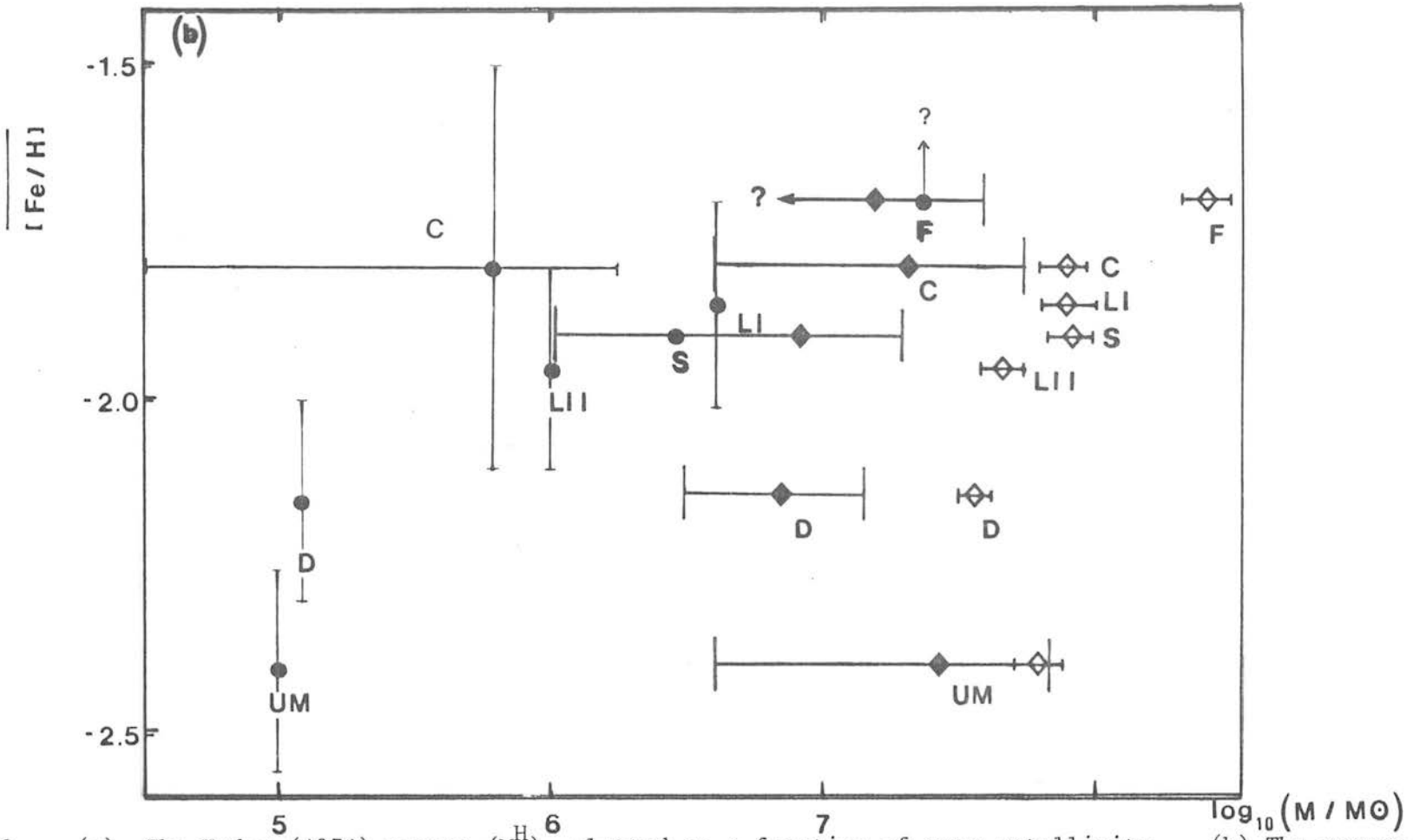

Figures 5.6a,b. (a) The Hodge (1971) masses (M^H) plotted as a function of mean metallicity. (b) The masses obtained from carbon star velocity dispersion measures (◆) and the masses obtained by assuming the velocity of escape from the dwarf spheroidals is large enough for these galaxies to retain nuclearly processed material blown from the surfaces of their red giants (◇) plotted as a function of mean metallicity (see table 5.4). C = Carina, UM = Ursa Minor, D = Draco, S = Sculptor, F = Fornax, LI = Leo I, LII = Leo II.

and the observed gas expansion rate for globular cluster giants undergoing mass loss is typically $\sim 50 kms^{-1}$ (Mallia and Pagel 1978). Hence, this means that if the core radius remained constant over the evolution of the dsph galaxy, the mass of the CDG would have to have been at least

$$\frac{M_c^E}{M_\odot} = (7.6 \pm 1.5) \times 10^7 \qquad (5.26)$$

to be able to retain the ejected material for further star formation episodes and to generate a metallicity spread as hinted at in chapter 3. This is about three times the mass found from (even) the velocity dispersion method discussed earlier. Figure 5.6b shows this predicted minimum mass M^E for all of the dsph galaxies. However, considering the (new) mass values (derived from carbon star velocity dispersions) which are up to~300 times that of the Hodge (1971) values, the apparent trend in figure 5.6a of increasing metallicity for more massive systems is not so clear, and all these masses fall below the M^E values for each of the dsph galaxies apart from Ursa-Minor's. This dsph galaxy is known to be different in horizontal branch type to those of the other dsph galaxies (having a predominantly blue one), and it could be that this dsph galaxy is (even now) massive enough to hold onto the nuclearly processed material blown from the surfaces of its red giants for more than one star formation episode. It is interesting to note however that the Fornax dsph galaxy (probably the most massive of these systems) is thought to contain stars as young as 2 Gyr (Aaronson and Mould 1985) and Draco and Ursa-Minor (probably the least massive) contain very little or no stars at all younger than 15 Gyr (Aaronson and Mould 1985). If the dwarf spheroidals did evolve as isolated systems, then it is unlikely that they are as massive (today) as equation 5.26 predicts, since as noted in chapter 1, there exists very little gas in these systems (Huchtmeier 1980). However, the observation of a planetary nebula in the Fornax dsph galaxy (see e.g. Danziger et al 1978, McDowell and Godwin 1986)

confirms that dsph galaxies of this order of mass (if the Hodge 1971 masses are taken as merely representing lower bounds) can retain this type of material. Could the low mass calculated here for the CDG by the Hodge (1971) method then, be due to a large proportion of this dsph galaxy's original membership being lost by tidal interactions over the time of its existence. This certainly seems plausible for the CDG, since even at the present time it could well be undergoing severe tidal disruption (see section 5.7), and it has (possibly) had time for several orbits around the Galactic centre. Alternatively, if the dsph galaxies originated in the Magellanic Clouds, then their observed metallicity dispersion could be explained by the inhomogeneity of the parent material, due to pollution from supernovae ejecta in different regions of the Clouds. The observed turn-off age of these dsph galaxies could then be thought of as the time that they were ripped away (with practically the same mass that equations 5.22 or 5.24 predict), by tidal interactions between the Clouds and the Galaxy. Star formation would cease at the instant of separation, and the nuclearly processed material would be lost giving the appearance today that these galaxies contain no gas.

5.6 : The relaxation and characteristic time scales

Two important time scales to be considered when examining the dynamics of stellar systems are the relaxation and crossing times. The relaxation time (T_r) is the time scale over which stellar encounters affect the stellar distribution and can be expressed in the (mean) form as

$$\overline{T}_r = 8.8 \sqrt{\frac{NR_*^3}{m}} \frac{1}{\log_{10} N - 0.45} \times 10^5 \text{ years} \qquad (5.27)$$

(Chandrasekhar 1942), where N is the total number of stars in the system, R_* is its 'mean' radius (usually taken to be the radius containing half the mass) in parsecs and m is the mass of a typical member star in units of $1M_\odot$ (T_r in general varies from point to point in a cluster, so this expression is an averaged value). It can be

thought of as the time required for the velocity distribution to approach Maxwellian equilibrium by individual stars exchanging energies.

The time scale associated with the orbital mixing process is called the characteristic or crossing time (T_c) and can be expressed in the form

$$T_c = 2.2 \times 10^7 \sqrt{\frac{R_*^3}{Nm}} \text{ years} \qquad (5.28)$$

What do these equations say about the importance of stellar encounters in determining the stellar distribution function of dsph galaxies? For large N, i.e. the situation that prevails in dsph galaxies and globular clusters, equations 5.27 and 5.28 yield

$$\frac{\bar{T}_r}{T_c} \propto \frac{N}{\log_{10} N} \qquad (5.29)$$

which implies $\bar{T}_r >> T_c$. This essentially means that the encounter term introduced on the right hand side of equation 5.8 can safely be neglected as found in sub-section 5.5.2. For globular clusters, $\bar{T}_r \sim 10^7$ to 10^8 years, and so it is expected that the velocity distribution of these clusters is close to Maxwellian. For the CDG, using the data derived in previous sections, $\bar{T}_r$ must be at least $\sim 2 \times 10^{11}$ years. Taking the relaxation times of the other dsph galaxies from Hodge (1971), the range of this time scale in these systems seems to be of the order 10^{11} to 10^{13} years which is older than the probable age of the Galaxy.

The large difference between the values of $\bar{T}_r$ for the dwarf galaxies and those of the globular clusters is due primarily to the difference in star density between the two systems, since the relaxation time can also be expressed in the form

$$T_r \propto \frac{v^3}{m^2 n} \qquad (5.30)$$

where v is a typical velocity in the system and n is the average number of these objects per unit volume (Hodge and Michie 1969). This again shows, that unlike the globular clusters, stellar encounters are not important in the modelling of the dsph galaxy's dynamics except at or very close to their centre. This would seem to contradict the fact that the radial profiles of the CDG and other dsph galaxies fit the (theoretically based) King models so well, since as already stated, these models take a Maxwellian function (minus a constant) as the assumed distribution function. This has however been explained by considering two relaxation mechanisms namely that due to energy exchange between the stars and star groups (since star-star relaxation times are so long) at the time of their formation and another due to the stars being in a time dependent gravitational potential leading to a change in the mean potential (Lynden-Bell 1967). This latter process has been shown to yield a distribution function similar to those models obtained by e.g. Michie (1963) from the Boltzmann equation.

5.7 The gravitational influence of the Galaxy

How and to what extent are the dsph galaxies interacting with the gravitational field of our own Galaxy? The predicted limiting radius at perigalacticon of a non-rotating stellar system moving in an elliptical orbit around the Galactic centre has been calculated by King (1962) to be

$$r_{lim} = R_p \left[\frac{M_d}{M_g(3+e)} \right]^{1/3} \qquad (5.31)$$

where M_g is the mass of the Galaxy, M_d the mass of the stellar system, e the eccentricity of its orbit, and R_p the perigalacticon radius. In calculating this quantity for any particular orbiting

system, R_p is taken to be its present distance from the centre of the Galaxy, and hence the value calculated from equation 5.31 is an upper bound for the actual r_{lim} (e is taken to be 0.5 i.e. elongated orbits). Figure 5.7 shows the observed tidal radius r_t divided by r_{lim} as a function of Galactocentric distance. The data used for the dsph galaxies comes from table 5.4, M_g has been taken to be equal to $(2.6\pm0.8)\times10^{11}M_\odot$ (Lynden-Bell, Cannon and Godwin 1983) and $M_d = M^H$ (note that Hodge 1971 quotes no errors on these values of M^H). The heliocentric distances of Hodge (1971) were corrected to Galactocentric distances by using a value for the Sun to Galactic centre distance = 8.8kpc (see e.g. Harris 1976).

This plot shows that for the Leo, Fornax and Draco systems, the expected behaviour occurs namely $r_{lim} > r_t$. For Sculptor and Carina, r_{lim} coincides with r_t to within the quoted errors whilst for Ursa-Minor, r_{lim} is <u>smaller</u> than the observed value r_t. This could be implying that the Galaxy's gravitational field is having a very significant effect on the structure of all these latter three galaxies, and can be investigated further by examining the ratio of the Galaxy's tidal to the dwarf spheroidal's internal gravitational attraction force. Hodge and Michie (1969) found that this could be expressed in the approximate form

$$\left|\frac{T_z}{V_z}\right| \sim \frac{2\left(\frac{b}{a}\right)M_g r_t^3}{D^3 M_d} \qquad (5.32)$$

where D is the Galactocentric distance to the stellar system, and b/a is the ratio of the semi-minor to semi-major axis of the system's mean isopleth. These values are calculated from the data in table 5.4 for each system, and are plotted against the mean ellipticity of their isopleths in figure 5.8. From this plot it is again evident that the closer the dsph galaxy is to the Galactic centre, the greater the role the Galactic tidal force plays in determining the structure of the outer regions (shown by the elongation of the isopleths). It can also be seen that the ratio $|T_z/V_z|$ is in fact ~ 1 or larger for the CDG, Sculptor, Draco and the Ursa-Minor dsph

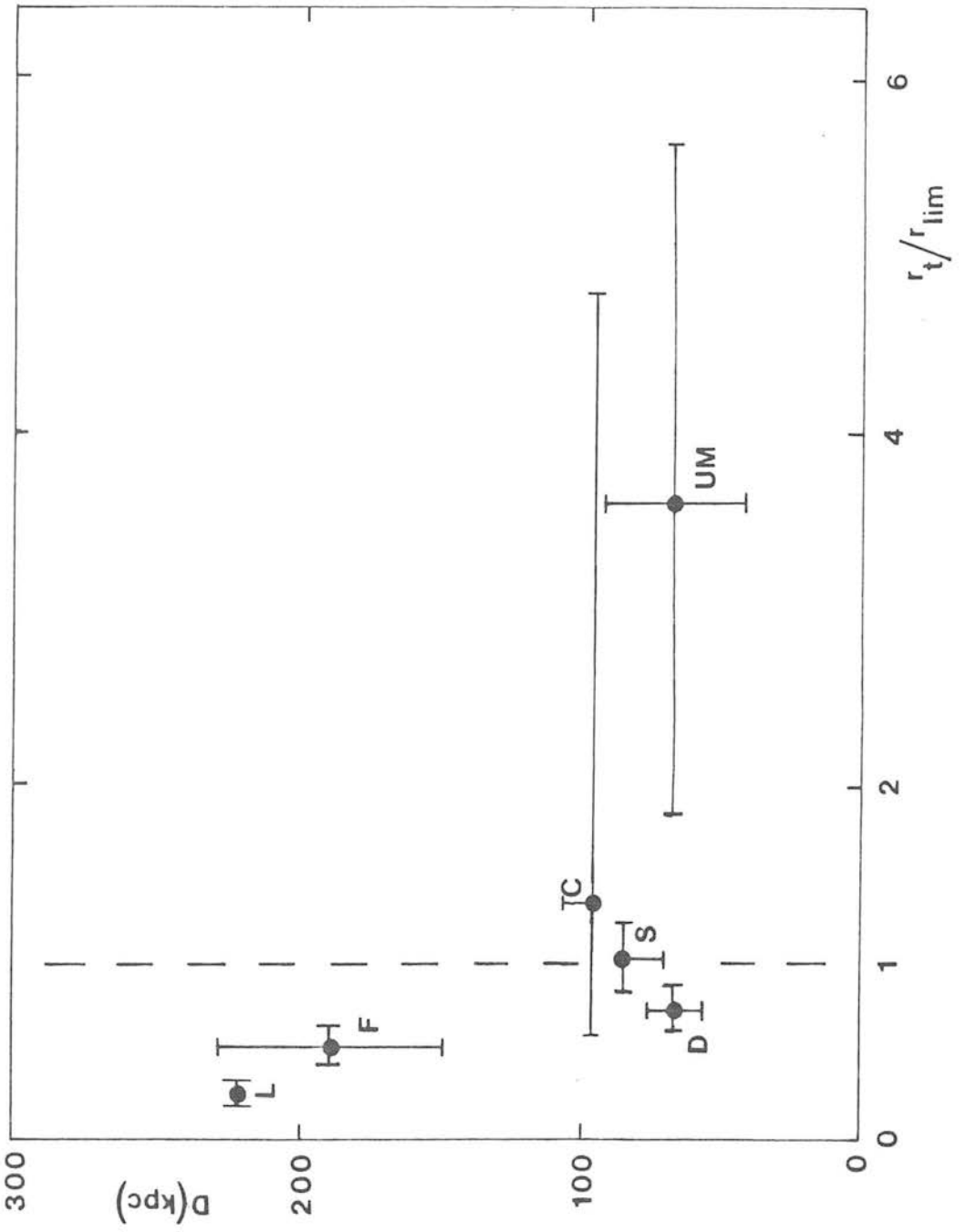

Figure 5.7. The ratio of the observed tidal radius (r_t) to the predicted one (r_{lim}) from King (1962) plotted as a function of Galactocentric distance. r_t/r_{lim} for the Leo systems overlap and so are plotted only once. Notation as in figures 5.6a and b.

TABLE 5.4 LOCAL GROUP DWARF SPHEROIDAL GALAXY DATA

Name	Ellipticity (e^*=1-b/a)	a_D (kpc)	b_D (kpc)	r_c (')	r_t (')	r_c (kpc)	r_t (kpc)	c
Sculptor	0.35±0.05	84±14	84±14	11.9	53±5	0.29±0.05	1.30±0.22	4.5±0.4
Fornax	0.35±0.10	188±40	190±40	16.0	50±6	0.87±0.19	2.73±0.58	3.1±0.4
Leo I	0.31±0.07	220±50	224±40	4.5	13.9±0.5	0.28±0.065	0.89±0.20	3.1±0.1
Leo II	0.01±0.10	220±50	223±40	2.5	9.6±1.5	0.160±0.036	0.61±0.14	3.8±0.6
Draco	0.29±0.04	67±10	67±10	6.5	26±2	0.127±0.019	0.51±0.08	4.0±0.3
Ursa-Minor	0.55±0.10	67±14	69±14	11.1	59±25	0.216±0.045	1.15±0.5	5.3±2.3
Carina[1]	0.31±0.03	91±9	93±9	9.7±0.8	38±10	0.260±0.050	(0.67,1.01,1.40)	4.4±1.2

M_V	$^2\rho_o$ ($\times10^{-3} M_\odot/pc^3$)	^{3}[Fe/H] (mean)	M^H ^{d}($\times10^5 M_\odot$)	M^V ^{e}($\times10^6 M_\odot$)	M^E ^{f}($\times10^7 M_\odot$)	$^4\ell$	^4b	$^4\alpha$ (1950)	$^4\delta$	$^5\sigma$ (kms^{-1})
-10.9	7.1	-1.9(±?)	30	(1, 8,19)	8.4±1.5	287.685	-83.133	00 57 44	-34 00.4	5.8±2.4
-13.6	1.7	-1.7(±?)	200	(?,15,39)	25±5	237.294	-65.654	02 37 50	-34 44.4	6.4±2.0
-11.4	6.0	-1.85±0.15	40		8.1±1.9	225.980	+49.109	10 05 46	+12 33.2	
- 9.8	13.0	-1.95±0.15	10		4.7±1.0	220.143	+67.236	11 10 50	+22 26.1	
- 8.0	3.5	-2.15±0.15	1.2	(3, 7,13)	3.7±0.5	086.363	+34.746	17 19 13	+57 57.5	9.0±2.0
- 8.0	1.1	- 2.4±0.15	1	(4,27,73)	6.3±1.3	104.969	+44.843	15 08 12	+67 23.0	11.0±3.0
(-8.8,-9.6, -10.8)	5±4	- 1.8±0.3	(0.3,6.1, 17.5)	(4,22,57)	7.6±1.5	260.113	-22.223	06 40 24	-50 55.0	10.4±3.0

TABLE 5.4 (cont'd.)

[1]All data for the Carina dwarf in this table has been derived in this Thesis apart from ℓ, b, α and δ.

[2]All data (apart from that for Carina dwarf) from Cowsik and Ghosh (1985).

[3]All data (apart from that for Carina dwarf) from Aaronson and Mould (1985).

[4]Webbink (1985).

[5]Ursa-Minor and Draco data from Aaronson (private communication - calculated from carbon and giant star spectra), Fornax and Sculptor data from Seitzer and Frogel (1985) (calculated from carbon star spectra only).

All other data in table taken or derived from that in Hodge (1971).

[a]Heliocentric distances.

[b]Galactocentric distances.

[c]Values obtained by using M^H as mass of dwarf spheroidal.

[d]Hodge (1971) masses (apart from Carina dwarf mass).

[e]Derived from carbon star velocity dispersion measures. Lower bound for Fornax uncertain since the value of μ cannot be easily derived (see King 1966) for the lower bound of the concentration parameter.

[f]Minimum mass (from velocity of espace arguments - see equation 5.25) for a dwarf spheroidal galaxy to retain material ejected from its red giants.

Bracketed values are in the form (min. value, mean, max. value).

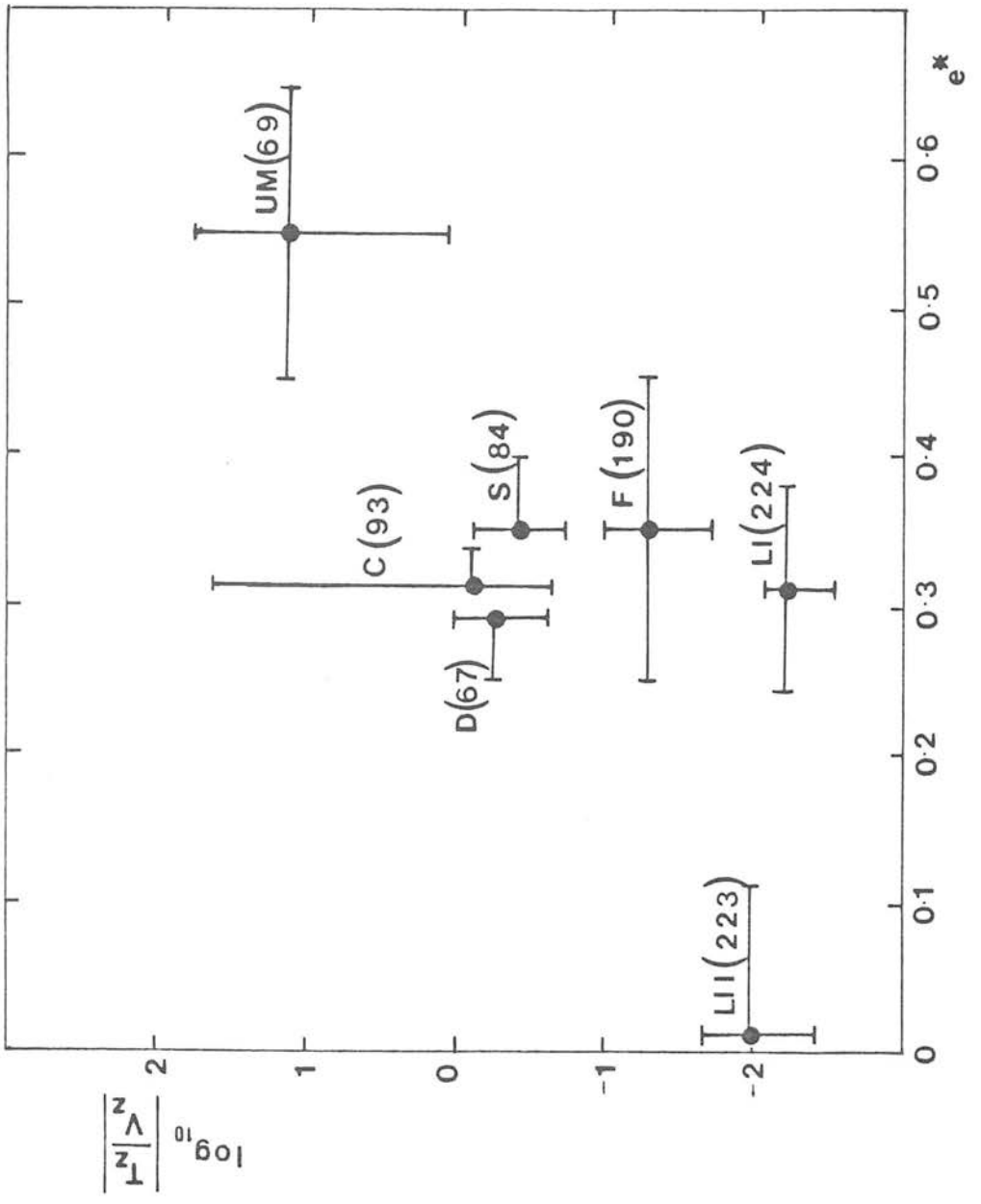

Figure 5.8. $\log_{10}\left|\frac{T_z}{V_z}\right|$ as a function of ellipticity for the Galaxy's dwarf spheroidal galaxy companions using Hodge (1971) data. Mean Galactocentric distances to the systems are in brackets (kpc). Part of the error bar on e* of the Carina data has been omitted to avoid confusion with the Draco data. Notation as in figures 5.6a and b.

galaxies, so again using the masses of the dsph galaxies derived by using the Hodge (1971) method, it must be concluded that the Galaxy is seriously disrupting these systems.

Can the CDG/Draco/Ursa-Minor 'discrepancies' in figures 5.7 and 5.8 be explained in any other way? In section 5.6, theoretical mechanisms to allow systems with the dwarf spheroidals' observed central densities to appear relaxed over a time equal to the probable age of the Galaxy (15 Gyr) were discussed. However, does the observed tidal radius reflect the <u>real</u> tidally imposed limit due to the Galactic potential i.e. have all the stars in these galaxies had the chance to be affected by the influence of the Galactic gravitational potential well? This can be examined by considering the ratio T_{orb}/T_c, where T_{orb} is the orbital period of the dwarf spheroidal around the Galactic centre. Taking the orbital period of the Sun around the Galactic centre as 2.5×10^8 years, from Kepler's Law it can be seen that if the presently observed distances to the dsph galaxies represent their time averaged distances, then the CDG has orbited about twice and the Draco and Ursa-Minor dwarfs about four times around the Galactic centre in a time span of 15 Gyr. From equation 5.28, in 15 Gyr, the average number of crossings that a star in the CDG will have done will be of the order fifty and possibly as many as 500 depending upon whether a mass $\sim 10^5$ (i.e. as the lower bounds of Hodge 1971 suggests) or $\sim 10^7 M_\odot$ (as velocity dispersion measures suggest) is adopted for the dwarf spheroidal masses respectively. This calculation shows that in either case, stars have had ample time to reach the boundary of the respective dsph galaxy. Once there though, do they have time to escape? - i.e. is a star's acceleration large enough in order that it is a sizable multiple (e.g. twice) of its (say) tidal radius away from the dsph galaxy in 15 Gyr. By calculating the magnitude of the relative acceleration of a star in the CDG in circular motion about the Galactic centre with the radius of its orbit equal to its present Galactocentric distance, a rough estimate of this time scale for the CDG is found to be (at most) 3 Gyr. If this approximation can be taken to be a good estimate of this time scale, then it seems reasonable to suppose that the observed tidal radius <u>does</u> reflect the tidally imposed limit due to the

Galaxy's gravitational field for the CDG.

Could it be that the equation derived by King (1962) (namely equation 5.31) to evaluate r_{lim} is not a very good approximation for the dwarf spheroidals, due to the angular velocity of these galaxies relative to that of our own Galaxy at their large Galactocentric distances not being negligible as King (1962) assumes? No information is currently available for the variation of velocity dispersion with radius for the dsph galaxies, so an observational estimate of this quantity is not easy to ascertain. However, the theoretical study of Innanen (1979) is a similar analysis to that of King (1962) but taking into account this effect, and shows that stars having retrograde orbits with respect to the direction of the stellar system's orbital motion can 'cling' onto the system well outside the theoretical tidal radius, hence producing an apparently larger r_t. Using e = 0.5 again, for a dwarf spheroidal in a direct orbit his calculations show that the tidal limit r_d (d for direct) = $0.7r_{lim}$. This makes the picture of Galactic tidal disruption depicted by figures 5.7 and 5.8 even worse (especially for Carina, Draco, Ursa-Minor, and Sculptor). Most tidally confined stars in globular clusters are believed to move in more rectilinear than circular orbits (see e.g. Heggie 1979), and so to survive near the tidal boundary it seems reasonable to suppose that some of the stars would need to be in retrograde orbits. For this to occur, Innanen's (1979) equations yield r_r (subscript r for retrograde) = $1.5r_{lim}$ and this gives the (better) situation of $r_r < r_{lim}$ for all the dwarf spheroidals (except Carina and Ursa-Minor (see figure 5.7), so the discrepancy still remains (both expressions for r_d and r_r are only weakly dependent upon the choice of e).

A much simpler way to obtain the predicted limiting radius at perigalacticon $\sim r_t$ (or larger) for all the dsph galaxies is to assume their masses are larger than Hodge (1971) predicts, say, in the case of the CDG, and Ursa-Minor dsph galaxies, increasing them by factors $\sim$ 2 and 50 respectively. This is smaller than the factors $\sim$ 36 and 270 predicted by the velocity dispersion measures and is consistent with the observation of very little neutral

hydrogen gas in these galaxies (Huchtmeier 1980) (cf. M^V in table 5.4). The values of $|T_z/V_z|$ are also affected by altering M_d. If the masses of the CDG and Ursa-Minor dwarf galaxies are increased by $\sim$36 and 270 respectively, then the value of $|T_z/V_z|$ for these galaxies are reduced by factors $\sim$ 0.03 and 0.004 respectively and one is lead to conclude that no severe tidal disruption is occuring. This result also (obviously) depends upon the value for the mass of our Galaxy that is being adopted. The value of $(2.6\pm0.8)\times10^{11}M_\odot$ obtained by Lynden-Bell, Cannon and Godwin (1983) from the radial velocity measurements of the outer Galactic halo clusters (including the dsph galaxies) assumed that the velocity distribution of these dsph galaxies was isotropic. This mass would be smaller if their velocities were predominantly radial and larger if they were predominantly transverse. It was shown in their paper (see appendix B) that for an appropriate choice of orbit eccentricity (less than that of the isotropic case, implying that the velocities are more transverse), consistent with the dsph galaxies surviving in the Galactic potential, that the Galaxy's mass could quite easily be pushed as high as $(10\pm3)\times10^{11}M_\odot$ out to a distance of about 100 kpc. Using this mass for the Galaxy, equation 5.31 implies that for the condition of $r_{lim} > r_t$ holding for all the dsph galaxies, M_d for the CDG and Ursa-Minor dsph galaxies would have to be factors of approximately 8 and 200 respectively larger than M^H i.e. if the carbon star velocity dispersion masses are correct then the dsph galaxies are not being disrupted.

5.8 : SUMMARY AND CONCLUSIONS

Core and tidal radii of the CDG have been found and used to show that if the dsph galaxies have a mass as derived by Hodge (1971) (by assuming that their luminosity functions are similar to those of the globular clusters), then the Carina, Sculptor and Ursa-Minor dsph galaxies are being disrupted by the Galaxy's gravitational attraction. The mean masses that the Hodge (1971) method predicts for the CDG is 125 times less than that required for the dsph galaxy to hold onto its nuclearly processed material for further star formation periods (see table 5.4). Hence the metallicity spread now found in

some of the dsph galaxies could suggest that this galaxy's strong tidal interaction with the Galaxy has led to a substantial fraction of its initial mass being lost if the dsph galaxies originated as isolated systems. However, if the velocity dispersion measures of carbon stars in the dsph galaxies reflect that of their parent galaxy, then the dsph galaxies could be substantially more massive than the mass predicted by Hodge (1971). If this is the case, then it has been shown that the dsph galaxies are stable against Galactic disruption, even if a heavy halo Galaxy model is used. The results are also consistent with the dsph galaxies originating in a more massive external system (such as a 'Greater' Magellanic Cloud) where their metal enrichment (and currently observable metallicity spread) originated, and later becoming satellites of our Galaxy when the hypothetical external system was disrupted. The M/L ratio calculated from the mass derived from the velocity dispersion measure of carbon stars indicates that there is a possibility of dark matter in the CDG, but the large error on this ratio makes any firm conclusion on this difficult to make.

It is clear from the discussion in this chapter that one of the major uncertainties in deducing the origin of the dsph galaxies is a reliable determination of their masses. The reliability of obtaining this from the observed velocity dispersion of carbon stars in the dsph galaxies is considered more fully in the next chapter.

6.1 : Introduction

Carbon stars have been found to be quite common in the Local Group galaxies. In the LMC, Westerlund et al (1978) and Sanduleak and Philip (1977) found more than 800 carbon stars, whilst Blanco, Blanco and McCarthy (1978) and Blanco, McCarthy and Blanco (1980) found enormous numbers in both of the Magellanic Clouds from grism surveys. The discovery of these stars in the dsph galaxies is also relatively recent. The very red stars in the Fornax dsph galaxy found by Demers and Kunkel (1979) were shown by Aaronson and Mould (1980) to be carbon stars, while Westerlund (1979) and Frogel et al (1982) found several in the Sculptor dsph galaxy. Three were identified in the Draco dsph galaxy by Aaronson, Liebert and Stocke (1981), and Aaronson, Olszewski and Hodge (1983) reported the discovery of these stars in the Leo I/II and Ursa-Minor galaxies.

Cannon, Niss and Norgaard-Nielson (1980) unexpectedly found two carbon stars in the CDG whilst examining the spectra of a sample of potential red giants. A systematic search of this galaxy was carried out on UKST low dispersion objective prism plates, and a further six candidates were found. Infra-red photometry (Mould et al 1982) and optical spectra (Lynden-Bell, Cannon and Godwin 1983) were obtained for all of these candidates, this latter work (see following, and appendix B) positively confirming six out of the (possible) eight candidates as carbon stars. Using a similar technique, but with COSMOS measures of AAT plates, a further carbon star candidate has been found in the CDG (see chapter 3 and figure 3.1a), confirmed later in the year (1985) as such by Azzopardi, Lequeux and Westerlund (1985) (hereafter ALW), who found an additional three in this galaxy.

Cool stars are usually classified into three MK spectral types, using the near infra-red spectral range (6800 to 8800Å). M stars are identified by their strong TiO bands; C stars by the 7945, 8125 and 8320Å CN bands and S stars by the LaO bands at 7403Å. Hotter carbon

stars, not showing sufficiently strong CN bands to be detected in the infra-red, can be detected at shorter wavelengths by their characteristic Swan C_2 bandheads at 4737, 5165 and 5635Å. Carbon stars are further classified according to their bandhead strengths; a C1 carbon star has weak bandheads whilst a C7 carbon star has strong ones. Automatic cross correlation techniques have been employed in this chapter to derive the heliocentric radial velocity of the CDG using the observed wavelengths of the Swan bandheads in carbon star spectra as redshift indicators. Aaronson (1983), using high resolution spectroscopy on carbon stars in the Draco dsph galaxy centred on one of the Swan bandheads (5636Å) and covering a spectral range of about 50Å at a resolution of 1/6Å, obtained a radial velocity with a claimed accuracy of $1 kms^{-1}$. He also used the technique to obtain a velocity dispersion in this galaxy of $\sim 6.5 kms^{-1}$. Stetson (1984) too has used the technique to show there is weak evidence against an internal velocity dispersion as great as $10 kms^{-1}$ in the same galaxy, and Aaronson and Cook (1983) found a 'significant' velocity dispersion in Ursa-Minor. Seitzer and Frogel (1985) found that the velocity dispersion in Fornax and Sculptor was 6.4 ± 2.0 and 5.5 ± 2.4 kms^{-1} respectively, but these were based only on five and three carbon star velocities respectively. The reliability of using carbon stars for infering the velocity dispersion of their parent galaxy is also considered in this chapter.

6.2 : The observations and reduction of data

6.2.1 : The RGO spectrograph and IPCS

All the spectra used to derive the radial velocities presented in this chapter were obtained over three nights during January 1983 using the RGO spectrograph at the f/8 focus of the AAT. The spectrograph contains two cameras; an 82cm focal length f/5.5 spherical mirror, and a 25cm f/1.67 Cassegrain-Maksutov system. For this observing run, the 25cm camera was used together with the 1200V grating (i.e. 1200 grooves/mm), with the blaze pointing towards the collimator; this combination of grating and blaze giving a dispersion of 33Å/mm. The Image Photon Counting system (IPCS) developed at

University College London (UCL) was used in conjunction with this spectrograph, and consists of four image tubes, the basic function of which is to register a 'flash' of light on a phosphor screen when a photon enters the system. This screen is scanned by a TV camera, via a transfer lens, and was used in 2D mode with the 2D computer memory formatted into 2040 'channels' (increments in the dispersion direction) by 50 'X-sections' (increments perpendicular to the dispersion direction). When a 'flash' occurs, corresponding to a photon colliding with this screen, the system automatically calculates its centre and increments the photon count in the appropriate part of the 2D memory of the computer by 1 count, thus gradually building up a 2D picture of the object. After the required time of integration, this stored data can be written to disc as a 2D image.

The IPCS tube can be adjusted so that the TV scans are perpendicular to the dispersion direction, and a variable time delay incorporated to straighten out the 'S distortion' of each spectrum caused by the magnetic focussing. This latter operation of focussing the system was done by comparing spectra obtained when alternate Hartmann shutters, each one covering half of the field of view, were closed.

6.2.2 : Reduction of data

In order to reduce the effects of image tube sensitivity variations (e.g. low efficiency, or 'dud' pixels), two 'apertures' were used for the observations; aperture A was centred on X-section 15 and aperture B on X-section 23. A copper-argon lamp was used for the purpose of wavelength calibration and by using a tungsten lamp in the spectrograph, flat fields could be obtained at the beginning and end of each observation night.

The general procedure used for each observation was then as follows:

(a) integration of the Cu-Ar arc for 100 seconds

(b) integration of the object through aperture A for 1000 seconds
(c) repeat of (a)
(d) repeat of (b) but using aperture B
(e) repeat of (a)

This procedure enabled the effect of 'flop' to be checked, whereby the instruments move as the telescope is slewed over certain regions of the sky.

Two grating angle settings were used to cover either the spectral range 4450 to 5350Å, which includes the 1-0 C_2 Swan bandhead at 4737Å and the 0-0 band at 5165Å, or the range 5000 to 5900Å which includes this latter bandhead and also the 0-1 band at 5636Å. Four Galactic carbon stars with known heliocentric velocities (McClure private communication, see table 6.1) were observed as standards and their spectra used as the templates for the cross correlation. Over the three nights, four of the carbon stars (C1,C3,C5,C6, this notation is not to be confused with the classification notation used in section 6.1) were observed over both the wavelength ranges mentioned above, and the remaining two (C2 and C4) only over the 4600 to 5300Å wavelength range (due to lack of observing time). The standard STARLINK spectral reduction package (SPICA) at the time the data was obtained, did not have a cross correlation subroutine that was working properly, and so the Edinburgh Spectral Package (ESP, Kelly private communication) had to be used (this package is primarily designed for obtaining galaxy redshifts).

The raw data was in a form so that each of the 2D images could be initially displayed on an ARGS TV monitor, and the number and position of the X-sections containing the spectrum (centred on aperture A or B) determined by using a cursor. A 1D spectrum was then obtained for each of the apertures by summing the data over these X-sections. The sky background measures were taken from the channels adjacent to the apertures used e.g. if the spectrum of the object covered three X-sections, then this signal was multiplied by two, and three X-sections of the sky signal either side of the relevant aperture subtracted from it. The calibration arc to calibrate the

TABLE 6.1

HELIOCENTRIC RADIAL VELOCITIES FOR STANDARD STARS

Standard	Radial velocity (kms^{-1}) (McClure private communication)	Mean
HD16115	19.2, 17.7, 18.1, 18.1	18.3 ± 0.6
HD52432	24.4, 24.5, 25.1, 21.5, 21.7, 21.2	23.1 ± 1.8
HD79319	-0.9, -1.0, -3.2, -3.4, -1.8, -0.2, -3.0, -2.8	-2.0 ± 1.2
HD223392	-20.0, -19.8, -20.0, -20.4, -20.6	20.2 ± 0.3

spectrum in each of the apertures was obtained in a similar fashion, by separately summing the two apertures used for the observations covered. These arc lines were then displayed on the ARGS TV monitor, and manually identified using the Schinckel, Phillips and Hill RGO spectrograph guide (1982), and a polynomial fit made to the (channel number, wavelength) values. Typically a fifth order fit was used. Each aperture observation was then individually 'scrunched' (i.e. this calibration was applied to the data) and the two aperture (A and B) measures for a particular object added and archived to disc.

The first stage of the reduction procedure to derive relative radial velocities of the various carbon stars was to choose the standard star against which the CDG carbon star redshifts were to be measured. Both the standard and object CDG spectra were smoothed by convolving them with a gaussian of width one pixel and then rebinned logarithmically to linearise the effects of the Doppler wavelength shifts. The continuum was computed using a 'Martin' recursive filter (which essentially removes the spikes from the spectrum) and the result was divided out of the rebinned spectra. The standard carbon star was then assigned a reference velocity of $0 kms^{-1}$ (the actual correction due to the motion of the standard star relative to the velocity of the CDG carbon star was put in manually at a later stage), and the two spectra cross correlated. For the cross correlation procedure in this reduction package to work effectively, a large portion of the spectral range of each spectrum had to be used. For this reason it was decided to use the whole of the wavelength ranges 5100 to 5800Å and 4600 to 5300Å, which would then include two Swan bandheads each, the 5165Å bandhead being common to both. The 5636Å bandhead is not affected by the presence of isotopes, but the 4737Å isotopic bands are well separated, so that the cross correlation package should be able to give strong weight to these features when present in the spectra. If the resulting cross correlation function (i.e. a plot of the difference in velocity between the two spectra against the correlation measure) was well defined in having a single peak, then this velocity was taken as the star's velocity relative to that of the standard.

If V_θ is the heliocentric radial velocity, V_{obs} the observed radial velocity and C the correction in velocity for the motion of the Earth around the Sun then

$$V^*_\theta = V^t_\theta + (V^*_{obs} - V^t_{obs}) + (C^* - C^t) \qquad (6.1)$$

where the superscript * refers to the Carina carbon star and 't' to the template star. These corrections were derived using a standard STARLINK package (Wallace private communication) and are listed in table 6.2, together with the derived (ESP) radial velocities in kms^{-1}. The consistency of these radial velocities is not good, since they depend upon e.g. which standard star template is used for the cross correlation, and also they vary depending upon which wavelength range is used.

In order to investigate the possibility of this being the case regardless of how the data was processed, the whole of the spectral data was re-analysed using the STARLINK SPICA cross correlation software when this became available (Hill, private communication) employing the fourier transform techniques of Tonry and Davis (1979). The wavelength calibration and logarithmic rebinning of the spectra were performed in precisely the same manner as before, but before cross correlation, the mean of each spectrum was subtracted from that spectrum, and its ends apodised with a cosine bell to smooth out any sharp features that might result in false measurements. Its fourier transform was then taken, and a bandpass filter applied to remove the high frequency components (see figure 6.1), and the spectra were then cross correlated as before. Unfortunately the routine did not return a normalised correlation function, and so this function as before had to be examined to see whether it was single peaked. The velocities derived by this method are also tabulated in table 6.2. This particular spectral package has been used more recently by Sagar (private communication) who used it to find the radial velocities of red giants in NGC1851. The results so obtained agreed excellently with previously published velocities, giving

TABLE 6.2

HELIOCENTRIC CORRECTIONS AND RADIAL VELOCITIES OF THE CARINA DWARF'S CARBON STARS

(i) 5100 to 5800 Å

		CARC6[1]	CARC5[1]	CARC1[1]	CARC3[3]
HD52432[1]	(a)	26	26	26	25
	(b)	261	236	234	253
	(c)	287	262	260	278
	(d)	211	225	242	245
HD79319[1]	(a)	-14	-14	-14	-15
	(b)	297	260	271	279
	(c)	282	246	257	264
	(d)	215	226	241	245
HD16115[1]	(a)	46	46	46	45
	(b)	203	192	203	203
	(c)	249	238	249	248
	(d)	218	229	241	240
HD223392[1]	(a)	8	8	8	7
	(b)	195	162	180	226
	(c)	203	171	189	233
	(d)	211	219	234	241

TABLE 6.2

(cont.)

(ii) 4600 to 5300 Å

		CARC6[2]	CARC5[3]	CARC1[3]	CARC3[2]	CARC4[2]	CARC2[2]
HD223392[2]	(a)	8	7	7	8	8	8
	(b)	135	194	192	167	140	260
	(c)	143	201	199	175	148	268
	(d)	216	230	244	236	220	242
HD16115[2]	(a)	46	45	45	46	46	46
	(b)	129	181	194	146	141	248
	(c)	175	226	239	192	187	294
	(d)	219	229	238	230	221	236
HD79319[2]	(a)	-14	-15	-14	-13	-14	-14
	(b)	199	244	221	230	193	265
	(c)	185	229	207	217	179	251
	(d)	223	235	249	239	220	240
HD52432[3]	(a)	29	28	28	29	29	29
	(b)	192	231	205	201	167	195
	(c)	221	259	233	230	196	224
	(d)	214	225	239	240	215	240

Superscripts indicate the night of observation. All velocities in kms^{-1}.

Entry (a): Total correction to apply to the relative velocity of the two labelled stars (as described in the text) to obtain a heliocentric velocity for the CDG carbon star.

Entry (b): The velocity of the CDG carbon stars relative to the standard stars using the ESP cross correlation package.

Entry (c): (a) + (b).

Entry (d): The heliocentric velocity of the CDG carbon star derived by applying the correction in (a) to the relative velocity of this carbon star with the standard star using the SPICA cross correlation package.

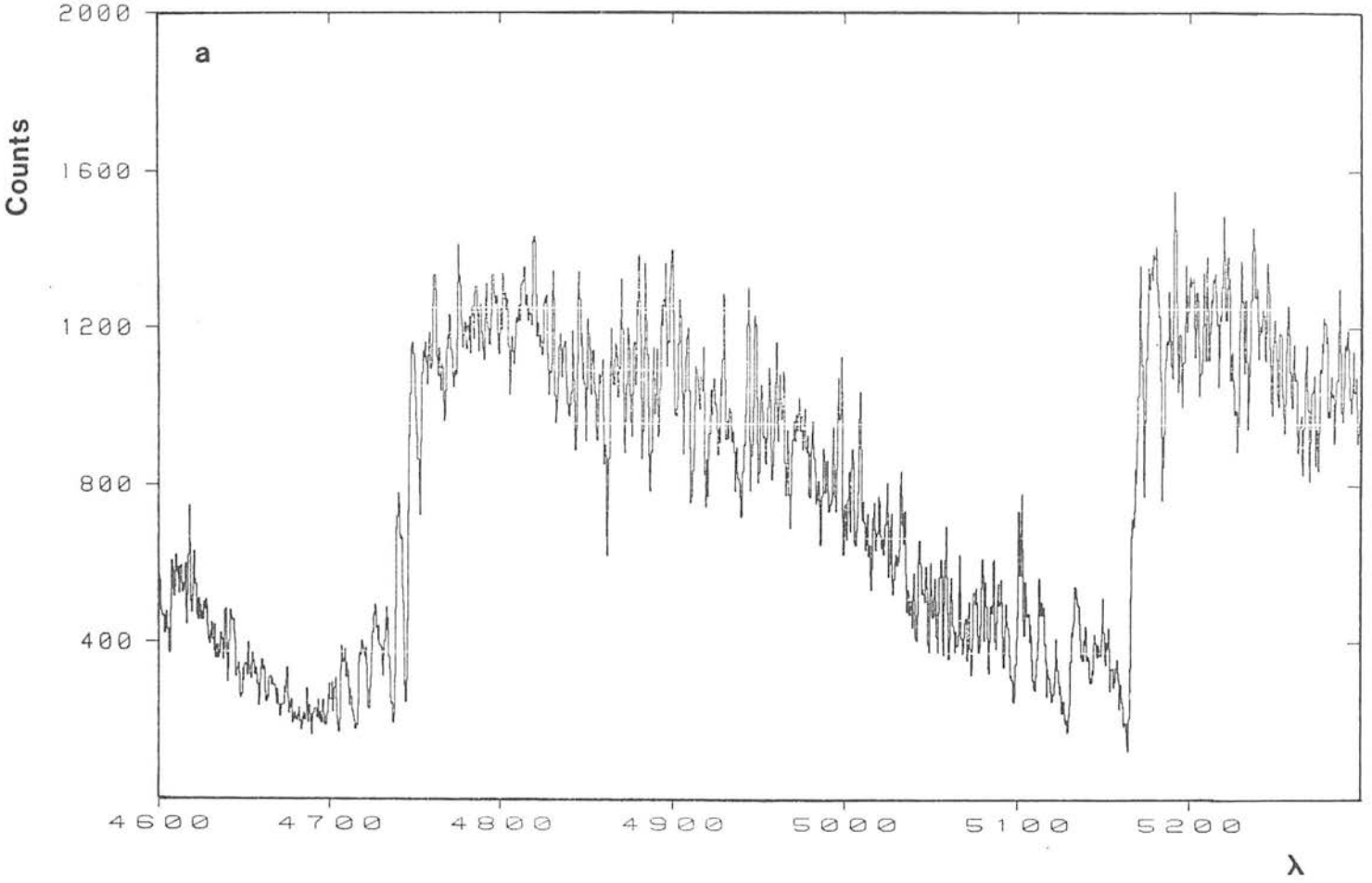

Figure 6.1a,b,c. (a) Original wavelength calibrated spectrum of HD16115, (b) log rebinned spectrum, (c) filtered spectrum.

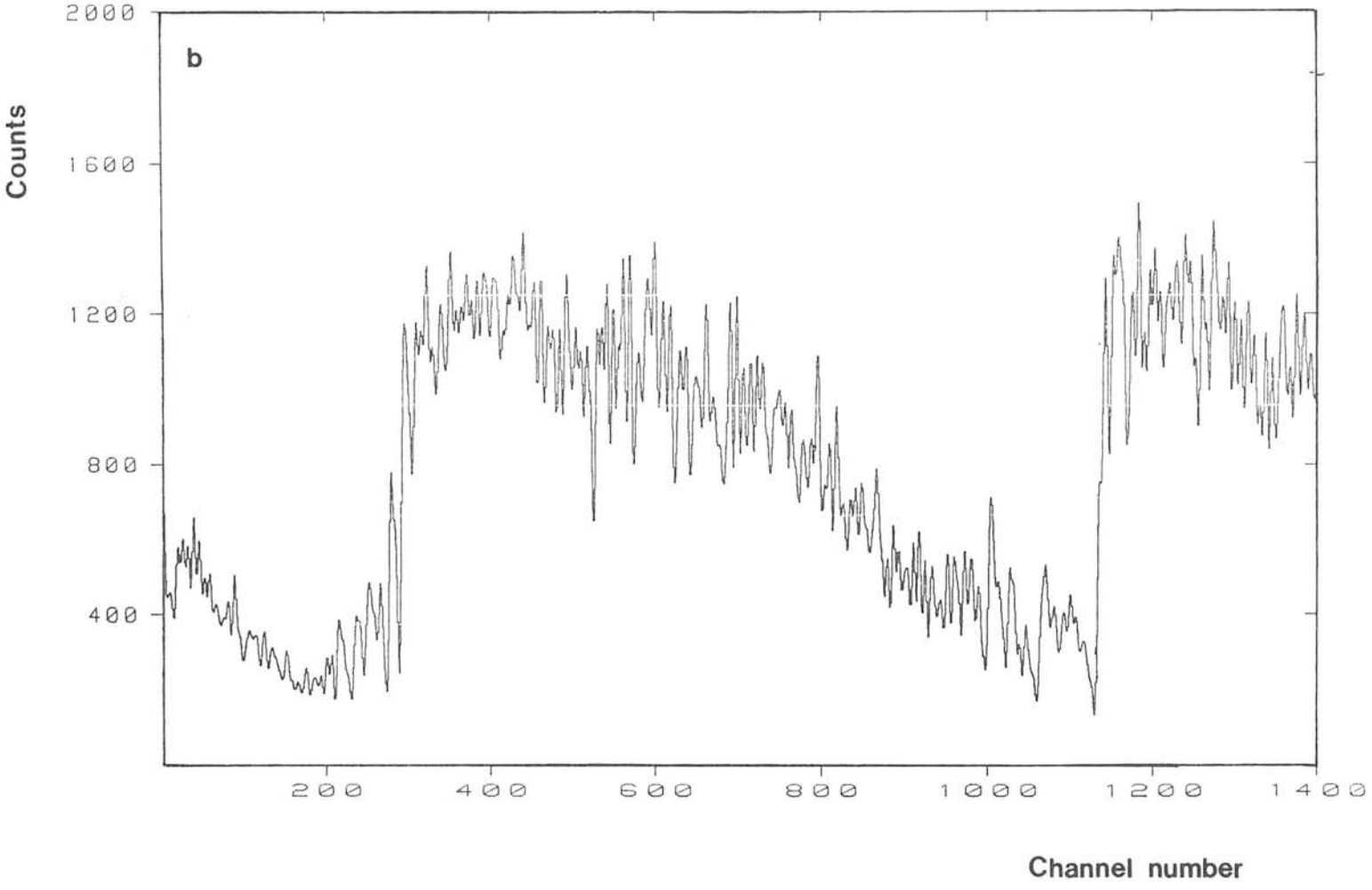

Figure 6.1 (cont.)

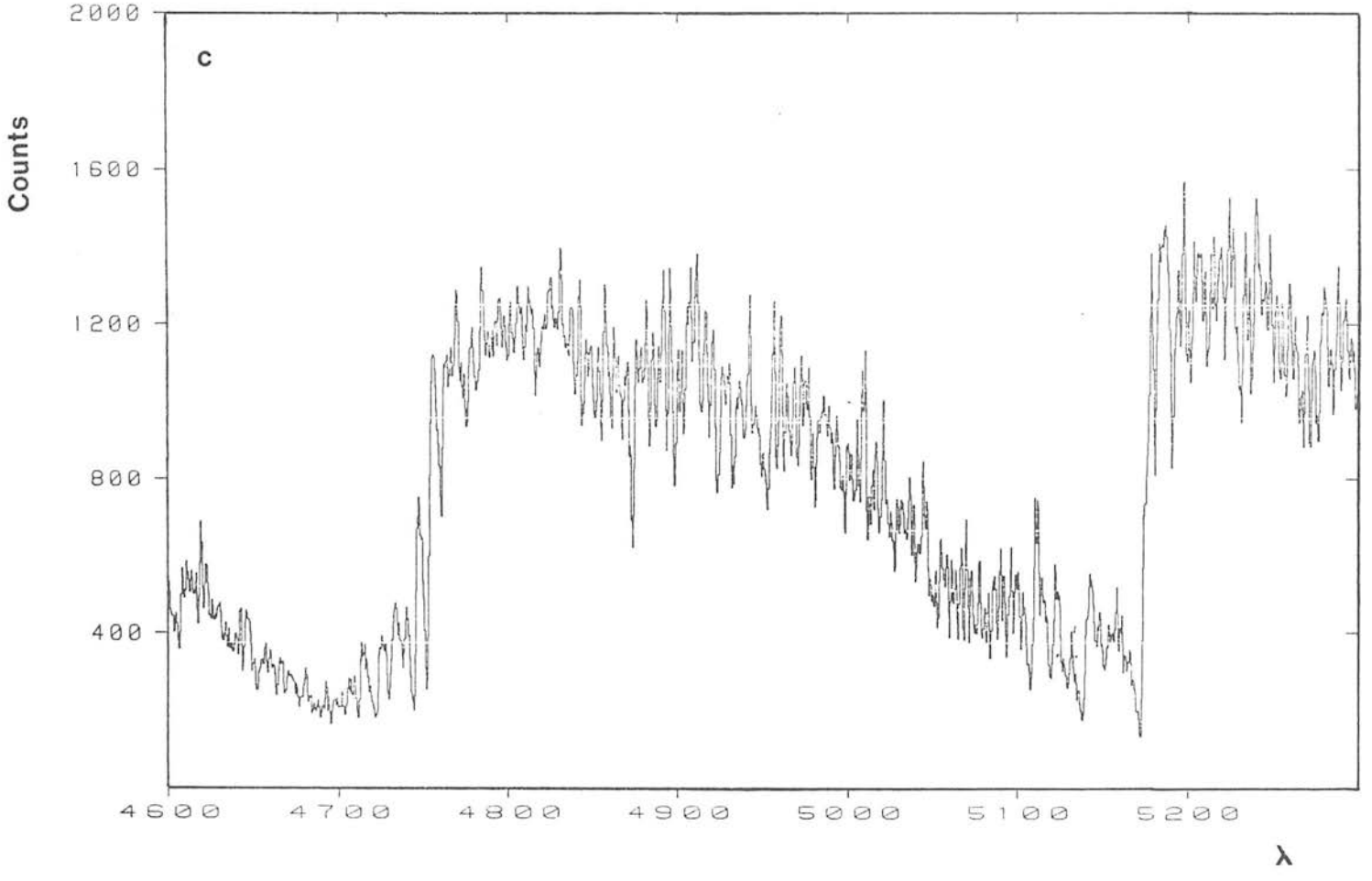

Figure 6.1 (cont.)

confidence that this package works satisfactorily for stellar spectra.

The biggest difference between the two reduction procedures is that the ESP package divides out the continuum of each spectrum before cross correlation. Since the carbon bands are absorption features in this continuum, a successful result can be difficult to achieve. If one (e.g. template) star was incorrectly processed due to this problem, then it could lead to systematic trends in the cross correlation e.g. in the 5100 to 5800Å range, HD52432 returns the highest correlated velocity with all of the CDG carbon stars (cf. table 6.2).

6.3 : Description of spectra

The wavelength calibrated spectra of the standard and CDG carbon stars are shown in figure 6.2. C7 and C8 (in the notation of Mould et al 1982) are not included since they did not show any of the Swan band features, and hence are not carbon stars. Maehara (private communication) classes C1 (which is similar to HD16115) as an early C3J type carbon star (the J implying that the spectrum contains C^{13} e.g. like HD52432 and HD 79319) and C3 as a normal (late) non-J carbon star of type C5, since normal carbon stars later than type C4 do not show Balmer lines. In relatively late carbon stars such as C3 and C4 in the CDG, most of the spectral features longward of the 5635Å $C_2(0,1)$ Swan bandhead are due to rotational lines of the CN red system, whilst in the early carbon stars such as C1 in the CDG, the atomic lines are generally weak in the region 4700 to 4900Å and so the cross correlation can make use of the strong atomic lines and CN features present in the region 5000 to 5900Å. The bandhead at 4737Å is usually not very well defined due to contamination by the $C^{12}C^{12}$, $C^{12}C^{13}$, $C^{13}{}_{C}{}^{13}$ isotopes which can be seen in some of the spectra shown in figure 6.2 (e.g. HD79319).

6.4 : Uses of the carbon star radial velocities

The radial velocities of the CDG carbon stars derived here will

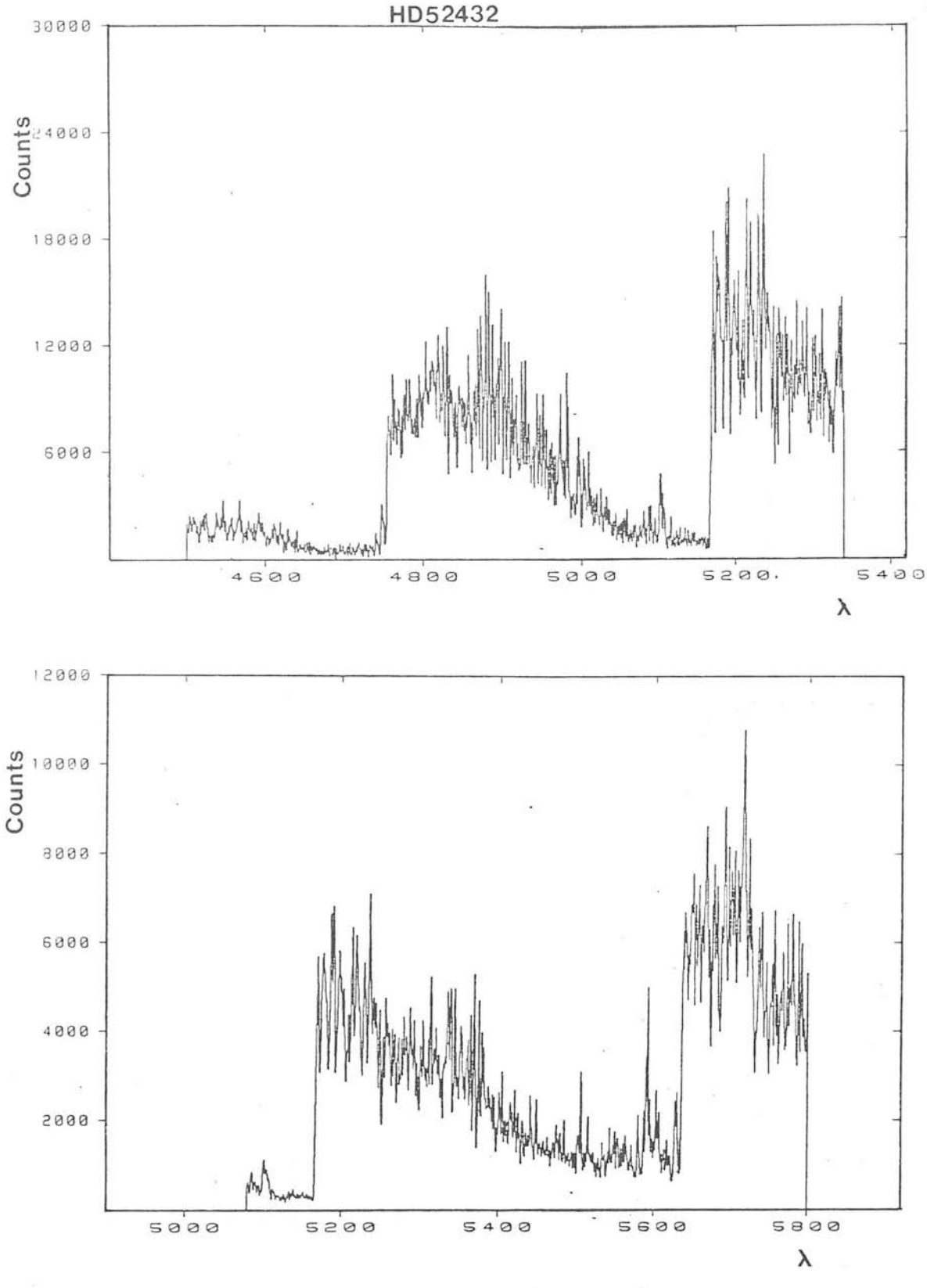

Figure 6.2. Wavelength calibrated spectra of the Galactic standard and Carina dwarf carbon stars derived in this thesis.

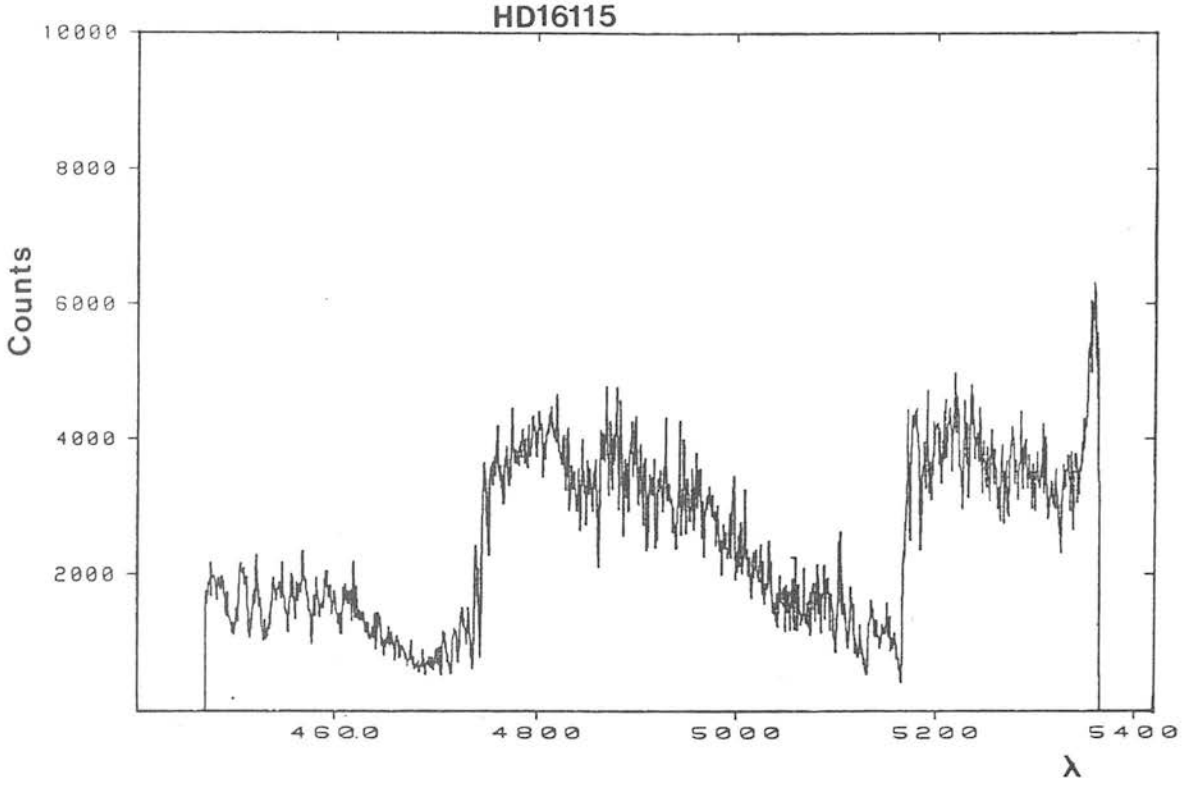

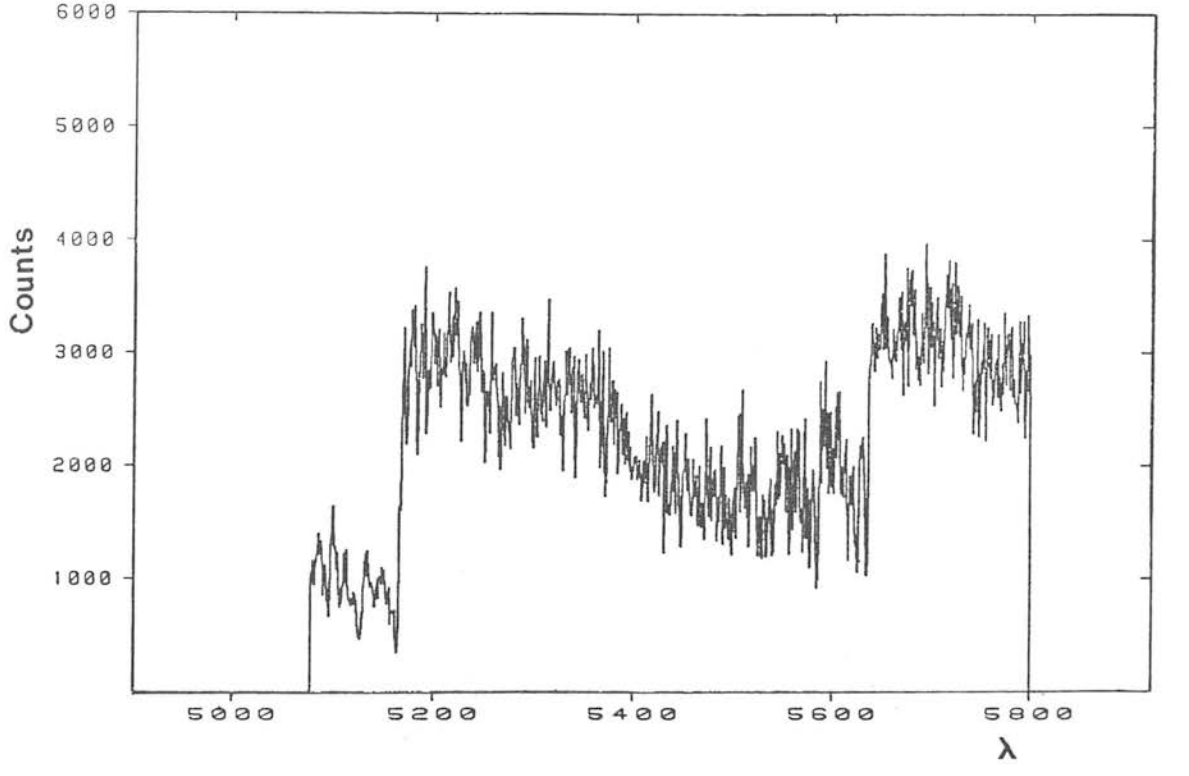

Figure 6.2 (cont.)

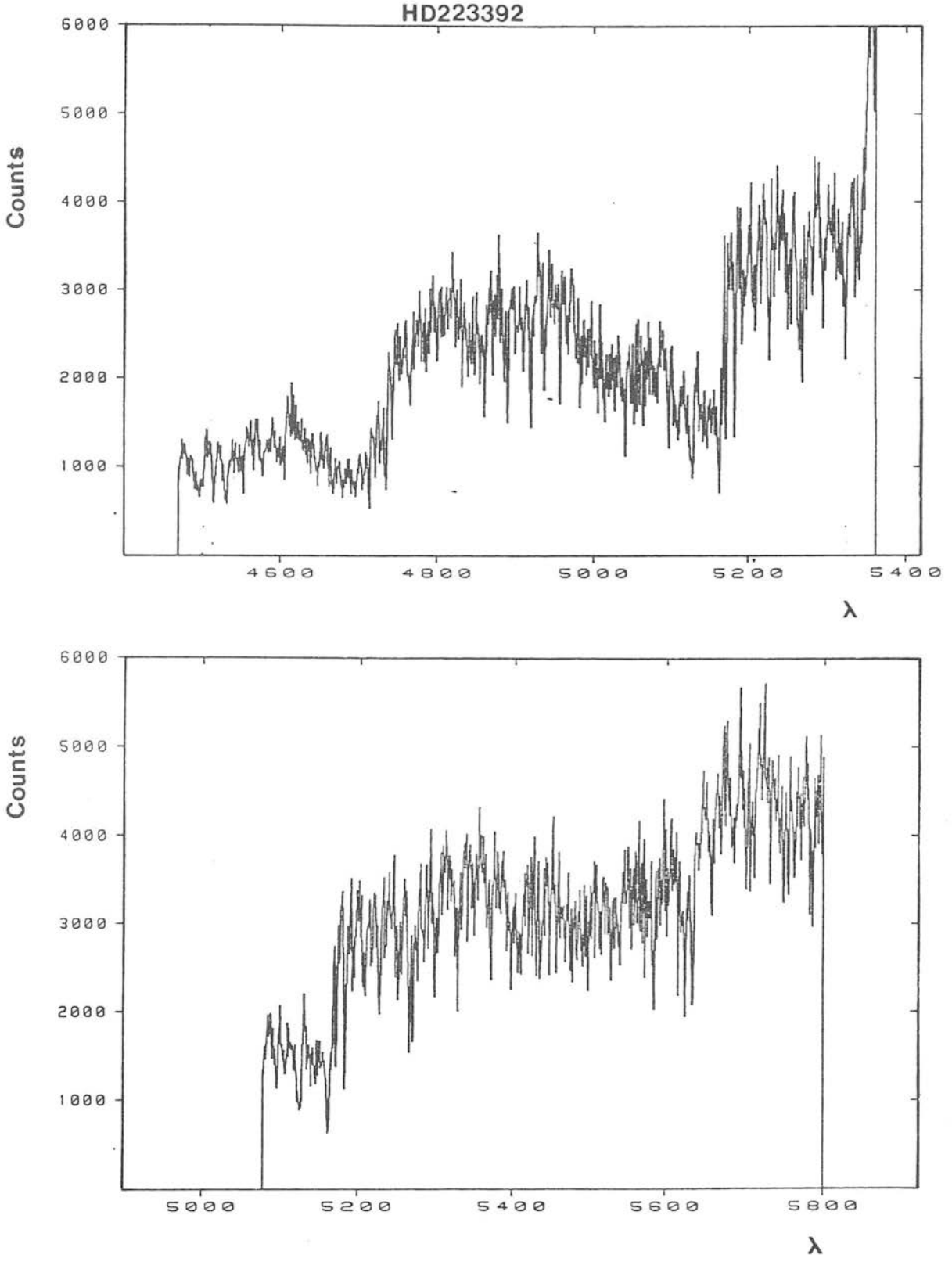

Figure 6.2 (cont.)

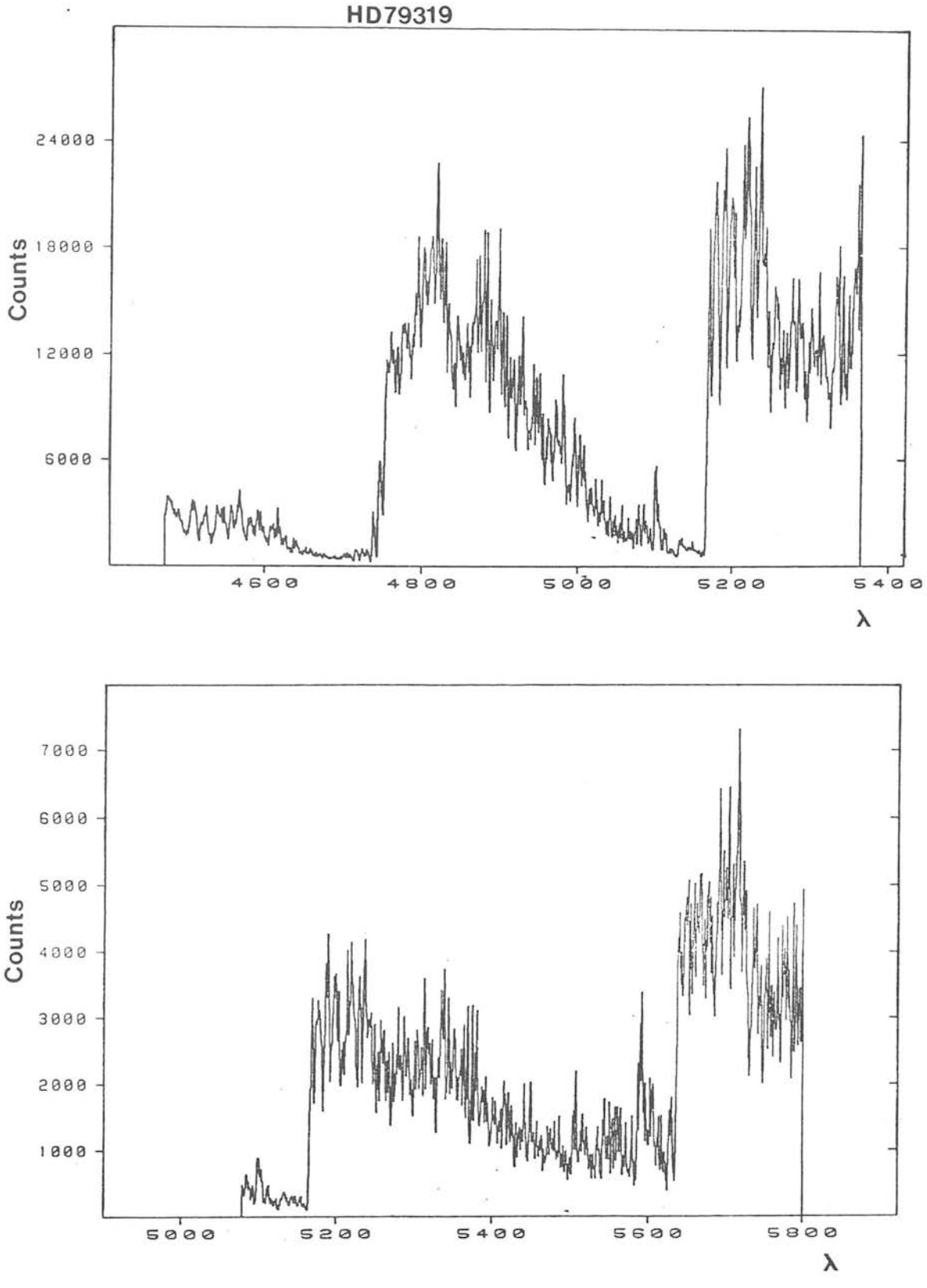

Figure 6.2 (cont.)

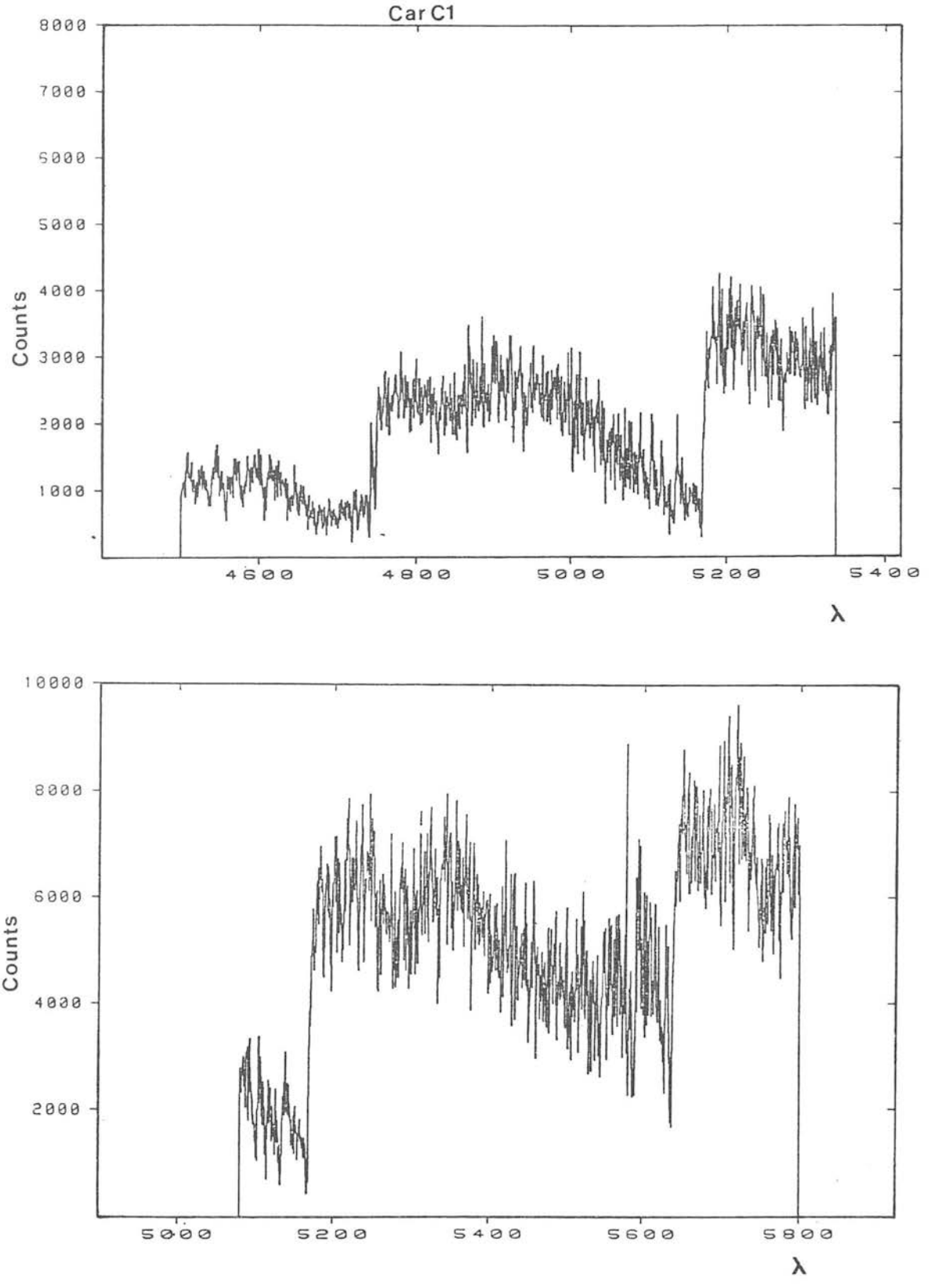

Figure 6.2 (cont.)

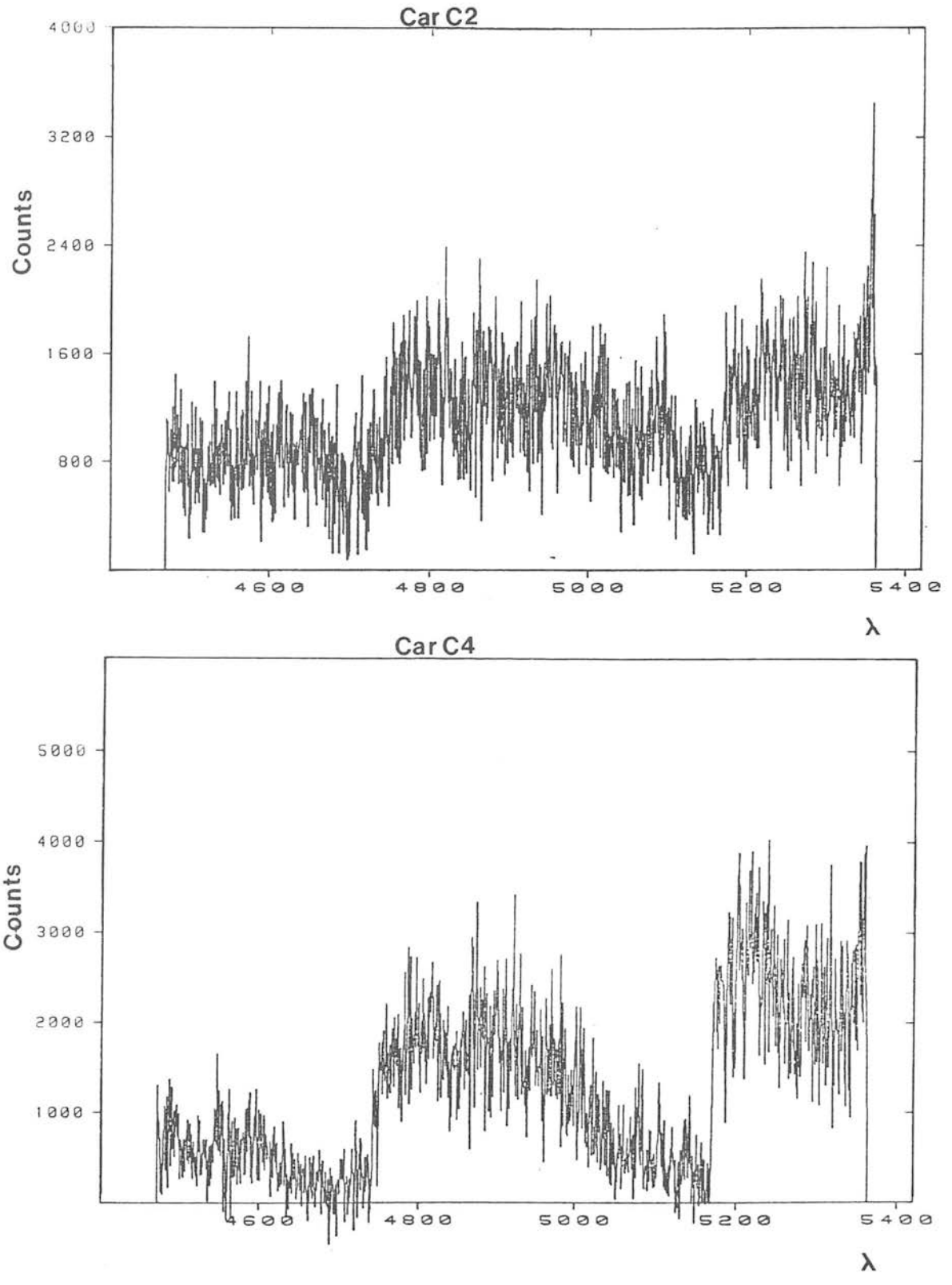

Figure 6.2 (cont.)

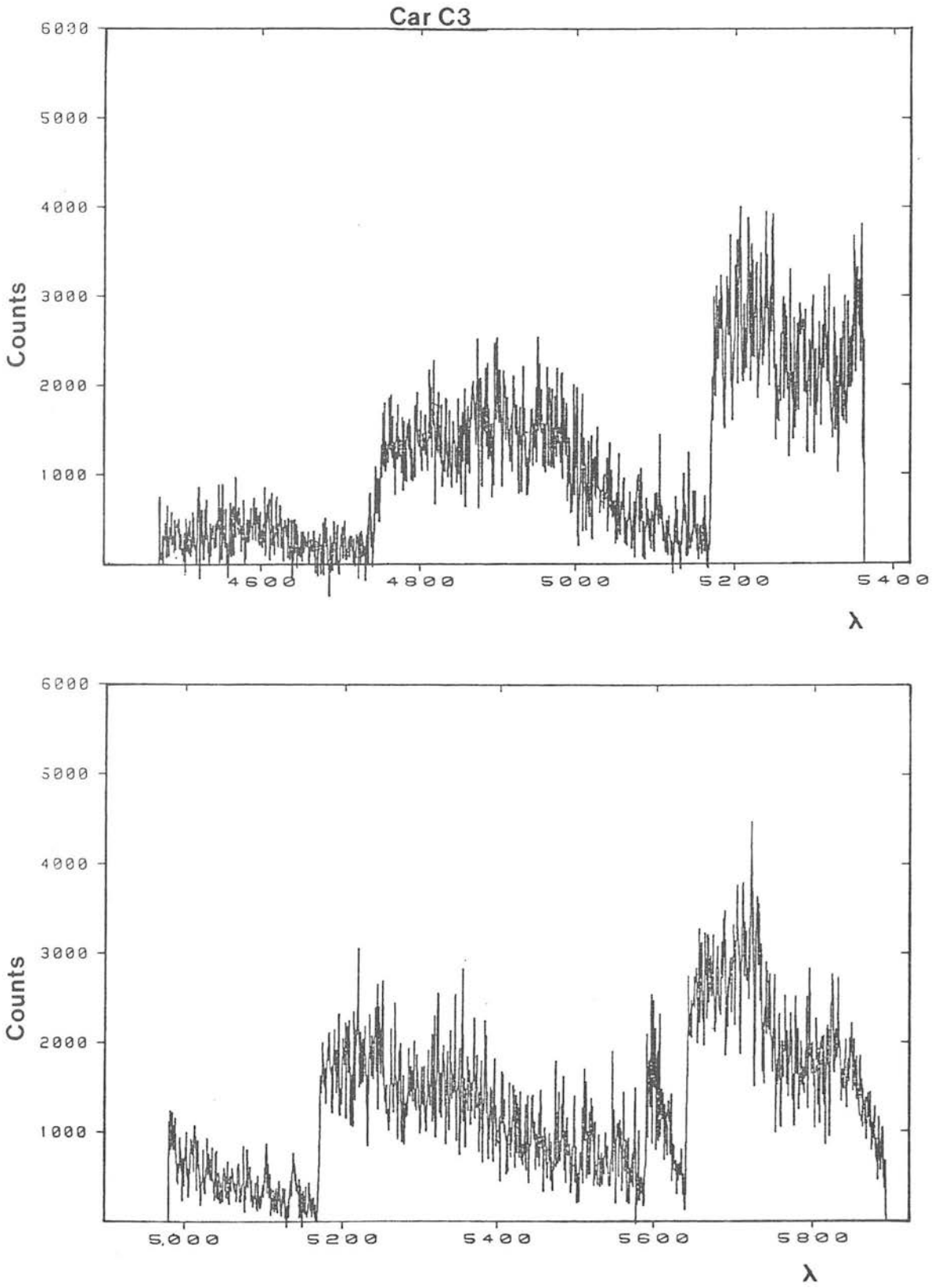

Figure 6.2 (cont.)

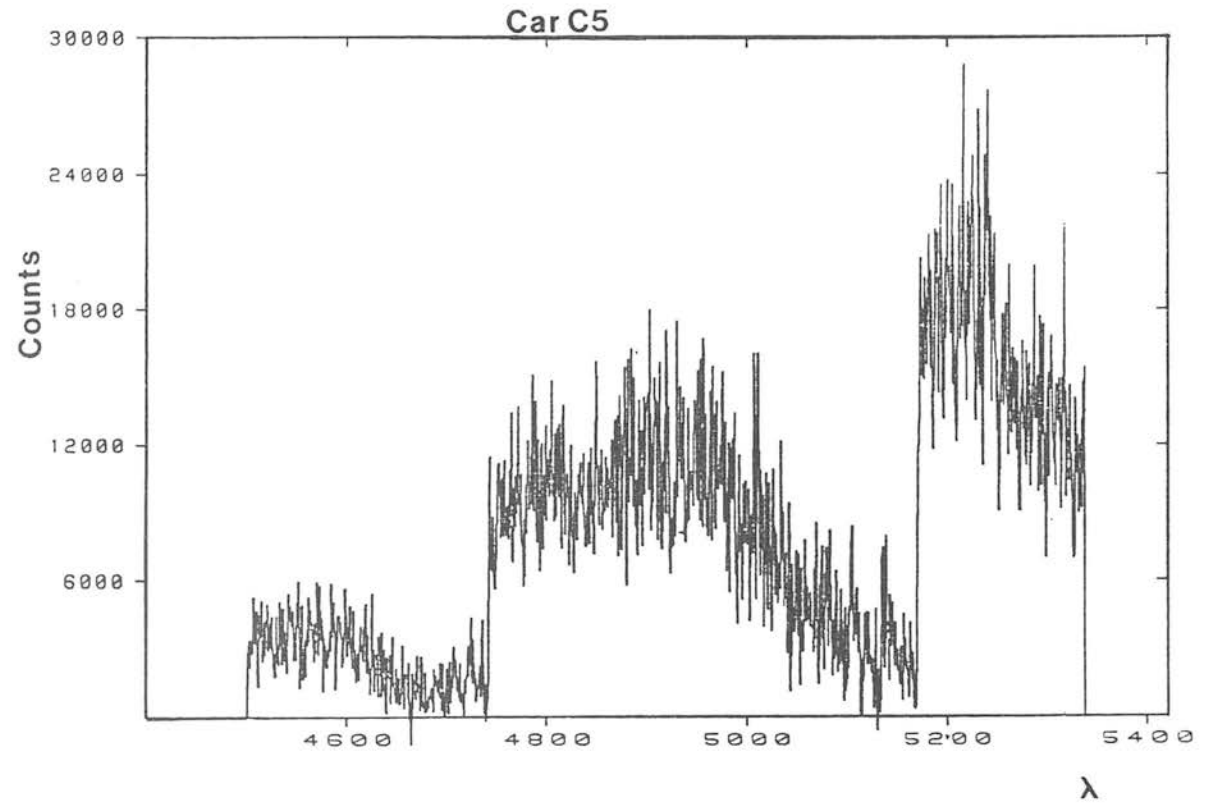

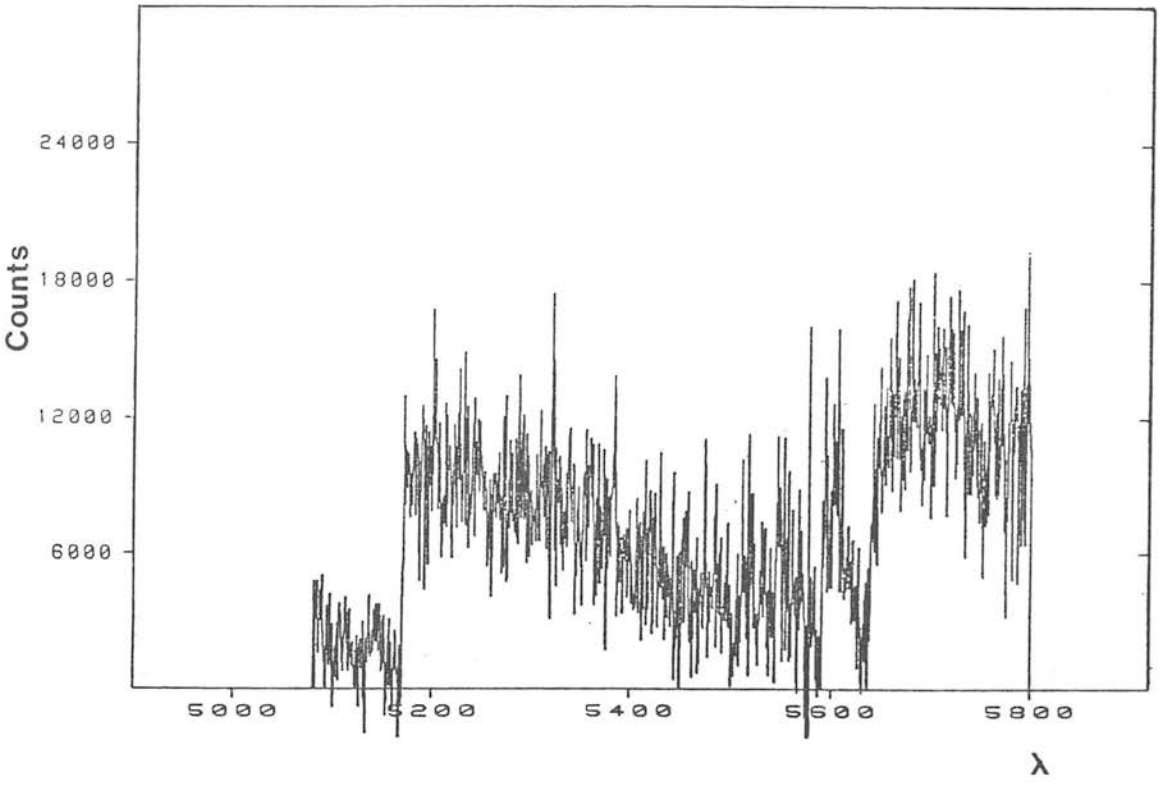

Figure 6.2 (cont.)

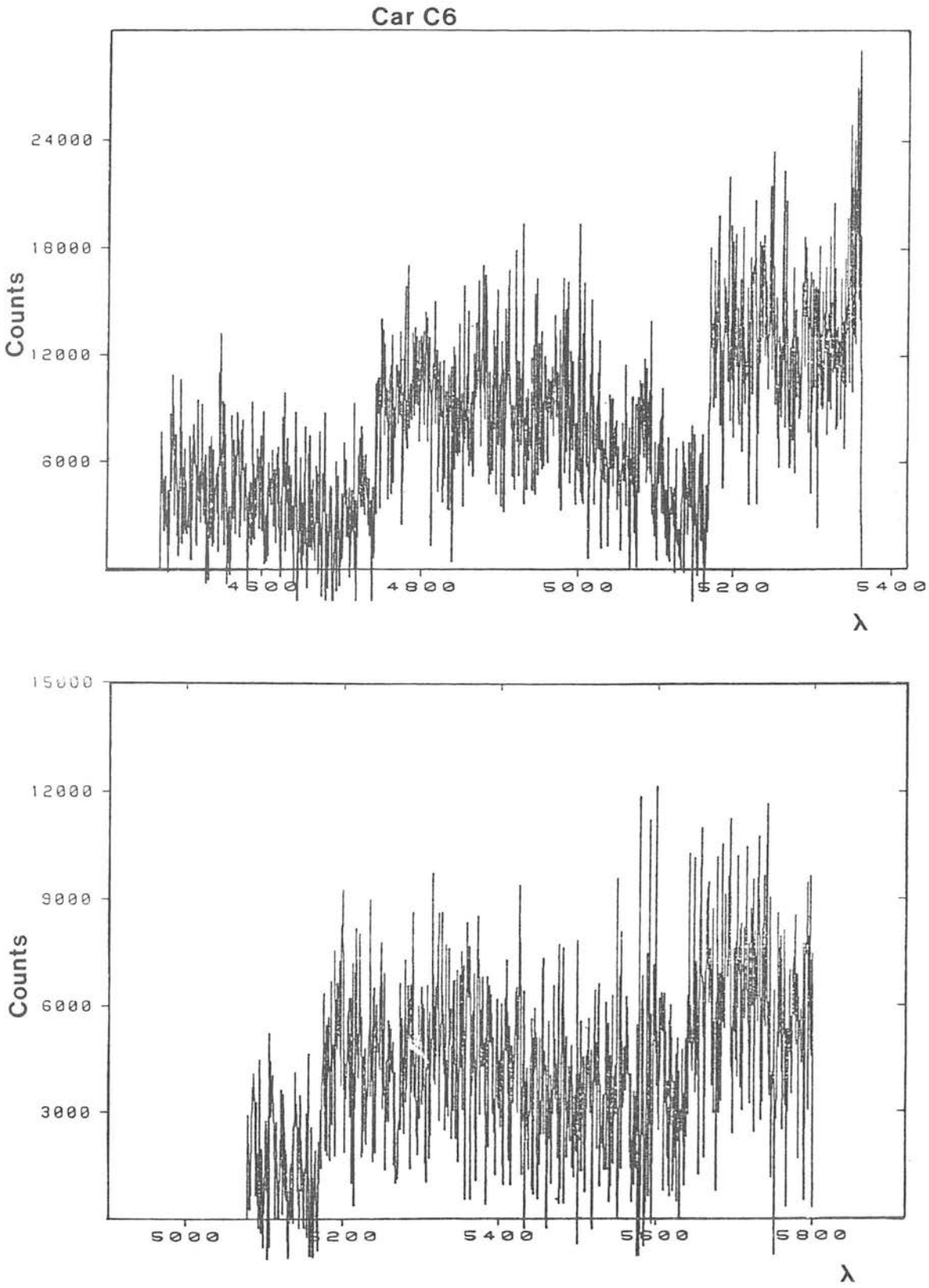

Figure 6.2 (cont.)

be used for two purposes namely (a) to investigate the possible variability that might be present in this type of star and (b) to consider if the velocity dispersion calculated from these velocities reflect that of their parent galaxy.

6.4.1 : The variability of carbon stars

Variability in Galactic carbon stars does not seem to be a new idea (e.g. Stephenson 1973). Two possible reasons for this phenomenon are connected with how current theory explains the actual existence of carbon in the atmospheres of these stars. The carbon stars in the CDG occupy two distinct positions in the theoretical HR diagram; Mould et al (1982) found that five of the six carbon stars considered here lie on the upper asymptotic giant branch well above the maximum luminosity attained by normal hydrogen burning giants, while C2 appears to be fainter and hotter. There are two favoured mechanisms for mixing carbon to the surface of stars; (a) that of the thermal pulses during the double shell source burning on the upper asymptotic giant branch (Iben 1984) and (b) mixing due to the binary mass transfer of carbon from a once more massive companion. Both these processes are capable of producing some degree of variability in a carbon star, in addition to any mixing instabilities which may be present. To date, thermal pulse models cannot account for the observed carbon stars with bolometric luminosities fainter than -4 magnitudes and so a separate mechanism for producing these latter stars (e.g. C2), if this theory is to be believed has to be forthcoming (Aaronson, Olszewski and Hodge 1983). Could it be that these low luminosity carbon stars have been formed by binary mixing, or is this mechanism responsible for the formation of all carbon stars? The argument against this is the fact that if the anomalous Cepheids are a result of binary mass transfer (Hirshfeld 1980), and if each evolves into a carbon star then the ratio of lifetimes predicted is one carbon star for every 10 anomalous Cepheids (Mould et al 1982). No variables to date have been detected in the CDG (see chapter 3), yet there exists at least 10 carbon stars in this galaxy (ALW) and so such a relation for the dsph galaxies seems unlikely.

A simple calculation shows that for a star in the region of the HR diagram that the carbon stars occupy (i.e. radius of star ~ 0.5 A.U., T$\sim$3000K), the period for atmospheric motions (2r/v where v is the velocity of sound in the star) is approximately 300 days. Hence the radial velocities of the CDG carbon stars obtained by Seitzer and Frogel (1985) 11 months later than our observations should enable an investigation into whether there exists any intrinsic variability of this kind in the velocity of the carbon stars over this time span.

In order to do this, careful attention must be paid to the question of the error on the carbon star velocities obtained here, so that statistical deductions can be made. If only random errors are present in the determination of the SPICA velocities listed in table 6.2, then the proper error to quote on the mean velocity of each star would be $\sigma/\sqrt{n}$, where n is the number of velocity measures taken for each star in deriving the mean, and σ is the standard deviation of the sample. However, although the standard stars were chosen to match as well as possible with the CDG carbon stars, it is clear from figure 6.2 that there do exist variations in their spectra which might result in systematic differences in the derived velocities (e.g. one standard star could be consistently giving the highest velocity for all of the CDG stars).

Hence, the error on each star's velocity probably lies somewhere <u>between</u> σ and $\sigma/\sqrt{n}$ (see table 6.3.1). Using this result, it can be seen from table 6.3.2, that the velocities of the CDG carbon stars derived using SPICA are independent of the wavelength range used to within 3σ, even using the most optimistic error of $\sigma/\sqrt{n}$ on each measure.

Seitzer and Frogel (1985) found velocities and associated errors for C4 and C5 relative to the mean velocity of the CDG from observations 11 months later than ours, and these are listed in table 6.4. Taking the velocity of C5 to be the same in both sets of data, even using the best possible error on the velocity for C4 from the SPICA data, the two velocities agree to within at least 2.5σ. Thus although the data sample is <u>very</u> limited in size, it is concluded

TABLE 6.3.1

'SPICA' CARBON STAR MEAN RADIAL VELOCITY RESULTS (kms^{-1})

	$\overline{V}$	σ	$\sigma/\sqrt{n}$	n
C6	216	4	1	8
C5	227	5	2	8
C4	219	3	1	4
C3	240	5	2	8
C2	240	3	1	4
C1	241	4	2	8

($\overline{V}$ = mean velocity taken over n measures).

TABLE 6.3.2

'SPICA' CARBON STAR MEAN RADIAL VELOCITIES (kms^{-1})
OVER DIFFERENT WAVELENGTH RANGES

	C6	C5	C4	C3	C2	C1
Mean of the 4 5100 to 5800 Å measures	214±3(2)	225±4(2)	-	243±3(1)	-	240±4(2)
Mean of the 4 4600 to 5300 Å measures	218±4(2)	230±4(2)	219±3(1)	236±5(2)	240±3(1)	243±5(3)

(most optimistic error ($\sigma/\sqrt{n}$) in brackets)

TABLE 6.4

	SPICA	SPICA velocities relative to mean velocity of Carina Dwarf galaxy	SEITZER + FROGEL (1986) velocities relative to mean velocity of Carina Dwarf galaxy
C5	227 ± 5(2)		+ 0.6 ± 3.2
C4	219 ± 3(1)	- 7 ± 7(4)	+ 3.2 ± 0.7

Let x_2 = mean velocity of Carina Dwarf galaxy. Corresponding velocities of C5 in the two sets of data are made equal, so that 227 ± 5(2) - x_2 = +0.6 ± 3.2, hence x_2 = 226 ± 6(4).

that if all the carbon stars in the CDG are carbon stars resulting from a single mechanism (that of C4), then they appear to show little if any variability over a time span of 11 months. Recent evidence to support the view of a single mechanism being responsible for carbon star formation comes from the work of Richer and Westerlund (1983) who argue that a smooth relation exists between the number of carbon stars in a dsph galaxy and its metallicity, which is most easily explained if this is the case. Further support for this view comes from a plot of parent galaxy luminosity against the contribution to this light of the constituent carbon stars (Aaronson, Olszewski and Hodge 1982, ALW). Both trends if accepted as real, indicate that the carbon stars form more easily as the metallicity of the dsph galaxy decreases, and hence there is no need for several mechanisms to explain the origin of these stars (ALW). Metallicity though is probably only one factor; since there are very few carbon stars found in young to intermediate age open clusters, age too seems to have a part to play in their production. Many more accurate comparisons of carbon star radial velocities in dsph galaxies will have to be done however, before this problem can be conclusively solved.

6.4.2 : Velocity dispersion

In this sub-section, it will be seen what the implications of the assumption that the velocity dispersion as measured from the individual radial velocities of carbon stars does reflect the velocity dispersion of the parent galaxy and is not due to some intrinsic variability of these stars, are on the mass of the CDG.

The observed velocity dispersion of a cluster is given by

$$\mu^2_{obs} = \frac{1}{N-1} \sum_{i=1}^{N} (v_i - \overline{V})^2 \qquad (6.2)$$

where N is the number of stars used, v_i is the velocity of the ith star, and $\overline{V}$ is the mean velocity of the N stars (Trumpler and Weaver 1952). This is made up of the true dispersion μ^2 and an instrumental

dispersion μ_I^2, produced by the errors in the observations i.e.

$$\mu^2 = \mu_{obs}^2 - \mu_I^2 \tag{6.3}$$

with the instrumental dispersion given by

$$\mu_I^2 = \frac{1}{N-1} \sum_{i=1}^{N} \varepsilon_i^2 \tag{6.4}$$

where ε_i is the mean error in v_i. The error in μ^2 comprises of (a) ε_s, the statistical error due to the finite number of stars used and (b) ε_I, the error caused by the inaccuracies in determining the mean error for an individual star (i.e. the errors in ε_i in equation 6.4). If it is assumed that the distribution of velocities and errors is gaussian, then the statistical error is given simply by

$$\varepsilon_s = \mu^2 \left(\frac{2}{N}\right)^{\frac{1}{2}} \tag{6.5}$$

and the error in ε_i is given by $\varepsilon_i/(2n_i)^{0.5}$, where n_i is the number of times the ith star has had its radial velocity measured (see e.g. Trumpler and Weaver 1952). Hence, using the combinatorial rules for independent errors

$$\varepsilon_I = \frac{\sqrt{2}}{N-1} \left(\sum_{i=1}^{N} \frac{\varepsilon_i^4}{n_i} \right)^{\frac{1}{2}} \tag{6.6}$$

Using the values obtained in table 6.3.1, $\mu^2_{obs} = 129.4$, $\mu_I^2 = 20$ implying that $\mu^2 = 109.4$. Also $\varepsilon_s = 62.9$, $\varepsilon_I = 4.6$, and so

$$\varepsilon = (\varepsilon_s^2 + \varepsilon_I^2)^{\frac{1}{2}} = 63.1 \tag{6.7}$$

showing that the statistical error due to the small number of stars dominates that due to the instrumental dispersion. Hence (using the σ errors on the velocities of the carbon stars, see table 6.3.1)

$$[<v^2>_r]^{\frac{1}{2}} = 10.4 \pm 3.0 \text{ kms}^{-1} \qquad (6.8)$$

This result ties in well with the work of Cook, Schecter and Aaronson (1983) and Seitzer and Frogel (1985) who found a velocity dispersion in the CDG $\sim 6\text{kms}^{-1}$. The mass value for the CDG calculated from this value in chapter 5 (see also table 5.4), makes it clear that what is required are more carbon star velocities, not necessarily more accurate than those obtained here, but a larger quantity to reduce the statistical error ε_s in order to obtain a narrower range for the mass estimate of this galaxy. To give an estimate of the numbers involved (neglecting the instrumental error), an accuracy of 1kms^{-1} on a real velocity dispersion of 6kms^{-1} requires $\sim$18 stars and the same accuracy on a velocity dispersion of 10kms^{-1} requires $\sim$50 stars. Here however is another problem in using carbon stars for determining the radial velocities of the dwarf spheroidals; the search for this type of star in chapter 3 and in ALW would seem to imply that most if not all of them have been identified in the CDG which on current estimates only amounts to 10.

With present techniques, the carbon stars have been used for the radial velocity determinations primarily because of their strong carbon bands. Normal giant star spectra usually only show weak features, but since there are many more of them, this has been seen as a way of reducing the statistical error mentioned. Some work has already been done on obtaining radial velocities from giant star spectra in dsph galaxies (e.g. Stetson 1984). Aaronson (private communication) has worked on data from the Ursa-Minor and Draco dsph galaxies and obtained a velocity dispersion of 11 ± 3 and 9 ± 2 kms^{-1} respectively, the error though still being too large to conclusively rule out (or confirm) a dark matter component in the dwarf

spheroidals from this data.

6.4.3 : Radial velocity determination for the Carina dwarf galaxy

Cannon, Niss and Norgaard-Nielson (1980) derived a mean heliocentric velocity of 450 $\pm$ 100 kms^{-1} for the CDG. However this value was known to have considerable uncertainty associated with it, mainly due to the low resolution of the spectra and the bandheads not being very well defined. A much more reliable mean heliocentric velocity of V = 231 $\pm$ 5 kms^{-1} ($\sigma/\sqrt{n}$ error quoted) can be obtained by taking the mean of the velocities (derived using SPICA) of the six carbon stars here. The correction to the local standard of rest (LSR) due to the Sun's motion of (9,12,7) kms^{-1} is $-15kms^{-1}$, while the correction for the motion of $220kms^{-1}$ of the LSR around the Galaxy is $-201kms^{-1}$. Hence the radial velocity of the CDG in the Galaxy's system of rest is $+15\pm5$ kms^{-1}. This compares with 235 ± 100 kms^{-1} used by Cannon, Niss and Norgaard-Nielsen (1980) and $24\pm10kms^{-1}$ derived from the ESP velocities (see Lynden-Bell, Cannon and Godwin 1983)i.e. this galaxy is practically stationary.

The implications of this result is that it removes some of the previous evidence for a Galactic heavy halo (see figure 1 in Lynden-Bell, Cannon and Godwin 1983), although it certainly does not rule out a heavy halo altogether. It is in agreement with the work of Wakamatsu (1981) who deduced the same result from dynamical arguments based on assuming that the boundaries of globular clusters and dwarf spheroidals arise from them being tidally limited (He assumed however, as Hodge (1971) did, that the dwarf spheroidals have the same mass to light ratio as the globular clusters $\sim$ 1.6). Evidence for a heavy halo can be found e.g. in the form of a very distant RR Lyrae star discovered by Hawkins (1983) to have a radial heliocentric velocity of around $-480kms^{-1}$. If this star is in a bound orbit of our Galaxy, then he estimated that a lower limit for the mass of the Galaxy was $1.4\times10^{12}M_{\odot}$. It is unknown though whether this star is a true member of the Galaxy or a star ejected from one of the Local Group systems.

The result obtained here though for the radial velocity of the CDG certainly does not rule out the possibility of a heavy halo for the Galaxy completely, since as discussed in Lynden-Bell, Cannon and Godwin (1983) and section 5.7, if the dsph galaxies have predominantly transverse velocities as opposed to the assumed isotropic distribution, then the mass of the Galaxy could easily be pushed as high as a few times $10^{12} M_{\odot}$.

6.5 : SUMMARY AND CONCLUSIONS

From the re-reduction of the data in Lynden-Bell, Cannon and Godwin (1983) using the standard STARLINK SPICA package, the Galactocentric velocity of the CDG has been found to be practically stationary and it has been further shown that there is some evidence to suppose that the carbon stars in the dsph galaxies have negligible variability over a period $\sim$ 11 months. If this is the case then the velocity dispersion of the CDG = 10.4 ± 3.0 kms^{-1} (internal errors used). If this measured dispersion truly reflects that caused by the presence of all the mass in the CDG (including any dark matter contribution), then the results of chapter 5 show that the dsph galaxies are indeed stable against Galactic tidal disruption, and that the M/L ratio for this galaxy could be substantially higher than that of the Galactic globular clusters.

Chapter 7 : CONCLUSIONS

7.1 : Summary and Conclusions

In this final chapter I shall review what has gone before, discuss the results and some of their uncertainties in a broader context and finally give suggestions for future work in the field.

The Carina dwarf galaxy is an extremely faint object, one of the faintest and least luminous known in the Local Group. Photographic photometry on plates taken with the Anglo-Australian telescope over an area which encloses a large portion of the object has been performed, and by stringent photometric and reduction procedures including the careful assessment of the effect of image contamination by Galactic stars and galaxies, the giant and horizontal branch region of the colour magnitude diagram has been determined and examined, giving a confident value for the system's mean metallicity. The giant branch morphology has been compared with model isochrones and demonstrated to be compatible with a lower bound for the Carina dwarf's age of 7 ± 2 Gyr, a mean metallicity $Z\sim0.0003$ and a helium content $Y=0.2$, if the convective mixing length parameter α is chosen <1.35 (but >1.0) rather than the conventional value of 1.5.

A reliable luminosity function for the giant branch has also been derived and an attempt made to link this with the luminosity function of the main sequence stars from the observations of other workers (Mould and Aaronson 1983). The latter observations, being confined to a very small region of the CDG, give rise to fitting errors, which having been assessed can then be used to compare this galaxy's luminosity function with that of a globular cluster of similar metallicity (M3). This together with the presence of carbon stars, lack of variables and the fitting of the isochrones mentioned above, all indicate that the CDG contains a population of stars which is of a relatively younger age than that found in the Galactic globular clusters. The age estimate of 7 ± 2 Gyr for the CDG given by Mould and Aaronson (1983) from the main sequence turn off point is certainly a lower

bound for the age of this galaxy, and the apparent total lack of variables in the CDG might suggest that there is little room for any much older population of stars i.e. that the vast majority of the CDG is 'young'. However, if multiple star formation episodes have occured in the CDG, then the observed main sequence turn off age of 7±2 Gyr only represents the last epoch of star formation. It has also been shown here that the slope of a giant branch theoretical isochrone, with the Carina dwarf's metallicity and an age greater than 12 Gyr is not consistent with the slope of this galaxy's giant branch. Hence the effect of any blue straggler population that may be present in the CDG making the main sequence turn off point apparently more luminous than it actually is and hence making the galaxy relatively younger, cannot rule out the fact that the CDG is at least 3 Gyr younger than the Galactic globular clusters (which have an age $\sim$ 15 Gyr old). The poorly defined main sequence turn off point in the Mould and Aaronson (1983) data could then be interpreted as due to the effects of multiple star formation episodes which is also the most probable explanation of the metallicity spread found in chapter 3 for the CDG.

This has a number of implications on the Carina dwarf's origin. If it evolved as an isolated system, and it is assumed that the metallicity spread originated due to the galaxy being able to hold onto its nuclearly processed material for more than one star formation episode, and not e.g. through any inhomogeneity of the material it formed out of or due to any peculiar mixing mechanisms within its red giants, then the mass M^H obtained in chapter 5 by assuming the globular cluster and dwarf spheroidals' luminosity functions are similar, implies that this galaxy has lost a substantial fraction of its mass (by comparing mean values, $\sim$ 99%) in subsequent evolution due to (perhaps) Galactic disruption. If the velocity dispersion measure for the CDG obtained in chapter 6 is correct, then the Carina dwarf's mean mass calculated from this is $\sim$36 times greater than the mean value of M^H (see table 5.4) and still indicates a large mass loss (using mean values again, $\sim$71%) if the CDG evolved in isolation. Since very little gas is presently observed in these dsph galaxies (Huchtmeier 1980), if the gas that was blown

off from their red giant stars was removed from the galaxy by simply having a velocity $> v_e$, then an upper bound for the Carina dwarf's mass has been found to be M^E ($= 7.6 \pm 1.5 \times 10^7 M_\odot$).

Alternatively, the results presented here are also consistent with the dsph galaxies originating within a more massive system (e.g. the Magellanic Clouds) where metal enrichment took place, and at an age indicated by their present main sequence turn off points were tidally ripped out with the mass predicted by e.g. their velocity dispersion measures. Gerola, Carnevali and Salpeter (1983) showed that if a large stellar system with total positive energy (e.g. one that has experienced a massive star formation burst) was allowed to expand indefinitely, a fraction of the total mass forms into virialised bound fragments with densities lower than the original one. Their simulations showed that the larger fragments originated from the central regions of the initially bound system, thus a metallicity gradient in this system can be turned into a mass-metallicity relation for the surviving fragments. Using the Hodge (1971) masses (figure 5.5a), this relation might seem to be reasonable, but with the carbon star velocity dispersion masses for Carina, Draco, Ursa-Minor, Fornax and Sculptor the trend is not so evident. If the original system is to be identified with a 'Greater Magellanic Cloud', then the alignment of the dwarf spheroidals in two planes (one containing the Magellanic Clouds) would seem to imply that this is a plausible picture. However, as discussed in chapter 1 there are uncertainties in this picture as well e.g. the dsph galaxies are now accepted to be metal poorer than the Magellanic Clouds. Hence it is still unclear as to whether the dsph galaxies are or have been in the past dynamically associated with the Magellanic Clouds. The orbital time scales of the dsph galaxies though (see chapter 5), show that they have had time to populate both the outer and inner halo, so if the picture of them evolving out of the proto-Galactic gas cloud is correct, then this could go some way to explain the blue horizontal branch found in the Ursa-Minor dsph galaxy, since this galaxy is found in the outer halo (cf the metallicity gradient of the galaxy in figure 3.8). However there is still the problem of why this latter galaxy appears to be old (from

isochrone fits) and metal poor (Olszewski and Aaronson 1985), but has a blue horizontal branch usually associated with metal rich systems.

How does the metallicity and stellar content of the CDG found here and in our Galaxy's other dsph companions compare with those of other known dwarf galaxies? Observations in the Virgo cluster indicate that there exists a metallicity range amongst these galaxies too, ranging from that of the bright ellipticals at the one end to the more metal rich Galactic globular clusters at the other. In fact, the infered relatively high metallicities derived cast some doubt on the origin of the dwarf spheroidals being dwarf irregulars (e.g. Lin and Faber 1983), since it is known that the gas of several dwarf irregulars is relatively metal poorer (Zinnecker and Cannon 1985). There is an indication from both photometry and spectroscopy that the Virgo dwarf ellipticals (dwarf 'ellipticals' by convention being the more luminous counterparts of the dwarf 'spheroidals') are more metal rich than a simple extrapolation down to the dsph galaxy absolute magnitude range might imply (Aaronson 1985). The majority of the Virgo dwarf ellipticals' stellar populations also appear from present data to have formed quite recently ($<$ 10Gyr ago) and over a much longer period than that of the giant ellipticals (see e.g. Zinnecker and Cannon 1985). Carbon stars have however now been positively identified in some of the nearby dwarf irregular galaxies (e.g. NGC 6822, IC1613 and NGC205) together with an extended asymptotic giant branch in the Andromeda II dwarf spheroidal (Aaronson et al 1985). This latter result, together with the data presented here and elsewhere on our Galaxy's dwarf spheroidals, implies that these two features could be inherent features of (all ?) dwarf spheroidals.

A second set of photographic plates, taken with the UK Schmidt telescope (which have a smaller plate scale than the AAT plates), allowed the entire CDG and the background field to be observed simultaneously. The plates, again measured automatically by COSMOS, allowed the star density profile to be determined. For the first time in this type of work, photometrically calibrated plates in two wavebands were used and counts were confined to the regime in the colour magnitude diagram which contains the dwarf galaxy stars, down

to M_V = 0.6, thus greatly improving the 'signal to noise' ratio. The star density profile was compared with model profiles, giving core and tidal radii and total counts to the chosen magnitude limit. From these counts and making certain assumptions regarding the luminosity function of the system, a total mass was calculated, within well defined limits, as well as this galaxy's core and tidal radii.

The main theoretical uncertainty in using the derived r_t to determine the interaction of the CDG with the Galaxy's gravitational potential field is whether it can be interpreted as a bona fide tidally imposed radius. Work on dwarf elliptical galaxies by Binggeli, Sandage and Tarenghi (1984) in the Virgo cluster showed that unlike the Local Group dwarf spheroidals, there is no evidence to suppose that these galaxies cluster around larger elliptical galaxies with the result that their 'tidal radii' as deduced from fits of the King (1966) sequence of profiles to their radial light profiles can only be 'tidal' if it is due to the action of the mass of the Virgo cluster as a whole. Hence it would seem that the fact that an observed radial density profile can be fitted by a King (1966) profile does not mean that the resulting values of r_t can be automatically taken as the usual 'tidal radius'.

Another problem is that Seitzer (1985) found from simulations of centrally concentrated systems (i.e. where tidal effects are negligible in their centres) that at least 50 orbits were required for them to attain a state of tidal relaxation. He concluded therefore that not much faith be put in the observed values of r_t for the dsph galaxies, since they probably reflected a combination of tidal and initial conditions (see e.g. Seitzer and Frogel 1986). However, Freeman (1985) pointed out that if the clusters form in not too eccentric orbits, then the tidally estimated masses may not be in serious error regardless of how many orbits have been done, since for the young globular clusters in the LMC, which are in low eccentricity orbits, their masses from tidal arguments agree excellently with those from velocity dispersion measures and luminosity functions, and yet their ages are only a fraction of their orbital time around the LMC. It has been shown here that if the King (1966) r_t can be

interpreted as a real tidal radius for the dwarf spheroidals as imposed by the Galaxy, then by taking the mass of the CDG as M^H (i.e. as derived by the Hodge 1971 method), this galaxy's observed tidal radius is larger than the radius r_{lim} predicted by King (1962) implying serious disruption of this system. This problem is made even worse by examining the motion of stars in direct orbits and still remains when retrograde orbits (which increases r_{lim}) are considered. This disruption has been confirmed by examining the ratio $|T_z/V_z|$ for the CDG (see figure 5.8) which measures the effect of the Galaxy's tidal field on the internal structure of the CDG, and implies that it could well be Galactic tidal disruption that has lead to the mass loss conjectured earlier in this chapter. However, analysis of the radial velocities of some of the Carina dwarf's carbon stars has allowed a dynamical mass for this galaxy to be determined from their velocity dispersion. This new mass is large enough to make the CDG stable against Galactic disruption, but is still not large enough to enable this galaxy to retain its nuclearly processed material blown from its red giants.

The implication of the greater value of this dynamical mass over the mass derived from the luminosity function comparison method of Hodge (1971) has already been discussed (see chapter 5). This difference is explored further below, in terms of the 'missing mass', as are the possibilities of other explanations to account for the apparent discrepancy.

What could this extra mass (over and above the visible component) be composed of? Recent results seem to suggest that the answer to this question is dark matter, but its existence in the Universe has been a contentious issue for numerous years. Two major pieces of evidence to suggest its presence are found in (a) the rotation curves of spiral galaxies and (b) the observed velocity dispersions in clusters of galaxies. In the former case, the circular velocity of a galaxy such as M31 (see e.g. Roberts 1975) at large galactocentric distances does not decline as $r^{-0.5}$ even when the visible edge is reached, which it should if the visible matter represents all the mass that is present. Instead, they are flat, or

in some cases still rise gently at large r (see e.g. Rubin 1979) indicating that these galaxies have extensive haloes of dark matter. In the latter case, the large observed velocity dispersions present in e.g. the Coma cluster of galaxies cannot be accounted for by the visible matter present, again indicating that there is a substantial contribution to the mass of galaxies from some form of non-luminous matter (see e.g. Faber and Gallagher 1979). What actually constitutes the dark matter is another controversy, as is the question of whether it is composed of all the same type of material. There are no convincing arguments to suggest that the answer to this latter question is 'yes' (see e.g. Gunn 1985), but there are numerous candidates for its constitution, the main ones being neutrinos and cold dark matter. Baryonic matter is now not generally considered as a serious candidate any longer, due to a number of serious inconsistencies when the theory is compared with observational constraints.

Cold dark matter (CDM) candidates (that is matter whose thermal velocity is cosmologically insignificant in the early Universe when compared to the velocity of the Hubble Flow) are numerous, the main ones being axions, gravitinos or moderate mass black holes. Since CDM has a significantly lower velocity dispersion than that of the neutrinos, it can cluster at scales $\sim 10^7 M_\odot$ and hence can account for dark matter in dsph galaxies (Blumenthal et al 1984, Primack and Blumenthal 1984).

If neutrinos ('hot dark matter') on the other hand dominate the contribution to the dark matter component in the Universe, then a cosmological constraint exists on their mass namely

$$\sum_i m_i \leq (100\text{eV}).\Omega.\left(\frac{h}{100\text{kms}^{-1}\text{Mpc}^{-1}}\right)^2 \qquad (7.1)$$

(see e.g. Padmanabhan and Vasanthi 1985, Cowsik and McClelland 1972), where h is Hubble's constant in units of $100\text{kms}^{-1}\text{Mpc}^{-1}$, Ω is the ratio between the presently observed mass density of the Universe and

that required for closure in the 'Big Bang' cosmological formalism and the sum is taken over all species of neutrinos. Tremaine and Gunn (1979) from phase density arguments found that a lower bound on the neutrino mass must satisfy

$$m_\nu > (101\text{eV}) \left(\frac{100\text{kms}^{-1}}{\sigma_\nu}\right)^{\frac{1}{4}} \left(\frac{1\text{kpc}}{r_{c\nu}}\right)^{\frac{1}{2}} g_\nu^{-\frac{1}{4}} \qquad (7.2)$$

where σ_ν is the one dimensional velocity dispersion of neutrinos bound in a gravitational potential well of core radius $r_{c\nu}$, and g_ν is the number of neutrino helicity states ($1 \leq g_\nu \leq 2$, Lin and Faber 1983). Assuming that (a) there exists only one species of neutrino, and (b) that $\Omega h^2 \sim 0.5$, then equation 7.1 implies that m_ν must be $\leq$ 50eV. However, if the further assumptions are made that (c) σ_ν for the neutrinos in the dwarf spheroidals is the same as that of the baryonic matter and (d) the core radius for the neutrinos is the same as that for the baryonic matter, then (for the CDG), m_ν must be greater than $\sim$300eV contradicting the result found from equation 7.1. Hence if neutrinos do constitute the non-luminous matter, then either (or both) of σ_ν and $r_{c\nu}$ must be increased in some fashion from these assumed values. Three different approaches have been considered to disentangle this contradiction

(a) Cowsik and Ghosh (1985) considered the case of large neutrino condensates (of dimensions slightly larger than rich clusters of galaxies) forming in the expanding Universe with the visible baryonic matter slowly cooling within them in the form of e.g. dwarf spheroidals, elliptical and spiral galaxies etc. which then find themselves embedded in the neutrino clouds. They found that the visual condensate when embedded in such a neutrino cloud will not be disrupted by the tidal forces of this cloud i.e. the galaxies are stable against disruption by the neutrino background.

(b) The dwarf spheroidals are embedded in a neutrino halo (extending out to some 250kpc) of our Galaxy.

(c) Unlike cases (a) and (b), the dwarf spheroidals actually have dark matter bound to them in the form of a halo with a core radius very much greater than that of the baryonic matter (e.g. r_c). Hence, for the CDG, if the constraints of equations 7.1 and 7.2 hold, $r_{c\nu}$ must be $\sim$30 to 40 times r_c or greater.

Padmanabhan and Vasanthi (1985) present arguments to suggest that approaches (a) and (b) are both theoretically and observationally unsound. The central factors to this conclusion being that after consideration of the mass and density profiles of our Galaxy, they find that the density enhancement between e.g. 10 and 100kpc from the Galactic centre (of a factor $\sim$100) cannot be treated at all as a small perturbation on a constant density background. Two more considerations are (i) if the dwarf spheroidals are not being disrupted by the Galaxy, then the velocity dispersion derived masses for the dwarf spheroidals (see e.g. chapters 5 and 6) imply that they have some form of dark matter bound to them, and (ii) the carbon star radial velocity data presented in chapter 6 also shows that the CDG is practically stationary in Galactocentric velocity coordinates. The previously derived radial velocity for the CDG of $235\pm100 kms^{-1}$ by Cannon, Niss and Norgaard-Nielsen (1981) gave 'evidence' to suppose that our Galaxy had a heavy halo (see e.g. figure 1 in Lynden-Bell et al 1983 in appendix B), but the new radial velocity here invalidates the use of the Carina dwarf as this lever pushing towards a heavy halo, if an isotropic distribution of velocities is assumed.

The evidence presented here therefore in the form of a high M/L ratio and velocity dispersion measure suggests the possible presence of dark matter in the CDG (and certainly does not rule out that possibility altogether), but more data is required to state conclusively that this matter exists in the dwarf spheroidals. Cold dark matter and neutrinos can still constitute this dark matter, the latter if it is distributed on a larger scale than the visible matter. The neutrino dominated picture of the Universe does have problems it cannot account for though, perhaps the main one being that the theory predicts that galaxy formation should have occured quite recently at redshifts $z < 2$ (Blumenthal et al 1984), which is

in contradiction with the existence of high redshift objects (usually taken to be the nuclei of galaxies). It is also still a controversial matter as to whether the neutrino actually has a mass, although experiments in the U.S.S.R. indicate that the mass of the neutrino associated with an electron, must lie somewhere in the range 20 to 40eV (Gribben 1986).

As has been seen, most of the evidence for the dsph galaxies having large masses comes directly from carbon star velocity dispersion measures. It is clear that since these dynamical masses depend upon the square of the velocity dispersion, checks still remain to be done when using this method which can really only be resolved with more observational data. Two of these checks are (a) the question of variability of these stars, which may not be too serious a problem (see chapter 6), and (b) a thorough assessment needs to be done on the possible external errors on the velocities used in calculating the velocity dispersion of the CDG by e.g. using a reasonable number of different observers' radial velocity data on the same stars. When these problems have been resolved, further progress will be able to be made in this field.

7.2 : Future Work

The study here is connected with only one dwarf spheroidal galaxy, that in Carina, and it is clear that further detailed studies on it and other dwarf galaxies are needed to answer a whole host of questions, some of which are discussed below:

(a) More photometry is required to establish the horizontal branch and subgiant branch regions more clearly in the CDG. In particular this is required for a more exhaustive search for RR Lyrae variables, since the magnitude limit adopted in this thesis is very close to that for the intrinsic magnitude of this type of star. CCD photometry, like that of Mould and Aaronson (1983), of a number of regions (their region is too small and hence has too few points in that part of the colour magnitude diagram to be useful) could be combined to fill this gap. This would also allow the luminosity

function to be defined more accurately along the entire range of magnitude than has been possible in the present thesis.

(b) Are the dsph galaxies distributed solely around larger galaxies indicating perhaps a coeval origin, or can they evolve in isolation? Are there any more dsph galaxy companions of our own Galaxy, perhaps at low Galactic latitudes, or at too faint levels to be detected at present? (e.g. around halo carbon stars). Large systematic searches are required here to solve these questions, but as indicated in chapter 5, they will certainly be hampered by the low surface brightness of these galaxies. COSMOS measures of e.g. UKST plates seems to provide an ideal way to attempt this problem though, once an algorithm has been developed to pick out diffuse objects satisfying various brightness criteria.

(c) Is the measured structure of the dwarf spheroidals dependent upon the luminosity of the stars counted? i.e. is there mass segregation of some sort in these galaxies that could possibly speed up their evolution? Large samples of stars fainter than the main sequence turn off point will be needed to examine this, as the giant branch stars (studied in this thesis) are essentially all of the same mass. This would also enable such questions as whether the observed tidal and core radii vary depending upon what magnitude limit is adopted and a tie up of the luminosity functions of M3 and the CDG over a larger portion of the ZAMS. Larger samples of stars than used previously (from e.g. COSMOS measures) could also help to determine whether the low luminosity asymptotic branches in the other dsph galaxies are in fact making their giant branches look broader than they actually are. This is again an area in which a lot of work still needs to be done, in order to confirm e.g. that the metallicity spread found from spectral scans of giant stars in some of the dsph galaxies is reflected in a corresponding breadth of the parent galaxy's giant branch.

For most of the dsph galaxies, no modern structural data exists. Two Leo I plates in different wavebands are scheduled to be taken on the AAT during April 1986 (Godwin, in preparation), and should enable

this to be tackled using the techniques applied in this thesis, together with the work of Hodge and Eskridge (private communication) who hope to study the Sculptor and Fornax dwarfs (again using some of the techniques developed here) from COSMOS measures of Palomar Schmidt and UKST photographic plates. A further dynamical investigation would also be able to consider whether all of the dsph galaxies fit King (1966) models better than (say) exponential models, or are there deviations that might be able to be interpreted in terms of e.g. tidal effects or stochastic self propagating star formation patterns as in the Gerola, Seiden and Schulman (1980) idea that these galaxies and the dwarf irregulars interchange identities as discussed in chapter 1. Also, does 'stellar clumping' exist in the dsph galaxies as tentatively found by Olszewski and Aaronson (1985) in a small region of the Ursa-Minor dwarf, perhaps giving more weight to the idea that these galaxies were once dwarf irregulars ?

(d) Do metallicity gradients exist in the dwarf spheroidals, and if so, what does this imply about their previous star formation history? (homogeneous star formation or just in isolated patches?). Elliptical galaxies are well known for their metallicity gradients (see e.g. Fall 1980), but it is not known whether this phenomenon occurs in the dwarf spheroidals. This is to be examined in the CDG by using a large number of recently obtained CTIO V and B photographic plates (Godwin 1986 in preparation, Saha private communication) and examining any changes of the colour magnitude diagram morphology of this galaxy from its outer edge inwards. Again, large samples of stars are required for this sort of project, to make real features in these diagrams statistically viable. Since the colour and luminosity of a star are strong functions of its mass, observations of colour gradients or changes in its luminosity function with position in the dsph galaxies might also be able to provide sensitive measurements of the amount of relaxation which has occured in various parts of these galaxies, if the data goes faint enough.

(e) In chapter 6, carbon stars were used to obtain the heliocentric velocity of the CDG, but their small number presented statistical problems in determining an accurate velocity dispersion and M/L

ratio. Also only internal errors on the velocities were used. This makes it clear that more data is required at separate epochs to confirm e.g. whether or not the carbon stars in the dsph galaxies vary or not, so that it can be proved conclusively one way or the other that the velocity dispersions obtained from their spectra are not simply a measure of the intrinsic variability of these stars, and hence whether a reliable mass for the parent galaxy can be deduced from them. To resolve this latter problem, more accurate radial velocities of red giants (in particular) will help to increase the statistical accuracy, and hence techniques will need to be developed to cross-correlate their very weak spectral features. More radial velocity data could also be used to investigate the presence or otherwise of retrograde motions in the dwarf spheroidals, and the corresponding implications on their predicted r_{lim} radii (see e.g. chapter 5). A better mass estimate would also enable the question of whether all the dsph galaxies have the same M/L ratio to be investigated further, or whether there is a spread in this quantity amongst these galaxies as Seitzer and Frogel (1985) have hinted at.

(g) The method of selecting the coolest of the carbon stars (as done in chapter 3, using a prism and direct plate) from a sample of red giants with magnitudes measured in a systematic way (such as with COSMOS), could prove useful in obtaining systematically large samples of carbon stars in e.g. the Magellanic Clouds and the remaining dsph galaxies. This is important since the carbon stars via e.g. their luminosity functions in the various systems can provide independent checks (to that of the colour magnitude diagrams) in determining e.g. the metallicity and distance to these galaxies (see e.g. Aaronson and Mould 1985). Also, Aaronson, Cook and Norris (1985) have shown that the carbon stars can be used to estimate the absolute magnitude of the galaxies they are contained in, since this latter quantity is correlated with the ratio C/M, where C and M are the number of carbon and M dwarfs in the galaxy respectively.

Finally, a brief mention is made of the Space Telescope. What impact will this instrument have on dwarf galaxy research? The greater resolution (at least 0.1") than present ground based

telescopes will allow observations to go some three magnitudes fainter in the optical region allowing data to be obtained well down the main sequence in the CDG. This should certainly allow some of the ideas discussed above to be explored further. The increase in resolution will also enable more reliable light profiles of e.g. the dwarf galaxies of the Virgo cluster to be made (the nuclei of these galaxies will be resolved 10 times further than presently possible), and further investigations into the kind of dynamical models that are relevant to these types of galaxy (see e.g. di Serego 1980).

Appendix A

#	X	Y	B	V	#	X	Y	B	V
1	96	103	20.72	20.10	61	98	131	20.73	19.76
2	96	107	13.57	12.63	62	98	133	18.96	17.50
3	95	108	18.73	18.04	63	99	134	19.09	17.80
4	95	116	15.37	14.78	64	99	135	21.12	20.76
5	95	117	20.78	20.13	65	99	140	20.99	20.31
6	95	133	19.90	18.62	66	99	143	15.78	14.95
7	96	134	18.50	17.89	67	98	146	20.35	19.83
8	95	138	20.15	19.07	68	100	146	21.12	20.54
9	95	152	20.86	19.91	69	98	153	21.00	20.35
10	95	156	16.46	15.56	70	98	155	19.90	18.45
11	95	169	16.67	16.18	71	98	159	17.74	16.87
12	95	171	19.84	18.93	72	100	162	20.95	20.33
13	95	172	17.87	17.24	73	99	166	20.70	19.11
14	95	178	19.27	18.82	74	98	169	17.86	17.11
15	96	179	19.27	17.99	75	99	172	21.05	20.29
16	96	183	20.94	19.77	76	99	181	16.74	16.10
17	95	184	19.15	18.43	77	99	182	20.10	19.94
18	97	95	20.98	20.21	78	99	187	20.16	19.82
19	97	96	21.54	20.72	79	99	189	15.22	14.64
20	98	105	19.16	18.76	80	98	193	12.26	11.98
21	96	106	21.33	20.48	81	100	194	18.78	17.12
22	97	109	17.14	16.35	82	102	96	20.41	19.46
23	96	109	20.60	19.83	83	100	104	21.03	20.19
24	98	121	20.00	19.18	84	101	106	20.45	19.56
25	97	126	18.66	18.03	85	102	111	19.01	18.37
26	98	129	21.47	20.42	86	102	120	21.61	20.62
27	96	132	20.99	20.46	87	101	121	20.43	18.91
28	96	135	16.95	16.04	88	100	120	21.12	19.56
29	98	136	19.11	18.42	89	102	122	21.27	20.34
30	97	138	18.23	17.42	90	100	126	18.54	17.92

31	98	143	20.19	19.38	91	100	128	19.56	19.11
32	98	144	20.68	19.89	92	102	131	21.15	20.36
33	96	159	20.26	19.65	93	100	131	20.28	19.51
34	97	161	20.20	18.73	94	101	133	21.06	20.31
35	97	166	20.42	19.98	95	102	136	19.14	18.63
36	96	169	19.78	18.70	96	101	138	20.95	20.16
37	97	169	21.15	20.50	97	101	139	18.34	17.80
38	97	170	17.77	16.83	98	102	139	20.83	20.22
39	97	174	20.80	19.39	99	100	144	17.11	16.69
40	97	175	16.11	15.53	100	102	147	21.33	20.63
41	96	180	16.24	15.81	101	101	151	20.44	19.50
42	97	185	20.30	19.43	102	101	151	16.23	15.74
43	97	186	16.32	15.38	103	100	152	20.87	20.09
44	97	189	20.95	19.59	104	102	155	19.96	18.98
45	97	190	20.01	18.53	105	101	157	20.43	19.79
46	97	194	19.52	18.99	106	100	157	16.71	15.70
47	99	102	21.00	20.30	107	100	168	20.44	19.29
48	99	107	20.19	19.18	108	100	169	19.87	18.37
49	100	107	20.98	20.12	109	101	173	18.24	17.50
50	99	107	21.19	20.51	110	101	175	20.62	19.67
51	98	108	14.76	13.81	111	100	187	14.38	13.92
52	100	108	20.03	19.08	112	102	95	18.41	17.46
53	99	109	21.16	20.45	113	103	97	20.51	18.90
54	98	112	20.89	20.32	114	103	98	20.43	19.16
55	100	116	21.18	20.31	115	103	100	20.30	19.36
56	98	119	20.82	20.07	116	102	101	20.92	20.03
57	99	122	21.04	20.33	117	103	110	18.57	17.46
58	99	127	21.18	20.27	118	102	112	19.12	17.97
59	99	128	20.97	20.26	119	103	113	20.96	20.20
60	100	129	20.31	19.96	120	103	113	20.67	19.69

121	102	113	17.97	17.33	181	108	113	17.45	16.62
122	102	115	20.22	19.66	182	106	114	20.21	19.37
123	104	115	21.20	20.62	183	107	123	20.57	19.70
124	104	119	21.26	20.60	184	106	131	21.54	20.47
125	102	119	21.02	20.40	185	108	136	20.78	20.16
126	103	120	20.16	19.55	186	107	137	16.61	15.75
127	103	120	18.81	17.49	187	106	140	20.34	19.89
128	102	121	19.49	18.66	188	107	140	21.26	20.55
129	103	123	21.28	20.66	189	108	145	18.28	17.47
130	102	129	19.23	18.17	190	106	146	18.64	18.10
131	104	128	21.16	20.52	191	107	148	21.39	20.00
132	104	129	20.23	19.50	192	107	150	17.75	17.18
133	103	139	17.20	16.53	193	108	153	17.86	17.39
134	104	143	20.97	20.36	194	107	154	20.81	20.07
135	104	145	18.72	17.67	195	107	155	20.18	19.31
136	104	147	20.90	20.35	196	106	159	18.62	17.64
137	103	148	18.87	17.53	197	108	162	20.89	20.02
138	104	148	21.79	20.78	198	108	163	21.18	20.14
139	103	149	20.47	19.77	199	107	166	19.96	19.05
140	104	155	19.35	18.84	200	107	173	17.43	16.71
141	104	162	21.34	20.57	201	107	177	19.99	19.24
142	104	163	18.24	16.97	202	106	181	19.08	18.23
143	102	165	17.77	16.97	203	107	185	21.47	20.00
144	103	166	20.04	19.14	204	107	188	18.92	17.66
145	103	168	19.55	19.06	205	107	189	20.74	19.86
146	104	175	20.41	19.46	206	108	190	19.93	18.88
147	103	176	18.15	17.59	207	108	192	19.92	18.49
148	103	181	12.79	11.45	208	109	95	19.82	18.89
149	102	183	19.50	18.74	209	109	97	21.02	20.26
150	103	184	19.99	19.12	210	109	99	17.43	16.89

151	104	185	21.64	20.15	211	108	102	19.85	18.72
152	102	192	18.11	17.55	212	110	105	19.73	19.19
153	105	115	17.91	17.29	213	110	106	20.94	20.09
154	106	116	18.55	17.99	214	108	106	20.93	20.44
155	105	120	20.23	19.27	215	108	107	18.52	18.08
156	104	127	19.77	19.18	216	109	115	20.44	18.87
157	106	135	18.68	17.91	217	110	118	21.18	20.73
158	105	147	20.94	20.29	218	110	123	19.51	18.55
159	105	150	20.65	19.29	219	109	125	16.17	14.91
160	105	156	16.46	15.93	220	108	126	20.31	19.50
161	106	157	19.43	18.33	221	109	129	19.87	18.95
162	104	159	19.11	18.34	222	108	132	20.02	19.19
163	106	165	17.35	16.74	223	109	134	21.44	19.99
164	104	166	19.65	18.23	224	108	135	20.44	19.47
165	104	168	18.72	17.59	225	109	135	20.53	20.03
166	106	172	16.42	15.75	226	109	136	17.63	16.82
167	106	175	16.18	15.61	227	108	138	21.05	20.34
168	104	178	17.34	16.09	228	110	139	18.90	18.20
169	106	179	20.08	19.39	229	110	142	18.35	17.50
170	105	180	21.13	19.67	230	109	151	21.52	20.21
171	106	185	18.35	16.75	231	110	152	21.08	20.47
172	107	98	14.65	14.11	232	110	152	20.96	20.17
173	107	99	19.74	18.34	233	109	155	20.52	19.29
174	107	103	21.72	20.18	234	109	158	20.92	20.71
175	106	104	21.23	20.46	235	109	159	13.16	12.43
176	107	104	19.76	18.84	236	108	169	19.78	18.78
177	108	106	18.77	18.63	237	109	171	21.65	21.09
178	107	106	20.11	19.16	238	109	172	19.09	18.08
179	106	106	20.63	19.75	239	109	173	20.83	20.61
180	106	113	21.01	20.29	240	109	178	19.68	18.76

241	110	95	20.08	19.31	301	114	128	20.47	19.97
242	111	98	18.69	18.10	302	113	133	17.53	16.64
243	112	99	19.86	18.61	303	113	135	20.97	20.35
244	110	103	20.36	19.59	304	113	139	21.01	20.26
245	112	104	19.03	17.85	305	114	142	19.06	18.65
246	111	104	21.01	19.54	306	113	146	18.52	17.92
247	111	105	19.27	18.12	307	114	146	21.03	20.35
248	111	105	18.54	17.85	308	113	146	21.07	20.40
249	112	109	21.58	20.77	309	112	150	20.83	20.69
250	111	114	19.02	18.45	310	113	150	21.07	20.57
251	111	114	21.17	20.67	311	113	152	20.83	20.48
252	112	117	18.16	17.22	312	113	157	20.62	19.82
253	110	117	20.54	19.66	313	113	158	19.07	17.68
254	110	117	20.02	19.19	314	114	160	20.92	20.22
255	112	118	21.73	20.88	315	114	168	16.60	16.02
256	112	120	19.75	18.51	316	114	180	18.75	17.99
257	112	122	19.69	19.21	317	114	190	19.91	18.89
258	111	123	21.10	20.40	318	113	193	19.82	18.38
259	112	124	21.27	20.35	319	116	96	19.49	18.11
260	112	126	17.94	17.19	320	116	98	21.16	20.38
261	112	127	17.70	16.71	321	115	103	19.11	18.19
262	111	128	20.94	20.43	322	116	106	20.63	19.88
263	112	128	21.02	20.34	323	114	108	20.78	20.08
264	110	129	20.70	20.15	324	116	108	19.77	18.86
265	111	130	21.37	20.64	325	116	114	20.74	20.23
266	111	132	21.22	20.57	326	116	116	20.25	19.74
267	112	134	18.83	18.39	327	115	118	21.63	20.93
268	110	136	21.28	20.50	328	116	120	20.49	19.92
269	112	138	20.92	20.33	329	114	124	20.81	20.02
270	111	141	21.05	20.50	330	116	125	18.68	17.90

271	111	142	20.20	19.31	331	116	126	20.75	19.25
272	112	143	16.09	15.53	332	115	130	20.88	20.66
273	111	151	21.06	20.55	333	115	130	20.87	20.32
274	110	153	20.02	19.23	334	115	138	18.20	17.58
275	112	154	13.24	12.68	335	114	147	17.87	16.58
276	110	157	18.89	17.68	336	116	147	16.28	15.63
277	111	160	14.49	13.78	337	116	148	20.12	17.75
278	112	162	14.99	14.16	338	116	152	15.78	15.24
279	111	169	20.96	20.54	339	114	153	20.01	19.33
280	112	169	20.16	19.26	340	115	154	13.98	13.25
281	112	170	20.10	19.11	341	115	157	20.22	19.28
282	111	171	17.54	16.87	342	116	157	20.84	20.59
283	112	173	21.48	20.17	343	116	159	20.98	20.63
284	111	176	19.58	18.23	344	116	160	20.97	20.14
285	112	178	20.83	19.96	345	116	165	20.44	19.89
286	111	189	20.17	19.36	346	115	165	20.39	19.48
287	114	96	18.27	17.66	347	116	169	19.43	18.26
288	114	97	20.24	19.11	348	116	170	19.03	18.27
289	112	103	21.04	20.40	349	115	171	20.70	20.46
290	114	104	21.05	19.97	350	115	172	19.40	18.18
291	114	104	20.83	20.33	351	115	178	20.92	20.33
292	113	105	15.37	14.31	352	115	179	21.09	20.38
293	114	107	20.68	20.08	353	115	184	20.00	18.99
294	114	109	20.72	19.92	354	116	185	15.30	14.51
295	113	113	17.43	16.41	355	116	189	18.87	17.37
296	113	116	20.89	19.93	356	115	191	20.72	19.29
297	112	116	21.15	20.42	357	116	192	19.86	18.98
298	113	118	17.32	16.79	358	116	98	21.24	20.03
299	114	119	21.21	20.50	359	117	101	19.87	19.10
300	113	120	20.97	20.22	360	118	101	17.52	16.81

361	118	107	21.14	20.46	421	119	150	21.13	20.64
362	117	111	17.33	16.76	422	120	150	20.95	20.36
363	116	118	16.91	16.10	423	121	151	21.39	19.76
364	117	121	16.97	16.41	424	118	152	19.52	18.64
365	118	121	21.22	20.39	425	120	153	21.15	20.44
366	117	124	20.60	19.68	426	120	155	20.99	20.29
367	118	125	21.01	20.49	427	120	156	19.58	18.50
368	117	125	18.64	18.09	428	119	157	20.47	19.60
369	118	127	18.97	17.50	429	120	157	18.46	17.60
370	116	127	20.36	19.45	430	120	161	20.65	19.89
371	118	131	20.94	20.05	431	119	162	21.24	20.55
372	117	132	19.58	18.53	432	119	167	20.16	19.34
373	117	136	21.33	20.72	433	120	167	20.94	20.12
374	117	137	19.10	18.53	434	119	168	20.33	19.42
375	118	137	20.21	19.42	435	120	171	20.08	19.09
376	117	143	21.30	19.68	436	118	172	20.19	18.69
377	116	146	21.22	20.51	437	120	175	19.04	17.68
378	118	147	20.58	19.71	438	120	180	20.42	19.90
379	117	148	20.90	19.96	439	119	183	20.20	18.58
380	117	149	21.22	20.55	440	119	185	15.47	14.75
381	118	157	18.10	17.63	441	119	188	17.06	16.29
382	117	157	20.52	19.69	442	121	95	20.28	19.70
383	117	161	19.40	18.36	443	122	98	19.98	19.45
384	116	164	20.67	19.94	444	121	99	21.14	20.08
385	118	166	17.74	17.08	445	121	100	21.45	19.61
386	118	171	18.69	18.02	446	123	105	19.57	18.49
387	117	173	20.82	19.47	447	122	105	20.97	20.62
388	116	178	20.66	19.20	448	122	107	20.49	19.62
389	117	180	19.83	19.24	449	121	107	15.62	14.76
390	117	187	20.22	18.85	450	121	108	20.06	19.14

391	116	188	21.02	19.86
392	117	188	21.20	20.77
393	119	101	20.70	19.21
394	119	106	15.76	15.10
395	119	111	19.53	19.16
396	119	111	21.04	20.43
397	119	111	20.57	19.71
398	119	115	20.96	20.17
399	120	119	16.96	16.36
400	120	120	20.27	19.39
401	121	120	19.56	18.87
402	119	120	20.98	20.18
403	119	120	20.85	20.19
404	120	124	19.63	18.90
405	119	129	19.97	19.17
406	120	131	19.70	18.82
407	118	133	21.10	20.42
408	120	133	21.00	20.38
409	120	137	19.72	18.85
410	118	138	20.71	20.21
411	119	139	20.22	19.71
412	119	139	21.03	20.43
413	120	140	21.15	20.49
414	120	140	19.97	18.56
415	121	145	19.93	19.19
416	119	146	19.92	19.11
417	119	146	20.26	19.31
418	119	147	20.96	20.19
419	120	148	21.00	20.49
420	120	149	20.86	19.71
451	121	111	21.36	20.59
452	121	112	20.89	20.18
453	121	114	18.62	18.02
454	121	114	21.28	20.57
455	121	122	14.42	13.61
456	121	126	18.19	16.80
457	122	128	21.23	20.37
458	121	130	19.05	18.02
459	121	132	20.83	20.03
460	121	134	20.60	19.16
461	121	136	20.95	20.18
462	121	141	19.05	17.57
463	122	142	20.46	19.59
464	122	147	20.66	19.93
465	121	148	20.78	20.07
466	122	148	19.99	19.43
467	122	150	19.21	17.91
468	121	150	20.88	20.33
469	122	155	21.07	20.22
470	122	157	13.95	13.47
471	121	161	20.56	19.67
472	121	164	21.41	20.62
473	122	166	18.37	17.53
474	120	166	16.50	15.71
475	122	167	20.38	19.37
476	121	173	19.89	19.18
477	120	177	13.63	12.77
478	121	179	20.04	18.96
479	121	181	17.68	16.64
480	122	182	21.33	20.74

481	122	183	20.90	20.19
482	121	186	19.17	18.58
483	121	188	19.71	19.25
484	124	99	20.82	20.32
485	123	100	20.60	19.49
486	124	100	20.22	19.60
487	124	102	19.67	18.72
488	123	107	17.42	16.85
489	123	109	19.79	18.72
490	124	109	19.92	19.56
491	123	111	20.94	19.97
492	123	114	21.02	20.20
493	123	115	20.54	20.06
494	123	117	18.22	17.56
495	122	119	19.13	18.34
496	122	119	20.17	19.30
497	124	120	21.09	20.91
498	123	120	20.17	19.65
499	123	123	21.14	20.35
500	124	123	16.69	15.92
501	123	125	21.33	20.50
502	124	126	19.71	18.66
503	123	126	19.49	18.52
504	124	131	20.42	19.22
505	123	131	21.22	20.87
506	124	134	19.23	17.81
507	123	137	21.06	20.46
508	122	140	19.83	18.87
509	123	145	17.81	17.15
510	123	146	19.66	19.00
541	125	125	16.55	15.74
542	126	125	20.72	20.08
543	125	127	17.58	17.03
544	125	128	20.19	19.28
545	126	129	20.96	20.03
546	126	141	20.97	20.33
547	125	142	20.91	20.17
548	125	143	21.14	20.25
549	126	143	21.20	20.49
550	125	146	16.22	15.62
551	126	149	20.60	18.95
552	126	150	20.76	19.96
553	126	152	20.30	19.60
554	126	153	21.71	20.74
555	125	153	16.91	16.40
556	126	154	21.05	19.82
557	125	154	17.69	17.08
558	126	155	19.14	17.99
559	126	156	21.15	20.44
560	125	156	21.16	20.45
561	126	161	20.39	19.70
562	125	162	20.94	19.91
563	126	165	20.44	19.83
564	125	168	14.80	14.02
565	125	172	20.21	19.48
566	125	173	18.21	17.08
567	126	175	20.57	19.61
568	126	175	17.41	16.86
569	126	179	20.91	20.08
570	126	181	17.05	16.26

511	123	147	21.17	20.37	571	125	185	19.47	18.80
512	124	148	19.82	18.15	572	125	188	20.35	19.79
513	123	160	20.81	20.21	573	126	189	19.88	19.05
514	124	160	16.24	15.34	574	125	192	20.79	19.89
515	123	161	20.92	20.38	575	127	95	20.61	19.72
516	123	162	20.01	19.12	576	127	96	18.94	18.61
517	123	163	17.87	17.09	577	127	102	20.94	20.21
518	123	164	20.79	20.02	578	127	107	21.10	20.30
519	123	169	21.23	20.48	579	128	108	20.23	19.67
520	123	170	20.35	19.46	580	127	109	20.12	19.16
521	124	171	20.01	18.94	581	127	110	20.70	19.97
522	124	171	20.66	20.21	582	128	111	19.30	18.36
523	124	173	18.95	18.85	583	127	115	20.59	19.61
524	123	174	20.16	19.28	584	127	116	20.05	18.52
525	123	177	18.13	17.35	585	127	118	19.01	18.30
526	124	186	20.83	20.34	586	127	119	21.44	20.69
527	124	186	20.51	19.33	587	128	119	20.26	19.67
528	126	97	19.35	18.03	588	127	120	21.05	20.34
529	126	97	20.52	19.68	589	128	120	21.33	20.67
530	125	101	21.23	19.90	590	127	121	19.16	17.85
531	126	108	20.78	20.29	591	128	122	20.20	18.98
532	125	109	19.76	18.74	592	127	124	16.39	15.81
533	125	110	18.07	17.24	593	127	125	20.72	20.16
534	126	111	21.27	20.07	594	128	129	21.30	20.43
535	125	111	20.85	19.89	595	127	130	20.98	20.24
536	125	112	19.33	18.30	596	127	130	20.49	19.63
537	125	114	20.66	20.14	597	127	130	19.72	19.20
538	125	117	16.23	15.58	598	128	131	15.94	14.96
539	126	123	18.99	17.53	599	128	133	19.98	19.12
540	126	124	20.09	19.04	600	128	136	20.67	19.79

601	127	136	17.47	16.96	661	130	156	21.08	20.41
602	128	137	20.82	20.16	662	129	157	20.91	20.13
603	128	137	21.24	20.27	663	129	158	19.66	18.62
604	127	141	21.20	20.45	664	130	159	20.06	18.68
605	128	141	21.13	20.44	665	129	161	16.36	15.51
606	128	141	21.14	20.38	666	129	164	20.01	19.12
607	128	142	20.92	20.07	667	129	165	19.91	19.00
608	127	143	20.90	20.26	668	129	168	19.15	17.86
609	127	146	19.44	18.25	669	130	168	21.00	20.06
610	128	148	20.89	20.47	670	130	170	17.40	16.28
611	129	153	20.48	20.07	671	129	172	17.66	17.02
612	127	157	17.61	16.33	672	130	175	18.06	16.51
613	128	157	20.36	19.71	673	130	186	20.48	19.38
614	127	159	19.89	19.01	674	129	188	20.15	18.70
615	127	159	20.92	20.42	675	131	96	21.05	20.38
616	127	160	20.42	19.84	676	132	97	21.42	20.11
617	128	162	16.33	15.51	677	131	97	19.23	18.17
618	127	164	16.88	16.03	678	131	100	17.19	16.50
619	127	165	19.64	18.89	679	131	102	18.53	17.50
620	128	167	20.90	20.69	680	132	103	20.79	19.98
621	128	169	20.44	19.60	681	133	104	20.30	19.08
622	128	171	18.74	17.64	682	131	107	18.79	17.59
623	128	171	21.09	20.19	683	131	108	21.38	20.06
624	128	176	20.61	20.04	684	132	113	20.73	20.14
625	127	179	20.76	19.80	685	132	114	17.88	17.27
626	127	184	18.70	18.22	686	132	115	21.56	20.46
627	127	190	21.10	20.57	687	131	118	20.33	18.76
628	128	189	13.64	13.08	688	132	119	20.93	20.43
629	128	191	20.64	19.54	689	132	120	19.01	17.80
630	130	95	20.42	19.51	690	133	122	19.90	18.99

631	130	101	20.28	19.39
632	129	102	19.72	19.04
633	129	104	16.59	16.06
634	129	105	18.41	17.32
635	129	106	21.26	20.33
636	129	107	20.95	20.15
637	130	111	16.48	15.90
638	129	116	19.40	18.21
639	130	118	21.07	20.60
640	130	120	21.18	20.32
641	130	120	19.31	18.07
642	130	123	19.46	18.33
643	130	123	19.08	17.86
644	130	125	20.51	19.85
645	129	126	20.86	20.15
646	129	129	21.03	20.09
647	129	132	17.62	16.40
648	130	137	20.95	20.27
649	130	138	21.12	20.36
650	130	139	20.95	20.02
651	130	140	20.60	19.82
652	130	142	20.89	20.22
653	129	142	20.52	20.16
654	130	143	17.81	17.21
655	129	145	20.19	19.43
656	129	152	21.19	20.45
657	130	152	18.63	17.43
658	130	154	21.02	20.16
659	129	154	20.34	19.61
660	129	154	19.75	18.55
691	131	122	20.94	19.59
692	132	125	21.21	20.47
693	131	127	18.88	16.88
694	131	128	19.88	19.44
695	131	136	20.40	19.55
696	132	139	21.06	20.32
697	131	140	21.21	20.61
698	132	141	15.30	14.56
699	132	145	18.83	17.63
700	132	145	21.57	20.54
701	131	146	17.86	16.96
702	131	147	21.20	20.45
703	131	148	18.87	18.63
704	132	151	20.79	20.12
705	131	153	19.64	18.44
706	131	154	20.85	20.25
707	132	155	20.93	20.52
708	132	157	20.28	19.45
709	133	163	20.84	20.72
710	132	165	20.52	19.62
711	132	165	20.85	20.30
712	132	167	21.00	20.41
713	132	169	20.55	20.08
714	131	169	20.39	18.85
715	132	170	20.80	20.15
716	131	173	18.62	18.00
717	131	179	20.02	18.77
718	131	186	20.05	19.18
719	133	193	20.07	19.53
720	131	194	20.59	19.80

721	134	95	18.63	17.81	781	136	116	21.02	20.25
722	134	98	20.24	19.49	782	136	117	21.71	20.27
723	135	98	20.89	19.59	783	137	121	20.82	20.05
724	133	104	19.49	18.91	784	136	123	20.73	20.15
725	133	107	19.52	17.96	785	135	126	21.07	20.70
726	134	110	20.19	19.14	786	136	127	21.35	20.67
727	133	112	20.70	19.82	787	137	127	19.30	18.11
728	134	116	21.02	19.93	788	137	138	21.24	20.64
729	134	118	19.45	18.27	789	136	138	20.97	20.13
730	134	119	21.45	20.63	790	135	139	20.73	19.74
731	133	120	19.20	18.57	791	136	140	21.19	20.82
732	134	121	21.35	20.56	792	136	142	20.85	19.56
733	133	123	19.57	18.45	793	136	145	20.06	18.92
734	134	125	16.81	16.37	794	136	148	20.68	19.84
735	133	128	19.16	17.64	795	135	151	20.71	19.87
736	134	129	20.96	20.40	796	135	151	20.68	20.20
737	133	130	21.01	20.76	797	136	152	19.53	18.74
738	134	133	21.21	20.53	798	135	154	20.87	20.25
739	134	133	20.06	19.60	799	135	155	19.19	18.33
740	133	134	20.87	20.22	800	135	156	20.69	20.07
741	134	134	20.78	20.09	801	136	157	21.04	20.33
742	134	136	19.70	19.11	802	136	158	20.48	19.66
743	133	138	20.32	19.09	803	135	160	21.10	20.47
744	134	138	19.94	18.97	804	137	160	19.33	18.56
745	134	141	21.23	20.51	805	135	161	21.33	20.84
746	134	142	20.37	19.51	806	135	165	20.89	20.30
747	133	144	20.65	18.92	807	135	167	21.16	20.75
748	134	145	16.66	16.10	808	135	168	20.34	19.14
749	134	146	19.34	18.22	809	137	168	21.01	20.36
750	134	147	19.46	18.93	810	136	171	21.03	20.68

751	134	152	20.67	19.86	811	137	171	20.68	20.05
752	135	153	20.35	19.52	812	135	172	21.21	19.70
753	133	154	19.43	18.41	813	135	175	19.04	17.67
754	134	160	21.29	20.46	814	135	176	20.15	20.05
755	133	161	20.72	20.15	815	136	185	18.50	18.01
756	134	161	21.27	20.73	816	135	190	20.83	20.21
757	135	161	20.70	19.13	817	139	96	20.33	19.74
758	135	161	20.34	19.60	818	138	97	20.93	19.86
759	134	163	18.39	17.52	819	137	101	19.64	18.61
760	134	167	16.15	15.46	820	138	106	20.93	20.30
761	134	171	21.04	20.42	821	138	107	20.24	19.57
762	133	172	16.58	15.96	822	139	109	20.30	19.50
763	134	174	19.98	19.06	823	138	111	21.11	20.50
764	134	175	20.81	20.38	824	139	112	21.06	19.61
765	134	178	20.72	19.90	825	138	112	20.95	19.48
766	134	180	19.97	19.04	826	137	112	16.95	16.34
767	133	180	16.82	15.46	827	139	116	20.04	19.11
768	134	184	17.30	16.61	828	139	119	21.09	20.50
769	135	189	20.98	20.20	829	137	120	21.21	20.73
770	133	189	16.74	15.43	830	137	121	19.04	17.65
771	135	95	17.54	17.03	831	138	123	18.90	18.26
772	136	96	20.37	18.99	832	137	124	19.87	18.74
773	136	97	19.25	18.46	833	139	125	20.18	19.46
774	136	102	19.75	18.68	834	138	138	20.11	19.17
775	136	104	20.37	19.44	835	137	139	21.63	20.98
776	137	106	13.12	12.66	836	139	141	20.81	20.22
777	136	107	20.78	19.78	837	137	141	20.90	20.18
778	136	107	20.34	19.69	838	138	143	21.41	20.57
779	135	109	19.54	18.41	839	138	143	18.32	17.58
780	135	113	17.88	16.50	840	137	145	21.17	20.86

841	137	147	19.14	17.79	901	139	194	14.20	13.51
842	138	148	21.15	20.01	902	142	103	21.16	20.33
843	138	151	19.90	19.61	903	141	114	20.58	19.59
844	137	153	20.60	19.72	904	142	114	20.92	20.50
845	138	154	17.05	15.54	905	142	117	19.55	18.57
846	139	159	21.07	20.31	906	142	121	20.96	20.53
847	137	160	21.16	20.54	907	141	127	20.95	20.42
848	138	161	20.29	19.52	908	141	128	20.90	20.31
849	137	164	20.98	20.23	909	141	129	20.27	19.16
850	138	165	18.35	17.79	910	143	129	20.53	19.94
851	138	167	15.60	14.74	911	141	133	21.30	20.17
852	139	172	19.60	18.40	912	142	133	20.13	19.76
853	137	173	12.16	11.79	913	143	133	21.21	20.49
854	138	178	18.19	17.36	914	141	136	18.26	17.34
855	138	181	18.35	17.71	915	142	140	17.81	17.31
856	138	181	20.73	19.26	916	142	142	21.16	20.62
857	138	186	21.30	20.58	917	141	142	18.84	17.44
858	139	187	16.44	15.86	918	141	145	20.91	20.10
859	138	192	19.14	18.64	919	141	146	19.04	17.76
860	141	101	12.89	12.21	920	143	147	19.00	17.89
861	141	104	13.77	12.91	921	143	149	20.29	19.76
862	140	105	20.42	19.88	922	143	150	19.69	18.82
863	141	107	18.68	17.13	923	142	151	21.11	20.42
864	141	109	20.85	20.09	924	142	152	20.82	20.04
865	141	112	20.52	19.73	925	143	155	17.37	16.68
866	139	113	18.85	17.46	926	141	156	20.45	19.80
867	141	114	19.61	18.64	927	142	159	21.08	20.39
868	140	115	18.15	17.29	928	143	162	20.93	20.32
869	139	116	19.42	18.28	929	141	163	16.99	16.31
870	140	119	18.94	18.25	930	143	163	20.94	20.28

871	140	122	21.23	20.94	931	141	167	19.35	18.20
872	139	123	20.86	19.51	932	141	168	19.54	18.75
873	141	123	20.56	19.94	933	141	173	20.77	19.52
874	139	129	19.66	17.37	934	142	174	15.39	14.70
875	141	129	20.02	19.41	935	141	182	20.48	19.14
876	140	129	21.13	20.49	936	142	183	19.74	19.33
877	139	135	20.75	20.31	937	143	189	20.83	20.31
878	139	135	20.71	19.87	938	144	96	20.34	19.92
879	141	138	18.27	17.54	939	144	103	17.85	17.25
880	141	139	19.54	19.42	940	144	109	20.78	19.90
881	139	140	19.04	17.68	941	143	110	17.77	16.96
882	139	143	20.49	19.17	942	144	112	20.20	19.67
883	140	143	20.23	19.28	943	143	116	21.19	20.60
884	141	144	20.78	20.24	944	144	119	21.24	20.64
885	139	146	19.88	19.01	945	143	119	19.49	18.27
886	141	147	21.08	20.29	946	145	120	19.03	17.60
887	140	148	18.35	17.59	947	144	120	20.30	19.24
888	139	152	19.71	18.25	948	144	121	18.60	18.00
889	141	158	21.03	20.30	949	143	123	20.30	19.36
890	139	159	21.11	20.64	950	144	124	20.36	19.56
891	140	163	19.24	18.23	951	144	126	20.15	19.28
892	141	166	20.90	20.32	952	144	128	21.17	20.93
893	139	168	20.84	20.18	953	144	131	21.07	20.74
894	139	172	20.80	20.02	954	144	131	21.17	20.58
895	141	174	20.77	20.00	955	144	133	19.27	17.98
896	139	175	20.79	20.78	956	143	134	21.17	20.50
897	139	182	20.66	19.04	957	144	134	16.73	15.72
898	139	183	19.24	18.01	958	145	137	19.18	18.60
899	140	190	16.64	16.14	959	144	141	20.38	19.61
900	139	192	19.18	18.66	960	144	141	19.71	18.65

961	145	142	21.07	20.52	1021	146	188	19.36	18.26
962	143	144	21.33	20.78	1022	147	192	20.90	19.98
963	144	145	21.60	20.13	1023	146	193	19.37	18.97
964	145	146	19.28	18.55	1024	148	97	19.03	18.29
965	144	147	19.78	18.90	1025	149	103	19.32	18.49
966	145	150	19.08	17.91	1026	149	107	19.79	19.17
967	144	150	19.83	18.93	1027	147	108	21.48	20.59
968	144	152	18.23	17.50	1028	149	111	18.61	17.95
969	145	152	20.97	20.41	1029	148	113	20.56	20.02
970	144	156	20.08	18.99	1030	149	118	20.95	20.00
971	143	158	14.77	14.20	1031	147	119	20.81	20.00
972	143	162	20.29	18.74	1032	148	123	19.51	18.43
973	145	165	18.90	17.54	1033	148	126	20.35	19.46
974	144	165	21.36	19.84	1034	147	127	20.93	20.24
975	144	167	21.07	20.31	1035	148	129	20.92	20.34
976	144	168	21.68	20.88	1036	148	133	20.92	20.21
977	143	169	20.88	20.31	1037	147	139	15.70	15.04
978	145	173	19.98	19.08	1038	148	141	17.59	16.93
979	143	174	19.95	18.99	1039	148	142	20.39	19.48
980	145	174	19.39	18.40	1040	148	143	21.00	20.22
981	144	179	20.44	19.61	1041	147	146	19.46	18.70
982	145	184	20.50	19.06	1042	149	149	18.87	18.04
983	144	187	20.08	18.99	1043	148	152	17.26	16.67
984	144	189	15.66	15.02	1044	147	154	19.96	19.17
985	144	190	16.92	16.18	1045	148	156	20.88	20.56
986	145	192	15.72	15.15	1046	149	158	20.59	19.61
987	147	95	16.90	15.95	1047	148	161	20.13	19.48
988	147	99	20.82	19.44	1048	149	171	18.07	16.98
989	146	103	21.05	20.41	1049	149	178	20.01	18.43
990	147	107	21.16	20.52	1050	147	182	19.59	18.27

991	145	109	20.95	20.13	1051	147	184	13.95	13.33
992	145	110	19.65	18.72	1052	148	187	17.34	16.61
993	147	114	21.23	20.24	1053	148	192	20.82	20.33
994	146	115	16.41	15.61	1054	149	194	20.48	19.03
995	145	116	16.05	15.01	1055	151	97	18.76	17.60
996	147	122	15.30	15.08	1056	150	98	20.29	19.34
997	147	125	20.53	19.66	1057	150	102	20.03	19.25
998	145	125	17.50	16.57	1058	149	108	20.67	19.77
999	147	131	17.96	17.35	1059	149	109	20.11	18.67
1000	145	135	16.85	16.16	1060	149	110	20.28	19.41
1001	146	138	21.50	19.79	1061	150	110	20.91	19.98
1002	145	140	20.37	18.81	1062	150	114	19.64	19.03
1003	146	144	18.84	17.53	1063	151	114	21.02	20.60
1004	146	145	20.29	19.35	1064	149	114	18.67	17.62
1005	145	145	20.92	20.29	1065	149	116	19.72	18.72
1006	146	147	14.02	12.89	1066	149	120	19.41	18.90
1007	146	149	20.81	20.25	1067	151	121	19.91	19.39
1008	146	152	19.86	18.84	1068	150	123	19.57	19.02
1009	146	157	21.06	19.84	1069	149	124	20.26	19.43
1010	146	158	19.10	17.83	1070	150	125	21.04	20.38
1011	147	160	20.68	19.88	1071	150	128	17.22	16.71
1012	146	160	20.77	19.46	1072	150	129	21.15	20.43
1013	147	162	20.91	20.66	1073	149	130	18.47	17.02
1014	145	163	20.85	20.01	1074	150	131	21.17	20.30
1015	147	166	21.06	19.91	1075	149	132	20.71	19.98
1016	146	167	20.30	19.71	1076	150	132	19.91	19.39
1017	146	169	19.09	17.84	1077	150	134	20.75	19.84
1018	146	173	16.34	15.83	1078	149	135	15.95	15.21
1019	146	182	14.78	13.88	1079	150	147	21.00	20.23
1020	146	183	20.86	20.72	1080	150	149	20.20	19.34

1081	151	150	21.34	20.90	1141	154	96	20.69	19.39
1082	150	153	21.08	20.32	1142	154	98	18.65	17.84
1083	150	159	20.70	19.91	1143	155	108	18.18	17.54
1084	151	160	20.47	19.23	1144	155	109	21.44	20.71
1085	149	160	20.30	19.41	1145	154	113	20.99	19.62
1086	151	161	20.40	19.12	1146	155	113	20.47	18.95
1087	149	162	20.23	19.56	1147	154	117	20.31	19.11
1088	150	163	21.42	19.69	1148	153	118	21.05	20.23
1089	150	177	19.88	19.41	1149	155	118	18.86	17.79
1090	150	177	20.62	19.68	1150	153	120	20.07	19.14
1091	151	178	20.97	20.31	1151	155	120	21.04	20.49
1092	151	178	18.57	17.98	1152	154	121	21.08	20.49
1093	149	181	18.09	17.45	1153	154	125	21.04	20.31
1094	150	181	21.05	20.44	1154	153	127	18.87	18.78
1095	150	182	20.92	19.35	1155	155	129	21.08	20.59
1096	151	185	19.80	18.86	1156	153	130	19.74	19.25
1097	150	185	21.05	20.06	1157	153	132	20.55	19.05
1098	150	186	20.90	20.78	1158	155	136	21.24	20.53
1099	150	193	21.67	20.32	1159	154	137	21.39	19.98
1100	150	193	19.75	18.83	1160	154	139	20.96	20.40
1101	152	102	18.71	17.52	1161	155	141	20.72	19.97
1102	151	107	19.51	18.21	1162	155	142	20.66	20.18
1103	152	108	21.12	20.42	1163	155	143	19.76	19.24
1104	152	118	16.66	15.79	1164	154	147	20.26	19.37
1105	151	118	20.22	19.42	1165	155	147	20.67	20.05
1106	152	119	19.10	17.75	1166	153	151	20.72	19.71
1107	153	123	21.00	20.65	1167	154	154	14.49	13.64
1108	152	125	19.63	18.59	1168	154	155	19.43	18.84
1109	153	126	19.96	19.00	1169	153	160	21.09	20.43
1110	153	127	20.56	19.77	1170	154	168	20.25	19.30

1111	152	127	20.65	19.92	1171	154	170	18.64	17.86
1112	151	129	19.48	18.25	1172	155	179	16.98	15.54
1113	151	133	13.39	12.32	1173	154	183	17.49	16.98
1114	153	134	20.98	20.53	1174	154	189	21.01	20.15
1115	152	140	19.59	19.00	1175	155	190	20.74	20.20
1116	151	141	19.26	17.28	1176	157	96	16.49	15.86
1117	152	145	20.94	20.44	1177	156	98	19.65	18.65
1118	152	150	20.97	20.40	1178	156	99	18.02	17.39
1119	153	152	21.03	20.41	1179	156	100	16.91	16.36
1120	152	154	20.02	19.04	1180	157	102	19.71	18.78
1121	152	155	19.97	19.15	1181	156	106	18.79	18.08
1122	153	156	19.55	18.35	1182	157	109	14.36	13.97
1123	152	157	20.95	20.32	1183	156	112	21.34	20.39
1124	152	158	15.93	15.13	1184	156	116	20.10	19.02
1125	153	165	20.56	20.16	1185	156	118	20.98	20.32
1126	152	165	21.09	20.43	1186	156	119	20.76	19.11
1127	153	170	20.40	19.39	1187	156	121	18.17	17.50
1128	152	172	18.57	17.97	1188	157	123	21.28	20.50
1129	153	172	21.18	20.70	1189	157	130	21.49	20.09
1130	151	173	20.90	20.18	1190	156	133	21.16	20.47
1131	153	176	20.68	19.78	1191	156	139	21.21	20.75
1132	152	177	21.00	20.54	1192	156	142	21.01	20.67
1133	153	181	19.14	18.52	1193	157	143	17.73	16.89
1134	153	184	20.97	20.44	1194	156	145	16.76	16.14
1135	153	185	21.13	20.46	1195	156	148	15.94	15.38
1136	152	186	20.89	20.13	1196	157	149	20.94	20.24
1137	153	186	19.86	18.34	1197	156	151	20.09	19.07
1138	151	189	20.07	19.64	1198	157	152	19.81	18.22
1139	152	191	20.90	20.16	1199	155	161	17.24	16.53
1140	153	96	20.96	20.80	1200	156	163	20.84	20.08

1201	157	171	21.07	19.83	1261	161	150	20.49	19.58
1202	157	175	19.01	18.23	1262	160	150	21.02	20.37
1203	156	176	20.61	20.10	1263	161	153	21.04	20.43
1204	155	176	18.06	16.51	1264	160	155	20.78	19.66
1205	155	186	21.46	20.59	1265	159	157	17.12	16.39
1206	157	187	21.13	19.67	1266	161	159	20.82	20.47
1207	157	191	19.88	18.92	1267	161	163	21.06	20.44
1208	156	193	19.17	18.42	1268	160	163	20.11	18.64
1209	159	95	20.82	20.64	1269	161	166	17.67	16.94
1210	158	101	19.15	17.55	1270	160	171	19.85	19.29
1211	158	101	20.47	19.47	1271	161	172	18.02	16.61
1212	159	101	15.63	15.07	1272	159	173	16.43	15.63
1213	158	113	19.01	17.81	1273	161	175	18.46	17.57
1214	158	115	20.74	19.35	1274	159	176	18.96	18.28
1215	159	116	19.87	18.60	1275	160	177	20.24	19.27
1216	158	116	18.01	17.29	1276	161	183	21.43	20.51
1217	158	124	20.86	20.62	1277	160	188	21.11	19.55
1218	158	127	18.75	17.99	1278	162	102	16.97	16.05
1219	158	129	20.67	19.95	1279	162	107	20.12	18.76
1220	159	130	20.18	19.20	1280	162	109	21.36	20.02
1221	159	131	21.13	20.65	1281	163	111	19.28	18.63
1222	159	132	17.99	16.73	1282	163	112	21.62	19.89
1223	157	134	21.24	20.77	1283	163	114	13.91	12.88
1224	159	138	19.55	18.45	1284	162	117	21.13	20.55
1225	159	140	21.12	19.90	1285	162	118	18.97	18.40
1226	158	141	21.24	20.50	1286	163	122	21.32	20.41
1227	158	142	20.13	19.48	1287	163	124	20.56	19.67
1228	159	148	19.66	18.53	1288	162	125	19.99	19.16
1229	159	153	18.94	17.49	1289	163	130	20.92	19.90
1230	158	157	21.30	19.66	1290	163	131	20.47	19.44

1231	159	158	21.21	20.35	1291	162	132	19.61	18.71
1232	158	167	18.71	18.16	1292	163	132	20.63	19.88
1233	158	170	15.54	14.89	1293	162	134	19.21	17.56
1234	157	172	20.33	19.49	1294	162	135	19.48	18.54
1235	157	182	16.39	15.66	1295	161	138	20.70	20.04
1236	158	183	20.16	19.58	1296	163	140	21.11	20.20
1237	158	189	20.91	19.67	1297	162	142	20.74	19.22
1238	158	192	18.31	17.62	1298	163	142	20.65	19.35
1239	159	193	17.38	16.34	1299	162	144	21.04	20.05
1240	160	95	15.54	14.66	1300	162	150	20.66	19.84
1241	160	99	19.34	18.45	1301	163	151	21.05	20.16
1242	161	101	20.43	19.87	1302	162	154	20.76	20.09
1243	160	106	21.24	19.48	1303	162	155	17.51	16.86
1244	161	109	18.46	17.57	1304	163	156	20.90	20.31
1245	160	114	15.71	14.98	1305	162	159	21.27	20.54
1246	160	118	20.75	20.13	1306	162	161	20.54	19.08
1247	160	126	21.06	19.59	1307	163	161	17.64	16.50
1248	160	125	20.26	19.43	1308	162	164	18.88	17.47
1249	161	128	20.78	20.05	1309	162	167	15.00	14.03
1250	160	131	20.23	19.26	1310	163	172	18.29	17.39
1251	160	131	21.12	20.44	1311	162	179	20.36	19.17
1252	160	132	21.16	20.75	1312	163	185	21.27	19.74
1253	160	135	20.90	19.88	1313	162	186	20.38	19.46
1254	161	140	19.91	18.63	1314	162	187	19.97	18.41
1255	160	140	21.02	20.27	1315	162	189	17.98	17.47
1256	160	143	18.73	18.18	1316	163	193	16.78	16.28
1257	161	143	17.43	16.82	1317	162	194	17.25	16.22
1258	161	144	20.62	19.54	1318	165	101	19.89	19.31
1259	159	145	16.37	15.75	1319	163	101	17.05	16.50
1260	160	146	21.06	20.17	1320	165	101	20.65	19.12

1321	164	107	21.18	20.08	1381	169	125	20.16	19.24
1322	165	112	19.67	18.08	1382	169	126	15.79	15.14
1323	164	114	20.86	19.25	1383	168	127	20.17	19.45
1324	163	116	16.40	15.45	1384	168	131	16.27	15.57
1325	164	118	20.91	19.83	1385	169	136	20.33	18.81
1326	165	118	17.62	16.09	1386	169	136	20.60	20.21
1327	164	120	20.03	19.08	1387	169	137	20.41	19.76
1328	164	120	19.99	19.14	1388	168	138	21.35	20.59
1329	165	125	20.20	19.66	1389	169	139	16.62	15.82
1330	164	132	21.17	20.12	1390	168	141	14.68	13.94
1331	164	135	20.64	19.84	1391	169	145	20.30	18.84
1332	165	138	18.20	17.54	1392	169	148	14.35	13.55
1333	165	140	17.15	16.60	1393	167	150	18.97	18.37
1334	165	147	20.99	19.87	1394	168	151	17.97	17.30
1335	165	155	17.96	17.26	1395	169	152	14.77	14.09
1336	165	163	17.62	17.03	1396	168	154	16.39	15.70
1337	164	169	20.28	19.47	1397	169	154	19.97	18.88
1338	165	176	19.38	18.12	1398	169	166	19.78	19.19
1339	165	181	17.73	17.13	1399	167	169	20.38	19.12
1340	165	187	20.36	19.69	1400	169	173	15.99	15.53
1341	165	189	18.72	18.00	1401	169	175	18.33	17.72
1342	165	192	21.21	19.85	1402	169	176	20.23	19.25
1343	163	193	21.31	20.18	1403	168	179	20.81	20.08
1344	166	99	20.67	19.88	1404	168	182	20.26	18.66
1345	166	102	20.57	19.92	1405	169	191	15.85	15.28
1346	166	109	20.17	18.97	1406	171	98	21.17	20.42
1347	167	115	20.41	19.43	1407	170	105	20.93	19.91
1348	167	116	20.75	19.26	1408	170	125	20.62	20.22
1349	167	117	20.95	19.51	1409	170	126	16.99	16.50
1350	166	121	19.82	18.30	1410	171	127	20.90	20.28

1351	166	122	16.57	15.06	1411	171	129	20.10	19.72
1352	166	129	18.68	17.80	1412	171	136	19.31	18.67
1353	166	133	18.62	17.93	1413	171	137	21.52	20.59
1354	166	143	20.88	19.39	1414	171	141	21.23	20.46
1355	167	148	20.27	19.60	1415	170	144	16.00	15.21
1356	166	148	17.07	16.59	1416	171	146	20.12	19.73
1357	167	152	21.01	20.43	1417	170	146	19.16	18.34
1358	167	152	21.86	20.39	1418	170	148	20.87	20.29
1359	167	155	18.39	16.75	1419	171	149	20.91	19.31
1360	165	157	19.48	18.46	1420	170	156	16.14	15.61
1361	166	157	20.56	19.74	1421	170	159	20.98	20.42
1362	166	159	17.48	16.87	1422	170	163	19.73	19.50
1363	166	161	20.69	19.74	1423	170	163	17.33	16.30
1364	166	167	20.73	19.60	1424	171	164	17.73	17.02
1365	166	168	17.84	16.51	1425	170	165	19.08	18.50
1366	167	173	19.78	18.85	1426	171	173	20.39	19.38
1367	166	174	20.50	20.06	1427	171	182	21.16	20.42
1368	167	184	20.77	19.73	1428	172	183	19.34	18.25
1369	167	186	17.92	17.35	1429	170	184	19.75	18.78
1370	167	192	19.00	18.52	1430	172	185	16.53	16.02
1371	168	95	20.29	19.58	1431	171	186	17.42	16.89
1372	169	100	18.95	18.37	1432	170	187	20.76	20.57
1373	169	102	20.38	19.43	1433	173	97	20.81	19.32
1374	168	102	20.45	19.54	1434	172	97	20.60	19.68
1375	168	108	16.95	15.98	1435	172	104	19.08	17.71
1376	168	114	17.08	16.15	1436	173	106	19.20	17.72
1377	169	115	17.74	16.86	1437	174	111	19.97	19.43
1378	168	116	19.46	18.45	1438	172	117	18.66	18.01
1379	169	118	17.96	17.33	1439	172	125	16.52	15.85
1380	169	123	15.35	14.93	1440	172	131	16.22	15.51

1441 173 132 19.81 19.49

1442 173 135 19.55 18.75

1443 172 137 20.44 19.58

1444 173 139 20.27 19.56

1445 172 139 13.73 13.58

1446 172 142 17.57 16.88

1447 173 144 20.52 19.49

1448 172 146 20.43 19.10

1449 173 146 21.33 20.77

1450 173 148 17.14 16.59

1451 173 158 18.22 17.56

1452 172 159 18.81 17.36

1453 172 164 19.73 19.15

1454 174 165 20.90 20.13

1455 173 169 17.70 17.00

1456 172 170 16.66 16.05

1457 172 172 20.83 20.27

1458 173 172 21.17 20.75

1459 172 177 18.84 18.38

1460 173 179 18.31 17.18

1461 173 181 15.47 14.81

1462 173 193 17.06 16.23

1463 174 108 20.02 19.18

1464 174 110 20.96 19.88

1465 174 114 20.89 19.54

1466 174 128 19.93 19.50

1467 174 138 18.50 17.54

1468 174 150 21.03 20.37

1469 174 161 15.06 14.49

1470 174 163 20.49 19.88

1471 174 185 20.67 19.25

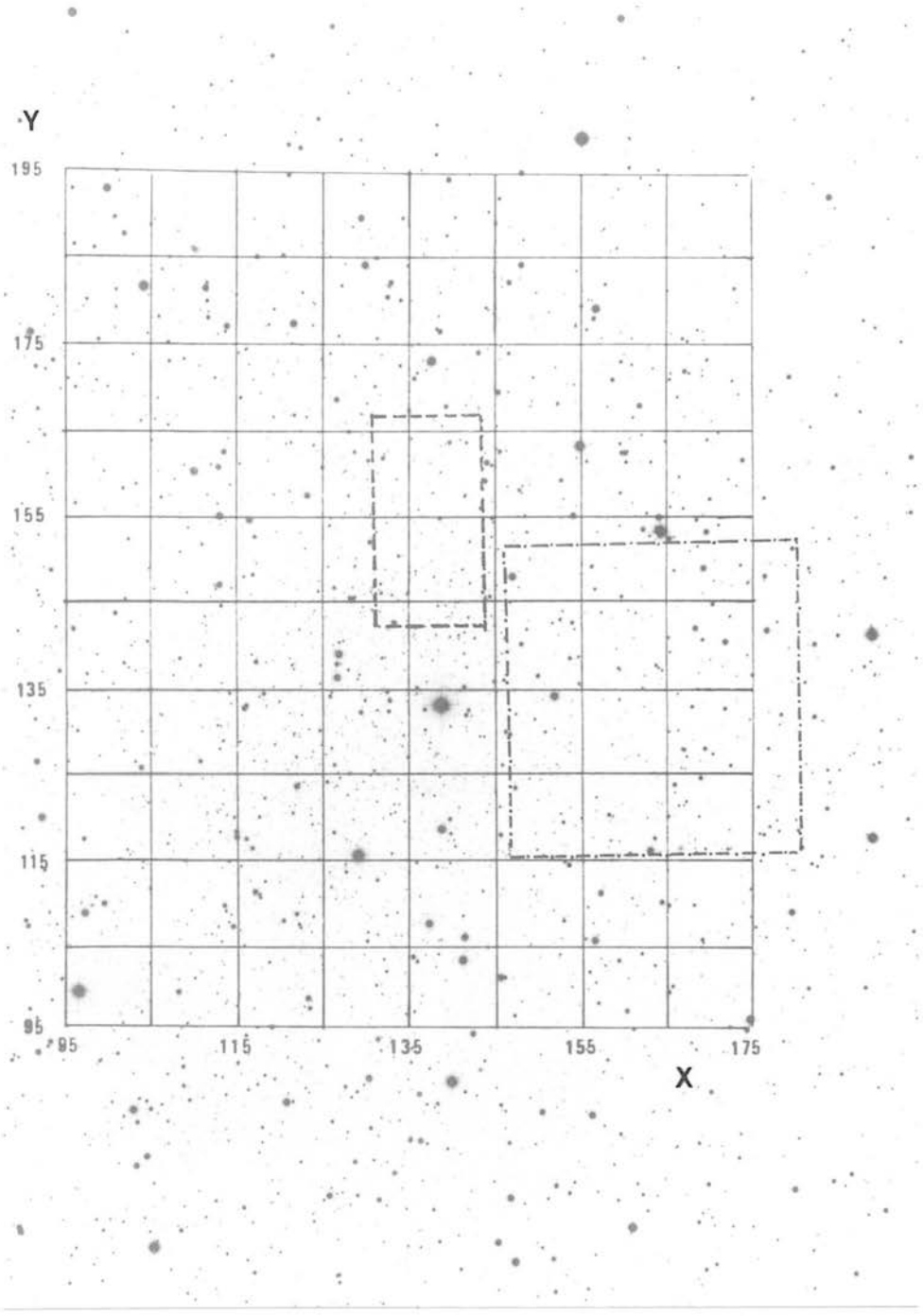

Plate A1. Area enclosed by solid line is that chosen from which stars were selected for the colour-magnitude diagram presented in chapter 3. Area enclosed by dashed line (----) is that over which the Mould and Aaronson (1983) sequence covers, and the dotted line (-·-·), that over which the Cannon et al (1986) and electronographic sequence derived in chapter 2 cover.

Appendix B

CORE AND TIDAL RADII OF THE CARINA DWARF SPHEROIDAL GALAXY FROM UK SCHMIDT TELESCOPE PLATES

P.J. Godwin
Department of Astronomy, University of Edinburgh
Blackford Hill, Edinburgh EH9 3HJ, Scotland, U.K.

ABSTRACT. Core and tidal radii of the Carina dwarf galaxy are determined by fitting King dynamical models to number count radial profiles, derived from COSMOS data. These values are compared with those of the other six known Local Group dwarf spheroidals.

PREPARATION AND REDUCTION OF DATA

Six good quality UK Schmidt Telescope plates (five IIIaJ, and one IIIaF), were mapped by COSMOS and then thresholded at 10% above the local sky background level in intensity space. This level was chosen as being a good compromise between (a) enabling faint images to be detected down to the horizontal branch with a relatively high S/N and (b) reducing the effects of crowding and hence making the blending of images less severe.

All the data were paired and calibrated enabling reliable J magnitudes to be determined and a (J-R, R) colour magnitude diagram drawn so that only the giant and horizontal branch stars could be used for the following analysis, thus eliminating to some extent the very high field star contamination ($l = 260.^{\circ}1$, $b = -22.^{\circ}2$). After being binned in 2′ bins, this data was contoured and finally smoothed using a 5 x 5 gaussian filter in order that the centre of the dwarf galaxy (XC, YC) could then be defined as the (x, y) coordinate of the bin with the maximum count. The (x, y) positions of the bins with a specified count starting at a value slightly higher than that of the background, could then be fitted (after transforming them to polar coordinates with origin at (XC, YC)), using a non-linear least squares procedure, to the generalised functional form of an ellipse, with the orientation and semi-major/minor axes left as the free fitting parameters. No significant variation of ellipticity with radius was found, but the effect of the bright central star SAO 234657 in the COSMOS data makes this result hard to confirm inconclusively with the present plate material. Work is now in progress (Godwin 1984), using the larger plate scale capacity of AAT prime focus plates to try and resolve this.

Hence a mean ellipticity (0.31) and orientation (72°) could then be found for all the fitted ellipses and the original data binned

J. Goodman and P. Hut (eds.), Dynamics of Star Clusters, 77–79.

in ellipses with these parameters. The background count was found by finding the value at which the counts summed over the ellipses levelled out. This was then subtracted from the original counts and the resulting mean radial profile with associated errors fitted to the empirical and theoretical models of King (1962, 1965, 1966). Values of $r_t = 47'$, $r_c = 9.6'$ were found. Taking the distance to the Carina dwarf galaxy as 91 kpc (Mould and Aaronson 1983), r_t comes out to be 1.24 kpc.

The effects of anisotropy in the outer regions of the Carina dwarf galaxy are now being investigated by fitting Michie models (Hodge and Michie 1969) to this radial profile (Godwin 1984).

DISCUSSION

The predicted limiting radius at perigalacticon of a stellar system moving in an elliptical orbit around the Galactic centre (King 1962) is

$$r_{lim} = R_p \left[\frac{M_d}{3.5 M_g} \right]^{1/3} \qquad (1)$$

assuming elongated orbits ($e \sim 0.5$). R_p is taken to be the present distance when calculating this quantity, and hence the value derived is an upper bound for the actual r_{lim}. If the observed tidal radius is larger than this upper bound, then the Galaxy must be seriously disrupting the system. Such is the case with Ursa-Minor and to a lesser degree with Draco and from the data here (see table I) Carina.

Hodge and Michie (1969) found that the ratio of the Galaxy's tidal, to the dwarf galaxy's internal gravitational force could be expressed in the approximate form

$$\left| \frac{T_z}{V_z} \right| \sim \frac{2\,(b/a)\,M_g\,r_t^3}{D^3 M_d} \qquad (2)$$

where D is the distance to the stellar system. Using $M_g = 3 \times 10^{11} M_\odot$, these values are recomputed from the data in table I, and plotted against the mean ellipticity of the isopleths (figure 1a). As Hodge and Michie (1969) noted, and as would be expected, the closer the dwarf galaxy to the Galactic centre, the greater the role that the Galactic tidal force plays in determining the structure of its outer regions. Figure 1b shows $|T_z/V_z|$ plotted against r_t/r_c. A large value of this former ratio, should be indicative of a large Galactic influence on the dwarf galaxy, producing a low stellar density envelope at large distances from its centre. As can be seen from these two figures, the Carina dwarf galaxy joins Draco and Ursa-Minor as satellites of our Galaxy seriously affected by the Galactic tidal field.

ACKNOWLEDGEMENTS

My thanks go to Drs. M.T. Brück, R.D. Cannon, D.C. Heggie, H.T. MacGillivray (COSMOS Unit, ROE), S.R. Heathcote and Mr S.M. Beard for helpful suggestions and comments.

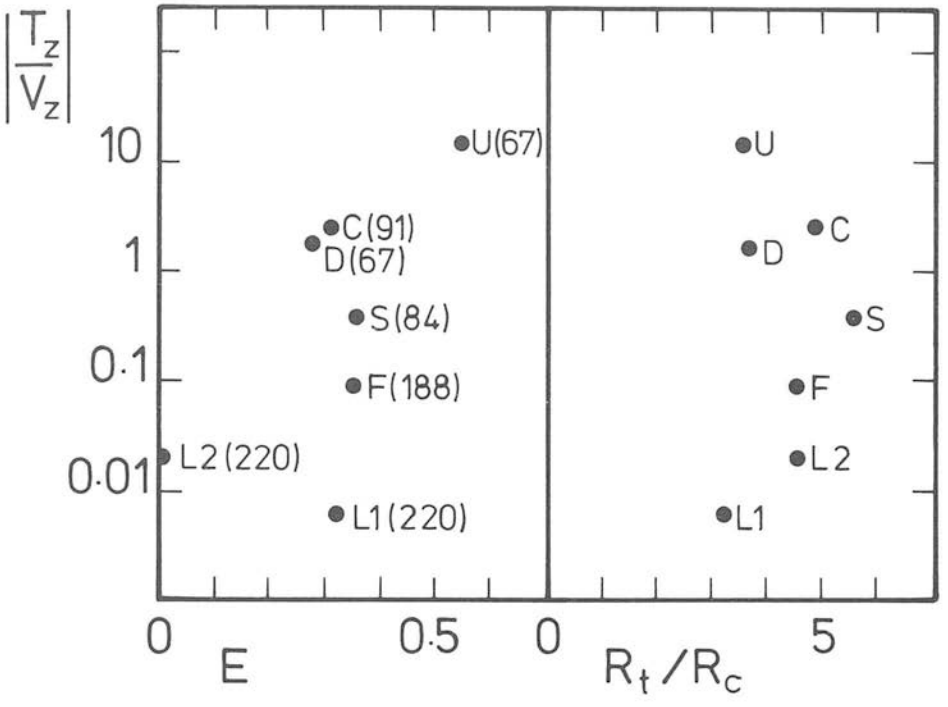

Fig. 1a,b. $|T_z/V_z|$ - ellipticity/concentration parameter relations for the Local Group dwarf spheroidals (distances in brackets).

Table I. Local Group dwarf spheroidal data.

Name	r_t'	r_t(kpc)	r_{lim}	r_c'	r_t/r_c	E	$M/M_\odot$	D(kpc)	T_z/V_z
Draco	35	0.51	0.33	9.27	3.85	0.29	1.2E+5	67	1.57
Leo I	13	0.91	3.44	4.33	3.13	0.31	4.0E+6	220	0.007
Leo II	10	0.65	2.16	2.28	4.43	0.01	1.0E+6	220	0.02
Sculptor	57	1.20	1.19	10.31	5.53	0.35	3.0E+6	84	0.38
Ursa-Minor	47	1.20	0.31	13.29	3.57	0.55	1.0E+5	67	15.51
Fornax	57	3.10	5.02	12.71	4.49	0.35	2.0E+7	188	0.09
Carina	47	1.24	0.71	9.60	4.90	0.31	5.0E+5	91	2.09

REFERENCES

Godwin, P.J. (1984) PhD Thesis, University of Edinburgh (in prep.)
Hodge, P.W., Michie, R.W. (1969) Astron. J. 74 p587
King, I.R. (1962) Astron. J. 67 p471
King, I.R. (1965) Astron. J. 70 p376
King, I.R. (1966) Astron. J 71 p64
Mould, J.R., Aaronson, M. (1983) Ap.J. 273 p530.

Mon. Not. R. astr. Soc. (1983) **204**, *Short Communication*, 87P–92P

Slippery evidence on the Galaxy's invisible heavy halo

D. Lynden-Bell *Institute of Astronomy, The Observatories, Madingley Road, Cambridge CB3 0HA*

R. D. Cannon *Royal Observatory, Blackford Hill, Edinburgh EH9 3HJ*

P. J. Godwin *Department of Astronomy, University of Edinburgh, Blackford Hill, Edinburgh EH9 3HJ*

Received 1983 May 24

Summary. New measurements have been made of the velocities of carbon stars in the Carina and other dwarf galaxies, and of the planetary nebula in Fornax. Carina, previously thought to be the Galaxy's fastest moving satellite, is shown instead to be moving very slowly. Evidence previously assembled on velocities of objects in the outer parts of the Galaxy is re-examined in the light of these and other new data. The new result for Carina combined with the revised velocity of Sculptor (and a new distance reported for Palomar 1) removes *some* of the evidence for a heavy halo, but more remains to be re-investigated. However, assuming the velocities are not preferentially oriented across the line-of-sight, the best modern data on all the nine satellites of the Galaxy now yield a total mass out to about 100 kpc of $(2.6 \pm 0.8) \times 10^{11} M_{\odot}$.

1 Introduction

In several past compilations of data on the outer reaches of the Galaxy (Lynden-Bell 1982a, 1983; Faber & Lin 1983), the Carina dwarf spheroidal galaxy (Cannon, Hawarden & Tritton 1977) takes pride of place as the object giving the greatest mass for the Galaxy (Fig. 1). The velocities of our dwarf spheroidal satellites have been notoriously hard to measure because the stars are faint and dispersed and they generally have very weak lines owing to their low abundances of the elements higher than helium. However, Cannon, Niss & Nørgaard-Nielsen (1980) discovered two carbon stars in Carina and we realized that the Swan band-heads would provide the strong spectral features lacking in other stars. The spectra of these first two stars in Carina were obtained in the expectation that they would be ordinary red giants, if indeed they were members of the dwarf galaxy at all. Thus no standard carbon stars were observed at the same time, while the dispersion was too low to use spectral features other than the Swan bands to determine velocities. Two galactic carbon stars were observed on the following night, and Cannon *et al.* (1980) derived a mean velocity of $450 \pm 100\,\mathrm{km\,s^{-1}}$, with a large and unknown possible systematic error. A systematic search led to the discovery of

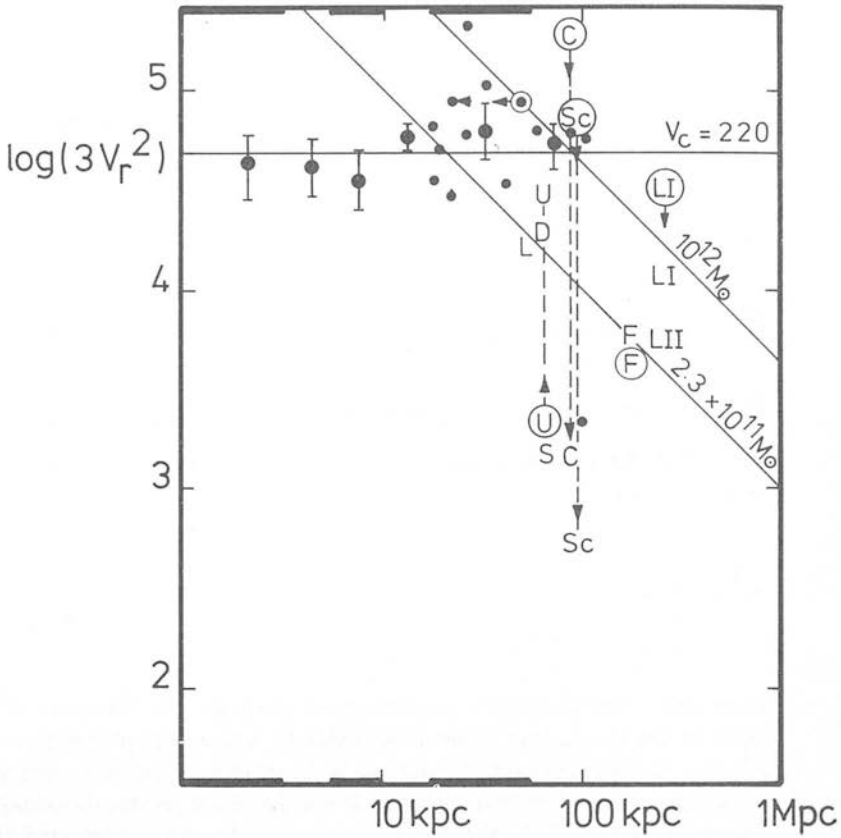

Figure 1. Velocities of globular clusters and satellite galaxies as a function of distance from the Galactic Centre. Heavy points are means of $3v_r^2$ for globular clusters in the columns indicated in the margins. The small points are the individual globular clusters in the outer parts of the Galaxy. The satellite galaxies are the Large Magellanic Cloud L, Small Magellanic Cloud S, Ursa Minor U, Draco D, Sculptor Sc, Carina C, Fornax F, Leo I LI and Leo II LII. Old radial velocity points are circles and have been replaced by the new uncircled ones, which represent results obtained by several authors within the last year.

several more carbon stars in Carina (Mould *et al.* 1982). Realizing that the preliminary Carina velocity was being widely used and that it was high enough to be a major influence on Galaxy mass determinations (Faber & Lin 1983; Lin & Faber 1983), we decided to try to obtain a more reliable value using higher dispersion spectra of a larger sample of stars. Carina also had enough carbon stars to give an opportunity to check the recent claim of Aaronson (1983) that the dwarf galaxies themselves may contain invisible mass. At the same time we realized that it should be possible to obtain a more precise velocity of the Fornax dwarf galaxy using its planetary nebula (Danziger *et al.* 1978).

2 Observational data

All the spectra were obtained on three nights during 1983 January, using the IPCS and the RGO spectrograph on the AAT. The 25-cm camera was used with grating 1200 V, yielding a reciprocal dispersion of 33 Å mm^{-1}. Two grating angle settings were used, to cover either the spectral range 4450–5350 Å which includes the 1–0 C_2 Swan band at 4737 Å and the 0–0 band at 5165 Å, or the range 5000–5900 Å which includes the 0–0 band and the 0–1 band

at 5636 Å. The 5636 Å band is not affected by isotopic shifts and should give reliable redshift information, while at this dispersion the 4737 Å isotopic bands are well separated and so should give good velocities as well as values for the C^{12}/C^{13} ratio. The 6165 Å band is liable to be confused.

All of the candidate carbon stars in Carina (Mould *et al.* 1982) were observed at least once; stars C7 and C8 were found not to be carbon stars. In addition, we observed one carbon star in each of the Fornax, Leo I and Leo II dwarf galaxies, and obtained two observations of the Fornax planetary nebula. Four galactic carbon stars with accurately known velocities (McClure, private communication) were observed as standards.

The carbon star spectra contain a wealth of information which warrants more discussion in a future paper. However, it is immediately apparent that the velocity of Carina is only about half the value originally quoted by Cannon *et al.* (1980), and the purpose of this paper is to discuss the implications of this drastic revision.

Two methods have been used to derive the carbon star velocities. One involves comparing the positions of the Swan bandheads on large-scale plots of the spectra, and the other utilizes a cross-correlation routine in the Edinburgh Spectrum Processing package (ESP; Kelly, private communication). In each case the velocities of the programme stars are determined relative to galactic standards. With either method it has proved possible to determine relative velocities to an accuracy of about 20 km s^{-1}, although we believe that a higher accuracy should be attainable. One of the difficulties is that the standard computer cross-correlation programs do not handle the dramatic carbon star spectra (see Cannon *et al.* 1980 for an illustration) very well, while another is that the galactic carbon stars are not particularly well matched to those in the dwarfs. In the case of the Fornax planetary nebula, the positions of the strong emission lines Hβ (λ 4861.3 Å) and the [O III] doublet ($\lambda\lambda$ 4958.9 Å, 5006.9 Å) were measured directly with respect to arc lines.

The results of our AAT observations are given in Table 1. Evidently the heliocentric radial velocity of Carina is really 240 ± 10 km s^{-1}. The correction to the LSR due to the Sun's motion of (9, 12, 7) km s^{-1} is -15 km s^{-1} while the correction for the motion of 220 km s^{-1} of the LSR around the Galaxy is -201 km s^{-1} so Carina's radial velocity in the Galaxy's system of rest is $+24 \pm 10$ km s^{-1}. This is to be compared with 235 ± 100 km s^{-1} used previously. Since velocities enter mass determinations in the form $v^2 r/G$, it is clear that any leverage Carina's velocity may have on the total mass of the Galaxy is now pushing towards a

Table 1. Velocities of stars in dwarf galaxies.

System	Star	Heliocentric V_{01} (manual)	Velocity V_{02} (cross-correlation)	Number of observations
Carina	C1	242	244	2
	C2	208:	268:	1
	C3	236	239	2
	C4	236	195	1
	C5	248	245	2
	C6	266:	212:	2
	Weighted mean	240 ± 5*	234 ± 9*	
Fornax	BM13	79 ± 20†	65 ± 25†	2
	Planetary nebula	36 ± 5†	Night 1	
		40 ± 5†	Night 2	

Notes:
* Formal internal errors.
† Estimated total errors.

small mass rather than a large one. A rather similar history may be recorded for Sculptor; Hartwick & Sargent (1978) obtained an uncertain heliocentric velocity off red giants of $196 \pm 70\,\mathrm{km\,s^{-1}}$. Re-determined by Richer & Westerlund (1983) using better data and the better carbon star method, the revised result is $20 \pm 22\,\mathrm{km\,s^{-1}}$. For Sculptor the correction to the LSR is -8 and onward to the GSR it is only -25, since it is close to the South Galactic Pole. Thus, in the galactic system of rest the old uncertain result of $163 \pm 70\,\mathrm{km\,s^{-1}}$ had been replaced by $-13 \pm 22\,\mathrm{km\,s^{-1}}$. Again evidence favouring a heavy mass for the Galaxy has evaporated on the basis of more accurate measurement.

For the planetary nebula in Fornax we obtained a mean velocity of $38 \pm 5\,\mathrm{km\,s^{-1}}$, compared with the original value of $10 \pm 40\,\mathrm{km\,s^{-1}}$ (Danziger *et al.* 1978). For the carbon star BM13 (Frogel *et al.* 1982) we obtained $70 \pm 25\,\mathrm{km\,s^{-1}}$, compared with $75 \pm 36\,\mathrm{km\,s^{-1}}$ for the same star by Richer & Westerlund (1983) who gave $+31 \pm 36\,\mathrm{km\,s^{-1}}$ for a second carbon star. The globular clusters in Fornax have also been measured by Humason, Mayall & Sandage (1956) who gave $+40$ and $+35 \pm 30$ $\mathrm{km\,s^{-1}}$ for two clusters, and by van den Bergh (1969) who gave $54 \pm 10\,\mathrm{km\,s^{-1}}$ for four clusters. Overall it seems that the best mean value for the Fornax galaxy as a whole is $45 \pm 5\,\mathrm{km\,s^{-1}}$. Our spectra for one very faint star in each of the Leo dwarfs are of low quality and have not yielded useful velocities.

The distant globular clusters have also given evidence on the total mass of the Galaxy (Hartwick & Sargent 1978). Recent work with charge coupled devices has confirmed the large distance for Pal 14 (Da Costa, Ortolani & Mould 1982) but Pal 1 is now at about 20 kpc from the Galactic Centre (Da Costa, private communication) in place of 52 kpc. It would be wise to remeasure the radial velocities of Pal 14, as well as of Pal 3 and Pal 4, before deciding whether our Galaxy has a heavy halo.

Regarding the velocity dispersion within Carina, the rms scatter between the velocities of the six carbon stars is of the order of $20\,\mathrm{km\,s^{-1}}$. However, the differences we obtain when using different reduction techniques, when using different spectral features or when comparing with different standards are also all of the order of $20\,\mathrm{km\,s^{-1}}$, and it is clear that we are not yet measuring a real intrinsic velocity dispersion for the dwarf galaxy. It is perhaps significant that our best-determined velocities (for C1, C3 and C5) cover a total range of only $12\,\mathrm{km\,s^{-1}}$, so that the true dispersion is presumably less than $10\,\mathrm{km\,s^{-1}}$, but since Carina is one of the smallest dwarfs this is not a useful upper limit. More sophisticated reduction procedures may yield better velocities and enable us to address the intriguing possibility that the dwarf galaxies are themselves over-massive (Aaronson 1983).

3 Implications for the mass of the Galaxy

In any set of observations the most outstanding new deductions can often be drawn from points that lie furthest away from the main distribution. In the above case, those with large v^2r are crucial. However, if the data set is corrupted by a few objects of very uncertain distance or very inaccurate radial velocity – so bad that the error dominates the value – then by selecting the extreme points for discussion, we are also selecting for points that have been sent away from the others by extreme errors. Objects at great distance are faint and hard to work on, they also have weak spectral features. Thus, the only objects that tell us of the outer reaches of the Galaxy are those in which we must expect the greatest error. Luckily technology is coming to our rescue and the much greater sensitivity of modern equipment will answer this problem. Some hint can already be found from the nine satellites of the Galaxy, seven of which now have good velocities.

Using the method of Lynden-Bell & Frenk (1981) we can calculate the rms circular velocity at the positions of the satellites from the formula $\langle V_c^2 \rangle = \langle \mathrm{v}^2 \rangle = 3\langle v_r^2 \rangle$. The last

Table 2.

	V_0 (km s^{-1})	± ϵ	V_{GSR} (km s^{-1})		r (kpc)	Velocity ref.
			V_c = 220	250		
LMC	+ 270	5	+ 76	+ 51	52	Yahil, Tammann & Sandage (1977)
SMC	+ 163	5	+ 22	+ 4	66	Yahil *et al.* (1977)
Draco	− 291	6	− 96	− 71	67	Aaronson (1983)
Ursa Minor	− 261	6	− 99	− 78	67	Aaronson (1983)
Sculptor	+ 20	22	− 13	− 16	84	Richer & Westerlund (1983)
Carina	+ 240	10	+ 24	− 3	85	This paper
Fornax	+ 45	5	− 44	− 54	188	This paper
Leo I	+ 168	40	+ 60	+ 46	220	Aaronson, Olszewski & Hodge (1983)
Leo II	+ 90	40	+ 46	+ 39	220	Aaronson *et al.* (1983)

Distances for dwarfs taken from Hodge (1971) except for Carina, which is from Mould *et al.* (1982). The Magellanic Cloud distances are means from several determinations.

equality assumes the true velocities are uncorrelated with the directions in which the objects lie. Applying this to the data in Table 2 we find $\langle V_c^2\rangle^{1/2} = 106 \pm 18\,\mathrm{km\,s^{-1}}$, a value much lower than the 220 to 250 km s^{-1} found near the Sun. This suggests that the main mass of the Galaxy lies inside this satellite system so a point mass approximation is appropriate. For elliptical orbits one has radial velocities v_r observed from the focus given by

$$v_r^2 r = GM\, e^2 \sin^2\phi/(1 + e\cos\phi)$$

where ϕ is measured from pericentre. Time averaging over the orbit,

$$\langle \sin^2\phi/(1 + e\cos\phi)\rangle = 1/2.$$

For a statistically steady assembly of such systems with various eccentricities one has

$$\langle v_r^2 r\rangle = GM\langle e^2\rangle/2.$$

Now Jeans (1928) showed that if the velocities were isotropically distributed, then e is distributed like $2\,e\,de$ between 0 and 1. We therefore expect $\langle e^2\rangle = 1/2$ and

$$M = 4\langle v_r^2 r\rangle/G.$$

Allowing for velocity errors ϵ we have $M = 4\langle (v_r^2 - \epsilon^2) r\rangle/G$. The mass would be smaller than this estimate if the velocities were predominantly radial and larger if they were predominantly transverse. The formula will be grossly in error if the satellite orbits are almost circular, but since most of them lie at quite high galactic latitudes and both the Magellanic stream (Mathewson, Cleary & Murray 1974) and the Fornax–Leo–Sculptor circle (Lynden-Bell 1982b; Hodge & Michie 1969) pass close to the Galactic Poles, this is unlikely. For a circular velocity at the Sun of 220 km s^{-1}, we obtain

$$M = (2.6 \pm 0.8) \times 10^{11} M_\odot.$$

The correction for other values of V_c at the Sun is approximately

$$\frac{M}{M_\odot} = -3.6 \times 10^9 (V_c - 220)/\mathrm{km\,s^{-1}}.$$

If this indicates that a heavy halo is not present in our Galaxy, *cf.* Miyamoto, Satoh & Ohoshi (1980) and Wakamatsu (1981), then we are by no means unique as Kalnajs (1983) and Gottesman & Hunter (1982) have shown. However, the above result is probably an underestimate of the Galaxy's mass because $\langle e^2\rangle = 1/2$ implies a typical $R_{min} \sim 1/6 R_{max}$.

Many of the dwarf spheroidals could not survive such close passages. This implies that the orbits of the surviving satellites will be less eccentric than those of an isotropic distribution, so the motions will be mainly transverse to the lines-of-sight. If instead we used the eccentricity distribution $8\,e\,de$ with a maximum e of 0.5, then $\langle e^2 \rangle = 1/8$ and our final result for the mass would be four times greater $(10 \pm 3) \times 10^{11} M_{\odot}$. Such a result is consistent with Hawkins's limit set from the velocity of one rapidly variable star in the distant halo which he takes to be a distant RR Lyrae. The history of radial velocities described above suggests that a second determination of the radial velocity of Hawkins's star (Hawkins 1983) at higher dispersion is necessary to ensure that history is not merely repeating itself. It is wise to withold judgement on our halo until we have a greater knowledge of the orbits of the distant satellites and better velocities for Leo I and Leo II.

Acknowledgments

We are grateful to Bob McClure, Paul Hodge, Marc Aaronson, Paul Schechter and Gary Da Costa for giving us access to as yet unpublished data.

References

Aaronson, M., 1983. *Astrophys. J.*, **266**, L11.
Aaronson, M., Olszewski, E. W. & Hodge, P. W., 1983. *Astrophys. J.*, **267**, 271.
Cannon, R. D., Hawarden, T. G. & Tritton, S. B., 1977. *Mon. Not. R. astr. Soc.*, **180**, 81P.
Cannon, R. D., Niss, B. & Nørgaard-Nielsen, H. U., 1980. *Mon. Not. R. astr. Soc.*, **196**, 1P.
Da Costa, G. S., Ortolani, S. & Mould, J., 1982. *Astrophys. J.*, **257**, 633.
Danziger, I. J., Dopita, M. A., Hawarden, T. G. & Webster, B. L., 1978. *Astrophys. J.*, **220**, 458.
Faber, S. M. & Lin, D. N. C., 1983. *Astrophys. J.*, **266**, L17.
Frogel, J. A., Blanco, V. M., McCarthy, M. F. & Cohen, J. G., 1982. *Astrophys. J.*, **252**, 133.
Gottesman, B. T. & Hunter, J. H., 1982. *Astrophys. J.*, **260**, 65.
Hartwick, F. D. A. & Sargent, W. L. W., 1978. *Astrophys. J.*, **220**, 453.
Hawkins, M. R. S., 1983. *Nature*, **303**, 406.
Hodge, P. W., 1971. *Ann. Rev. Astr. Astrophys.*, **9**, 35.
Hodge, P. W. & Michie, R. W., 1969. *Astr. J.*, **74**, 587.
Humason, M. L., Mayall, N. U. & Sandage, A. R., 1956. *Astr. J.*, **61**, 97.
Jeans, J. H., 1928. *Astronomy and Cosmology*, p. 297, Cambridge University Press.
Kalnajs, A. J., 1983. *IAU Symp. 100, Internal Kinematics and Dynamics of Galaxies*, p. 109, ed. Athanassoula, E. Reidel, Dordrecht, Holland.
Lin, D. N. C. & Faber, S. M., 1983. *Astrophys. J.*, **266**, L21.
Lynden-Bell, D., 1982a. Vatican Conference 1981, *Pont. Acad. Scripta Varia*, **48**, p. 85.
Lynden-Bell, D., 1982b. *Observatory*, **102**, 202.
Lynden-Bell, D., 1983. Vancouver Conference 1982, *Kinematics, Dynamics and Structure of the Milky Way*, p. 349, ed. Shuter, W. L. H., Reidel, Dordrecht.
Lynden-Bell, D. & Frenk, C. S., 1981. *Observatory*, **101**, 200.
Mathewson, D. S., Cleary, M. N. & Murray, J. D., 1974. *Astrophys. J.*, **190**, 291.
Miyamoto, M., Satoh, C. & Ohashi, M., 1980. *Astr. Astrophys.*, **90**, 215.
Mould, J. R., Cannon, R. D., Aaronson, M. & Frogel, J. A., 1982. *Astrophys. J.*, **254**, 500.
Richer, H. B. & Westerlund, B. E., 1983. *Astrophys. J.*, **264**, 114.
Van den Bergh, S., 1969. *Astrophys. J. Suppl.*, **19**, 145 (Appendix).
Wakamatsu, K., 1981. *Publ. astr. Soc. Pacif.*, **93**, 707.
Yahil, A., Tammann, G. A. & Sandage, A., 1977. *Astrophys. J.*, **217**, 903.

Aaronson M. (1983), Ap.J. 266, L11.

Aaronson M. (1985), talk presented at Star Forming Dwarf Galaxies and related objects, Paris, France.

Aaronson M. and Cook K. (1983), Bull. Am. Astron. Soc. 15, 907.

Aaronson M., Gordon G., Mould J.R., Olszewski E. and Suntzeff N. (1985), Ap.J. Lett. 296, L7.

Aaronson M., Cook K. and Norris J. (1985), preprint.

Aaronson M., Liebert J. and Stocke J. (1982), Ap.J. 254, 507.

Aaronson M. and Mould J.R. (1980), Ap.J. 240, 804.

Aaronson M. and Mould J.R. (1982), Ap.J. Suppl. 48, 161.

Aaronson M. and Mould J.R. (1985), Ap.J. 290, 191.

Aaronson M., Olszewski E.W. and Hodge P.W. (1983), Ap.J. 267, 271.

Allen C.W. (1955), in "Astrophysical Quantities" University of London, Athlone Press.

Appleton P.N. and Davies R.D. (1983), IAU Symposium no.100, "Internal Kinematics and Dynamics of Galaxies", ed. E. Athanassoula (Reidel:Dordrecht) p.95.

Argue A.N. and Sullivan C. (1980), The Observatory 100, 152.

Armandroff T.E. and Demarque P. (1984), Astron. Astrophys. 139, 305.

Audouze J. and Tinsley B.M. (1976), Ann. Rev. Astr. Astrophys. 14, 43.

Azzopardi M., Lequeux J. and Westerlund B.E. (1985), preprint (to

appear in Astron. Astrophys.).

Bell R.A. and Gustafsson B. (1978), Astron. Astrophys. Suppl. 34, 229.

Bertola F. (1980), in "Structure and Evolution of Normal Galaxies", NATO advanced study, I.O.A., eds. Fall S.M. and Lynden-Bell D., (C.U.P.), p.13.

Bevington P.R. (1969), in "Data reduction and error analysis for the physical sciences", McGraw-Hill.

Binggeli B., Sandage A. and Tarenghi M. (1984) Astron.J. 89, 64

Blair M. and Gilmore G. (1982), P.A.S.P. 94, 752.

Blanco B.M., Blanco V.M. and McCarthy M.F. (1978), Nature 271, 638.

Blanco V.M., McCarthy M.F. and Blanco B.M. (1980), Ap.J. 242, 938.

Blumenthal G.R., Faber S.M., Primack J.R. and Rees M.J. (1984), Nature 311, 517.

Bruck M.T. and Hawkins M.R.S. (1983), Astron. Astrophys. 124, 216.

Buonanno R., Corsi C.E. and Fusi-Pecci F. (1981) M.N.R.A.S. 196, 435.

Buonnano R., Corsi C.E., Fusi-Pecci F., Hardy E. and Zinn R. (1984a), P.A.S.P. 96, 785.

Buonanno R., Corsi C.E., Fusi-Pecci F., Alcaino G. and Liller W. (1984b), Astron. Astrophys. Suppl. 57, 75.

Burstein D. and Heiles C. (1978), Ap.J. 225, 40.

Burstein D. and Heiles C. (1983), Astron.J. 87, 1165.

Cacciari C. and Renzini A. (1976), Astron. Astrophys. Suppl. 25, 303.

Cannon R.D. (1968), Ph.D. Thesis Cambridge University.

Cannon R.D. (1974), M.N.R.A.S. 167, 551.

Cannon R.D. (1984), in "Astronomical Photography 1984", IAU Working Group on Photographic Problems, Edinburgh, eds. Sim M.E. and Ishida K., p.119.

Cannon R.D. and Stobie R.S. (1973), M.N.R.A.S. 162, 207.

Cannon R.D., Hawarden T.G. and Tritton S.B. (1977), M.N.R.A.S. 180, 81P.

Cannon R.D., Niss B and Norgaard-Nielsen H.U. (1980), M.N.R.A.S. 196, 1P.

Cannon R.D., Demers S., Hawkins M.R.S., Kunkel W.E. and Pritchet C. (1986), in preparation.

Cannon R.D., Hawkins M.R.S. and Sagar R.S. (1985), in proceedings of X1X IAU General Assembly, New Delhi (in press).

Canterna R. and Schommer R.A. (1978a), Ap.J. 219, L119.

Canterna R. and Schommer R.A. (1978b), IAU Symposium no.80 "The HR diagram", eds. Davis Philip A.G. and Hayes D.S., (Reidel:Dordrecht), p.177.

Carney B.W. (1984), P.A.S.P. 96, 841.

Castellani V. and Tornambe A. (1981), in "Effects of mass loss on Stellar Evolution", Astrophysics and Space Science library, eds. Chiosi C. and Statio R., (Reidel:Dordrecht), p.357.

Chandrasekhar S. (1942), in "Principles of Stellar Dynamics",

(Dover:New York).

Ciardullo R.B. and Demarque P. (1977a), Yale Transactions, 33.

Ciardullo R.B. and Demarque P. (1977b), Yale Transactions, 34.

Ciardullo R.B. and Demarque P. (1977c), Yale Transactions, 35.

Ciardullo R.B. and Demarque P. (1979), in "Problems of calibration of multicolour photometric systems", Dudley Obs. Report 14, 317, ed. Davis Philip A.G.

Clube S.V.M. and Dawe J.A. (1980), M.N.R.A.S. 190, 591.

Cook K., Schecter P. and Aaronson M. (1983), Bull. Am. Astron. Soc. 15, 907.

Cowsik R. and Ghosh P. (1985), preprint.

Cowsik R. and McClelland J. (1972), Phys. Rev. Lett. 29, 669.

Da Costa G.S. and Freeman K.C. (1976), Ap.J. 206, 128.

Da Costa G.S. (1982), Astron.J. 87, 990.

Da Costa G.S. (1984), Ap.J. 285, 483.

Danziger I.J., Dopita M.A., Hawarden T.G. and Webster B.L. (1978), Ap.J. 220, 458.

Demarque P. and Hirshfeld A.W. (1975), Ap.J. 202 ,346.

Demarque P., Sweigart A.V. and Gross P.G. (1972), Nature (Physical Review) 239, 85.

Demers S., Beland S. and Kunkel W.E. (1983), P.A.S.P. 95, 354.

Demers S. and Kunkel W.E. (1979), P.A.S.P. 91, 761.

Demers S., Kunkel W.E. and Hardy E. (1979), Ap.J. 232, 84.

Demers S., Kunkel W.E. and Krautter A. (1980), Astron.J. 85, 1587.

Demers S. and Harris W.E. (1983), Astron.J. 88, 329.

Deupree R.G. (1979), Ap.J. 234, 228.

de Vaucouleurs G. (1958), in "Handbuch der Physik", ed. Flugge S. (Springer:Berlin), 53,311.

Di Serego S. (1980), ESO/ESA Workshop on the need for coordinated ground based observations "Dwarf Galaxies", Geneva, eds. Tarenghi M. and Kjar K., p.183.

Eggen O.J., Lynden-Bell D. and Sandage A.R. (1962), Ap.J. 136, 748.

Faber S.M. and Gallagher J.S. (1979), Ann. Rev. Astr. Astrophys. 17, 135.

Faber S.M. and Lin D.N.C. (1983), Ap.J. 266, L17.

Fall S.M. (1980) in "Structure and Evolution of Normal Galaxies", NATO advanced study, I.O.A., eds. Fall S.M. and Lynden-Bell D. (C.U.P.), p.1.

Flannery B.P. and Johnson B.C. (1982), Ap.J. 263, 166.

Freedman W.L. (1984), Ph.D. Thesis, David Dunlap Observatory, Department of Astronomy, University of Toronto.

Freeman K.C. (1985), see Seitzer P.O. (1985).

Freeman K.C. and Norris J. (1981), Ann. Rev. Astr. Astrophys. 19, 319.

Frogel J.A., Blanco V.M., McCarthy M.F. and Cohen J.G. (1982), Ap.J. 252, 133.

Fujimoto M. and Murai T. (1983), IAU Symposium no. 108 "Structure and Evolution of the Magellanic Clouds", eds. van den Bergh S. and de Boer K.S., (Reidel:Dordrecht), p.115.

Fusi-Pecci F. and Renzini A. (1979) in "Astronomical uses of the Space Telescope", ESO publication.

Gerola H., Carnevali P. and Salpeter E.E. (1983), Ap.J. 268, L75.

Gerola H., Seiden P.E. and Schulman L.S. (1980), Ap.J. 242, 517.

Green E.M. (1981), University of Texas Publication in Astronomy, 18.

Gribben J. (1986), New Scientist 1490, 37.

Gunn J.E. (1985), preprint of paper to appear in proceedings of IAU Symposium no. 117 "Dark matter in the Universe".

Hardy E. and Durand D. (1984), Ap.J. 279, 567.

Hardy E., Buonanno R., Corsi C.E., Janes K.A. and Schommer R.A. (1984), Ap.J. 278, 592.

Harrington R.G. and Wilson A.G. (1950) P.A.S.P. 62, 118.

Harris W.E. (1976), Astron.J. 81, 1095.

Harris W.E. and Racine R. (1979), Ann. Rev. Astr. Astrophys. 17, 241.

Hartwick F.D.A. (1968), Ap.J. 154, 475.

Hartwick F.D.A. (1976), Ap.J. 209, 418.

Hartwick F.D.A. and Sargent W.L.W. (1978), Ap.J. 221, 512.

Hawkins M.R.S. (1979), M.N.R.A.S. 188, 691.

Hawkins M.R.S. (1981), M.N.R.A.S. 194, 1013.

Hawkins M.R.S. (1983), Nature 303, 406.

Hayashi C. (1961), Publ. Astr. Soc. Japan 13, 450.

Heggie D.C. (1979), M.N.R.A.S. 188, 525.

Heiles C and Cleary M.N. (1979), Aust. J. of Physics, Astrophys. Suppl. 47, 1.

Hirshfeld A.W. (1980), Ap.J. 241, 111.

Hodge P.W. (1961a), Astron.J. 66, 249.

Hodge P.W. (1961b), Astron.J. 66, 384.

Hodge P.W. (1962), Astron.J. 67, 125.

Hodge P.W. (1963), Astron.J. 68, 470.

Hodge P.W. (1964a), Astron. J. 69, 438.

Hodge P.W. (1964b), Astron. J. 69, 853.

Hodge P.W. (1971), Ann. Rev. Astr. Astrophys. 9, 35.

Hodge P.W. (1977), Ap.J. Suppl. 33, 69.

Hodge P.W. (1978), Ap.J. Suppl. 37, 145.

Hodge P.W. (1983), Ap.J. 264, 470.

Hodge P.W. and Michie R.W. (1969), Astron. J. 74, 587.

Hodge P.W. and Smith D.W. (1974), Ap.J. 188, 19.

Huchtmeier W.K. (1980), ESO/ESA Workshop on the need for coordinated space and ground based observations. "Dwarf Galaxies", Geneva, eds. Tarenghi M. and Kjar K., p.57.

Iben I. (1968), Nature 220, 143.

Iben I. (1974), Ann. Rev. Astr. Astrophys. 12, 215.

Iben I. (1984), IAU Symposium no. 105 "Observational Tests of the Stellar Evolution Theory", eds. Maeder A. and Renzini A., (Reidel:Dordrecht), p.3.

Illingworth G. (1975), IAU Symposium no. 69 "Dynamics of Stellar Systems", ed. Hayli A., (Reidel:Dordrecht), p.151.

Illingworth G. (1976), Ap.J. 204, 73.

Innanen K.A. (1979), Astron. J. 84, 960.

Janes K. (1981), IAU Colloquium no. 68 "Astrophysical parameters for Globular Clusters", eds. Davis Philip A.G. and Hayes D.S., (L. Davis Press:Schenectady, N.Y.), p.349.

Jones W.B., Obitts D.L., Gallet R.M. and de Vaucouleurs G. (1967), Publ. of the Department of Astronomy, University of Texas at Austin, Series II, Vol. 1., no.8, 1.

King I.R. (1962), Astron. J. 67, 471.

King I.R. (1965), Astron. J. 70, 376.

King I.R. (1966), Astron. J. 71, 64.

King I.R. (1978), Ap.J. 222, 1.

Kraft R.P. (1979), Ann. Rev. Astr. Astrophys. 17, 309.

Kraft R.P., Trefzger C.F. and Suntzeff N. (1979), IAU Symposium no. 84 "The Large-Scale Characteristics of the Galaxy", ed. Burton W.B. (Reidel:Dordrecht), p.463.

Kuiper G.P. (1942), Ap.J. 95, 201.

Kunkel W.E. (1979), Ap.J. 228, 718.

Kunkel W.E. and Demers S. (1977), Ap.J. 214, 21.

Larson R.B. (1974), M.N.R.A.S. 169, 229.

Lee S.W. (1976), Ph.D. Thesis ANU Canberra, Australia.

Lin D.N.C. and Faber S.M. (1983), Ap.J. 266, L21.

Luyten W. (1939), Publ. Astr. Obs. Univ. Minnesota, volume 2, no. 7.

Lynden-Bell D. (1967), M.N.R.A.S. 136, 101.

Lynden-Bell D. (1976), M.N.R.A.S. 174, 695.

Lynden-Bell D. (1982a), The Observatory 102, 7.

Lynden-Bell D. (1982b), The Observatory 102, 202.

Lynden-Bell D., Cannon R.D. and Godwin P.J. (1983), M.N.R.A.S. 204, 87P.

Madore B. (1978) in "Globular Clusters", NATO advanced study. I.O.A., eds. Hanes D.S. and Madore B., (C.U.P.), p.21.

Maeder A. (1975), Astron. Astrophys. 43, 61.

Maeder A. (1976), Astron. Astrophys. 47, 389.

Mallia E.A. and Pagel B.E.J. (1978), M.N.R.A.S. 184, 55P.

Mathewson D.S., Cleary M.N. and Murray J.D. (1974), Ap.J. 190, 291.

Mathewson D.S., Schwartz M.P. and Murray J.D. (1977), Ap.J. 217, L5.

McClure R.D. and Hesser J.E. (1981), Ap.J. 246, 136.

McDowell J.C. and Godwin P.J. (1986), The Observatory 106, 19.

Mengel J.G., Sweigart A.V., Demarque P. and Gross P.G. (1979), Ap.J. Suppl. 40, 733.

Michie R.W. (1963), M.N.R.A.S. 125, 127.

Mould J.R. (1982), Ann Rev. Astr. Astrophys. 20, 91.

Mould J.R. and Aaronson M. (1980), Ap.J. 240, 464.

Mould J.R. and Aaronson M. (1983), Ap.J. 273, 530.

Mould J.R., Cannon R.D., Aaronson M. and Frogel J.A. (1982), Ap.J. 254, 500.

Norris J. and Bessell M.S. (1978), Ap.J. 225, L49.

Norris J. and Zinn R. (1975), Ap.J. 202, 335.

Norris J. and Freeman K.C. (1983), Ap.J. 266, 130.

Olszewski E.W. and Aaronson M. (1985), preprint.

Padmanabhan T. and Vasanthi M.M. (1985), J. Astrophys. Astr. 6, 261.

Pagel B.E.J. and Edmunds M.G. (1981), Ann. Rev. Astr. Astrophys. 19, 77.

Penny A.J. (1976), Ph.D. Thesis, Sussex University.

Peterson C.J. and King I.R. (1975), Astron. J. 80, 427.

Pilachowski C.A. (1984), Ap.J. 281, 614.

Primack J.R. and Blumenthal G.R. (1984) in "Formation and Evolution of Galaxies and large scale structures in the Universe", eds. Audouze J. and Tran Thanh van J., (Reidel:Dordrecht), p.163.

Reaves G. (1967), in "Modern Astrophysics", ed. Hack M., (Gunthier-Villars:Paris), p.337.

Renzini A. (1981), in "Effects of mass loss on Stellar Evolution", Astrophysics and Space Science library, eds. Chiosi C and Statio R. (Reidel:Dordrecht), p.319.

Renzini A., Mengel J.G. and Sweigart A.V. (1977), Astron. Astrophys. 56, 369.

Richer H.B. and Westerlund B.E. (1983), Ap.J. 264, 114.

Robin A. and Creze M. (1984), preprint (to appear in Astron. Astrophys.).

Roberts M.S. (1975), IAU Symposium no.69 "Dynamics of Stellar Systems", ed. Hayli A., (Reidel:Dordrecht), p.331.

Rood R.T. (1973), Ap.J. 184, 815.

Rood R.T. and Seitzer P.O. (1981), IAU Colloquium no.68 "Astrophysical parameters for Globular Clusters", eds. Davis Philip, A.G. and Hayes D.S. (L. Davis Press:Schenectady, N.Y.), p.369.

Rubin V.C. (1979), IAU Symposium no.84 "The Large Scale Characteristics of the Galaxy", ed. Burton W.B., (Reidel:Dordrecht), p.211.

Saito M. (1979), Publ. Astr. Soc. Japan 31, 193.

Salpeter E.E. (1955), Ap.J. 121, 161.

Sandage A. (1957), Ap.J. 125, 422.

Sandage A. (1970), Ap.J. 162, 841.

Sandage A. (1982), Ap.J. 252, 553.

Sandage A. and Katem B. (1982), Astron.J. 87, 537.

Sandage A. and Smith L.L. (1966), Ap.J. 144, 886.

Sandage A. and Wallerstein G. (1960), Ap.J. 131, 598.

Sandage A. and Wildey R. (1967), Ap.J. 150, 469.

Sanduleak N. and Philip A.G.D. (1977), Publ. Warner and Swasey Obs. 2, no. 5.

Schinckel A.E., Phillips M.M. and Hill P.W. (1982), "A guide to wavelength identifications for the Cu-Ar lamp of the RGO spectrograph".

Schommer R.A., Olszewski E.W. and Cudworth K.M. (1981), IAU Colloquium no. 68 "Astrophysical parameters for Globular Clusters", eds. Davis Philip A.G. and Hayes D.S. (L. Davis Press:Schenectady, N.Y.), p.453.

Schommer R.A., Olszewski E.W., and Kunkel W.E. (1978), IAU Symposium no. 80 "The HR diagram" eds. Davis Philip A.G. and Hayes D.S. (Reidel:Dordrecht), p.269.

Searle L. and Zinn R. (1978), Ap.J. 225, 357.

Seitzer P.O. (1985), IAU Symposium no. 113 "Dynamics of Star Clusters", eds. Goodman J. and Hut P., (Reidel:Dordrecht), p.343.

Seitzer P.O. and Frogel J.A. (1985), Astron.J. 90, 1796.

Shanks T., Stevenson P.R.F., Fong R. and MacGillivray H.T. (1984), IAU Colloquium no. 74 "Astronomy with Schmidt type telescopes", ed. Capaccioli M., (Reidel:Dordrecht), p.499.

Shapley H. (1938), Harvard Bull. 908, 1.

Shapley H. (1939), Proc. Nat. Acad. Science U.S. 25, 565.

Simoda M. and Iben I. (1970), Ap.J. Suppl. 22, 81.

Smith G.H. and Dopita M.A. (1983), Ap.J. 271, 113.

Stetson P.B. (1979a), Astron.J. 84, 1056.

Stetson P.B. (1979b), Astron.J. 84, 1149.

Stetson P.B. (1979c), Astron.J. 84, 1167.

Stetson P.B. (1980), Astron. J. 85, 398.

Stetson P.B. (1984), P.A.S.P. 96, 128.

Stetson P.B., VandenBerg D.A. and McClure R.D. (1985), P.A.S.P. 97, 908.

Stephenson C.B. (1973), Publ. Warner and Swasey Observatory 1, no. 4.

Stobie R.S. (1982), COSMOS user manual, Royal Observatory Edinburgh.

Sweigart A.V. (1978), IAU Symposium no. 80 "The HR diagram", eds. Davis Philip A.G. and Hayes D.S., (Reidel:Dordrecht), p.333.

Sweigart A.V. and Gross P.G. (1978), Ap.J. Suppl. 36, 405.

Tammann G.A. (1980), ESO/ESA Workshop on the need for coordinated ground based observations, "Dwarf Galaxies", Geneva, eds. Tarenghi M. and Kjar K., p.3.

Tanaka K.I. and Hamajima K. (1982), Publ. Astr. Soc. Japan 34, 417.

Tinsley B.M. (1981), M.N.R.A.S. 194, 63.

Tonry J. and Davis M. (1979), Astron. J. 84, 1511.

Tremaine S.D. and Gunn J.E. (1979), Phys. Rev. Lett. 42, 407.

Trumpler R.J. and Weaver H.F. (1952) in "Statistical Astronomy", University of California Press.

van Agt S.L.T.J. (1973) IAU Colloquium no. 21 "Variable stars in Globular Clusters and in related Systems", ed. Fernie J.D., (Reidel:Dordrecht), p.35.

VandenBerg D.A. (1983), Ap.J. Suppl. 51, 29.

VandenBerg D.A. and Bridges T.J. (1984), Ap.J. 278, 679.

Van den Bergh S. (1972), Ap.J. 171, L31.

Van den Bergh S. (1980), in "Structure and Evolution of Normal Galaxies", NATO advanced study, I.O.A., eds. Fall S.M. and Lynden-Bell D. (C.U.P.), p.201.

Van den Bergh S. and Lafontaine A. (1984), P.A.S.P. 96, 869.

Van Rhijn P.J. (1936), Groningen Publlication no. 47.

Wakamatsu K. (1981), P.A.S.P. 93, 707.

Webbink R.F. (1985), preprint (IAU Symposium no. 113, "Dynamics of Star Clusters", eds. Goodman J. and Hut P., (Reidel:Dordrecht), p.541.

Westerlund B.E. (1979), ESO messenger 19, 7.

Westerlund B.E. and Glaspey J. (1971), Astron. Astrophys. 10, 1

Westerlund B.E., Olander N., Richer H.B. and Crabtree T.R. (1978), Astron. Astrophys. Suppl. 31, 61.

Wheeler J.C. (1979), Ap.J. 234, 569.

Wilson A.G. (1955), P.A.S.P. 67, 27.

Yoshii Y. and Saio H. (1979), Publ. Astr. Soc. Japan 31, 339.

Zinn R. (1978a), Ap.J. 225, 790.

Zinn R. (1978b), in "Globular Clusters", NATO advanced study, I.O.A., eds. Hanes D.S. and Madore B. (C.U.P.), p.191.

Zinn R. (1981), Ap.J. 251, 52.

Zinn R. and Dahn C.C. (1976), Astron. J. 81, 527.

Zinn R. and Persson S.E. (1981), Ap.J. 247, 849.

Zinn R. and Searle L. (1976), Ap.J. 209, 734.

Zinn R. and West M.J. (1984), Ap.J. Suppl. 55, 45.

Zinnecker H. and Cannon R.D. (1985), talk presented at Star Forming Dwarf Galaxies and Related Objects, Paris, France.